Generalized Parton Distributions and their covariant extension : towards nucleon tomography

Nabil Chouika

Thèse de doctorat

Generalized Parton Distributions and their covariant extension: towards nucleon tomography

Thèse de doctorat de l'Université Paris-Saclay
préparée à l'Université Paris-Sud
au sein de l'Irfu/DPhN du CEA Saclay

École doctorale n°576 PHENIICS
Particules, Hadrons, Énergie, Noyau,
Instrumentation, Imagerie, Cosmos et Simulation

Spécialité de doctorat : Physique hadronique

Thèse présentée et soutenue à Saclay, le 17 septembre 2018, par

Nabil Chouika

Composition du Jury :

Jaume Carbonell	Directeur de recherche IPN Orsay	(Président du jury)
Barbara Pasquini	Associate Professor Université de Pavie	(Rapporteur)
Lech Szymanowski	Professeur NCBJ, Varsovie	(Rapporteur)
Bernard Pire	Directeur de recherche CPhT, École Polytechnique	(Examinateur)
José Rodriguez-Quintero	Associate Professor Université de Huelva	(Examinateur)
Hervé Moutarde	Ingénieur chercheur CEA Saclay, Irfu/DPhN	(Directeur de thèse)

À Anass,

Acknowledgements

The most difficult part to write is probably these first lines of the manuscript, and that is why they are written last. Even with the best words I can come up with, I would probably not do justice to the persons I will acknowledge here (nor obviously to the ones I will forget). I must still try nonetheless.

First and foremost I would like to thank my supervisor Hervé Moutarde who showed from the first time I met him a genuine enthusiasm to work with me and kept encouraging me throughout the internship and then the thesis. Hervé was always available, even when he had to juggle both research and his new bureaucratic duties. His natural curiosity makes him knowledgeable on all things related to QCD in particular, but also Physics and Mathematics in general. When encountering an issue, I always knew that I could turn successfully to Hervé, because even when he didn't know the answer, he would gladly sit through the afternoon with me while we tried to find a solution together. Thank you for trusting me, Hervé.

I would like also to thank the two other members of what Hervé calls I think the "gang of four": Pepe Rodríguez-Quintero and Cédric Mezrag. Hervé initiated with them this "covariant extension" project and I was lucky to come and reap the rewards of this work by implementing it. Pepe was as encouraging and available as any supervisor could be, despite not being officially one[1], and his cheerfulness had no limits. When it comes to Cédric, I must thank him also for his thesis manuscript. He was Hervé's previous PhD student, and I could not have survived in the GPD field without having his thesis to turn to in moments of need. I hope I wrote in turn a thesis pedagogical enough to be even if only half as useful for the next students as his was for me. It was a pleasure to work with all of you.

To continue with the collaborators, I would like to thank all the PARTONS collaboration. In particular Bryan Berthou and Pawel Sznajder. Bryan conceived with Hervé the PARTONS software as it is today, and taught us all physicists numerous lessons of software development, be it pragmatically for work, or for our personal benefit during lunch breaks. After Bryan had to leave, Pawel took upon himself to carry the project and push for more and more improvements and he continues to do so. His mastery of the software makes him the first interlocutor when it comes to PARTONS, and he never fails to help. Thank you again.

To achieve a good thesis, there is not only need of good collaborators, but also a good place to work at. Therefore, I would like to thank all the people at DPhN[2] who make it such a wonderful working environment. In particular I would like to thank the members (past and present) of the CLAS group at Saclay: my office neighbour Maxime for being always available to answer my questions on the experimental side of GPDs, Francesco who kindly suggested to help me for my defense rehearsal when Hervé was absent, Guillaume and Noélie who both

---

[1]For the anecdote, he was supposed to be my co-supervisor before the CEA scholarship saved us all from the bureaucratic nightmares of a *co-tutelle*. So I suppose I should not forget to thank the *Haut Commissaire*.

[2]Always SPhN in our hearts.

Acknowledgements

separately shared my office for a time and had to cope with my probably infuriating habit playing with the pencil, and many others. Of course I cannot forget the other students and post-docs of the lab: Christopher who had to immigrate from so far away and make incredible efforts of integration by learning French for instance (which as everyone knows is fundamentally different from his native language, *le marseillais*) and whose constant cheerfulness during lunch breaks I would never trade back, Mehdi[3] with whom I followed the same road to DPhN from our M2, his soulmate Pierre[3] who is behind his rugbyman stature one of the nicest persons I've met, Simon who helped me find a good teaching job, Arek and Saba, as both need to be praised for their incredible spy abilities[4], the duo Benjamin and Raphaël whose Shakespearean relationship is heartwarming, Aurélie, Antoine, Loïc and many more. But the student life at DPhN would not have been as interesting as it is without the efforts of Jason and Nancy who took to heart the difficult task of bringing us together. I would like also to thank the administrative side of DPhN, with Danielle Coret and Isabelle Richard at the forefront making our life easier by smoothing the horrible bureaucracy, and the heads of the lab, Franck Sabatié, Jacques Ball and Christophe Theisen, for their constant efforts in the interest of all the research held here.

Going back to the thesis process, I would like to thank Bernard Pire and Jaume Carbonell who accepted to sit at my examination panel and also discussed our covariant extension approach enthusiastically with Hervé and me at previous occasions. I was also very lucky that Barbara Pasquini and Lech Szymanowski kindly accepted to review my manuscript with inestimable comments and encouragements. Barbara in particular pointed out many corrections that improved the manuscript significantly. Thank you both for your time. I wish I could also mention Daniele Binosi as one of the jury members as he kindly accepted my offer, but unfortunately had conflicting schedules which prevented him from participating. Nevertheless, Daniele was very supportive all the way back to when we worked together on Dyson-Schwinger solvers and afterwards helped me considerably for the post-doc applications, and I thank him for all that. I am also grateful to Cédric Lorcé for fruitful exchanges and his valuable inputs on the last months of this thesis.

In a perhaps not so common way, I would now like to thank some people that I have never actually met (or only briefly) but whose work was immensely helpful for this thesis. The first one is Markus Diehl, whose incredible output on GPDs in the previous decades is simply impressive. When something was not clear or seemed new to me (or other collaborators), you could bet that it was actually already dealt with in Markus's review [1]. After perhaps a few days of tearing your hair out, going back to this bible closed the issue in 90% of cases as it was at least discussed there if not solved. Sometimes, when it was only briefly mentioned, you could be sure to find the detailed answer in the second testament: Belitsky and Radyushkin's review [2]. I would like to thank in general all the physicists who took the time to review their field for newcomers. But this thesis has also a strong numerical component, and for that I would like to thank all the contributors to open-source softwares that I used throughout these years, in particular the numerical tools in Python [3, 4].

Last but not least, I would like of course to thank my friends here in Paris who put up with

---

[3]Both tried to explain to me patiently and so many times what are *ab initio* methods in nuclear structure, but still without success I am ashamed to say.

[4]I completely fell for their act!

me during the previous years and my family in Morocco, in particular my mom, who I know suffered a lot from the distance and from seeing me only for a brief month each year, and my sister Dalal without whom nothing would have been possible.

Contents

Contents

Contents

Résumé

1. Distributions de Partons Généralisées

Les Distributions de Partons Généralisées (GPDs) [5–7] encodent les corrélations entre l'impulsion longitudinale et la position transverse des partons[1] dans les hadrons et peuvent donc fournir une représentation de la structure du nucléon en 2+1 dimensions Elles ont été étudiées théoriquement et expérimentalement pendant près de deux décennies et une nouvelle ère expérimentale visant à les extraire vient de débuter à Jefferson Lab (JLab) aux États-Unis et au CERN avec l'expérience COMPASS, et à l'avenir à un collisionneur électron-ion (EIC).

Ces GPDs sont définies comme des transformées de Fourier sur le cône de lumière d'un élément de matrice non-diagonal d'opérateur bi-local, ce qu'on peut par exemple écrire dans le cas simple d'une GPD twist-2 de quark dans le pion à chiralité paire :

$$H^q\left(x,\xi,t\right) = \frac{1}{2}\int \frac{\mathrm{d}z^-}{2\,\pi}\, e^{i\,x\,P^+ z^-} \left\langle \pi, P+\frac{\Delta}{2}\left|\bar{\psi}^q\left(-\frac{z}{2}\right)\gamma^+ \psi^q\left(\frac{z}{2}\right)\right|\pi, P-\frac{\Delta}{2}\right\rangle\Bigg|_{\substack{z^+=0 \\ z_\perp=0}}, \quad (1)$$

où $t=\Delta^2$ est la variable de Mandelstam de transfert d'impulsion et $\xi = -\frac{\Delta^+}{2\,P^+}$ est la variable d'asymétrie (*skewness*). Dans le cas du nucléon, d'autres GPDs de chiralité paire interviennent : E (qui intervertit l'hélicité du nucléon), $\tilde{H}$ et $\tilde{E}$ (GPDs polarisées). Nous garderons surtout l'exemple simple du pion dans ce qui suit.

L'une des principales motivations derrière l'étude des GPDs est l'interprétation probabiliste de leur limite d'asymétrie nulle $H(x,\xi=0,t)$ [8], qui est reliée par transformée de Fourier à une densité numérique de partons

$$\rho^q\left(x,\boldsymbol{b}_\perp\right) = \int \frac{\mathrm{d}^2\boldsymbol{\Delta}_\perp}{(2\pi)^2}\, e^{-i\,\boldsymbol{b}_\perp\cdot\boldsymbol{\Delta}_\perp}\, H^q\left(x,0,-\boldsymbol{\Delta}_\perp^2\right) \quad (2)$$

d'impulsion longitudinale x et de position transverse $\boldsymbol{b}_\perp$ (aussi appelé paramètre d'impact). Malheureusement, pour l'instant l'accès à ces objets est seulement possible de manière indirecte à travers des convolutions de la forme [9]

$$\mathcal{H}\left(\xi,t,Q^2\right) = \int_{-1}^{1}\frac{\mathrm{d}x}{\xi}\sum_{a=g,u,d,\ldots} C^a\left(\frac{x}{\xi},\frac{Q^2}{\mu_F^2},\alpha_S\left(\mu_F^2\right)\right)H^a\left(x,\xi,t,\mu_F^2\right). \quad (3)$$

où $\mathcal{H}$ est un Facteur de Forme Compton (CFF) associé à la GPD H, C est un noyau de diffusion dure calculé à un certain ordre en théorie des perturbations, μ_F est l'échelle de factorisation, α_S est la constante de couplage fort et Q^2 est la virtualité du photon sondant le hadron par

---

[1]Nom désignant à la fois les quarks et les gluons, degrés de liberté fondamentaux de la chromodynamique quantique (QCD).

Résumé

exemple dans un processus tel que la Diffusion Compton Profondément Virtuelle (DVCS). De plus, seules des valeurs non nulles de $\xi \in [\xi_{\min}, \xi_{\max}]$ sont accessibles. Une extrapolation à asymétrie nulle est donc nécessaire en plus de la tâche déjà difficile de déconvolution de la dépendance en x.

Par conséquent, un des principaux défis dans ce domaine est de produire des modèles de GPDs qui satisfont à la fois aux propriétés de *polynomialité* et de *positivité*[2]. Ces contraintes sont cruciales pour pouvoir extrapoler de manière correcte l'information extraite des données expérimentales et peuvent être formulées comme suit :

Polynomialité Les moments de Mellin $\int_{-1}^{1} \mathrm{d}x\, x^m\, H\left(x, \xi, t\right)$ d'une GPD H sont des polynômes en la variable d'asymétrie ξ, de degré au plus $m+1$. Ceci découle de l'invariance de Lorentz.

Positivité La GPD est bornée par des inégalités de la forme [1,10]

$$\left. \left|H^q(x, \xi, t)\right|\right|_{x \geq \xi} \leq \sqrt{q\left(\frac{x-\xi}{1-\xi}\right) q\left(\frac{x+\xi}{1+\xi}\right)}, \tag{4}$$

où la borne de la GPD de quark H^q est donnée en fonction de sa limite vers l'avant, c.-à-d. la PDF q. Ceci est dû à la positivité d'une norme dans un espace de Hilbert, où le théorème de Cauchy-Schwarz peut être appliqué.

Il y a deux chemins généralement suivis dans une approche de théorie quantique du champ menant à un calcul de GPDs.

Approche covariante Le premier est basé sur une analyse diagrammatique et covariante qui, dans la plupart des cas, suppose une approximation d'impulsion, autrement appelé calcul de diagramme triangle. Il a l'avantage de produire des GPDs sur tout leur domaine cinématique respectant la polynomialité, mais présente plusieurs problèmes comme l'absence de positivité ou des anomalies concernant les symétries discrètes quand les vertex considérés dépendent de l'impulsion [11–14].

Approche sur le cône de lumière Le deuxième est de considérer le développement dans l'espace de Fock en termes de Fonctions d'Onde sur le Front de Lumière (LFWFs). Ce faisant, la positivité est naturellement satisfaite du fait que les GPDs sont représentées comme un produit scalaire de LFWFs, p. ex. dans la région DGLAP (cf. le chapitre 6 pour les notations et plus de détails)

$$H^q\left(x, \xi, t\right) = \sum_{N, \beta} \left(\sqrt{1-\xi^2}\right)^{2-N} \sum_a \delta_{f_a, q} \int \left[\mathrm{d}\bar{x}\right]_N \left[\mathrm{d}^2\bar{\boldsymbol{k}}_\perp\right]_N \delta\left(x - \bar{x}_a\right) \tag{5}$$
$$\times\, \Psi_{N, \beta}^*\left(x_1^{\mathrm{out}\prime}, \boldsymbol{k}_{\perp 1}^{\mathrm{out}\prime}, \ldots, x_a^{\mathrm{out}\prime}, \boldsymbol{k}_{\perp a}^{\mathrm{out}\prime}, \ldots\right) \Psi_{N, \beta}\left(x_1^{\mathrm{in}}, \boldsymbol{k}_{\perp 1}^{\mathrm{in}}, \ldots, x_a^{\mathrm{in}}, \boldsymbol{k}_{\perp a}^{\mathrm{in}}, \ldots\right),$$

où des LFWFs de même nombre de partons se recoupent. En revanche, il est difficile de tronquer cette somme sur les états de Fock de manière cohérente à la fois dans les régions

---

[2]Dans ce résumé, nous ne considérerons pas les autres propriétés et contraintes. Pour plus de détails à ce sujet, voir le chapitre 4 et les références à cet égard.

DGLAP ($|x| \geq \xi$) et ERBL ($|x| \leq \xi$). En effet, dans cette dernière, le recoupement des LFWFs est asymétrique en le nombre N de partons. Ceci rend peu vraisemblable que la polynomialité soit satisfaite ou que la GPD obtenue soit cohérente dans les deux régions (continue à la frontière $|x| = \xi$ en particulier, ce qui est crucial pour la factorisation des processus exclusifs comme DVCS) à un quelconque ordre fini de troncature N. On s'attend plutôt à ce que ce soit vérifié quand tous les états de Fock sont sommés.

2. Extension covariante

En pratique, on est souvent limités à une troncature aux ordres les plus bas, p. ex. une LFWF à deux corps dans le cas du pion. La GPD dans la région DGLAP en est obtenue directement. Mais le problème ensuite peut être énoncé comme suit : quelle est la contribution ERBL correspondante ? Et comment la reconstruire ?

Pour cela, on peut utiliser la représentation naturelle de la propriété de polynomialité : les Double Distributions (DDs). En considérant la GPD comme une transformée de Radon [15, 16] de la façon suivante [17] :

$$H(x, \xi) = (1 - x) \int_\Omega \mathrm{d}\beta \mathrm{d}\alpha \, h(\beta, \alpha) \, \delta(x - \beta - \alpha\xi) = (1 - x) \, \mathcal{R}h(x, \xi), \qquad (6)$$

on peut utiliser la région DGLAP pour inverser l'équation et en déduire la DD h, ce qui nous permet ensuite d'étendre la GPD à la région ERBL [18]. Les différents domaines d'intérêt sont schématisés sur la figure 1.
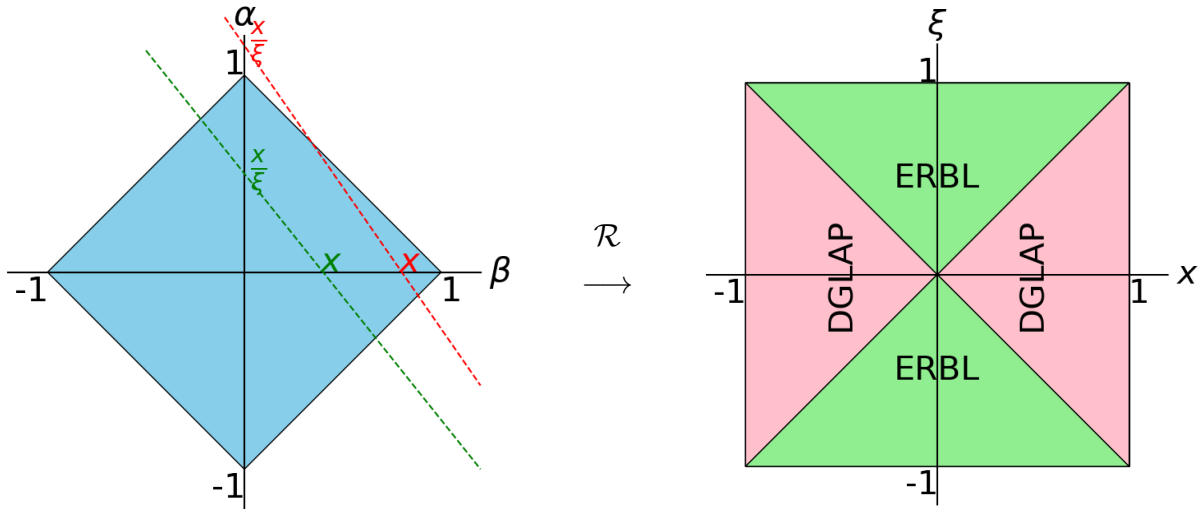
Figure 1. Le domaine $\Omega = \{(\beta, \alpha) \, / \, |\beta| + |\alpha| \leq 1\}$ des Double Distributions (à gauche) et les domaines DGLAP et ERBL des GPDs (à droite). La transformée de Radon $\mathcal{R}f(x, \xi) = \int \mathrm{d}\beta \mathrm{d}\alpha \, f(\beta, \alpha) \, \delta(x - \beta - \alpha\xi)$, c.-à-d. une intégration de f sur des lignes paramétrées par (x, ξ), est l'opération qui relie ces espaces. Les lignes rouges qui traversent l'axe des α en $x/\xi > 1$ correspondent aux cinématiques DGLAP, tandis que les lignes ERBL sont représentées en vert.

Résumé
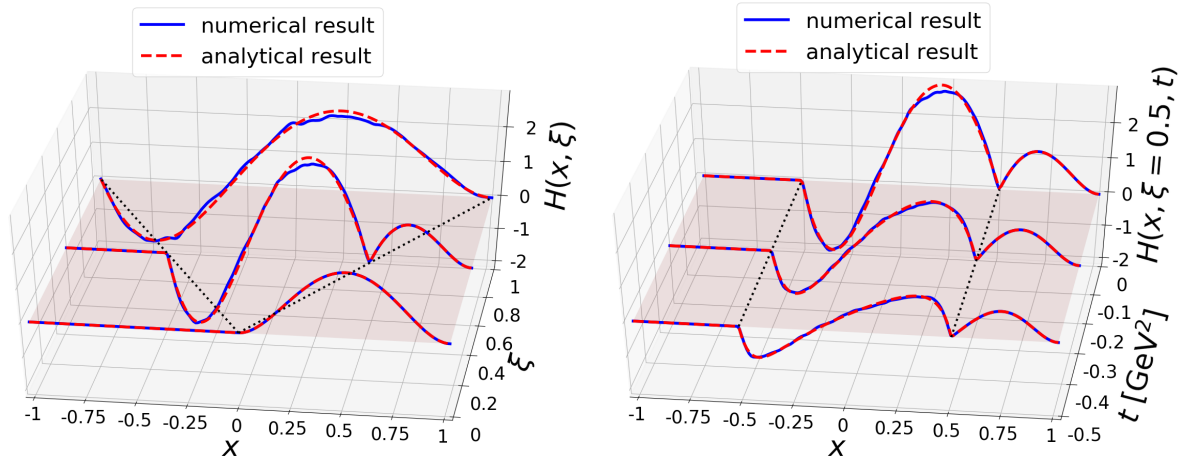
Figure 2. Comparaison entre les résultats analytiques et numériques pour la GPD de pion modélisée dans les Refs. [13, 19]. Les courbes en trait plein bleu présentent le résultat numérique, tandis que celles en tirets rouges montrent le résultat analytique obtenu dans le cas présent. Le panneau de gauche concerne le cas $t = 0$ pour trois valeurs de $\xi = [0, 0.5, 1]$, tandis que celui de droite présente l'évolution en t pour les trois valeurs $[0, -0.25, -0.5]$ à $\xi = 0.5$. Pour plus de détails, voir la légende de la même figure 9.1 et la section 9.1 correspondante.

Le principal avantage de cette méthode est qu'elle est générale, c'est-à-dire que l'inversion peut être faite numériquement avec une procédure identique pour tout modèle de LFWFs en entrée. Cependant, certains modèles permettent de trouver un résultat analytique simple pour la DD et fournissent donc des benchmarks pour tester la procédure numérique. On peut citer par exemple le modèle de diquark scalaire pour le nucléon étudié dans la Ref. [20] et qui est à l'origine de cette idée d'extension covariante. Ici, on présente sur la figure 2 un autre benchmark avec une GPD de pion construite à partir d'un modèle algébrique simple basé sur une représentation de Nakanishi [13, 19]. L'inversion numérique se base sur l'information de la seule région DGLAP, avec pour objectif d'étendre à la région ERBL. Par conséquent, la comparaison des résultats numériques et analytiques sur la région ERBL (c.-à-d. entre les lignes en pointillés noirs) est le principal résultat de cette figure. Comme on peut le voir, cette extrapolation numérique est très bonne.

Pour résoudre numériquement ce problème inverse, une discrétisation inspirée des méthodes d'éléments finis a été utilisée, avec notamment des fonctions de base linéaires par morceaux dans l'espace des DDs. Dans l'espace des GPDs, un échantillonnage aléatoire de la région DGLAP peut être réalisé de telle sorte à inclure le plus d'informations possibles. Du fait du caractère mal posé de l'inversion de la transformée de Radon, il est important cependant de régulariser [21] le problème discret pour obtenir une solution qui a du sens.

3. La bibliothèque PARTONS

Le logiciel PARTONS [22] a été conçu comme une réponse aux défis théoriques rencontrés par la modélisation des GPDs, avec comme objectif d'accompagner les programmes expérimentaux actifs où on attend de nettes augmentations de précision et de couverture cinématique. Il

fournit une bibliothèque C++ visant à la fois les expérimentateurs et les phénoménologues.

PARTONS traite la chaîne de calcul complète d'un observable dans un canal expérimental donné lié aux GPDs. Ceci peut être décomposé en trois niveaux :

Grandes distances Ce niveau concerne le calcul des GPDs elles-mêmes, comme des fonctions de x, ξ, t, etc, eu égard à différents paramètres de modèles. La dépendance en l'échelle de factorisation est décrite par des équations d'évolution.

Petites distances Le deuxième niveau est celui des fonctions coefficients décrivant les phénomènes de diffusion dure. En pratique, ceci implique de convoluer les GPDs et le résultat obtenu consiste en des CFFs (cf. p. ex. Eq. (3)).

Processus final Finalement, ce niveau concerne le calcul des sections efficaces et autres observables pouvant être directement mesurés expérimentalement.

À chacun de ces niveaux, le framework est assez flexible pour permettre n'importe quel choix d'hypothèses de modélisation, l'inclusion de corrections d'ordre supérieur, etc. En effet, PARTONS a été conçu pour être modulaire et fonctionne sur la base de classes abstraites uniquement, laissent la liberté à l'utilisateur de choisir la physique qu'il souhaite implémenter.

Pour l'instant, seul le canal DVCS est implémenté, mais les autres processus exclusifs (TCS et DVMP notamment) sont aussi prévus, et l'architecture a été pensée pour traiter n'importe quel canal. Parmi les modules disponibles, on peut citer le modèle de GPDs dit « GK » très utilisé dans la communauté [23], ou encore les dernières formules de sections efficaces du formalisme Belitsky-Müller [24]. La version actuelle de PARTONS en somme dispose de tous les outils nécessaires pour étudier le DVCS à NLO (deuxième ordre de perturbation) et twist-2, mais d'autres modèles et

Figure 3. Logo PARTONS.

fonctionnalités peuvent être ajoutées (ou branchées par l'utilisateur) du fait de sa modularité.

4. Phénoménologie de modèles de quarks

En utilisant les développements de physique déjà implémentés dans PARTONS, on peut maintenant tirer profit de la méthode d'extension covariante présentée dans la section 2 pour produire des observables DVCS à partir de modèles du type quarks constituants, en vue d'une phénoménologie systématique. On fait le choix ici du *Chiral Quark Soliton Model* (χQSM) pour le nucléon, étudié dans la Ref. [25] au travers d'une troncature au premier état de Fock (c.-à-d. trois quarks de valence). Cette troncature signifie que seule la région DGLAP des GPDs est accessible, ce qui limite la phénoménologie DVCS au premier ordre en perturbation (LO), vu que seule la ligne de frontière $x = \xi$ intervient dans ce cas avec l'addition d'au moins une constante de soustraction dans le cadre de l'approche des relations de dispersion (cf. p. ex. Ref. [26] et les références à cet égard). On ne peut pas aller plus loin dans la théorie des perturbations, et on ne peut pas non plus évoluer la GPD de l'échelle basse $Q_0^2 = 0.259 \, \text{GeV}^2$ du modèle vers celle de l'expérience.

Résumé
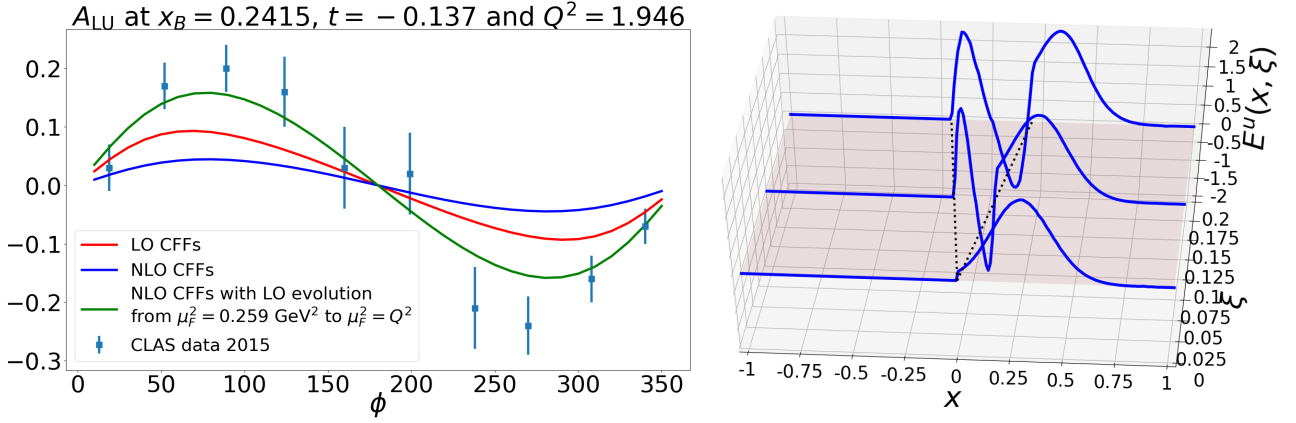
Figure 4. Test du modèle χQSM de la Ref. [25]. **Gauche** : Asymétrie de spin de faisceau pour le processus DVCS avec comparaison aux données CLAS de Ref. [27]. **Droite** : GPD E^u à $t = -0.34$ GeV^2 avec extension à la région ERBL.

En étendant de manière covariante ces GPDs à la région ERBL, ces études deviennent maintenant possibles. La figure 4 (panneau de droite) illustre cette extension dans le cas de la GPD E^u. On peut donc utiliser ces GPDs étendues H, E et $\tilde{H}$[3] pour chaque saveur u et d pour produire des observables DVCS et les comparer aux données expérimentales. Un exemple d'un tel calcul est présenté sur la figure 4 (panneau de gauche) avec une asymétrie de spin de faisceau définie en fonction de la section efficace du processus $ep \to ep\gamma$ comme :

$$A_{\mathrm{LU}}^-(\phi) = \frac{\mathrm{d}\sigma^{\vec{\rightarrow}}(\phi) - \mathrm{d}\sigma^{\vec{\leftarrow}}(\phi)}{\mathrm{d}\sigma^{\vec{\rightarrow}}(\phi) + \mathrm{d}\sigma^{\vec{\leftarrow}}(\phi)}, \qquad (7)$$

où ϕ est l'angle entre le plan leptonique et le plan de production, les flèches désignant l'hélicité et le signe « $-$ » la charge du faisceau[4]. La cinématique de JLab choisie pour illustrer cela fait partie d'un jeu de données publié par la collaboration CLAS [27].

Il ne s'agit pas ici de dire quoi que ce soit sur la justesse de ce modèle, le but présent étant simplement d'illustrer la procédure. Celle-ci peut être appliquée systématiquement à n'importe quel modèle de quarks de valence pour produire des GPDs qui satisfont toutes les contraintes théoriques et prêtes à l'emploi pour de la phénoménologie de DVCS sous diverses hypothèses perturbatives. Étant donné la publication prochaine de nouvelles données de JLab 12 GeV dans la région de valence, ce type d'études serait le bienvenu. Cela permettrait en effet de tester la pertinence à basse échelle d'une troncature de valence des LFWFs et d'ouvrir la voie à une phénoménologie systématique des LFWFs à travers les processus exclusifs et les GPDs. Cela pourrait mener *in fine* à une phénoménologie unifiée avec à la fois les GPDs et les TMDs.

---

[3]On néglige la GPD $\tilde{E}$.

[4]JLab ne dispose que de faisceaux d'électrons.

Introduction

A few years ago, the particle that gives their mass to the other elementary particles of the Standard Model (SM) was discovered at the Large Hadron Collider (LHC), several decades after the theoretical discovery of the Brout-Englert-Higgs mechanism. This completed the SM and led the Particle Physics community in two directions, both going to higher and higher energies: the main one devoted to challenging the SM and finding new physics, the other consisting in a finer metrology of the SM. But one should not forget that some parts of the Standard Model are not even fully understood yet, in particular what is known as the non-perturbative regime of Quantum Chromodynamics (QCD), which is the theory of the strong interaction that binds nucleons together. At low energies, Nuclear Physics aims at describing the structure of nuclei, while at medium energies enters Hadron Physics with among other things the goal of understanding how hadrons (such as the nucleons or the pions) are made in terms of the fundamental degrees of freedom of QCD; the quarks and gluons.

One of the difficulties of QCD is that quarks and gluons which carry a color quantum number cannot be observed; they are *confined* inside hadrons which are colorless bound-states. Explaining this confinement is a major challenge. A second issue is the dynamical mass generation of hadrons. Indeed, the Higgs mechanism contributes to no more than a few percents of the visible mass of the universe. The rest is due to the strong interaction; gluons and quarks interact inside the proton for instance and this energy makes up for almost all its mass. We could say that a world where the Higgs does not couple to quarks would not be much different from ours, as the mass of the bare quarks is negligible compared to this *Dynamical Chiral Symmetry Breaking* phenomenon. These are the mysteries Hadron Physics aims at shedding light[1] on.

To achieve this, one uses scattering experiments at moderate to high energies and can often count on *factorization* to separate:

- the small distance phenomena of the hard probe interacting with almost free constituents of the hadrons, calculable with perturbative QCD thanks to the *asymptotic freedom* behavior;

- from the large distance phenomena (of the order of the proton size for instance) that are linked to the structure of the probed hadron and are intrinsically non-perturbative.

In the processes that interest us in the present thesis, the hard probe is a photon, usually virtual and produced by a lepton. This allows us to access distributions of quarks and gluons inside the hadron.

These distributions are non-perturbative objects that cannot be computed in principle, unless one applies a discretization to solve the field theory as in Lattice QCD — but the

---

[1]Often virtual.

ability to compute such complex objects in this framework is still very limited — or relies on models reproducing some QCD features (constituent quark models, Dyson-Schwinger equations, etc). For this thesis, we are mostly interested in Generalized Parton Distributions (GPDs), introduced in the late 90s, which encompass both elastic Form Factors (FFs) and Parton Distribution Functions[2] (PDFs), which were studied starting from the 60s and 70s and are already quite well known. The latter are distributions of longitudinal momentum of partons inside the hadron, while the former are related to distributions of charge (in the transverse plane). GPDs provide additional information on the correlation between the longitudinal momentum and the transverse position of partons.

Experimentally, this tomography of hadrons led to a large experimental program in the numerous facilities around the world dedicated to Hadron Physics. In particular, for GPDs, DESY in Germany and Jefferson Lab (JLab) in Virginia, USA, have been at the forefront of the effort towards their extraction, with first data published at the start of the 2000s. A new GPD era is starting with both the 12 GeV upgrade at JLab, which promises a larger kinematic coverage in the valence region and a higher accuracy in upcoming data, and the COMPASS collaboration (at CERN) providing new data in the sea quark region. *In fine*, the Electron Ion Collider (EIC) project is driven in part by the promise of hadron tomography, and in particular the extraction of GPDs in a wide kinematic region including the gluon dominated one at a very high luminosity. All this new input with high accuracy will without doubt challenge the current models of GPDs.

Phenomenologically, the difficulty resides in the fact that GPDs are not directly accessible in experiment. The observables are convolutions of GPDs with a hard scattering kernel and therefore an inverse problem needs to be solved. This is usually done by using functional forms with free parameters that are fitted to the experimental data. However, GPDs are constrained by several important properties, which renders the task more difficult as one often has to choose between flexible parametrizations reproducing the data well but with poor predictive power or take into account all the constraints with a parametrization too strict for data compatibility. All this was acceptable within the range of accuracy previously achieved with experimental data, but will not be sustainable with the new high precision era.

Naturally, the way to go is through *ab initio* computations, *i.e.* to use the state-of-the-art modelling techniques developed to fulfill most QCD features. But even then, the issue arises when it comes to GPDs that not all constraints are met at once. One interesting method consists in using the *Light-Front Wave-functions* (LFWFs) expansion, but in practice does not allow to access all the kinematic domain of GPDs, which is necessary for phenomenology. The novel method of this thesis consists in extending this limited-domain GPD by solving a Radon transform inverse problem in a general way and deriving the corresponding Double Distribution (DD), which in doing so allows to fulfill a missing constraint. This approach can help model building achieve the long promised goal of hadron tomography.

In Part. I, we introduce the fundamentals of the field of GPDs (and hadron tomography in general), with Chap. 2 in particular laying down the physics case[3]. Parts II and III are

---

[2]PDFs constitute the main uncertainty in experiments at the LHC and their knowledge at high accuracy is therefore crucial also for Particle Physics applications.

[3]As a reading advice, a newcomer to the field may want to skip Chap. 2 in a first reading as it may be difficult to digest at first, and then come back to it later with enough distance. On the contrary, someone familiar with the field (such as a GPD experimentalist) may want to skip chapters 1 and 3 in which they would

the core of this thesis, with the former establishing the necessary theoretical ground[4] and the latter delving into the aforementioned *covariant extension* method. In Part. III, we start by motivating the approach and explaining its principle (chapter 7), then we detail the chosen numerical procedure in Chap. 8 and finally we illustrate how this can be applied to extend LFWF-based models of GPDs in Chap. 9 with a few relevant examples (mainly in the pion case).

---

probably find nothing new, but still read Chap. 2 which reviews the interesting physics of hadron tomography motivating the existing experimental programs.

[4]Reading it is necessary to fully understand the subsequent part, but it can also be of interest as a standalone review of GPDs (chapter 4), DDs (chapter 5) and LFWFs (chapter 6).

Part I.

Nucleon tomography

Chapter 1.

Probing the nucleon: a long story short

We start by introducing very succinctly the main milestones [28–30] in the field of hadron structure and more generally QCD physics, its direct parent. We will cover in this chapter the history of the field up to the 1970s, while the more recent formalism will be introduced in the next chapters.

1.1. From the hydrogen atom...

1.1.1. Discovery of the proton

The proton was discovered in 1919 by Rutherford who noticed that a hydrogen nucleus is liberated from a nitrogen atom once disintegrated [31]. This hydrogen nucleus was thought of as an elementary particle, the *proton*, and its spin was confirmed to be $\frac{1}{2}$ in 1927 [32]. The first hints of an internal structure of the proton came only in 1933 when experiments [33–36] shed light on its magnetic moment, much larger than what was expected for a point-like fermion obeying Dirac's equation. In other words, it was found to be:

$$\mu_p = (1 + \kappa)\, \frac{e}{2\, M_p} > \frac{e}{2\, M_p}\,, \tag{1.1}$$

where we denoted by κ the anomalous magnetic moment, e the positron charge and M_p the proton mass.

1.1.2. Elastic scattering and charge radius

Therefore, to confirm the spatial extension of the proton, several scattering experiments were pursued. In the context of particle physics, an elastic scattering means that we have identical particles in the final state. Here, we are considering a scattering of an electron off a proton (and more generally a nucleon), as sketched in Fig. 1.1 (left panel). On top of the notations of the diagram, we also define the momentum transfer[1], corresponding to the photon virtuality, which is space-like:

$$\Delta \equiv P_2 - P_1 = l - l'\,, \qquad\qquad t \equiv \Delta^2 < 0\,. \tag{1.2}$$

This virtuality is the only independent Lorentz scalar.

---

[1]We choose here a consistent notation with that of GPDs in Chap. 4, despite this virtuality being usually denoted $-Q^2$.
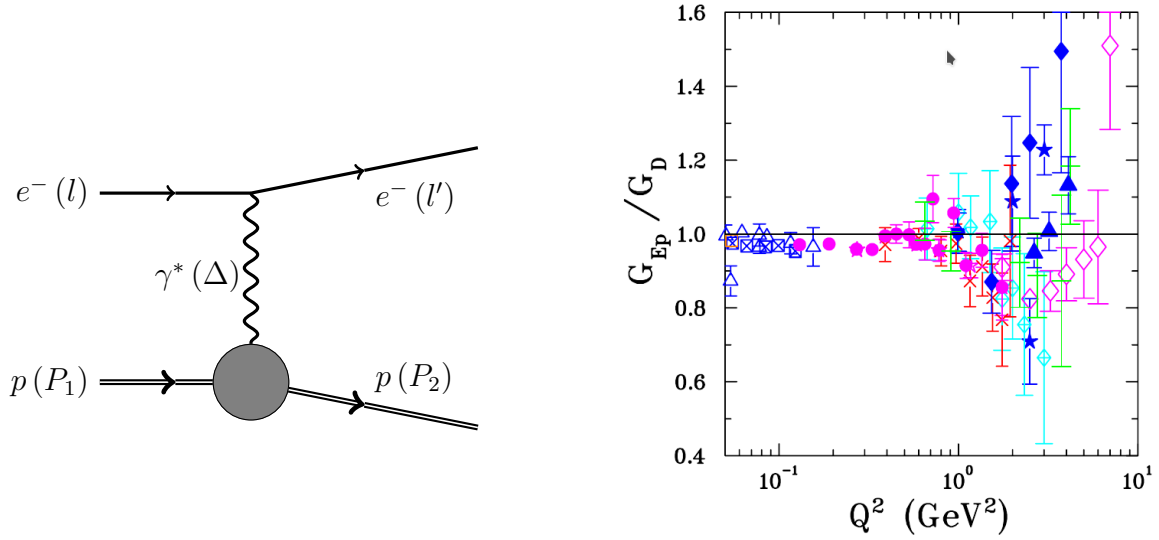
Figure 1.1. **Left**: Elastic Scattering of a lepton (*e.g.* electron) off a nucleon (*e.g.* proton) target, with a single photon exchange. **Right**: Proton electric Form Factor divided by the dipole Form Factor $G_D\left(Q^2\right) = \left(1 + \frac{Q^2}{0.71\ \text{GeV}^2}\right)^{-2}$. Data taken from worldwide experiments. See Ref. [37], where the figure was taken, for details.

We can write the amplitude of the process, at the lowest order in QED, in the form:

$$\mathcal{M}_{ep \to ep} = \frac{e^2}{\Delta^2}\, \bar{u}\left(l'\right) \gamma^\mu u\left(l\right) \langle p, P_2 | J_\mu^{\text{em}}\left(0\right) | p, P_1 \rangle\ , \tag{1.3}$$

where we omitted the spin dependence of spinors and states. Despite not being able to compute directly the matrix element of the proton electromagnetic current, we can parametrize it with only two real functions of the Lorentz scalar Δ^2 in the space-like region:

$$\langle p, P_2 | J_\mu^{\text{em}}\left(0\right) | p, P_1 \rangle = \bar{u}\left(P_2\right) \left(F_1\left(\Delta^2\right) \gamma_\mu + i\, F_2\left(\Delta^2\right) \frac{\sigma_{\mu\nu}\Delta^\nu}{2\, M_N}\right) u\left(P_1\right)\ , \tag{1.4}$$

where we denoted the nucleon mass M_N and we refer to the appendix A.1 for a summary of the notations for spinors and Dirac matrices. This reduction can be obtained by applying the Dirac equation (for the spinors), current conservation and hermiticity [38].

F_1 and F_2 are called Dirac and Pauli Form Factors (FFs) and they are normalized such that their value at $\Delta^2 = 0$ gives respectively the charge of the nucleon (in units of the positron charge) and its anomalous magnetic moment κ. A point-like particle would have a vanishing Pauli Form Factor, and a constant Dirac Form Factor. Another parametrization, from Sachs, is also possible in terms of electric and magnetic FFs:

$$G_E\left(\Delta^2\right) = F_1\left(\Delta^2\right) + \frac{\Delta^2}{4\, M_N^2} F_2\left(\Delta^2\right)\ , \tag{1.5}$$

$$G_M\left(\Delta^2\right) = F_1\left(\Delta^2\right) + F_2\left(\Delta^2\right)\ . \tag{1.6}$$

These Form Factors can be interpreted as the three-dimensional Fourier transform of the charge and magnetization densities, respectively, when one considers the Breit Frame (see Sec. 2.3), in the non-relativistic limit.

The root mean square (rms) charge radius can be inferred as:

$$\langle r^2 \rangle = -6 \frac{\mathrm{d}G_E}{\mathrm{d}(-t)}(0) \, , \tag{1.7}$$

but an extrapolation is necessary, as experimentally we can access only finite values of Δ^2. To this day, despite very precise measurements, the determination of the proton radius remains an open subject, due to significant discrepancies between these elastic scattering and several electronic hydrogen atomic measurements on one hand and muonic hydrogen Lamb shift measurements on the other. See *e.g.* Ref. [39] and references therein.

But coming back to our historical journey, elastic scattering experiments conducted between 1954 and 1957 at SLAC showed that indeed the proton has a spatial extension [40, 41], by measuring the Δ^2-dependence of these FFs, with the Rosenbluth [42] formula for the cross-section:

$$\frac{\mathrm{d}\sigma}{\mathrm{d}^2\Omega} = \frac{\alpha_{em}^2}{4\,E^2 \sin^4 \frac{\theta}{2}} \frac{E'}{E} \left(\frac{G_E^2 + \tau G_M^2}{1 + \tau} \cos^2 \frac{\theta}{2} + 2\tau G_M^2 \sin^2 \frac{\theta}{2} \right) \, , \tag{1.8}$$

where $\alpha_{em} = \frac{e^2}{4\pi}$ is the QED coupling constant or fine structure constant, $\tau = \frac{-\Delta^2}{4\,M_N^2}$ and the cross-section is expressed in the lab frame, *i.e.* the nucleon target rest frame. Note that for a given beam energy E (for the incoming electron), there is only one independent variable θ (the angle between the incoming and outgoing electrons) or equivalently Δ^2. The outgoing electron energy E' is constrained by:

$$E' = \frac{E}{1 + 2\frac{E}{M_N} \sin^2 \frac{\theta}{2}} \qquad \Longleftrightarrow \qquad P_1 \cdot \Delta + \frac{1}{2}\Delta^2 = 0 \, . \tag{1.9}$$

By varying the incident energy E and the angle θ, while keeping $\Delta^2 = -4EE' \sin^2 \frac{\theta}{2}$ fixed for instance, it is possible to separate the Form Factors. See Fig. 1.1 (right panel) for a recent compilation of measurements of the electric Form Factor.

1.2. . . . to quarks and gluons

To understand this composite particle that is the proton, and the many other *hadrons* that were experimentally discovered in the mean time, two approaches were historically followed. One consisted in the spectroscopy of these hadrons, *i.e.* classifying them (in terms of mass, spin, and other quantum numbers). The second one, closer to the subject of this thesis, consisted in high energy experiments aiming at "breaking" these hadrons to reveal their inner constituents.

1.2.1. Quark model and spectroscopy

The spectroscopy experiments led to two important theoretical steps in the road to QCD: the *Eightfold Way* [43, 44], and then the *Quark Model* [45, 46], both of which are due to Gell-Mann, at the beginning of the 1960s. This allowed to classify hadrons in terms of octets, nonets and
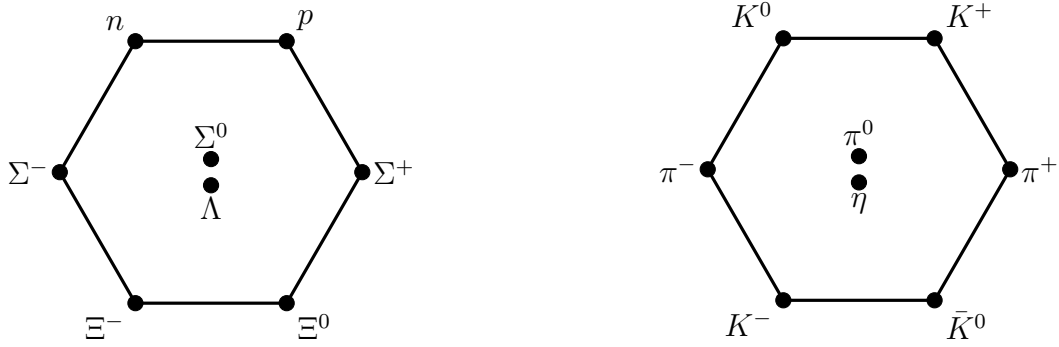
Figure 1.2. Baryon (left) and pseudo-scalar meson (right) octets, $\frac{1}{2}^+$ and 0^- respectively. Horizontal lines associate particles of same strangeness, while diagonal lines are for the same charge.

decuplets, in the sort of diagrams represented in Fig. 1.2, with the same spin and parity J^P, and correctly predicted new composite particles such as the Ω^-.

The basic idea [47] is that of the flavor symmetry group $SU(3)$, expanding the previous isospin group $SU(2)$ of Heisenberg where the fundamental representation consisted of nucleons (proton and neutron). In the case of $SU(3)$, there is no observed fundamental representation (3-dimensional), the hadrons being only in decuplets (10-dimensional representation), octets (8-dimensional) and singlets, the latter two being usually assembled into a nonet for mesons. This led to introduce the *quarks u, d* and *s* as only mathematical objects forming this fundamental representation, their antiquarks being in the conjugate representation. The Quark Model asserts that the baryons are composed of three quarks, while the mesons are composed of a pair quark-antiquark. In mathematical language, the hadrons belong to irreducible representations of direct products of the fundamental representation. For mesons, we have:

$$\mathbf{3} \otimes \bar{\mathbf{3}} = \mathbf{8} \oplus \mathbf{1} \,, \tag{1.10}$$

while for baryons:

$$\mathbf{3} \otimes \mathbf{3} \otimes \mathbf{3} = \mathbf{10} \oplus \mathbf{8} \oplus \mathbf{8} \oplus \mathbf{1} \,. \tag{1.11}$$

We recover the aforementioned decuplets, octets and singlets.

These quarks being spin-$1/2$ particles, they should obey Pauli's exclusion principle, which causes a problem for instance for the baryon Δ^{++}, a *uuu* state. This prompted the introduction of *color* [48–51] as an additional quantum number with the postulate that only color-singlet states are observable (colorless hadrons). This comes with the introduction of an exact symmetry with the group $SU(3)$ of color. This was not necessary for mesons, since pairs of quark-antiquark can never have a completely symmetric wave-function, but it is crucial for baryons, since looking at Eq. (1.11) but interpreting it now for $SU(3)_{\text{color}}$ instead of $SU(3)_{\text{flavor}}$, we can show that the singlet representation is completely antisymmetric, which means that the rest of the wave-function needs to be completely symmetric (for orbital angular momentum, spin and flavor). The issue is thus solved, and later, QCD will be born as a gauge theory for this color group [52–54].
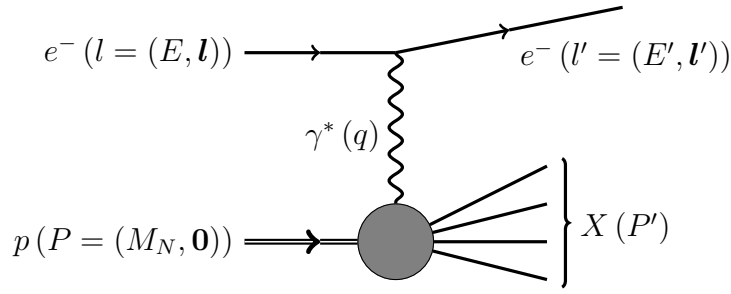
Figure 1.3. Deep-Inelastic Scattering of a lepton (*e.g.* electron) off a nucleon (*e.g.* proton) target. The four-vectors are expressed in the target rest frame.

1.2.2. Deep Inelastic Scattering and Parton model

But in the road to QCD, a crucial role was played by the Deep Inelastic Scattering (DIS) off a nucleon, an experimental program started at SLAC [55, 56] at the end of the 1960s. This $ep \to eX$ process (where X denotes the many particles that can be produced by breaking the proton) is represented in Fig. 1.3, and we define the following notations:

$$Q^2 \equiv -q^2 > 0\,, \qquad\qquad x_B \equiv \frac{Q^2}{2\,P \cdot q}\,, \qquad\qquad (1.12)$$

the former being the virtuality of the photon, and the latter is called Bjorken's scaling variable. We define also the *deep inelastic regime* as the limit where both Q^2 and $P \cdot q$ are large but their ratio x_B stays finite. This is also called the *Bjorken limit*.

We could follow the same reasoning as in Sec. 1.1.2 and introduce a hadronic electromagnetic current at the level of the amplitude, then integrate to take into account all the possible final state particles (it is an *inclusive* reaction). Instead, we will consider directly the cross-section, which can be written as:

$$\frac{\mathrm{d}\sigma}{\mathrm{d}^2\Omega \mathrm{d}E'} = \frac{\alpha_{em}^2}{Q^2}\frac{E'}{E}L^{\mu\nu}W_{\mu\nu}\,, \qquad\qquad (1.13)$$

where the leptonic tensor describes the pure QED vertex:

$$L^{\mu\nu} = \frac{1}{2}\,\mathrm{Tr}\left(\slashed{k}'\gamma^\mu\,\slashed{k}\gamma^\nu\right) = 2\left(k^\mu k'^\nu + k^\nu k'^\mu - k \cdot k'\eta^{\mu\nu}\right)\,, \qquad\qquad (1.14)$$

and the hadronic tensor can be again parametrized by only two *structure functions*, when using hermiticity and current conservation:

$$W^{\mu\nu} = -W_1\left(\eta^{\mu\nu} + \frac{q^\mu q^\nu}{Q^2}\right) + \frac{W_2}{M^2}\left(P^\mu + \frac{P \cdot q}{Q^2}q^\mu\right)\left(P^\nu + \frac{P \cdot q}{Q^2}q^\nu\right)\,. \qquad (1.15)$$

We end up with the equivalent of the Rosenbluth formula for inclusive inelastic scattering:

$$\frac{\mathrm{d}\sigma}{\mathrm{d}^2\Omega \mathrm{d}E'} = \frac{\alpha_{em}^2}{4\,E^2\sin^4\frac{\theta}{2}}\left(2W_1\sin^2\frac{\theta}{2} + W_2\cos^2\frac{\theta}{2}\right)\,, \qquad\qquad (1.16)$$

Note that now, these structure functions depend on two Lorentz scalars Q^2 and x_B, just as there are two independent variables E' and θ for experimentalists to play with, for a given

incident energy E. We can recover the elastic case when $x_B = 1$, *i.e.* with the constraint of Eq. (1.9) which is relaxed here. In other words, setting

$$W_1\left(x_B, Q^2\right) \longrightarrow \frac{G_M^2\left(q^2\right)}{2\,M_N}\,\delta\left(x_B - 1\right) \tag{1.17}$$

$$W_2\left(x_B, Q^2\right) \longrightarrow \frac{1}{2\,M_N\,\tau}\frac{G_E^2\left(q^2\right) + \tau G_M^2\left(q^2\right)}{1 + \tau}\,\delta\left(x_B - 1\right)\,, \tag{1.18}$$

and integrating over E' gives back the elastic cross-section (1.8). We denoted by $\delta\left(\,\cdot\,\right)$ the Dirac distribution.

At high enough energy, we can say that the photon interacts directly with the constituents of the proton, and that they are seemingly free. Suppose these *partons*[2] are spin-1/2 point-like particles carrying a fraction x_q of the proton momentum: $p_q = x_q P$. The partonic cross-section for a constituent q can be inferred from Eq. (1.16) but with the following trivial structure functions:

$$W_1^q = \frac{e_q^2}{2\,m_q}\,\delta\left(x_B^q - 1\right) \quad = \frac{e_q^2}{2\,M_N}\,\delta\left(x_B - x_q\right)\,, \tag{1.19}$$

$$W_2^q = \frac{2\,m_q\,e_q^2}{Q^2}\,\delta\left(x_B^q - 1\right) = \frac{2\,M_N\,x_q^2\,e_q^2}{Q^2}\,\delta\left(x_B - x_q\right)\,. \tag{1.20}$$

We simply used here Eqs. (1.17)-(1.18) for a point-like particle, *i.e.* $G_E = G_M =$ charge, and denoted by e_q and $m_q = x_q M_N$ respectively the charge (in units of the positron charge) and mass[3] of the parton q, whereas the fractional Bjorken variable is defined naturally for partons as:

$$x_B^q \equiv \frac{Q^2}{2\,p_q \cdot q} = \frac{x_B}{x_q}\,. \tag{1.21}$$

The next step is to sum incoherently (*i.e.* adding the probabilities and not the amplitudes) the partonic contributions to the cross-section:

$$W_1 = \sum_q \int_0^1 \mathrm{d}x_q\, q\left(x_q\right) W_1^q = \frac{1}{2\,M_N}\sum_q e_q^2\, q\left(x_B\right)\,, \tag{1.22}$$

$$W_2 = \sum_q \int_0^1 \mathrm{d}x_q\, q\left(x_q\right) W_2^q = \frac{2\,M_N\,x_B^2}{Q^2}\sum_q e_q^2\, q\left(x_B\right)\,, \tag{1.23}$$

where $q\left(x\right)$ is the probability density for the parton q to carry a momentum fraction x.

We retrieve two results:

Bjorken scaling law In the Bjorken limit of large Q^2 and finite x_B, the structure functions[4] $F_1 \equiv M_N W_1$ and $F_2 \equiv \frac{Q^2}{2\,M_N\,x_B} W_2$ do not have a Q^2 dependence [58]. This is a consequence of the point-like nature of these partons.

---

[2]Term coined by Feynman [57] when quarks were not yet taken seriously, but now refers to the elementary constituents of hadrons, *i.e.* both quarks and gluons.

[3]This variable mass of partons may be surprising, but this reasoning can be made more rigorous by working in the infinite momentum frame where all masses are neglected.

[4]These notations, due to Bjorken, should not be confused with the Pauli and Dirac electromagnetic Form Factors.

Callan-Gross relation For spin-1/2 partons [59], the structure functions obey the relation

$$2\,x_B\,F_1\left(x_B\right) = F_2\left(x_B\right) . \tag{1.24}$$

Both of these predictions were confirmed experimentally [55, 56]. This really puts a constraint on the charged constituents of the proton, and hints that they are indeed the quarks of Gell-Mann. Moreover, the fact that they come in three colors was also confirmed with the process of hadron production with electron-positron scattering $e^+e^- \to$ hadrons. See *e.g.* Fig. 51.6 of Ref. [60] (Particle Data Group).

Let us now redefine $q\left(x\right)$ to be the number density[5] of quarks of flavor q carrying the momentum fraction x. We call this object a *Parton Distribution Function* (PDF) and it encodes the soft (or large distance) physics, that is due to QCD. If we consider the composition of the proton to be strictly *uud* as in the Quark model, we would need

$$\int_0^1 \mathrm{d}x\,x\,u\left(x\right) + \int_0^1 \mathrm{d}x\,x\,d\left(x\right) = 1\,, \tag{1.25}$$

i.e. the proton momentum is carried entirely by the quarks u and d, but this is not verified experimentally. Only about half of it is accounted for by the quarks. This provides indirect evidence[6] to the existence of gluons and their contribution to the proton momentum in average consists of the missing half. In fact, these gluons are constantly interacting and producing quark-antiquark pairs. But only the original *uud* quarks of Gell-Mann contribute to the quantum numbers of the proton and we call them *valence* quarks. The extra quarks (resp. antiquarks) are referred to as *sea* quarks (resp. antiquarks). The virtual photon can couple to any charged particle, including the sea quarks and antiquarks. We should therefore consider their contribution and we note, for $q = u, d, s$, etc:

$$q\left(x\right) = q_{\text{val}}\left(x\right) + q_{\text{sea}}\left(x\right)\,, \qquad \text{with} \quad \begin{cases} q_{\text{val}} \equiv q - \bar{q} & , \\ q_{\text{sea}} = \bar{q}_{\text{sea}} \equiv \bar{q} \end{cases} \tag{1.26}$$

where we used the fact that the quarks and antiquarks of the sea come always in pairs. Hence, the structure function should be in total (if we restrict ourselves to the three light flavors):

$$F_2\left(x\right) = x\left(\left(\frac{2}{3}\right)^2\left[u\left(x\right) + \bar{u}\left(x\right)\right] + \left(-\frac{1}{3}\right)^2\left[d\left(x\right) + \bar{d}\left(x\right) + s\left(x\right) + \bar{s}\left(x\right)\right]\right) . \tag{1.27}$$

Note that these distributions are constrained by the number of valence quarks:

$$\int_0^1 \mathrm{d}x\,\left[u\left(x\right) - \bar{u}\left(x\right)\right] = 2\,, \qquad \int_0^1 \mathrm{d}x\,\left[d\left(x\right) - \bar{d}\left(x\right)\right] = 1\,, \tag{1.28}$$

and similar relations in the case of other hadrons. Figure 1.4 (right panel) shows recent extractions of these PDFs, where we notice that valence quark contributions are peaked around one third of the proton momentum, but that at lower fractions, sea quarks and then mainly gluons become dominant.

---

[5]Notice that now the quarks of the same flavour are indistinguishable in the definition, contrary to before where we indexed all the constituents independently. The PDF $u\left(x\right)$ would be the sum of the probability densities for each quark u.

[6]The observation of a three-jet event in $e^+e^- \to$ hadrons is a more direct evidence for gluons.
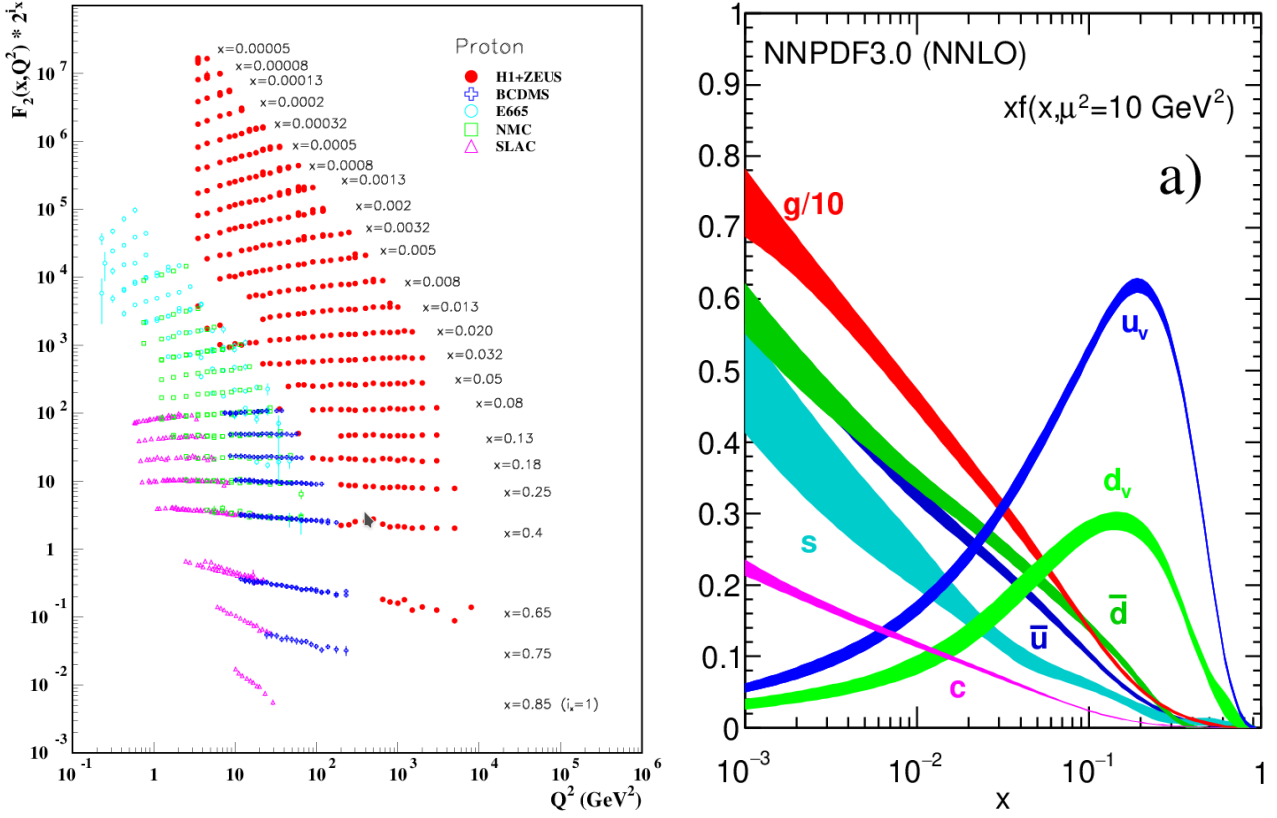
Figure 1.4. **Left**: Structure function F_2 of the proton from worldwide measurements. **Right**: Unpolarized PDFs of the proton at scale 10 GeV^2 from the NNPDF collaboration [61]. Figures taken from Ref. [60] (Particle Data Group).

1.2.3. QCD Factorization

The Parton model implies a factorization between the soft physics (*i.e.* large distance) and the hard scattering with partons (*i.e.* small distance). We can recover this behavior in the context of perturbative QCD with more rigorous techniques such as the Operator Product Expansion (OPE), and actually the leading order (LO) in α_S (the strong coupling constant) corresponds to the result of the Parton model. But contrary to the simple assumptions we made, the structure functions do have a scale dependence; the quarks are not free inside the proton. This appears for instance with next-to-leading order (NLO) computations. The experimental confirmation of Bjorken's scaling law is due to the x_B-region originally considered, but subsequent data with better precision did show a logarithmic scale dependence, as shown in Fig. 1.4 (left panel).

Thus, in general, the structure function F_2 for instance can be written as a convolution of parton distributions and a hard scattering kernel [62]:

$$F_2\left(x_B, Q^2\right) = \sum_{a=g,u,d,\dots} \int_0^1 \mathrm{d}x\, C_2^a\left(\frac{x_B}{x}, \frac{Q^2}{\mu_F^2}\right) a\left(x, \mu_F^2\right) + \mathcal{O}\left(\frac{M_N^2}{Q^2}\right), \qquad (1.29)$$

where we neglected higher-twist contributions. C_2 is a coefficient function, obtained via

perturbation theory, which depends on the factorization scale μ_F. The structure function being observable, it should not depend on that scale, and this means that the dependence is cancelled with that of the PDF. The latter is governed by the so-called DGLAP[7] equations [63–65], which writes for instance for a valence distribution:

$$\mu_F^2 \, \frac{\partial}{\partial \mu_F^2} q_{\text{val}}\left(x, \mu_F^2\right) = \frac{\alpha_S\left(\mu_F^2\right)}{2\pi} \int_x^1 \frac{\mathrm{d}y}{y} \, P_{qq}\left(\frac{x}{y}\right) q_{\text{val}}\left(y, \mu_F^2\right) \, , \tag{1.30}$$

where the so-called splitting function P_{qq} can be found in textbooks (*e.g.* [66]). The PDFs can thus be parametrized at a given low scale, and then evolved to a higher scale for phenomenology (as we usually take $\mu_F = Q$ for convenience).

Note that in this factorization, PDFs are universal and not restricted to DIS. They can be extracted from one channel and used to interpret experimental data in another, such as the Drell-Yan process.

---

[7]Dokshitzer–Gribov–Lipatov–Altarelli–Parisi.

Chapter 2.

Partonic structure of hadrons

After introducing the notion of parton distributions in a phenomenogical way, we can now turn to their more general framework with the full zoology of these distributions, which can in principle allow us to understand the spin, spatial and momentum structure of hadrons. We will start with the most fundamental object, that is the relativistic Wigner distribution.

2.1. Wigner distributions

2.1.1. In Quantum Mechanics

In classical mechanics, the phase-space distribution function $f(\boldsymbol{p}, \boldsymbol{q}, t)$ obeying Liouville's theorem, where $\boldsymbol{q}$ and $\boldsymbol{p}$ are respectively the generalized position and momentum, provides a probabilistic interpretation; f is a number density of particles around $(\boldsymbol{p}, \boldsymbol{q})$ in phase space at a given time t.

To generalize this to Quantum Mechanics, Wigner introduced the quasiprobability distribution [67]:

$$\rho(\boldsymbol{p}, \boldsymbol{q}, t) = \int \mathrm{d}^3 \boldsymbol{r} \, \psi^* \left(\boldsymbol{q} - \frac{1}{2} \boldsymbol{r}, t \right) \psi \left(\boldsymbol{q} + \frac{1}{2} \boldsymbol{r}, t \right) e^{-i \boldsymbol{p} \cdot \boldsymbol{r}} , \tag{2.1}$$

where ψ is the wave-function of a pure state. This distribution is no longer necessarily positive, as it encodes quantum interference. But integrating it yields the usual probability densities:

$$\int \frac{\mathrm{d}^3 \boldsymbol{p}}{(2\pi)^3} \, \rho(\boldsymbol{p}, \boldsymbol{q}, t) = \psi^*(\boldsymbol{q}, t) \, \psi(\boldsymbol{q}, t) , \tag{2.2}$$

$$\int \mathrm{d}^3 \boldsymbol{q} \, \rho(\boldsymbol{p}, \boldsymbol{q}, t) = \tilde{\psi}^*(\boldsymbol{p}, t) \, \tilde{\psi}(\boldsymbol{p}, t) , \tag{2.3}$$

where $\tilde{\psi}$ is the Fourier transform of ψ.

The Wigner distribution is closely related to the so-called density operator (or density matrix) $\hat{\rho}$, as they are linked through a Wigner-Weyl transform[1]:

$$\rho(\boldsymbol{p}, \boldsymbol{q}, t) = \int \mathrm{d}^3 \boldsymbol{r} \left\langle \boldsymbol{q} + \frac{1}{2} \boldsymbol{r} \middle| \hat{\rho}(t) \middle| \boldsymbol{q} - \frac{1}{2} \boldsymbol{r} \right\rangle e^{-i \boldsymbol{p} \cdot \boldsymbol{r}} . \tag{2.4}$$

This, in passing, generalizes the Wigner distribution to a mixed state $\hat{\rho} = \sum_k p_k |\psi_k\rangle \langle\psi_k|$, with probabilities p_k for each state ψ_k. For a pure state $\hat{\rho} = |\psi\rangle \langle\psi|$, we recover Eq. (2.1). The

---

[1]More precisely, this is the Wigner transform, and its inverse is the Weyl quantization [68].

Wigner distribution allows to compute expectation values of an operator $\hat{A}$ [69]:

$$\langle \hat{A} \rangle (t) = \int \mathrm{d}^3 \boldsymbol{q} \, \frac{\mathrm{d}^3 \boldsymbol{p}}{(2\pi)^3} \, \rho\left(\boldsymbol{p}, \boldsymbol{q}, t\right) \, a\left(\boldsymbol{p}, \boldsymbol{q}\right) . \tag{2.5}$$

where a is the associated phase-space function of the operator; *i.e.* its Wigner transform, as in Eq. (2.4)).

2.1.2. In Quantum Field Theory

The generalization of this distribution to the relativistic framework of QCD was first attempted by Ji [70, 71]. Unfortunately, it is difficult to relate it to observable quantities. Indeed, in the case of a three-dimensional localization in space, relativistic corrections spoil the interpretation as a Fourier transform of some parton distributions with respect to momentum transfer, as we will illustrate in the simpler case of Form Factors in Sec. 2.3.

To circumvent this issue, Lorcé and Pasquini [72] defined a five-dimensional alternative; two-dimensional in impact parameter space and three-dimensional in momentum space. It writes for a quark of flavor q in two equivalent forms:

$$\rho_{[\Gamma]}^q \left(\boldsymbol{b}_\perp, \boldsymbol{k}_\perp, x, \boldsymbol{S}\right) = \int \mathrm{d}^2 \boldsymbol{D}_\perp \left\langle P^+, -\frac{1}{2}\boldsymbol{D}_\perp, \boldsymbol{S} \left| \hat{W}_{[\Gamma]}^q \left(\boldsymbol{b}_\perp, \boldsymbol{k}_\perp, x\right) \right| P^+, \frac{1}{2}\boldsymbol{D}_\perp, \boldsymbol{S} \right\rangle \tag{2.6}$$

$$= \int \frac{\mathrm{d}^2 \boldsymbol{\Delta}_\perp}{(2\pi)^2} \left\langle P^+, \frac{1}{2}\boldsymbol{\Delta}_\perp, \boldsymbol{S} \left| \hat{W}_{[\Gamma]}^q \left(\boldsymbol{b}_\perp, \boldsymbol{k}_\perp, x\right) \right| P^+, -\frac{1}{2}\boldsymbol{\Delta}_\perp, \boldsymbol{S} \right\rangle , \tag{2.7}$$

where the Wigner operator

$$\hat{W}_{[\Gamma]}^q \left(\boldsymbol{b}_\perp, \boldsymbol{k}_\perp, x\right) = \frac{1}{2} \int \frac{\mathrm{d}z^- \mathrm{d}^2 \boldsymbol{z}_\perp}{(2\pi)^3} \, e^{i\left(x P^+ z^- - \boldsymbol{k}_\perp \cdot \boldsymbol{z}_\perp\right)} \, \bar{\psi}^q \left(b - \frac{z}{2}\right) \Gamma \mathcal{W} \psi^q \left(b + \frac{z}{2}\right) \Big|_{\substack{z^+=0 \\ b^+=b^-=0}} \tag{2.8}$$

is sandwiched between hadronic states of definite longitudinal momentum and either definite transverse position in Eq. (2.6) or transverse momentum in Eq. (2.7), with a polarization $\boldsymbol{S}$. The hadron has vanishing average transverse position and momentum, hence $\boldsymbol{b}_\perp$ and $\boldsymbol{k}_\perp$ can be interpreted as the relative average position and momentum of the quark in the transverse plane. We note $x = k^+/P^+$ the longitudinal momentum fraction of the quark with respect to the hadron (see App. A.1 on light-cone coordinates), Γ a given Dirac matrix and $\mathcal{W}$ is a Wilson line joining the fields at different points to ensure gauge invariance. The spatially localized state is simply related to the state of definite transverse momentum via Fourier transform:

$$\left| P^+, \boldsymbol{R}_\perp \right\rangle = \int \frac{\mathrm{d}^2 \boldsymbol{P}_\perp}{(2\pi)^2} \, e^{i \boldsymbol{P}_\perp \cdot \boldsymbol{R}_\perp} \left| P^+, \boldsymbol{P}_\perp \right\rangle . \tag{2.9}$$

This localization is possible when working in the Infinite Momentum Frame [8, 73] (IMF) where P^+ is large or in light-cone formulation (see Chap. 6), due to the Galilean subgroup of transverse boosts where plus-momentum plays the role of mass in non-relativistic mechanics, and $\boldsymbol{R}_\perp$ corresponds to the center of plus-momentum of the hadron [74, 75]:

$$\boldsymbol{R}_\perp = \sum_i x_i \, \boldsymbol{b}_{\perp i} , \tag{2.10}$$
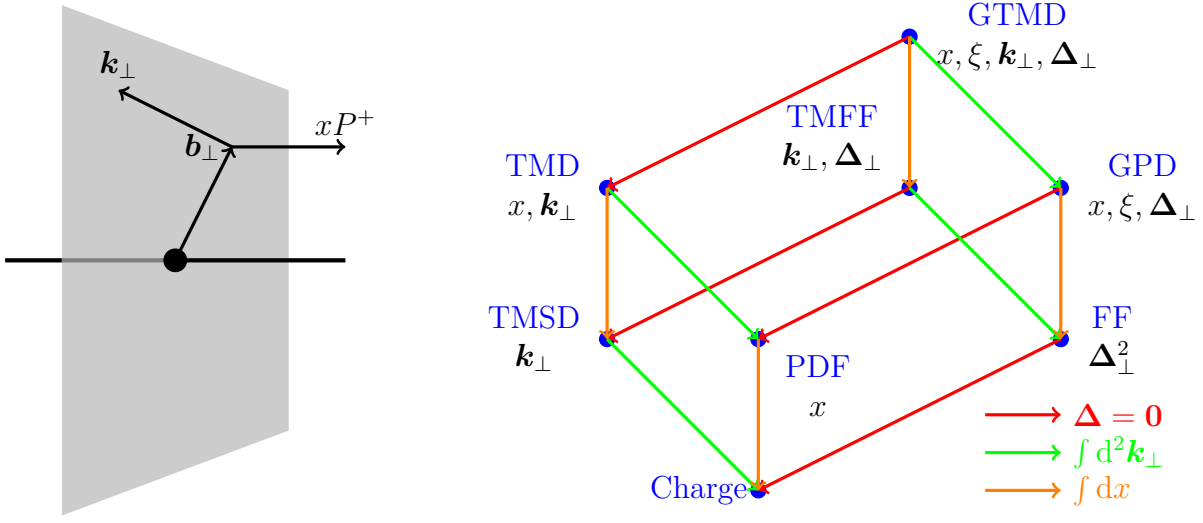
Figure 2.1. Left: Transverse plane representation of the Wigner distribution variables: impact parameter $\boldsymbol{b}_\perp$, transverse momentum $\boldsymbol{k}_\perp$ and longitudinal momentum fraction x of partons. **Right**: Full zoology of parton distributions. See Ref. [25] for more details.

where $\boldsymbol{b}_{\perp i}$ is the transverse position of each parton. This conserved quantity is the equivalent of the center of mass in a non-relativistic framework.

These five-dimensional Wigner distributions are related by Fourier transform to the quark-quark correlators defining the so-called Generalized Transverse Momentum Dependent parton distributions (GTMDs) [76,77]:

$$W^q_{[\Gamma]}\left(\boldsymbol{\Delta}_\perp, \boldsymbol{k}_\perp, x, \boldsymbol{S}\right) = \int \mathrm{d}^2\boldsymbol{b}_\perp \, e^{-i\boldsymbol{\Delta}_\perp \cdot \boldsymbol{b}_\perp} \, \rho^q_{[\Gamma]}\left(\boldsymbol{b}_\perp, \boldsymbol{k}_\perp, x, \boldsymbol{S}\right) \tag{2.11}$$

$$= \left\langle P^+, \frac{1}{2}\boldsymbol{\Delta}_\perp, \boldsymbol{S} \left| \hat{W}^q_{[\Gamma]}\left(\boldsymbol{0}_\perp, \boldsymbol{k}_\perp, x\right) \right| P^+, -\frac{1}{2}\boldsymbol{\Delta}_\perp, \boldsymbol{S} \right\rangle, \tag{2.12}$$

taken at vanishing Δ^+, where in the passage to the second line we used translation invariance in the transverse plane [74], *i.e.*

$$\left\langle P^+, -\frac{1}{2}\boldsymbol{D}_\perp, \boldsymbol{S} \left| \hat{W}^q_{[\Gamma]}\left(\boldsymbol{b}_\perp, \boldsymbol{k}_\perp, x\right) \right| P^+, \frac{1}{2}\boldsymbol{D}_\perp, \boldsymbol{S} \right\rangle \tag{2.13}$$

$$= \left\langle P^+, -\frac{1}{2}\boldsymbol{D}_\perp - \boldsymbol{b}_\perp, \boldsymbol{S} \left| \hat{W}^q_{[\Gamma]}\left(\boldsymbol{0}_\perp, \boldsymbol{k}_\perp, x\right) \right| P^+, \frac{1}{2}\boldsymbol{D}_\perp - \boldsymbol{b}_\perp, \boldsymbol{S} \right\rangle.$$

2.2. 3D tomography of hadrons

GTMDs are mother distributions to both Generalized Parton Distributions (GPDs) and Transverse Momentum Dependent parton distributions (TMDs). Indeed, integrating Eqs. (2.6)-(2.7) over $\boldsymbol{b}_\perp$ or, equivalently, setting $\boldsymbol{\Delta}_\perp = 0$ in Eq. (2.12) yields the correlators defining TMDs. On the other hand, integrating Eq. (2.12) over $\boldsymbol{k}_\perp$ yields the zero-skewness correlators defining

GPDs[2]. Figure 2.1 summarizes this and sketches the full zoology of parton distributions with their relations to each other.

It would be tempting to consider $\boldsymbol{b}_\perp$ and $\boldsymbol{k}_\perp$ as two conjugate Fourier variables, but this is not true. TMDs and GPDs are independent objects that share only the forward limit, *i.e.* PDFs, as limiting case. In fact, average positions (resp. momenta) are Fourier conjugates of differences of momenta (resp. positions) [75]:

$$\text{average transverse momentum} \qquad \boldsymbol{k}_\perp \overset{\mathcal{F}}{\longleftrightarrow} \boldsymbol{z}_\perp \qquad \text{difference of transverse positions}$$

$$\text{average transverse position} \qquad \boldsymbol{b}_\perp \overset{\mathcal{F}}{\longleftrightarrow} \boldsymbol{\Delta}_\perp \qquad \text{momentum transfer}$$
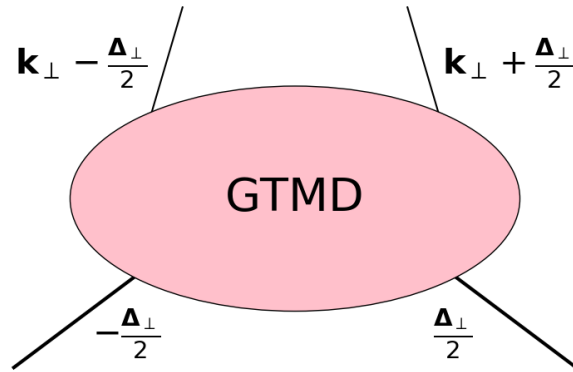

Figure 2.2. GTMD diagram with only transverse variables. Thick lines represent hadrons, whereas thin lines represent partons.

In Fig. 2.2, we sketch the general diagram of GTMDs in terms of transverse variables. We ignore longitudinal ones for simplicity. The corresponding matrix element would be roughly:

$$\int \mathrm{d}^2 \boldsymbol{z}_\perp \, e^{-i\,\boldsymbol{k}_\perp \cdot \boldsymbol{z}_\perp} \left\langle -\frac{\boldsymbol{\Delta}_\perp}{2} \middle| \bar{\psi}^q \left(-\frac{\boldsymbol{z}_\perp}{2} \right) \dots \psi^q \left(\frac{\boldsymbol{z}_\perp}{2} \right) \middle| \frac{\boldsymbol{\Delta}_\perp}{2} \right\rangle$$

which, if integrated over $\boldsymbol{k}_\perp$ (*i.e.* assigning $\boldsymbol{z}_\perp = \boldsymbol{0}_\perp$) and once taking into account the longitudinal variables, would give a GPD matrix element (but this is written rigorously in Chap. 4). Likewise, taking $\boldsymbol{\Delta}_\perp = \boldsymbol{0}_\perp$ yields a TMD matrix element.

Therefore, both GPDs and TMDs give a 3D picture of hadrons. But in the case of GPDs, we should first consider their inverse Fourier transform: Impact Parameter Distributions[3] (IPDs). As their name suggest, they depend on the impact parameter $\boldsymbol{b}_\perp$:

$$\text{IPD}\left(x, \boldsymbol{b}_\perp^2 \right) = \int \frac{\mathrm{d}^2 \boldsymbol{\Delta}_\perp}{(2\pi)^2} \, e^{i\,\boldsymbol{b}_\perp \cdot \boldsymbol{\Delta}_\perp} \, \text{GPD}\left(x, \xi = 0, t = -\boldsymbol{\Delta}_\perp^2 \right) , \tag{2.14}$$

but only via its square, due to rotation invariance. Notice that we take the skewness $\xi = -\Delta^+ / (2P^+)$ (see Chap. 4) to be vanishing. This is crucial for the probabilistic interpretation [8] as a density of partons with longitudinal momentum fraction x and transverse

---

[2]See Chap. 4 for the full definition of such matrix elements, in the general case of non-vanishing skewness.
[3]Also called Impact Parameter Dependent PDFs.

distance $\boldsymbol{b}_\perp$ from the hadron's center of plus-momentum (2.10). For a nucleon of polarization $\boldsymbol{S}$ and a parton of helicity λ, this density[4] writes [78–80] in terms of the IPDs H, E and $\tilde{H}$[5]:

$$\rho\left(x, \boldsymbol{b}_\perp, \lambda, \boldsymbol{S}\right) = \frac{1}{2}\left[H\left(x, \boldsymbol{b}_\perp^2\right) - S_\perp^i \epsilon^{ij} b_\perp^j \frac{1}{M_N}\frac{\partial}{\partial \boldsymbol{b}_\perp^2} E\left(x, \boldsymbol{b}_\perp^2\right) + \lambda\Lambda\tilde{H}\left(x, \boldsymbol{b}_\perp^2\right)\right] , \qquad (2.15)$$

where we wrote $\boldsymbol{S}_\perp$ and Λ respectively the transverse and longitudinal components of the spin vector at rest $\boldsymbol{S}$, and ϵ^{ij} is the Levi-Civita symbol. In the helicity basis considered in Sec. 4.2, states with a transverse polarization can be written as:

$$\left|\boldsymbol{S}_\perp, \Lambda\right\rangle = \cos\theta/2 \left|+\right\rangle + e^{i\phi}\sin\theta/2 \left|-\right\rangle , \qquad (2.16)$$

where $\boldsymbol{S} = (\boldsymbol{S}_\perp, \Lambda) = (\sin\theta\cos\phi, \sin\theta\sin\phi, \cos\theta)$. Notice that we do recover $\left|\boldsymbol{0}_\perp, \pm\right\rangle = \left|\pm\right\rangle$, as the longitudinal polarization corresponds to the light-cone helicity. For the case of a transversely polarized partons, we refer to the literature [79, 80].

The promise of nucleon tomography in three dimensions — one of longitudinal momentum and two of either transverse position (in the case of GPDs) or momentum (for TMDs) — is the main reason driving the various experimental programs in this field. In this thesis, we will consider only the GPD side. In particular, the next chapter will review the efforts to extract these GPDs by performing exclusive processes.

2.3. Breit frame vs transverse plane interpretations

We have seen that the electromagnetic Form Factors are interpreted as Fourier transforms of the charge and magnetization densities in the Breit frame. This frame is defined such that $\boldsymbol{P_1} + \boldsymbol{P_2} = 0$, where $P_1 = (E_1, \boldsymbol{P_1})$ and $P_2 = (E_2, \boldsymbol{P_2})$ are the incoming and outgoing nucleon momenta respectively (see Sec. 1.1.2), and it allows one to write the matrix element of Eq. (1.4) as:

$$\left\langle p, P_2\right| J_0^{\text{em}}\left(0\right)\left|p, P_1\right\rangle = 2\,M_N\,G_E\left(\Delta^2\right) , \qquad (2.17)$$

after some manipulations with spinors, and similarly for the magnetic form factor. The question now is can this be considered the three-dimensional Fourier transform of the charge distribution. To verify this, we will consider the simple case of a spinless hadron, for which there is only one electromagnetic Form Factor F defined as:

$$\left\langle P_2\right| J_\mu^{\text{em}}\left(0\right)\left|P_1\right\rangle = \left(P_{1\,\mu} + P_{2\,\mu}\right)\,F\left(\Delta^2\right) , \qquad (2.18)$$

and there is no need to choose the Breit frame anymore.

Following Ref. [8], we will consider a wave packet

$$\left|\psi\right\rangle = \int\frac{\mathrm{d}^3\boldsymbol{P}}{(2\pi)^3\sqrt{2E}}\,\psi\left(\boldsymbol{P}\right)\left|\boldsymbol{P}\right\rangle \qquad (2.19)$$

---

[4]If we do not take into account the parton helicity, summing over $\lambda = \pm 1$ would yield a density equal to the IPD H (in an unpolarized or longitudinally polarized nucleon), as it is the case for a spinless hadron such as the pion.

[5]These IPDs correspond to the inverse Fourier transform (2.14) of the GPDs defined in Sec. 4.2.

where the energy is constrained by the on-shell relation, *i.e.* $E = \sqrt{M_N^2 + \boldsymbol{P}^2}$. This way, the charge density can be well defined and we write its Fourier transform:

$$F_\psi\left(\boldsymbol{\Delta}'\right) = \int \mathrm{d}^3\boldsymbol{r}\, e^{-i\boldsymbol{\Delta}'\cdot\boldsymbol{r}} \left\langle\psi\right| J_0^{\mathrm{em}}\left(\boldsymbol{r}\right)\left|\psi\right\rangle \tag{2.20}$$

$$= \int \mathrm{d}^3\boldsymbol{r}\, e^{-i\boldsymbol{\Delta}'\cdot\boldsymbol{r}} \int \frac{\mathrm{d}^3\boldsymbol{P_1}\,\mathrm{d}^3\boldsymbol{P_2}}{(2\pi)^6\,\sqrt{2E_1\,2E_2}}\,\psi^*\left(\boldsymbol{P_2}\right)\psi\left(\boldsymbol{P_1}\right)\left\langle\boldsymbol{P_2}\right| J_0^{\mathrm{em}}\left(\boldsymbol{r}\right)\left|\boldsymbol{P_1}\right\rangle .$$

Then, using

$$\left\langle\boldsymbol{P_2}\right| J_0^{\mathrm{em}}\left(\boldsymbol{r}\right)\left|\boldsymbol{P_1}\right\rangle = e^{i\boldsymbol{r}\cdot\left(\boldsymbol{P_2}-\boldsymbol{P_1}\right)}\left\langle\boldsymbol{P_2}\right| J_0^{\mathrm{em}}\left(0\right)\left|\boldsymbol{P_1}\right\rangle , \tag{2.21}$$

which introduces a delta function constraining $\boldsymbol{\Delta}' = \boldsymbol{P_2} - \boldsymbol{P_1} = \boldsymbol{\Delta}$, we end up with

$$F_\psi\left(\boldsymbol{\Delta}\right) = \int \frac{\mathrm{d}^3\boldsymbol{P_1}}{(2\pi)^3\,\sqrt{2E_1\,2E_2}}\,\psi^*\left(\boldsymbol{P_1}+\boldsymbol{\Delta}\right)\psi\left(\boldsymbol{P_1}\right)\left\langle\boldsymbol{P_1}+\boldsymbol{\Delta}\right| J_0^{\mathrm{em}}\left(0\right)\left|\boldsymbol{P_1}\right\rangle$$

$$= \int \frac{\mathrm{d}^3\boldsymbol{P_1}}{(2\pi)^3}\,\frac{E_1+E_2}{2\sqrt{E_1\,E_2}}\,\psi^*\left(\boldsymbol{P_1}+\boldsymbol{\Delta}\right)\psi\left(\boldsymbol{P_1}\right) F\left(\Delta^2\right) , \tag{2.22}$$

where in the last line we used the definition (2.18) of the form factor. Notice that the form factor depends on $\Delta^2 = \left(E_2 - E_1\right)^2 - \boldsymbol{\Delta}^2$ and therefore cannot be taken out of the integral, unless one takes the non-relativistic limit. This would imply $\frac{E_1+E_2}{2\sqrt{E_1\,E_2}} \sim 1$ and $\Delta^2 \sim -\boldsymbol{\Delta}^2$. If we also choose a wave packet broad in momentum space, *i.e.* localized in position space, we end up with the desired result:

$$F_\psi\left(\boldsymbol{\Delta}\right) = F\left(-\boldsymbol{\Delta}^2\right) \int \frac{\mathrm{d}^3\boldsymbol{P_1}}{(2\pi)^3}\,\psi^*\left(\boldsymbol{P_1}\right)\psi\left(\boldsymbol{P_1}\right) \tag{2.23}$$

$$= F\left(-\boldsymbol{\Delta}^2\right) .$$

Unfortunately, relativistic corrections would spoil this identification. They come with terms of the form $\frac{\boldsymbol{P_1}\cdot\boldsymbol{\Delta}}{E_1^2}$ and $\frac{\boldsymbol{\Delta}^2}{E_1^2}$, and shift for instance the rms charge radius (1.7) obtained from $F_\psi\left(\boldsymbol{\Delta}\right)$ with respect to the one we would obtain from $F\left(\Delta^2\right)$. This suggests to work in the Infinite Momentum Frame, as in that case $E_1 \to \infty$ whereas $\boldsymbol{P_1}\cdot\boldsymbol{\Delta}$ and $\boldsymbol{\Delta}^2$ stay finite. Contrary to before, we would consider a wave packet localized only in the transverse plane, as it is the case in Eq. (2.9), with a plane wave in the longitudinal direction with a very large longitudinal momentum, and we would probe this system only with a transverse momentum transfer $\boldsymbol{\Delta}_\perp^2$. Doing so, the relativistic corrections would be negligible [8] and we would recover:

$$\int \mathrm{d}^2\boldsymbol{b}_\perp\, e^{-i\boldsymbol{\Delta}_\perp\cdot\boldsymbol{b}_\perp} \left\langle\psi\right| J_0^{\mathrm{em}}\left(\boldsymbol{b}_\perp\right)\left|\psi\right\rangle = F\left(-\boldsymbol{\Delta}_\perp^2\right) . \tag{2.24}$$

Note that, due to the two-dimensional Fourier transform, the rms impact parameter would be:

$$\left\langle\boldsymbol{b}_\perp^2\right\rangle = -4\,\frac{\mathrm{d}F}{\mathrm{d}\left(\boldsymbol{\Delta}_\perp^2\right)}\left(0\right) , \tag{2.25}$$

instead of Eq. (1.7) with the factor 6. For a spin-$1/2$ hadron, F should be replaced by the Dirac form factor F_1.

The reasoning is the same for GPDs (resp. GTMDs). In order to relate them to IPDs (resp. Wigner distributions), we can probe the hadron only with a transverse momentum transfer. This means setting the skewness $\xi = 0$, *i.e.* $\Delta^+ = 0$. Hence why we introduced only five-dimensional Wigner distributions and GTMDs. We will nevertheless consider the skewed GPDs in Chap. 4, as the skewness is crucial for phenomenology, experimental access at vanishing skewness being out of reach. An interpretation in impact parameter space at non-zero skewness was given in Ref. [74], but the probabilistic interpretation is lost, as the IPD would no longer be positive. Moreover, only in the case $\xi = 0$ does the Fourier conjugate of $\boldsymbol{\Delta}_\perp$ correspond to the impact parameter $\boldsymbol{b}_\perp$, interpreted as the distance of the active parton from the center of plus-momentum of the hadron (2.10). In general, it is not true. For instance, for $x = \xi$, the Fourier conjugate of $\boldsymbol{\Delta}_\perp$ is the distance, usually denoted $\boldsymbol{r}_\perp$, of the active parton from the spectators center of plus-momentum [75, 81].

Note that using only the IMF for this probabilistic interpretation is not really a restriction, as it is precisely in this frame that the physical picture of a hadron as a collection of partons holds, all of them moving fast and the light-cone momentum P^+ of the hadron becoming proportional to the longitudinal momentum P^3 and to its energy.

2.4. Spin decomposition

Another historical incentive for studying GPDs was the spin budget "puzzle". Indeed, Ji suggested in Ref. [82] a gauge invariant decomposition of the nucleon spin, in terms of quark spin, quark orbital angular momentum and gluon total angular momentum, and related this to sum rules of GPDs.

First, we need to start with the Belifante energy-momentum tensor $T^{\mu\nu}$, which is the sum over the quark and gluon contributions:

$$T_q^{\mu\nu} = \psi^q \gamma^{(\mu} i \overset{\leftrightarrow}{D}{}^{\nu)} \psi^q \,, \qquad\qquad T_g^{\mu\nu} = G^{\mu\rho} G^\nu_\rho + \frac{1}{4} \eta^{\mu\nu} G^{\rho\sigma} G_{\rho\sigma} \,, \qquad (2.26)$$

where $(\dots)$ denotes a symmetrization of indices, $\overset{\leftrightarrow}{D}$ is the left-right covariant derivative (see Sec. 4.1.4), ψ^q are the quark fields, and $G^{\mu\nu}$ the gluon field strength tensor. We can then define the total angular momentum density as:

$$M^{\rho\mu\nu}(x) = T^{\rho\nu}(x)\, x^\mu - T^{\rho\mu}(x)\, x^\nu \,. \qquad (2.27)$$

The z-component of the spin for a nucleon at rest can be taken to be the light-cone helicity for a nucleon moving along the z-direction:

$$J^3 = \int \mathrm{d}x^- \mathrm{d}^2\boldsymbol{x}_\perp \, M^{+12}(x) \qquad (2.28)$$

as the two operators give the same expectation values [83] on the nucleon states respectively described above. The separation into quark and gluon contributions

$$J^3 = \sum_q J_q^3 + J_g^3 \,, \qquad\qquad \text{with}^6 \qquad \left\langle J^3 \right\rangle = \frac{1}{2} \,, \qquad (2.29)$$

gives the following result:

$$\left\langle J_q^3 \right\rangle = \frac{1}{2} \left(A_q \left(0 \right) + B_q \left(0 \right) \right) , \qquad \left\langle J_g^3 \right\rangle = \frac{1}{2} \left(A_g \left(0 \right) + B_g \left(0 \right) \right) , \qquad (2.30)$$

where A and B are *Gravitational Form Factors* defined, along with the form factors C[7] and $\bar{C}$, as (for $a = q, g$):

$$\left\langle P + \frac{\Delta}{2} \middle| T_a^{\mu\nu} \middle| P - \frac{\Delta}{2} \right\rangle = \bar{u} \left(P + \frac{\Delta}{2} \right) \left(A_a \left(t \right) P^{(\mu} \gamma^{\nu)} + B_a \left(t \right) P^{(\mu} i \sigma^{\nu)\rho} \frac{\Delta_\rho}{2 \, M_N} \right.$$
$$\left. + \frac{C_a \left(t \right)}{M_N} \left(\Delta^\mu \Delta^\nu - \eta^{\mu\nu} t \right) + \bar{C}_a \left(t \right) M_N \, \eta^{\mu\nu} \right) u \left(P - \frac{\Delta}{2} \right) \quad (2.31)$$

with again $t = \Delta^2$. Due to the polynomiality property (see Secs. 4.1.4 and 4.2.2), we can relate these form factors to the GPDs H and E through sum rules:

$$\int_{-1}^{1} \mathrm{d}x \, x \left[H^q \left(x, \xi, t \right) + E^q \left(x, \xi, t \right) \right] = A_q \left(t \right) + B_q \left(t \right) , \qquad (2.32)$$

$$\int_{0}^{1} \mathrm{d}x \left[H^g \left(x, \xi, t \right) + E^g \left(x, \xi, t \right) \right] = A_g \left(t \right) + B_g \left(t \right) , \qquad (2.33)$$

then, using Eq. (2.30), we end up with what is called Ji's sum rule:

$$\left\langle J_q^3 \right\rangle = \frac{1}{2} \int_{-1}^{1} \mathrm{d}x \, x \left[H^q \left(x, 0, 0 \right) + E^q \left(x, 0, 0 \right) \right] , \qquad (2.34)$$

and similarly for gluons.

Ji's decomposition[8] of the quark total angular momentum $\left\langle J_q^3 \right\rangle = \left\langle S_q^3 \right\rangle + \left\langle L_q^3 \right\rangle$ is as follows [87]:

$$S_q^3 = \frac{1}{2} \int \mathrm{d}^3 x \, \psi^{q\dagger} \sigma^{12} \psi^q , \qquad L_q^3 = - \int \mathrm{d}^3 x \, \psi^{q\dagger} \left(x^1 i D^2 - x^2 i D^1 \right) \psi^q , \qquad (2.35)$$

with the spin and orbital contributions respectively. The former is simply given in terms of the polarized PDFs:

$$\left\langle S_q^3 \right\rangle = \frac{1}{2} \int_0^1 \mathrm{d}x \left[\Delta q \left(x \right) + \Delta \bar{q} \left(x \right) \right] , \qquad (2.36)$$

and given that the part due to H in Eq. (2.34) is a sum rule of unpolarized PDFs (see the forward limit of GPDs in Sec. 4.2.2), we can *in fine* access the contribution of the quark orbital angular momentum to the nucleon spin, if we are able to extract the GPD E.

---

[6]The notation $\langle \ldots \rangle$ here means $\frac{\langle P | \ldots | P \rangle}{\langle P | P \rangle}$.

[7]Just as A and B are related to the angular momentum of partons inside a nucleon at rest, C can be related to shear forces experienced by partons inside the nucleon [84]. On the other hand, $\bar{C}$ cancels out when summing contributions from all quark flavors and gluons, due to the conservation of the energy-momentum tensor. See *e.g.* Ref. [85] for a recent review on the subject.

[8]Other decompositions were suggested, and we refer to Ref. [86] for a thorough study of the subject.

Chapter 3.

Exclusive processes and extraction of Generalized Parton Distributions

We have seen in the previous chapter the extent of the information encoded in GPDs and hence why we are so interested in them. Now, we will see how we can access them experimentally.

3.1. Compton amplitudes

As we have seen in Sec. 1.2.2, DIS is an *inclusive* process, meaning that the final state is not characterized (apart from the emitted electron). The processes where GPDs intervene are fundamentally different, they are coined *exclusive*, as every particle in the final state is detected. Nevertheless, as PDFs are a limiting case of GPDs, they can be linked to the same kind of Compton amplitude. This Compton amplitude (with different kinematics) intervenes in exclusive processes where GPDs play a role: Deeply Virtual Compton Scattering (DVCS), Time-like Compton Scattering (TCS) [88], or even Double Deeply Virtual Compton Scattering (DDVCS) [89, 90]. It is sketched in Fig. 3.1 in three different cases. The first one concerns DIS, the squared amplitude of which is related through the optical theorem to the imaginary part of the forward Compton amplitude:

$$|\mathcal{M}_{\mathrm{DIS}}|^2 \overset{\mathrm{opt. \ th.}}{\propto} \mathrm{Im}\,\mathcal{A}\left(\gamma^* p \to \gamma^* p\right) . \tag{3.1}$$

Another exclusive process of interest is the Deeply Virtual Meson Production (DVMP) [91–93], where the final photon is replaced by a hard meson. For all these processes, the virtual photon is produced with electrons $e \to \gamma^* e$, or produces an electron-positron pair if in the final state $\gamma^* \to e^+ e^-$. The relevant experimental process for DVCS for instance is therefore the photon electroproduction $ep \to ep\gamma$, whereas TCS is accessed through $\gamma p \to e^+ e^- p$.

The DVCS process in particular will be detailed in the next section, but first let us see quickly how these processes allow to access parton distributions. As mentioned in Sec. 1.2.3, this is possible of course due to a factorization between soft and hard phenomena. In broad terms, it consists on organizing the Feynman diagrams into hard and collinear subgraphs after considering the Bjorken limit of large Q^2 (and finite x_B and t). It is indeed proven that these diagrams are dominated by distinct momentum regions [62, 94, 95]. When separating the subgraphs, we keep only the diagrams with the smallest possible number of lines between them,
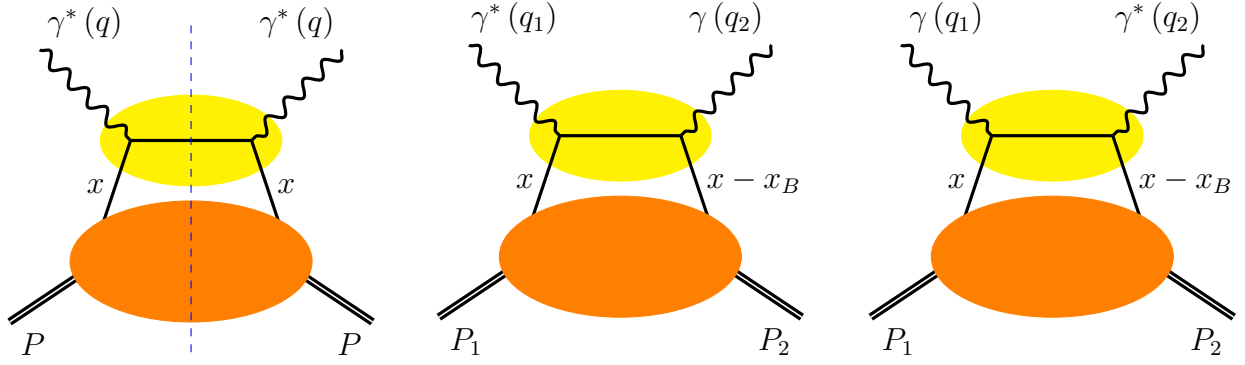
Figure 3.1. Handbag diagrams for the forward Compton amplitude (left panel) whose imaginary part gives the DIS cross-section, DVCS (middle panel) with $q_1^2 < 0$ and TCS (right panel) with $q_2^2 > 0$. For DDVCS, both photons would be virtual. Collinear subgraph in orange and hard part (here at leading order) in yellow.

as the more lines the more suppressed the diagram is in powers of $1/Q$. This power suppression corresponds to a "collinear" twist[1] expansion:

- twist-2: leading term in the Bjorken limit,

- twist-3: suppressed by $1/Q$,

- twist-4: suppressed by $1/Q^2$, etc.

This leads to convolutions of a hard scattering part where incoming and outgoing partons are treated as exactly collinear and on-shell, with the contribution from the collinear subgraphs that are expressed as matrix elements of quark (or gluon) fields (these are the parton distributions).

Historically, for the factorization of DVCS (and Compton scattering in general), three different approaches were pursued: one using the α-Schwinger representation [6, 97], others using a Feynman parametrization [98, 99] and a more formal one with Operator Production Expansion [5]. We will not detail any of these developments, but we can sketch the contribution of the hard scattering part of the handbag diagrams (*i.e.* leading order diagrams in α_S and leading-twist) of Fig. 3.1 as [75]:

$$\frac{1}{x - x_B + i\epsilon} + \{\text{crossed graph}\} = \text{p.v.} \frac{1}{x - x_B} - i\pi\delta\left(x - x_B\right) + \{\text{crossed graph}\}, \qquad (3.2)$$

where p.v. denotes Cauchy's principal value distribution[2]. Note that in this section (and only in this section), in order to keep a consistent notation between DIS and Compton scattering, we use the asymmetrical plus-momentum fractions of Radyushkin:

$$x = k_1^+/P_1^+, \qquad\qquad x - x_B = k_2^+/P_1^+, \qquad (3.3)$$

---

[1]For the definition of twist, see Ref. [96].

[2]See *e.g.* Ref. [100], appendix A4, for the derivation of this relation.

in the frame where $\boldsymbol{P}_{\perp 1} = \boldsymbol{0}_\perp$, instead of the symmetrical ones of Ji:

$$x = \frac{k_1^+ + k_2^+}{P_1^+ + P_2^+}, \qquad\qquad \xi = \frac{P_1^+ - P_2^+}{P_1^+ + P_2^+}, \qquad (3.4)$$

in the symmetric frame $\boldsymbol{P}_{\perp 1} + \boldsymbol{P}_{\perp 2} = \boldsymbol{0}_\perp$, that are used throughout this thesis. The next section will treat the case of DVCS more rigorously and with the usual notations. We denoted by k_1 and k_2 the momenta of the emitted and reabsorbed quarks in the handbag diagrams of Fig. 3.1.

The hard part (3.2) is then convoluted with the parton distributions in an integral over x. In the case of DIS, only the imaginary part of the Compton amplitude matters, so we find something of the form:

$$\operatorname{Im} \mathcal{A}\left(\gamma^* p \to \gamma^* p\right) \propto \sum_q e_q^2 \left[q\left(x_B\right) + \bar{q}\left(x_B\right)\right] + (\ldots), \qquad (3.5)$$

where the dots stand for the crossed graph and polarized PDFs, higher order in α_S and higher-twist contributions. For DVCS, both real and imaginary parts of Eq. (3.2) need to be taken into account and the amplitude looks like:

$$\mathcal{A}\left(\gamma^* p \to \gamma p\right) \propto \sum_q e_q^2 \left[\text{p.v.} \int \mathrm{d}x \frac{H^q\left(x, x_B, t\right)}{x_B - x} + i\pi H^q\left(x_B, x_B, t\right)\right] + (\ldots). \qquad (3.6)$$

This amplitude then needs to be squared, contrary to DIS where the factorization happens at the level of the cross-section due to the optical theorem.

3.2. Deeply Virtual Compton Scattering
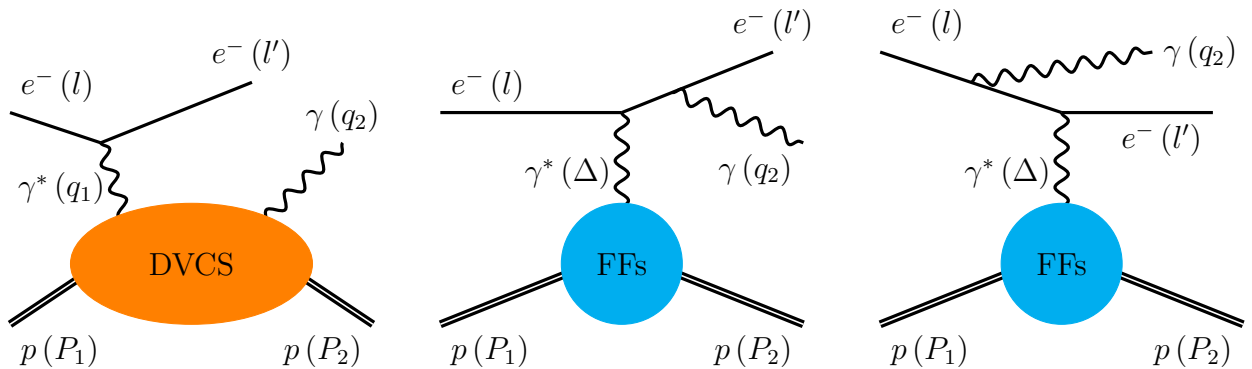
3.2.1. Cross-section and kinematics

Figure 3.2. DVCS (left) and Bethe-Heitler (middle and right) contributions to the photon electroproduction $ep \to ep\gamma$.

Chapter 3. Exclusive processes and extraction of GPDs

The DVCS process interferes coherently with the Bethe-Heitler (BH) process in the photon electroproduction, and each separate contribution is represented in Fig. 3.2. We use notations similar to Chap. 1:

$$q_1 \equiv l - l', \qquad Q^2 \equiv -q_1^2 > 0, \qquad x_B \equiv \frac{Q^2}{2P_1 \cdot q_1},$$

$$P \equiv \frac{P_1 + P_2}{2}, \qquad \Delta \equiv P_2 - P_1, \qquad t \equiv \Delta^2 < 0, \qquad (3.7)$$

but it should be pointed out that only in the case of DVCS does Q^2 represent the photon virtuality. We also add the following definitions:

$$y \equiv \frac{P_1 \cdot q_1}{P_1 \cdot l}, \qquad \epsilon \equiv 2\, x_B \frac{M_N}{Q}, \qquad \xi \equiv \frac{(P_1 - P_2) \cdot (q_1 + q_2)}{(P_1 + P_2) \cdot (q_1 + q_2)}, \qquad (3.8)$$

with $y = \dfrac{Q^2}{2\, x_B M_N E}$ in the target rest frame, where E is the incoming electron energy. The skewness ξ can be written as:

$$\xi = \frac{x_B}{2 - x_B \left(1 - \frac{t}{Q^2}\right)} \simeq \frac{x_B}{2 - x_B}, \qquad (3.9)$$

and we recover approximately the GPD variable:

$$\xi \simeq \frac{P_1^+ - P_2^+}{P_1^+ + P_2^+}. \qquad (3.10)$$

The total cross-section then writes:

$$\frac{\mathrm{d}^5\sigma}{\mathrm{d}x_B \,\mathrm{d}Q^2 \,\mathrm{d}\,|t|\,\mathrm{d}\phi\,\mathrm{d}\phi_S} = \frac{\alpha_{em}^3 x_B}{16\pi^2 Q^4 \sqrt{1 + \epsilon^2}} |\mathcal{T}|^2, \qquad (3.11)$$

as five-fold differential on the kinematic variables. The angles ϕ and ϕ_S are defined in Fig. 3.3. The amplitude $\mathcal{T} = \mathcal{T}_{\mathrm{BH}} + \mathcal{T}_{\mathrm{DVCS}}$ is the coherent sum of Bethe-Heitler and DVCS contributions and we denote by $\mathcal{I}$ the interference term:

$$|\mathcal{T}|^2 = |\mathcal{T}_{\mathrm{BH}}|^2 + |\mathcal{T}_{\mathrm{DVCS}}|^2 + \mathcal{I}. \qquad (3.12)$$

The angular dependence of these squared amplitudes is known and can be written as Fourier harmonics [9]:

$$|\mathcal{T}_{\mathrm{BH}}|^2 = \frac{1}{x_B^2 t \left(1 + \epsilon^2\right)^2 \mathcal{P}_1(\phi)\,\mathcal{P}_2(\phi)} \left(c_0^{\mathrm{BH}} + \sum_{n=1}^{2} c_n^{\mathrm{BH}} \cos n\phi + s_1^{\mathrm{BH}} \sin\phi\right), \qquad (3.13)$$

$$|\mathcal{T}_{\mathrm{DVCS}}|^2 = \frac{1}{Q^2} \left(c_0^{\mathrm{DVCS}} + \sum_{n=1}^{2} \left[c_n^{\mathrm{DVCS}} \cos n\phi + s_n^{\mathrm{DVCS}} \sin n\phi\right]\right), \qquad (3.14)$$

$$\mathcal{I} = \frac{-e_\ell}{x_B t y \mathcal{P}_1(\phi)\,\mathcal{P}_2(\phi)} \left(c_0^{\mathcal{I}} + \sum_{n=1}^{3} \left[c_n^{\mathcal{I}} \cos n\phi + s_n^{\mathcal{I}} \sin n\phi\right]\right), \qquad (3.15)$$
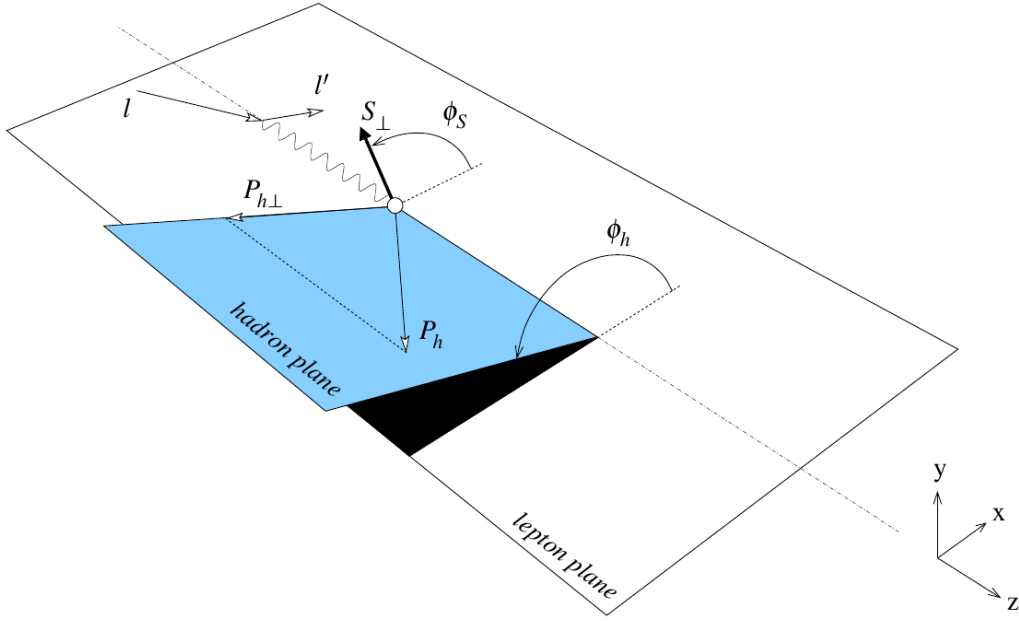
Figure 3.3. Definition of the angles $\phi = \phi_h$ between the lepton plane and hadron plane and ϕ_S between the lepton plane and the target transverse polarization. For the photon electroproduction, the lepton plane is defined by the incoming and outgoing electrons, whereas the hadron plane is defined by the outgoing proton and real photon. The longitudinal direction is that of the virtual photon (or more generally $\boldsymbol{q_1}$, as it is not the virtual photon momentum in the Bethe-Heitler process). Figure taken from Ref. [101] defining the Trento convention.

where e_ℓ is the lepton charge (*i.e.* $e_\ell = -1$ for an electron beam), and $\mathcal{P}_1(\phi)\,\mathcal{P}_2(\phi)$ are the lepton propagators of the Bethe-Heitler diagrams. It should be noted that the Fourier coefficients c_n and s_n still keep an angular dependence on $\phi - \phi_S$, for this combination is taken as an independent variable in Refs. [9, 24, 102, 103]. For instance, we can write [104]:

$$c_1^{\text{DVCS}} = c_{1,\text{U}}^{\text{DVCS}} + \Lambda\, h_\ell\, c_{1,\text{L}}^{\text{DVCS}} + S_\perp \left[\sin\left(\phi - \phi_S\right) c_{1,\text{N}}^{\text{DVCS}} + h_\ell \cos\left(\phi - \phi_S\right) c_{1,\text{S}}^{\text{DVCS}} \right], \qquad (3.16)$$

and similar relations for the other coefficients. We wrote $S_\perp$ and Λ the transverse and longitudinal polarization of the target (with respect to the virtual photon direction) and h_ℓ the lepton polarization. The subscripts U, L, N and S indicate the target polarization and respectively mean "unpolarized", "longitudinal", "normal" and "sideways". The last two are both for a transverse polarization; "N" means that it is normal to the hadron plane ($\phi - \phi_S = \frac{\pi}{2}$), while "S" means that the transverse polarization belongs to the hadron plane ($\phi = \phi_S$). Note that Ref. [24] uses the alternative notation "TP−" and "TP+".

The most up-to-date set of formulas[3] for these Fourier coefficients are given in Ref. [24]. The BH coefficients are simply expressed in terms of Dirac and Pauli FFs (with a quadratic dependence) [9], whereas the DVCS amplitude is expressed linearly either in terms of helicity amplitudes for the Compton scattering $\gamma^* p \to \gamma p$ or equivalently in terms of Compton Form Factors (CFFs). These CFFs thus enter the interference term linearly (multiplied by the elastic

---

[3]Note that an alternative but unpublished set of formulas [105] is also widely used (*e.g.* in Refs. [23, 106]), on top of the numerical code VGG [107].

FFs) and the squared DVCS amplitude quadratically. The Bethe-Heitler process is dominant in the high-x_B region, which means that the interference term is what practically allows to access CFFs in that case. For small-x_B, the DVCS becomes dominant.

3.2.2. Compton Form Factors

Compton Form Factors are the analog of DIS structure functions and are often the observables experimentalists and phenomenologists seek to extract from data, but they are not the end of the story. Due to the factorization theorems, leading-twist CFFs are convolutions of a hard scattering kernel (the coefficient function) and the non-perturbative twist-2 matrix element, *i.e.* the GPD. Following *e.g.* Refs. [108–110], we can write for instance for the CFF $\mathcal{H}$ and associated GPD H:

$$\mathcal{H}\left(\xi, t, Q^2\right) = \int_{-1}^{1} \frac{\mathrm{d}x}{\xi} \sum_{a=g,u,d,\dots} C^a \left(\frac{x}{\xi}, \frac{Q^2}{\mu_F^2}, \alpha_S\left(\mu_F^2\right)\right) H^a\left(x, \xi, t, \mu_F^2\right) . \tag{3.17}$$

Just like DIS structure functions, these CFFs are observable and therefore cannot depend on the arbitrary factorization scale μ_F. This leads to a known factorization scale evolution for GPDs (section 3.3).

The coefficient function can be calculated perturbatively and writes at leading order for the quark GPD:

$$C^q = e_q^2 \left(\frac{1}{1 - \frac{x}{\xi} - i\epsilon} - \frac{1}{1 + \frac{x}{\xi} - i\epsilon}\right) + \mathcal{O}\left(\alpha_S\right) . \tag{3.18}$$

Using the relation (3.2), we obtain the real and imaginary parts of the CFF:

$$\mathrm{Re}\,\mathcal{H}\left(\xi, t, Q^2\right) \underset{\mathrm{LO}}{=} \mathrm{p.v.} \int_{-1}^{1} \mathrm{d}x \sum_{q=u,d,\dots} e_q^2 \left(\frac{1}{\xi - x} - \frac{1}{\xi + x}\right) H^q\left(x, \xi, t, \mu_F^2\right) , \tag{3.19}$$

$$\mathrm{Im}\,\mathcal{H}\left(\xi, t, Q^2\right) \underset{\mathrm{LO}}{=} \pi \sum_{q=u,d,\dots} e_q^2 \left[H^q\left(x = \xi, \xi, t, \mu_F^2\right) - H^q\left(x = -\xi, \xi, t, \mu_F^2\right)\right] , \tag{3.20}$$

and we recover what we sketched in Eq. (3.6). Note that for gluons, the first contribution is at NLO. Note also that even though the GPD itself may depend on the factorization scale μ_F, the r.h.s. of Eqs. (3.19)-(3.20) do not, as the dependence cancels order by order in α_S [1]. And since the LO kernel does not depend on $\frac{Q^2}{\mu_F^2}$, this means that the LO CFF does not have a Q^2-dependence, just like the structure functions of DIS in the Parton model. The scale dependence appears at NLO.

Using dispersion relation techniques (see *e.g.* Ref. [26] and references therein), one can relate both real and imaginary parts of the CFF and write *in fine* the result in terms of the GPD at the cross-over line $x = \xi$ with the addition of (at least) a subtraction constant:

$$\mathrm{Re}\,\mathcal{H}\left(\xi, t, Q^2\right) \underset{\mathrm{LO}}{=} \mathrm{p.v.} \int_{-1}^{1} \mathrm{d}x \sum_{q=u,d,\dots} e_q^2 \left(\frac{1}{\xi - x} - \frac{1}{\xi + x}\right) H^q\left(x, x, t, \mu_F^2\right) + \mathcal{C}_{\mathcal{H}}\left(t, \mu_F^2\right) . \tag{3.21}$$

The subtraction constant is linked to the so-called D-term (introduced in Sec. 4.2.2 and Sec. 5.3.3) via the integral:

$$\mathcal{C}_{\mathcal{H}} = \sum_{q=u,d,\dots} e_q^2 \int_{-1}^{1} \mathrm{d}\alpha \frac{2\,D^q\left(\alpha\right)}{1 - \alpha} . \tag{3.22}$$

This means the information contained in the LO CFFs is limited to the cross-over line of the GPD and (an integral of) the D-term. Note that this can be alternatively derived [111–113] using Double Distributions (introduced in Chap. 5).

3.2.3. Observables

To access these CFFs, experimental collaborations measure either total and differential cross-sections or asymmetries. The latter are easier to measure due to the cancellation of normalizations. For instance, the HERA experiments having access to both positron and electron beams could measure the beam charge asymmetry:

$$A_{\mathrm{C}}\left(\phi\right) = \frac{\left(\mathrm{d}\sigma^{\overset{+}{\rightarrow}}\left(\phi\right) + \mathrm{d}\sigma^{\overset{+}{\leftarrow}}\left(\phi\right)\right) - \left(\mathrm{d}\sigma^{\overset{-}{\rightarrow}}\left(\phi\right) + \mathrm{d}\sigma^{\overset{-}{\leftarrow}}\left(\phi\right)\right)}{\left(\mathrm{d}\sigma^{\overset{+}{\rightarrow}}\left(\phi\right) + \mathrm{d}\sigma^{\overset{+}{\leftarrow}}\left(\phi\right)\right) + \left(\mathrm{d}\sigma^{\overset{-}{\rightarrow}}\left(\phi\right) + \mathrm{d}\sigma^{\overset{-}{\leftarrow}}\left(\phi\right)\right)} \, , \tag{3.23}$$

which allows to access the real part of CFFs. We have denoted by a sign "$\pm$" the beam charge e_l and by an arrow the beam helicity h_l. The other possible combinations when controlling both the beam charge and helicity are:

$$A_{\mathrm{LU,DVCS}}\left(\phi\right) = \frac{\left(\mathrm{d}\sigma^{\overset{+}{\rightarrow}}\left(\phi\right) - \mathrm{d}\sigma^{\overset{+}{\leftarrow}}\left(\phi\right)\right) + \left(\mathrm{d}\sigma^{\overset{-}{\rightarrow}}\left(\phi\right) - \mathrm{d}\sigma^{\overset{-}{\leftarrow}}\left(\phi\right)\right)}{\left(\mathrm{d}\sigma^{\overset{+}{\rightarrow}}\left(\phi\right) + \mathrm{d}\sigma^{\overset{+}{\leftarrow}}\left(\phi\right)\right) + \left(\mathrm{d}\sigma^{\overset{-}{\rightarrow}}\left(\phi\right) + \mathrm{d}\sigma^{\overset{-}{\leftarrow}}\left(\phi\right)\right)} \, , \tag{3.24}$$

$$A_{\mathrm{LU,I}}\left(\phi\right) = \frac{\left(\mathrm{d}\sigma^{\overset{+}{\rightarrow}}\left(\phi\right) - \mathrm{d}\sigma^{\overset{+}{\leftarrow}}\left(\phi\right)\right) - \left(\mathrm{d}\sigma^{\overset{-}{\rightarrow}}\left(\phi\right) - \mathrm{d}\sigma^{\overset{-}{\leftarrow}}\left(\phi\right)\right)}{\left(\mathrm{d}\sigma^{\overset{+}{\rightarrow}}\left(\phi\right) + \mathrm{d}\sigma^{\overset{+}{\leftarrow}}\left(\phi\right)\right) + \left(\mathrm{d}\sigma^{\overset{-}{\rightarrow}}\left(\phi\right) + \mathrm{d}\sigma^{\overset{-}{\leftarrow}}\left(\phi\right)\right)} \, , \tag{3.25}$$

where we denoted by the first letter "L" the beam polarization (longitudinal) and by the second one the target polarization (unpolarized here). On the other hand, when only one lepton charge is available, such as at Jefferson Lab, one can only measure the beam spin asymmetry:

$$A_{\mathrm{LU}}^{e_\ell}\left(\phi\right) = \frac{\mathrm{d}\sigma^{\overset{e_\ell}{\rightarrow}}\left(\phi\right) - \mathrm{d}\sigma^{\overset{e_\ell}{\leftarrow}}\left(\phi\right)}{\mathrm{d}\sigma^{\overset{e_\ell}{\rightarrow}}\left(\phi\right) + \mathrm{d}\sigma^{\overset{e_\ell}{\leftarrow}}\left(\phi\right)} \, . \tag{3.26}$$

For longitudinally polarized targets, asymmetries A_{UL} defined similarly to Eq. (3.26) can also be measured. We can note that the HERMES collaboration had also access to transversely polarized targets, which allowed to access ϕ_S-unintegrated asymmetries. Finally, we can point out that instead of the ϕ-dependence of asymmetries, the HERMES collaboration published only Fourier harmonics of the form (*e.g.* for the beam charge asymmetry):

$$A_{\mathrm{C}}^{\cos n\phi} = \frac{1}{\pi} \int_0^{2\pi} \mathrm{d}\phi \, \cos n\phi \, A_{\mathrm{C}}\left(\phi\right) \, , \tag{3.27}$$

which can be approximately related to combinations of CFFs. We can quote for instance:

$$A_{\mathrm{C}}^{\cos \phi} \propto \mathrm{Re}\left(F_1 \mathcal{H} + \xi\left(F_1 + F_2\right)\hat{\mathcal{H}} - \frac{t}{4M_N^2}F_2\mathcal{E}\right) \, , \tag{3.28}$$

$$A_{\mathrm{LU}}^{-,\sin \phi} \propto \mathrm{Im}\left(F_1 \mathcal{H} + \xi\left(F_1 + F_2\right)\hat{\mathcal{H}} - \frac{t}{4M_N^2}F_2\mathcal{E}\right) \, , \tag{3.29}$$

and other similar combinations. For each such observable, there is usually a real or imaginary part of some CFF that dominates kinematically. Having a complete set of asymmetries allows to discriminate between the different contributions.

We refer *e.g.* to Refs. [23, 110] for a thorough review of the observables measured or planned and the information they give on CFFs.

3.3. Evolution

As PDFs evolve according to the DGLAP equations, GPDs follow also their own evolution equations. In principle, these are integro-differential equations that mix gluons and quark flavors. They can be nevertheless almost diagonalized in flavor space by using "non-singlet" (NS) combinations that can evolve independently of the gluon GPD. These NS combinations correspond to an exchange of charge conjugation $C = -1$ (C-odd) and do not mix with gluons (C-even). One example is the valence[4] combination:

$$H^{q(-)}(x, \xi, t) = H^q(x, \xi, t) + H^q(-x, \xi, t) . \qquad (3.30)$$

They follow the autonomous evolution equation [1]:

$$\mu_F^2 \frac{\partial}{\partial \mu_F^2} H_{\text{NS}}\left(x, \xi, t, \mu_F^2\right) = \int_{-1}^1 \frac{\mathrm{d}y}{|\xi|} V_{\text{NS}}\left(\frac{x}{\xi}, \frac{y}{\xi}\right) H_{\text{NS}}\left(y, \xi, t, \mu_F^2\right) \qquad (3.31)$$

where V_{NS} is the non-singlet evolution kernel. On the other hand, the singlet combination

$$\sum_q H^{q(+)}(x, \xi, t) = \sum_q \left[H^q(x, \xi, t) - H^q(-x, \xi, t)\right] \qquad (3.32)$$

mixes with gluons as the combination $H^{q(+)}$ is C-even, and we end up with a similar equation but in matrix form; *i.e.* with the substitution $V_{\text{NS}} \to \boldsymbol{V}_{\text{S}}$ and $H_{\text{NS}} \to \boldsymbol{H}_{\text{S}}$ defined by

$$\boldsymbol{V}_{\text{S}}\left(\frac{x}{\xi}, \frac{y}{\xi}\right) = \begin{pmatrix} V^{qq}\left(\frac{x}{\xi}, \frac{y}{\xi}\right) & \frac{1}{\xi} V^{qq}\left(\frac{x}{\xi}, \frac{y}{\xi}\right) \\ \xi V^{gq}\left(\frac{x}{\xi}, \frac{y}{\xi}\right) & V^{gg}\left(\frac{x}{\xi}, \frac{y}{\xi}\right) \end{pmatrix} , \qquad (3.33)$$

$$\boldsymbol{H}_{\text{S}}\left(x, \xi, t, \mu_F^2\right) = \begin{pmatrix} \frac{1}{2N_f} \sum_q H^{q(+)}\left(x, \xi, t, \mu_F^2\right) \\ H^g\left(x, \xi, t, \mu_F^2\right) \end{pmatrix} . \qquad (3.34)$$

Note that differences of $H^{q(+)}$ for different quark flavors are also C-odd and therefore non-singlet. In total, we need $2N_f + 1$ independent combinations (in the non-diagonalized basis, we have $H^{q(+)}$ and $H^{q(-)}$ for each quark flavor, plus the gluon GPD). The singlet and gluon GPD in the coupled system count for two, and the valence combinations $H^{q(-)}$ for N_f. The differences $H^{u(+)} - H^{d(+)}$, $H^{d(+)} - H^{s(+)}$, etc, for instance, can make up for the missing $N_f - 1$ NS combinations. The system is maximally diagonalized this way.

The kernels are known at LO and NLO (in α_S) and can be found *e.g.* in Refs. [2, 114–117]. The limit $\xi \to 0$ gives back the DGLAP equations, even for non-zero t, *i.e.* for t-dependent

---

[4]The denomination comes from its forward limit $q_{\text{val}} = q - \bar{q}$. See Sec. 4.2.2.

PDFs. On the other hand, at $\xi \to \pm 1$, we recover the evolution kernels of another non-perturbative object, the (Generalized) Distribution Amplitude (introduced in Sec. 5.2.4). These are the ERBL[5] equations [118, 119].

To solve these evolution equations, one can use classical numerical methods such as Runge-Kutta, as in Ref. [120]. Another possibility is to rely on Mellin moments for PDFs (see *e.g.* Ref. [62]), or conformal moments for GPDs (see *e.g.* Refs. [1, 2]), to get rid of the integral and end up only with a differential equation. This is referred to as a diagonalization, as we go from coupled equations in x-space (*i.e.* the integral of Eq. (3.31)) to decoupled ones in m-space (at least at LO) with the Mellin moments $\int_0^1 \mathrm{d}x\, x^m q(x)$ or similarly the conformal moments.

The evolution of parton distributions is crucial for phenomenology as it allows to relate measurements at different energy scales. Without it, we would not be able to interpret consistently data taken at colliders with large Q^2, such as the H1 and ZEUS experiments at DESY or the future electron-ion collider (EIC), and fixed-target data for which Q^2 can be much lower, such as the experiments at Jefferson Lab or HERMES at DESY. It also allows to extract from high-energy experiments information on the low-energy hadronic phenomena.

3.4. Extraction of Generalized Parton Distributions

3.4.1. Experimental status

DVCS measurements started in the early 2000s at DESY in Hamburg, Germany, and at Jefferson Laboratory in Newport News, Virginia, USA.

Two different kinds of DVCS experiments were pursued at DESY, all of them held at the HERA accelerator: a fixed-target one by the HERMES collaboration [121–127], and collider experiments by the H1 [128–131] and ZEUS [132, 133] collaborations. The last two allowed us to access small-x_B regions ($\sim 10^{-4}$–10^{-2}), where DVCS is dominant, and therefore managed to measure directly the DVCS part of the cross-section, either the total one, or the t-differential one, for values of Q^2 up to 100 GeV^2 but mainly around 10 GeV^2. They also published beam charge asymmetries, having access to both positron and electron beams. The HERMES collaboration on the other hand used a fixed proton target that could be both longitudinally and transversely polarized, and published a complete set of asymmetries in the moderate x_B region, for values of Q^2 mainly around $\sim$ 2–3 GeV^2, allowing a very convenient disentanglement of the different CFFs. These HERA experiments ended in 2007, with the last HERMES results published in 2012.

The CLAS [27, 134–138] and Hall A [139, 140] collaborations at Jefferson Lab pursued a similar program to HERMES (moderate values of $Q^2 \sim 2$ GeV^2), but still active today. CLAS measured observables over a wide kinematical range ($x_B \sim 0.1$–0.5), whereas Hall A focused on a restricted set ($x_B \sim 0.35$–0.4) with a higher luminosity and therefore precision. CLAS published both asymmetries and ϕ-dependent cross-sections, while Hall A published the latter.

All in all, this experimental effort confirmed the factorization of DVCS. It showed that the leading-twist approximation holds even for moderate values of Q^2, within the statistical accuracy achieved. But a recent reanalysis of Hall A data [140, 141] hinted at the important

---

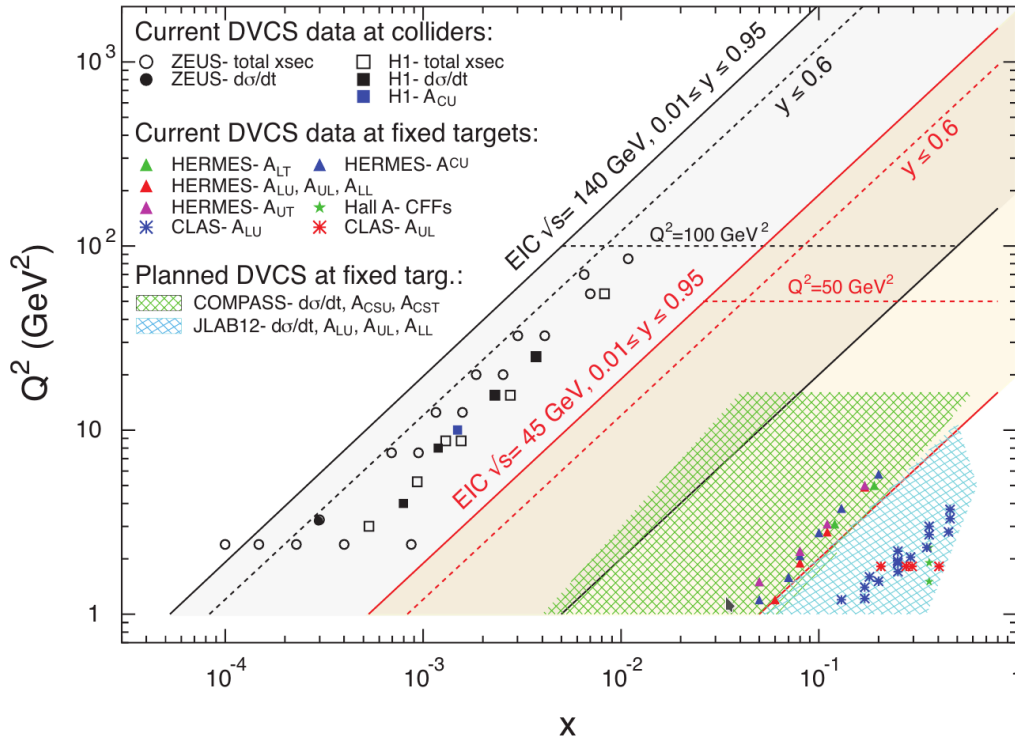[5]Efremov–Radyushkin–Brodsky–Lepage.

Figure 3.4. Summary of the available (in 2012) and planned DVCS measurements. Figure taken from Ref. [142]. Here, "x" should be understood as the Bjorken variable x_B, which is related to the skewness ξ, and not as the mute variable x of GPDs.

role played by gluons, either through higher-twist contributions or NLO effects, which was not necessarily expected at high values of x_B.

In the near future, the COMPASS collaboration at CERN will provide us with cross-sections in an intermediate x_B region, hoping to bridge the gap between the previous collider and fixed-target experiments, while the different halls at Jefferson Lab should continue to contribute to the effort in the 12 GeV era with increased kinematical coverage and precision of upcoming data. On a longer time scale, the EIC project [142] aims at covering a very large kinematical region, including *in fine* the very small-x_B region of the past collider experiments, with a high luminosity, to really seek out the gluon realm. Figure 3.4 summarizes the currently available measurements relatively to the planned kinematic coverage, although more recent asymmetries and cross-sections have since been published by CLAS and Hall A (in 2015).

3.4.2. Fits to data

As illustrated in Fig. 1.4 (right panel), PDFs extraction is working very well, with different fitting groups using different methods cross-checking their results that are in very good agreement (see *e.g.* the review of the PDG [60], section 19.3). One may hope that the situation would be the same for GPDs, if not now at least in the future, as *a priori* one has to perform the same sort of deconvolution; indeed the CFF convolution (3.17) looks similar to that of the DIS structure function (1.29). But GPD extraction faces two important issues:

- First, contrary to PDFs who do not depend on the external Bjorken variable x_B in the factorization (1.29) but only on the mute variable x, GPDs do depend on the external variable, *i.e.* the skewness ξ, in Eq. (3.17), which renders this deconvolution a completely different problem and makes it much more difficult. Indeed, we lose information when going from GPDs to CFFs with the projection (3.17) from four variables to only three, which does not happen for PDFs.

- Second, the so-called *curse of dimensionality* is a serious obstacle as any increase in the dimension of the domain space implies a more sparse available data. The theoretical constraints detailed in Chap. 4 do not help much in this matter, as they imply only a decrease in the domain volume, but not its dimension.

For now, the fitting efforts have been devoted to extract CFFs, not GPDs, as it is already very challenging itself. Two main approaches have been followed:

Local fits [106, 143–148] This method consists on fitting the CFFs themselves as free parameters, for a given kinematic bin. It has the advantage of being completely model-independent (apart from the twist-2 approximation), but lacks the ability to do any extrapolation.

Global fits [106, 147, 149–151] In this approach, CFFs are parametrized through a functional form for the GPD. The term "global" refers to the fact that we consider all the kinematic points at once, and fit the parameters of the chosen functional form. We should stress that it is still a fit at the level of the CFFs, even though the GPD can be directly parametrized, as it carries an inherent model-dependence. The advantage is that the functional forms allow to reliably extrapolate CFFs to other kinematics. These fits are very successful in reproducing the data (although the very accurate Hall A data can present some difficulty), moreover they generally agree with the local fits presented above.

We refer to the recent review [110] on DVCS fitting for more details on the subject. We can point out in passing that fits to other processes such as DVMP [152, 153] were also performed. The GK model in particular, although tuned for DVMP only, gives also accurate predictions for DVCS [23], which is a good test of the universality of GPDs. On another note, we can mention the first efforts of CFF fitting using neural networks [154], in good agreement with previous approaches.

3.4.3. PARTONS software

As we have seen, GPDs belong to an active field of research where still theoretical questions are to be solved and the lack of a general first principle parametrization justifies the need for several models. In parallel, the active experimental program with a foreseen increased accuracy requires a careful design of tools to exploit these experimental data. Those tools should also be used for the physics case of future experiments (*e.g.* at the EIC). The PARTONS framework [22] was born with the aim of accomplishing this. It provides a C++ library aimed both at experimentalists and phenomenologists.

PARTONS encompasses the whole chain of computation of an observable in a given channel related to GPDs. This can be divided into three main levels:

Large distance This level concerns the computation of GPDs themselves, with respect to different model parameters, as functions of x, ξ, t, etc. The factorization scale dependence is described by evolution equations.

Small distance The second level is that of the small distance coefficient functions. In practice, it means convoluting the GPDs and the end results are the CFFs (see *e.g.* Eq. (3.17)).

Full process Finally, this level concerns the cross-sections and various other observables (see Sec. 3.2.3) that can be directly accessed in experiments.

Figure 3.5. PARTONS logo.

At any such level, the framework is flexible enough to allow any choice of model assumption, the inclusion of higher order corrections, etc. Indeed, PARTONS is modular by design, and Fig. 3.6 sketches an example of the different steps in a calculation with corresponding choices of modules. This is possible in practice through class inheritance, as for instance the module `GPDGK11` is a child class of the abstract class `GPDModule` and can be plugged by the user in the computation chain independently of the choice of other modules. PARTONS works only on the basis of the needed abstract classes, unknowingly of what the user chooses for the physics content. We showed an example going up to the observable level, but of course a computation at any step in the chain can also be performed (if one wants *e.g.* only GPDs as end result, or alternatively CFFs).

So far, only the DVCS channel is implemented in PARTONS, but the other exclusive processes (TCS and DVMP) are also planned, and the architecture was thought of to accommodate any such channel. The following modules are currently available:

GPD The popular GK model [152, 155, 156] (both as it was originally conceived and with numerical integration) and VGG model [92, 107, 157], and various other GPD models used in Refs. [109, 120, 158].

Evolution Code by Vinnikov [120].

CFF The up-to NLO evaluation of Refs. [108, 109], its extension to massive quarks [159], and the historical LO evaluation of the VGG code.

DVCS The unpublished set of formulas [105], the latest one in the BM formalism [24] (referred to as BMJ), and the historical numerical code VGG.

The current version of PARTONS has all the necessary tools to study DVCS at NLO and leading-twist, but this list is by no means limiting, as other models and features can easily be added (or plugged) due to its modularity.

We should note also that on top of the default C++ interface, PARTONS also allows one to use XML files[6] as scenarios to compute automated tasks, for users who do not need to add their own modules or simply do not want to delve into coding when the task is very straightforward.

---

[6]These are meant *in fine* to be the "configuration files" for the foreseen visualization interface.
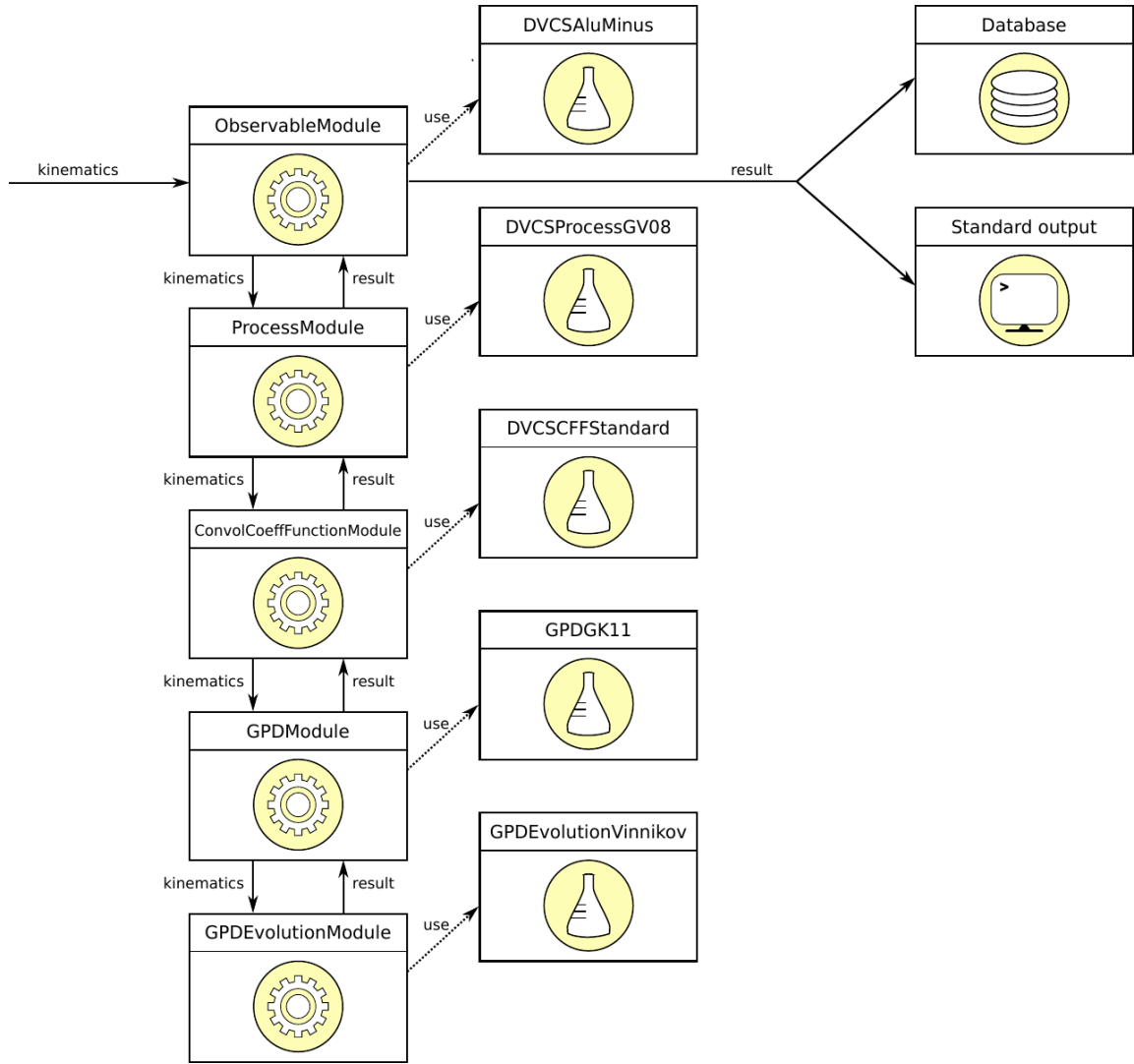
Figure 3.6. Example of computation of a beam spin asymmetry with the PARTONS library. Figure taken from Ref. [22].

Examples of such scenarios are given in Ref. [22], and a complete documentation is available on the web[7].

---

[7]http://partons.cea.fr/

Part II.

Theory of Generalized Parton Distributions

Chapter 4.

Definition and properties of Generalized Parton Distributions

GPDs were independently introduced by Müller et al [5], Radyushkin [6] and Ji [7] under various names[1]. They are defined as a Light-front projection of a non-diagonal hadronic matrix element of a bi-local operator. This general statement applies to all kinds of GPDs, but without delving into the full zoology, we will first consider the simple pion case, which can already illustrate all the properties that interest us. We will then move to the nucleon case in a second phase, with its (un)fortunate complications due to its spin and non-negligible mass.

We will use throughout the conventions of Refs. [1, 160] and mostly the notations therein (see also App. A.1).

4.1. Generalized Parton Distributions of the pion

4.1.1. Definition

The twist-2 chiral-even quark GPD of a spin-0 hadron writes:

$$H_\pi^q (x, \xi, t) = \frac{1}{2} \int \frac{\mathrm{d}z^-}{2\pi} e^{i x P^+ z^-} \left\langle \pi, P + \frac{\Delta}{2} \left| \bar{\psi}^q \left(-\frac{z}{2} \right) \gamma^+ \psi^q \left(\frac{z}{2} \right) \right| \pi, P - \frac{\Delta}{2} \right\rangle \Bigg|_{\substack{z^+=0 \\ z_\perp=0}}, \quad (4.1)$$

where, as sketched in Fig. 4.1, we use the following notations:

- $P = \frac{P_1 + P_2}{2}$ is the momentum average of the hadron incoming (1) and outgoing (2) states,

- $\Delta = P_2 - P_1$ is the momentum transfer,

- $t = \Delta^2$ is the Mandelstam variable of momentum transfer,

- $x = \frac{k^+}{P^+}$ is the longitudinal average momentum fraction of the quarks,

- $\xi = -\frac{\Delta^+}{2 P^+}$ is the longitudinal transfer momentum fraction, *i.e.* the *skewness* variable.

q classically stands for the quark flavor, hence here the operators ψ^q are quark fields. We used here the light-cone gauge, hence no Wilson line joining the fields at different positions is needed. In other gauges, it should be added.

---

[1] "Off-forward", "non-diagonal", "skewed", ... parton distributions, to quote some of them.

This quark GPD of the pion will be used heavily as case study and benchmark in Part. III. Here it will allow us to present all the important properties of such objects. Note however that there is also a chiral-odd GPD in the case of the pion, *i.e.* with a parton helicity flip, called the transversity GPD $H_{T,\pi}$, but we will not consider it here. Likewise, we do not discuss gluon GPDs.

4.1.2. Basic Properties

Limiting case

This GPD encodes information on both the pion *electromagnetic form factor* and the pion *parton distribution function*. Indeed, taking $\Delta = 0$ in Eq. (4.1) leaves us with a diagonal matrix element defining a quark PDF. In other words,

$$H_\pi^q(x, 0, 0) = q_\pi(x)\,\theta(x) - \bar{q}_\pi(-x)\,\theta(-x) \,, \tag{4.2}$$

where we denote by $\theta(\,\cdot\,)$ the Heaviside step function.

On the other hand, integrating Eq. (4.1) over x yields the local operator defining the Elastic Form Factors:

$$\begin{aligned}
\int_{-1}^{1} H_\pi^q(x, \xi, t)\,\mathrm{d}x &= \frac{1}{2}\int \frac{\mathrm{d}z^-}{2\pi}\int_{-1}^{1}\mathrm{d}x\, e^{i\,x\,P^+z^-} \left\langle \pi, P_2 \middle| \bar{\psi}^q\left(-\frac{z}{2}\right)\gamma^+\psi^q\left(\frac{z}{2}\right) \middle| \pi, P_1 \right\rangle \Bigg|_{\substack{z^+=0 \\ z_\perp=0}} \\
&= \frac{1}{2\,P^+}\int \mathrm{d}z^-\,\delta(z^-)\left\langle \pi, P_2 \middle| \bar{\psi}^q\left(-\frac{z}{2}\right)\gamma^+\psi^q\left(\frac{z}{2}\right) \middle| \pi, P_1 \right\rangle \Bigg|_{\substack{z^+=0 \\ z_\perp=0}} \\
&= \frac{1}{2\,P^+}\left\langle \pi, P_2 \middle| \bar{\psi}^q(0)\,\gamma^+\psi^q(0) \middle| \pi, P_1 \right\rangle .
\end{aligned} \tag{4.3}$$

We thus obtain that the zeroth Mellin moment of a quark GPD is the quark's contribution to the electromagnetic form factor[2]:

$$\int_{-1}^{1} H_\pi^q(x, \xi, t)\,\mathrm{d}x = F_\pi^q(t) \,. \tag{4.4}$$

Notice that there is no ξ-dependence.

Domain

From the definition of ξ as:

$$\xi = \frac{P_1^+ - P_2^+}{P_1^+ + P_2^+} \,, \tag{4.5}$$

and given that the plus-momenta of physical states are positive (see App. A.1), one can easily see that the domain is limited to $\xi \in [-1, 1]$. In truth, ξ is also bounded by an additional maximal value defined by t and the mass of the hadron M_H, as will be detailed in the next

---

[2]This form factor was defined in Eq. (2.18), and the electromagnetic current can be written in terms of the quark fields as: $J_\mu^{\mathrm{em}}(0) = \sum_q e_q\,\bar{\psi}^q(0)\,\gamma_\mu\psi^q(0)$. Hence, the quark contributions are defined such that $F = \sum_q e_q\,F^q$.
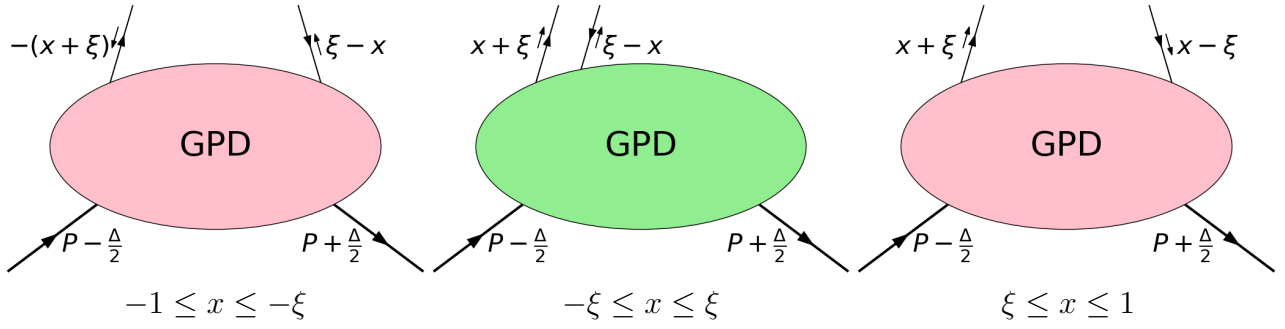
Figure 4.1. GPD diagram with associated momenta of hadrons and partons, interpreted differently in each region. Internal arrows indicate the flow of charge, while external arrows indicate momentum flow.

section 4.2.2. But for the pion, we will usually work in the chiral limit and neglect the pion mass. We will therefore ignore this additional bound and consider the full domain $t \leq 0$ (space-like values) and $\xi \in [-1, 1]$ as physical.

In this ξ domain, the support is such that $x \in [-1, 1]$. This can be shown by considering the analytic properties of the scattering amplitude of an off-shell quark off an on-shell hadron, of which the GPD of Eq. (4.1) is a projection [2, 161].

The region $|x| > |\xi|$ is called DGLAP, while the other $|x| < |\xi|$ is called ERBL, both names referring to the kernels involved in each region for the QCD evolution in the factorization scale. See section 3.3.

ξ-parity

By considering the discrete symmetry of time reversal, represented by the anti-linear and anti-unitary operator $\mathcal{T}$ [162, 163]:

$$\mathcal{T}\left[u\left|\Phi\right\rangle + v\left|\Psi\right\rangle\right] = u^*\mathcal{T}\left|\Phi\right\rangle + v^*\mathcal{T}\left|\Psi\right\rangle , \tag{4.6}$$
$$\left\langle\mathcal{T}\Phi|\mathcal{T}\Psi\right\rangle = \left\langle\Phi|\Psi\right\rangle^* = \left\langle\Psi|\Phi\right\rangle ,$$

we can show that the matrix element (4.1) transforms as:

$$\left\langle \pi\left(P_2\right)\left|\bar{\psi}^q\left(-\frac{z}{2}\right)\gamma^+\psi^q\left(\frac{z}{2}\right)\right|\pi\left(P_1\right)\right\rangle = \left\langle\mathcal{T}\pi\left(P_2\right)\left|\mathcal{T}\bar{\psi}^q\left(-\frac{z}{2}\right)\gamma^+\psi^q\left(\frac{z}{2}\right)\right|\pi\left(P_1\right)\right\rangle^*$$
$$= \left\langle \pi\left(P_1\right)\left|\bar{\psi}^q\left(-\frac{z}{2}\right)\gamma^+\psi^q\left(\frac{z}{2}\right)\right|\pi\left(P_2\right)\right\rangle, \tag{4.7}$$

where the details of the derivation are given for instance in Refs. [2, 12] and the effect of time reversal on quark fields is given in textbooks (*e.g.* Refs. [66, 163]). It follows that the GPD (4.1) is even in ξ:

$$H_\pi^q\left(x, -\xi, t\right) = H_\pi^q\left(x, \xi, t\right) . \tag{4.8}$$

From now on, ξ will be considered ≥ 0, unless stated otherwise in some situations where the full domain needs to be considered.

Real-valued function

Similarly, taking the hermitian conjugate of the matrix element in Eq. (4.1) leaves us with:

$$\left\langle \pi, P_2 \left| \bar{\psi}^q \left(-\frac{z}{2}\right) \gamma^+ \psi^q \left(\frac{z}{2}\right) \right| \pi, P_1 \right\rangle^* = \left\langle \pi, P_1 \left| \bar{\psi}^q \left(\frac{z}{2}\right) \gamma^+ \psi^q \left(-\frac{z}{2}\right) \right| \pi, P_2 \right\rangle . \qquad (4.9)$$

This implies (after a change of variable $z^- \leftrightarrow -z^-$ in Eq. (4.1)) the property:

$$\left(H_\pi^q (x, \xi, t)\right)^* = H_\pi^q (x, -\xi, t) . \qquad (4.10)$$

Combined with Eq. (4.8), this shows that the GPD is real.

Partonic interpretation

The partonic exchange can be interpreted differently in each region:

- For $-1 \leq x \leq -\xi$ (that we will denote by DGLAP<), the interpretation is that of an emission of an antiquark of plus-momentum fraction $\xi - x$ and its reabsorption with a plus-momentum fraction $-(x + \xi)$. We have an antiquark distribution.

- The region $-\xi \leq x \leq \xi$ (ERBL) corresponds to an emission of a pair quark-antiquark of plus-momentum fractions $x + \xi$ and $\xi - x$ respectively. This is reminiscent of a meson Distribution Amplitude (DA). See sections 5.2.4 and 6.1.7.

- In the region $\xi \leq x \leq 1$ (DGLAP>), there is emission of a quark of plus-momentum fraction $x + \xi$ and its reabsorption with plus-momentum fraction $x - \xi$. This corresponds to a quark distribution.

This is sketched in Fig. 4.1.

4.1.3. Isospin symmetry and charge conjugation

From isospin symmetry, we can write the following relations (see for instance Refs. [1,2,164, 165]), defining at the same time the two isospin combinations of GPDs and stating that there are at most two independent quark GPDs for the pions:

$$H_{\pi^c}^u (x, \xi, t) + H_{\pi^c}^d (x, \xi, t) = H_\pi^{I=0} (x, \xi, t) , \qquad \forall c = 0, \pm , \qquad (4.11)$$

$$H_{\pi^c}^u (x, \xi, t) - H_{\pi^c}^d (x, \xi, t) = c \, H_\pi^{I=1} (x, \xi, t) . \qquad (4.12)$$

Notice that each equation represents three equalities. From this, we deduce the relations:

$$H_{\pi^c}^u (x, \xi, t) = H_{\pi^{-c}}^d (x, \xi, t) , \qquad \forall c = \pm , \qquad (4.13)$$

$$H_{\pi^0}^u (x, \xi, t) = H_{\pi^0}^d (x, \xi, t) = \frac{1}{2} \left(H_{\pi^c}^u (x, \xi, t) + H_{\pi^c}^d (x, \xi, t) \right) . \qquad (4.14)$$

Using now charge conjugation yields:

$$H_{\pi^c}^q (x, \xi, t) = -H_{\pi^{-c}}^q (-x, \xi, t) , \qquad \forall c = 0, \pm \text{ and } q = u, d , \qquad (4.15)$$

and combining this with the previous relations allows us to write:

$$H^u_{\pi^c}(x, \xi, t) = -H^d_{\pi^c}(-x, \xi, t) , \qquad\qquad \forall c = 0, \pm . \qquad (4.16)$$

All in all, this shows that there is actually only one independent quark GPD, for instance $H^u_{\pi^+}$, and that the isospin GPDs are the x-even and x-odd contributions to it:

$$H^I_\pi(x, \xi, t) = H^u_{\pi^+}(x, \xi, t) - (-1)^I H^u_{\pi^+}(-x, \xi, t) . \qquad (4.17)$$

These combinations are also called "singlet" for the isoscalar $H^{I=0}_\pi$ and "non-singlet" (or "valence") for the isovector $H^{I=1}_\pi$.

In this thesis, when the subscripts and superscripts are not explicitly written, it is implied that the GPD considered is $H^u_{\pi^+}$.

4.1.4. Polynomiality

Let us now derive the same kind of matrix element of a local operator as in Eq. (4.3), but for a general mth Mellin moment, that we will denote by H^m:

$$\begin{aligned} H^{q,m}_\pi(\xi, t) &= \int_{-1}^{1} x^m H^q_\pi(x, \xi, t)\, \mathrm{d}x \\ &= \frac{1}{2}\int \frac{\mathrm{d}z^-}{2\pi} \int_{-1}^{1} \mathrm{d}x\, x^m e^{i\,x\,P^+ z^-} \left\langle \pi, P_2 \middle| \bar{\psi}^q\left(-\frac{z}{2}\right) \gamma^+ \psi^q\left(\frac{z}{2}\right) \middle| \pi, P_1 \right\rangle \bigg|_{\substack{z^+=0 \\ z_\perp=0}} \\ &= \frac{(-i)^m}{2\,(P^+)^{m+1}} \int \mathrm{d}z^- \left(\frac{\partial}{\partial z^-}\right)^m \left[\delta\left(z^-\right)\right] \left\langle \pi, P_2 \middle| \bar{\psi}^q\left(-\frac{z}{2}\right) \gamma^+ \psi^q\left(\frac{z}{2}\right) \middle| \pi, P_1 \right\rangle \bigg|_{\substack{z^+=0 \\ z_\perp=0}} \\ &= \frac{i^m}{2\,(P^+)^{m+1}} \left\langle \pi, P_2 \middle| \left(\frac{\partial}{\partial z^-}\right)^m \left(\bar{\psi}^q\left(-\frac{z}{2}\right) \gamma^+ \psi^q\left(\frac{z}{2}\right)\right) \middle| \pi, P_1 \right\rangle \bigg|_{z=0} \\ &= \frac{1}{2\,(P^+)^{m+1}} \left\langle \pi, P_2 \middle| \bar{\psi}^q(0)\, \gamma^+ \left(i\, \overleftrightarrow{\partial}^+\right)^m \psi^q(0) \middle| \pi, P_1 \right\rangle , \end{aligned} \qquad (4.18)$$

where the last line is just a convenient rewriting of the previous line by using the notation $\overleftrightarrow{\partial} = \frac{1}{2}\left(\overrightarrow{\partial} - \overleftarrow{\partial}\right)$ for the left-right partial derivative, with $\partial^+ = \frac{\partial}{\partial z^-}$.

This operator $\bar{\psi}^q(0)\, \gamma^+ \left(i\, \overleftrightarrow{\partial}^+\right)^m \psi^q(0)$ is a special case of twist-2 local operators of the form:

$$\mathcal{O}^{\mu_0\mu_1\ldots\mu_m}_q = \bar{\psi}^q \gamma^{\{\mu_0} i\overleftrightarrow{D}^{\mu_1} \ldots i\overleftrightarrow{D}^{\mu_m\}} \psi^q \qquad (4.19)$$

where D is the covariant derivative[3] and $\{\ldots\}$ denotes a full symmetrization and trace subtraction[4], and the fields are taken at the same position (*e.g.* $z = 0$). A matrix element of this operator has the following structure in terms of the two four-vectors P^μ and Δ^μ and the only scalar invariant $t = \Delta^2$ (given that $P \cdot \Delta = 0$ and $P^2 = M_H^2 - \frac{\Delta^2}{4}$):

$$\langle \pi, P_2| \mathcal{O}^{\mu_0\mu_1\ldots\mu_m}_q(0) |\pi, P_1\rangle = 2 \sum_{k=0}^{m+1} H^{q,m}_{\pi,k}(t) \left(-\frac{\Delta^{\{\mu_0}}{2}\right) \ldots \left(-\frac{\Delta^{\mu_{k-1}}}{2}\right) P^{\mu_k} \ldots P^{\mu_m\}} , \qquad (4.20)$$

---

[3]The covariant derivative appears when considering a general gauge with a Wilson line for the bi-local operator. Here, we used the light-cone gauge and ended up with the usual derivative in Eq. (4.18).

[4]Our operator in Eq. (4.18) indeed fulfills that since we have only plus-indices.

where H_k^m are *Generalized Form Factors* (GFFs)..

We immediately deduce from this the structure of the Mellin moment of Eq. (4.18):

$$
\begin{aligned}
H_\pi^{q,m}(\xi,t) &= \frac{1}{(P^+)^{m+1}} \sum_{\substack{k=0 \\ k \text{ even}}}^{m+1} H_{\pi,k}^{q,m}(t) \left(-\frac{\Delta^+}{2}\right)^k (P^+)^{m+1-k} \\
&= \sum_{\substack{k=0 \\ k \text{ even}}}^{m+1} H_{\pi,k}^{q,m}(t) \, \xi^k .
\end{aligned}
\tag{4.21}
$$

This is the so-called *Polynomiality* property: the mth x-moments of the GPD are polynomials of order $m+1$ in the skewness ξ. We should remark that only the k-even form factors are non-vanishing, due to the ξ-parity of the GPD.

4.1.5. Positivity

On top of polynomiality, the second main constraint on GPDs is called *Positivity*. For the quark GPD in the scalar case of Eq. (4.1), it takes the following form:

$$
|H_\pi^q(x,\xi,t)| \leq \sqrt{q_\pi\left(\frac{x+\xi}{1+\xi}\right) q_\pi\left(\frac{x-\xi}{1-\xi}\right)},
\tag{4.22}
$$

in the region $x \geq \xi$, with a similar relation involving the anti-quark PDF $\bar{q}_\pi$ in the region $x \leq -\xi$. This gives a bound on the GPD in the DGLAP region, in terms of its forward limit (the PDF) for the emitted and reabsorbed partons of momentum fractions $k_1^+/P_1^+ = (x+\xi)/(1+\xi)$ and $k_2^+/P_2^+ = (x-\xi)/(1-\xi)$ with respect to the initial and final hadron momenta respectively.

A weaker bound (involving a prefactor $1/\sqrt{1-\xi^2}$) for the pion was first derived in Ref. [10]. Here, we are considering a stronger bound as in Ref. [1] for instance. The proof can be straightforward when using the overlap representation of GPDs in terms of Light-front wave-functions. We will therefore postpone it to Chap. 6.

4.2. Generalized Parton Distributions of the nucleon

Let us now extend the scalar case to a spin-$^1/_2$ hadron, the nucleon. Contrary to the pion case, we will not use any subscript nor specify the particle in the hadron states. In its absence, the nucleon (and often especially the proton) is implied.

4.2.1. Definition

The same matrix element as in Eq. (4.1) gives rise now to two independent GPDs H and E due to the spin-$^1/_2$ structure of the hadron:

$$
\begin{aligned}
F_{\Lambda_2,\Lambda_1}^q &= \frac{1}{2} \int \frac{\mathrm{d}z^-}{2\pi} e^{i\,x\,P^+ z^-} \langle P_2,\Lambda_2| \bar{\psi}^q\left(-\frac{z}{2}\right) \gamma^+ \psi^q\left(\frac{z}{2}\right) |P_1,\Lambda_1\rangle \Big|_{\substack{z^+=0 \\ z_\perp=0}} \\
&= \frac{1}{2P^+} \left[H^q(x,\xi,t)\,\bar{u}(P_2,\Lambda_2)\gamma^+ u(P_1,\Lambda_1) + E^q(x,\xi,t)\,\bar{u}(P_2,\Lambda_2)\frac{i\sigma^{+\mu}\Delta_\mu}{2M_H}u(P_1,\Lambda_1) \right],
\end{aligned}
\tag{4.23}
$$

where M_H is the hadron mass and we refer to the appendix A.1 for the Dirac spinor and matrices notations.

Additionally, we can now consider also the axial-vector sector, which defines two other chiral-even GPDs $\tilde{H}$ (which was vanishing in the scalar case due to parity invariance) and $\tilde{E}$, often called *polarized* GPDs:

$$\tilde{F}^q_{\Lambda_2,\Lambda_1} = \frac{1}{2} \int \frac{\mathrm{d}z^-}{2\pi} e^{i\,x\,P^+z^-} \left. \langle P_2, \Lambda_2| \bar{\psi}^q \left(-\frac{z}{2}\right) \gamma^+\gamma_5 \psi^q \left(\frac{z}{2}\right) |P_1, \Lambda_1\rangle \right|_{\substack{z^+=0\\z_\perp=0}}$$
$$= \frac{1}{2\,P^+} \left[\tilde{H}^q(x,\xi,t)\, \bar{u}\,(P_2,\Lambda_2)\, \gamma^+\gamma_5 u\,(P_1,\Lambda_1) + \tilde{E}^q(x,\xi,t)\, \bar{u}\,(P_2,\Lambda_2)\, \frac{\gamma_5\Delta^+}{2\,M_H} u\,(P_1,\Lambda_1) \right]. \tag{4.24}$$

We will not consider chiral-odd quark GPDs as they do not intervene in DVCS phenomenology, but we can introduce chiral-even gluon GPDs as they do enter the DVCS cross-section at NLO. The gluon matrix elements defining H^g, E^g, $\tilde{H}^g$ and $\tilde{E}^g$ are as follows:

$$F^g_{\Lambda_2,\Lambda_1} = \frac{1}{P^+} \int \frac{\mathrm{d}z^-}{2\pi} e^{i\,x\,P^+z^-} \left. \langle P_2, \Lambda_2| G^{+\mu} \left(-\frac{z}{2}\right) {G_\mu}^+ \left(\frac{z}{2}\right) |P_1, \Lambda_1\rangle \right|_{\substack{z^+=0\\z_\perp=0}}$$
$$= \frac{1}{2\,P^+} \left[H^g(x,\xi,t)\, \bar{u}\,(P_2,\Lambda_2)\, \gamma^+ u\,(P_1,\Lambda_1) + E^g(x,\xi,t)\, \bar{u}\,(P_2,\Lambda_2)\, \frac{i\sigma^{+\mu}\Delta_\mu}{2\,M_H} u\,(P_1,\Lambda_1) \right], \tag{4.25}$$

$$\tilde{F}^g_{\Lambda_2,\Lambda_1} = \frac{1}{iP^+} \int \frac{\mathrm{d}z^-}{2\pi} e^{i\,x\,P^+z^-} \left. \langle P_2, \Lambda_2| G^{+\mu} \left(-\frac{z}{2}\right) {\tilde{G}_\mu}^+ \left(\frac{z}{2}\right) |P_1, \Lambda_1\rangle \right|_{\substack{z^+=0\\z_\perp=0}}$$
$$= \frac{1}{2\,P^+} \left[\tilde{H}^g(x,\xi,t)\, \bar{u}\,(P_2,\Lambda_2)\, \gamma^+\gamma_5 u\,(P_1,\Lambda_1) + \tilde{E}^g(x,\xi,t)\, \bar{u}\,(P_2,\Lambda_2)\, \frac{\gamma_5\Delta^+}{2\,M_H} u\,(P_1,\Lambda_1) \right], \tag{4.26}$$

where $G^{\mu\nu}$ is the gluon field strength tensor.

To extract the GPDs H^a, E^a,... from the helicity-dependent matrix elements F^a and $\tilde{F}^a$, with $a = q, g$, we can use the following dictionary [1, 25, 166]:

$$F^a_{++} = F^a_{--} = \sqrt{1-\xi^2} \left[H^a - \frac{\xi^2}{1-\xi^2} E^a \right], \tag{4.27}$$

$$F^a_{-+} = -\left(F^a_{+-}\right)^* = \frac{\Delta^1 + i\,\Delta^2}{2\,M_H\,\sqrt{1-\xi^2}}\, E^a, \tag{4.28}$$

$$\tilde{F}^a_{++} = -\tilde{F}^a_{--} = \sqrt{1-\xi^2} \left[\tilde{H}^a - \frac{\xi^2}{1-\xi^2} \tilde{E}^a \right], \tag{4.29}$$

$$\tilde{F}^a_{-+} = \left(\tilde{F}^a_{+-}\right)^* = \frac{\Delta^1 + i\,\Delta^2}{2\,M_H}\, \frac{\xi}{\sqrt{1-\xi^2}}\, \tilde{E}^a, \tag{4.30}$$

where the subscripts $+$ or $-$ denote the hadron helicities as explicitly written in Eq. (4.23), and Δ^j, $j = 1, 2$, are the components of $\mathbf{\Delta}_\perp$. We can see now why E is considered the hadron helicity flip GPD (and therefore is absent in the scalar case), while H conserves hadron helicity.

4.2.2. Properties

Similarly to the scalar case, we will list the important properties of the thus defined nucleon GPDs, but without explaining the derivation this time.

Forward limit

The limit $\Delta = 0$ gives the following relations:

$$H^q\left(x, 0, 0\right) = q\left(x\right)\theta\left(x\right) - \bar{q}\left(-x\right)\theta\left(-x\right), \qquad H^g\left(x, 0, 0\right) = |x|\, g\left(|x|\right), \qquad (4.31)$$

$$\tilde{H}^q\left(x, 0, 0\right) = \Delta q\left(x\right)\theta\left(x\right) + \Delta\bar{q}\left(-x\right)\theta\left(-x\right), \qquad \tilde{H}^g\left(x, 0, 0\right) = x\,\Delta g\left(|x|\right), \qquad (4.32)$$

where a and Δa are respectively the unpolarized and polarized PDFs, for $a = q, g$.

We can say nothing about the forward limit of E (or $\tilde{E}$), given the prefactor linear in Δ (see for instance Eq. (4.23)). Its contribution to the matrix element vanishes when $\Delta = 0$, despite the GPD itself not necessarily vanishing. In fact, this forward limit is crucial to understanding the nucleon spin decomposition, as made explicit by Ji's sum rule (2.34), but it cannot be linked to any PDF extracted from inclusive processes. Only the exclusive processes can allow to access this information, with an extrapolation of the GPD for non-vanishing momentum transfer Δ.

Domain

As was mentioned in Sec. 4.1, the domain for (x, ξ) is $[-1, 1]^2$.

In addition to this, the relation[5]

$$-t = \frac{4\,\xi^2\,M_H^2 + \mathbf{\Delta}_\perp^2}{1 - \xi^2}, \qquad (4.33)$$

with $\mathbf{\Delta}_\perp^2 \geq 0$, implies that $-t$ is bounded from below or, equivalently, that ξ has an upper bound:

$$-t \geq -t_{\min}\left(\xi\right) = \frac{4\,\xi^2\,M_H^2}{1 - \xi^2}, \qquad |\xi| \leq \xi_{\max}\left(t\right) = \sqrt{\frac{-t}{-t + 4\,M_H^2}}. \qquad (4.34)$$

This significantly limits the accessible region in ξ, which is a considerable issue for the covariant extension of Part. III. For example, with a value of $-t = 0.2$ GeV^2, we have $\xi_{\max} \sim 0.23$ for the nucleon. In principle, we can extend the GPD by analytic continuation to imaginary values of $\Delta_\perp$ (negative $\mathbf{\Delta}_\perp^2$), and therefore consider the full domain in ξ (as it is possible for fully algebraic models such as the one of Sec. 9.2), but these are non-physical values of ξ.

Symmetries

As in the scalar case, we can show that all GPDs considered here are real-valued and even in ξ:

$$\left(\text{GPD}^a\left(x, \xi, t\right)\right)^* = \text{GPD}^a\left(x, -\xi, t\right) = \text{GPD}^a\left(x, \xi, t\right), \qquad (4.35)$$

---

[5]It can be derived from the parametrization of Eqs. (6.8)-(6.9).

with GPD $= H, E, \tilde{H}, \tilde{E}$ and $a = q, g$.

In addition, gluons being their own anti-particles, we have the following parity relations in x:

$$H^g\left(-x,\xi,t\right) = H^g\left(x,\xi,t\right) , \qquad\qquad \tilde{H}^g\left(-x,\xi,t\right) = -\tilde{H}^g\left(x,\xi,t\right) , \qquad (4.36)$$

$$E^g\left(-x,\xi,t\right) = E^g\left(x,\xi,t\right) , \qquad\qquad \tilde{E}^g\left(-x,\xi,t\right) = -\tilde{E}^g\left(x,\xi,t\right) , \qquad (4.37)$$

i.e. x-even unpolarized and x-odd polarized gluon GPDs.

Polynomiality

The sum rules for each nucleon GPD are:

$$H^{q,m}\left(\xi,t\right) = \int_{-1}^{1} x^m H^q\left(x,\xi,t\right) \mathrm{d}x = \sum_{\substack{k=0 \\ k\,\mathrm{even}}}^{m} H_k^{q,m}\left(t\right)\xi^k + \mathrm{mod}\left(m,2\right) D^{q,m}\left(t\right)\xi^{m+1} , \qquad (4.38)$$

$$E^{q,m}\left(\xi,t\right) = \int_{-1}^{1} x^m E^q\left(x,\xi,t\right) \mathrm{d}x = \sum_{\substack{k=0 \\ k\,\mathrm{even}}}^{m} E_k^{q,m}\left(t\right)\xi^k - \mathrm{mod}\left(m,2\right) D^{q,m}\left(t\right)\xi^{m+1} , \qquad (4.39)$$

$$\tilde{H}^{q,m}\left(\xi,t\right) = \int_{-1}^{1} x^m \tilde{H}^q\left(x,\xi,t\right) \mathrm{d}x = \sum_{\substack{k=0 \\ k\,\mathrm{even}}}^{m} \tilde{H}_k^{q,m}\left(t\right)\xi^k , \qquad (4.40)$$

$$\tilde{E}^{q,m}\left(\xi,t\right) = \int_{-1}^{1} x^m \tilde{E}^q\left(x,\xi,t\right) \mathrm{d}x = \sum_{\substack{k=0 \\ k\,\mathrm{even}}}^{m} \tilde{E}_k^{q,m}\left(t\right)\xi^k , \qquad (4.41)$$

$$H^{g,m}\left(\xi,t\right) = \int_{-1}^{1} x^m H^g\left(x,\xi,t\right) \mathrm{d}x = \mathrm{mod}\left(m+1,2\right)\left[\sum_{\substack{k=0 \\ k\,\mathrm{even}}}^{m+1} H_k^{g,m}\left(t\right)\xi^k + D^{g,m}\left(t\right)\xi^{m+2}\right] ,$$
$$(4.42)$$

$$E^{g,m}\left(\xi,t\right) = \int_{-1}^{1} x^m E^g\left(x,\xi,t\right) \mathrm{d}x = \mathrm{mod}\left(m+1,2\right)\left[\sum_{\substack{k=0 \\ k\,\mathrm{even}}}^{m+1} E_k^{g,m}\left(t\right)\xi^k - D^{g,m}\left(t\right)\xi^{m+2}\right] ,$$
$$(4.43)$$

$$\tilde{H}^{g,m}\left(\xi,t\right) = \int_{-1}^{1} x^m \tilde{H}^g\left(x,\xi,t\right) \mathrm{d}x = \mathrm{mod}\left(m,2\right)\sum_{\substack{k=0 \\ k\,\mathrm{even}}}^{m+1} \tilde{H}_k^{g,m}\left(t\right)\xi^k , \qquad (4.44)$$

$$\tilde{E}^{g,m}\left(\xi,t\right) = \int_{-1}^{1} x^m \tilde{E}^g\left(x,\xi,t\right) \mathrm{d}x = \mathrm{mod}\left(m,2\right)\sum_{\substack{k=0 \\ k\,\mathrm{even}}}^{m+1} \tilde{E}_k^{g,m}\left(t\right)\xi^k . \qquad (4.45)$$

Several crucial points should be noticed:

- The GPDs being ξ-even, only the even powers in ξ have non-vanishing coefficients.

- Specializing for $m = 0$, we have again the sum rules linking GPDs to the Elastic Form Factors:

$$\int_{-1}^{1} H^q\left(x,\xi,t\right) \mathrm{d}x = F_1^q\left(t\right) , \qquad\qquad \int_{-1}^{1} \tilde{H}^q\left(x,\xi,t\right) \mathrm{d}x = G_A^q\left(t\right) , \qquad (4.46)$$

$$\int_{-1}^{1} E^q\left(x,\xi,t\right) \mathrm{d}x = F_2^q\left(t\right) , \qquad\qquad \int_{-1}^{1} \tilde{E}^q\left(x,\xi,t\right) \mathrm{d}x = G_P^q\left(t\right) , \qquad (4.47)$$

where F_1 and F_2 are the Dirac and Pauli electromagnetic form factors, whereas G_A and G_P are the axial-vector and pseudo-scalar form factors, respectively. See Sec. 1.1.2.

- The Gravitational Form Factors A, B and C introduced in Eq. (2.31) correspond for quarks to $H_0^{q,1}$, $E_0^{q,1}$ and $\frac{1}{4}D^{q,1}$ respectively in Eqs. (4.38)-(4.39), and for gluons to $\frac{1}{2}H_0^{g,0}$, $\frac{1}{2}E_0^{g,0}$ and $\frac{1}{8}D^{g,0}$ in Eqs. (4.42)-(4.43).

- H^q and E^q share the same $(m+1)$-degree coefficient (*i.e.* the dominant one when m is odd):

$$H_{m+1}^{q,m} = -E_{m+1}^{q,m} = D^{q,m} \,. \tag{4.48}$$

This means in particular that the sum rule of $H^q + E^q$ is a polynomial of degree m, just like the polarized GPDs. The same type of remark can be made for gluons, by adapting the degrees ($m+2$ instead of $m+1$). Moreover, the coefficients D^m define what is called the D-term:

$$\int_{-1}^{1} \alpha^m D\left(\alpha, t\right) \mathrm{d}\alpha = D^m\left(t\right) \,, \tag{4.49}$$

which is an odd function of α (consequence of the ξ-parity). The D-term will play an important role when it comes to the Double Distributions representation (Chap. 5) and the covariant extension of GPDs (Part. III).

- The gluon GPDs having a definite x-parity (4.36)-(4.37), only the m-even moments of H^g and E^g and m-odd moments of $\tilde{H}^g$ and $\tilde{E}^g$ are non-vanishing.

Positivity

We can write the following positivity bound for unpolarized quark GPDs [167]:

$$\left[H^q\left(x,\xi,t\right) - \frac{\xi^2}{1-\xi^2}E^q\left(x,\xi,t\right)\right]^2 + \left[\frac{\Delta_\perp E^q\left(x,\xi,t\right)}{2\,M_H\,\left(1-\xi^2\right)}\right]^2 \leq \frac{1}{1-\xi^2}\, q\left(\frac{x+\xi}{1+\xi}\right) q\left(\frac{x-\xi}{1-\xi}\right)\,. \tag{4.50}$$

But more general and stronger bounds (involving all kinds of PDFs, not just the unpolarized one) can also be found in Ref. [168].

The simple bound for H as seen for the pion (4.22) is not valid for the nucleon, but one can derive from Eq. (4.50) a weaker bound depending on t, as done in Ref. [167].

Chapter 5.

Polynomiality and the Double Distributions representation

Throughout this chapter, the pion-quark case will be considered for simplicity. To lighten the notation, the subscript π, the t-dependence and superscript q will be dropped, unless necessary. This is because t is only a fixed parameter in the following, and the flavour plays no significant role.

5.1. Fulfilling Polynomiality

We have seen in the previous chapter the polynomiality property of GPDs, that we can rewrite here:

$$H^m\left(\xi\right) = \int_{-1}^{1} x^m H\left(x,\xi\right)\mathrm{d}x = \sum_{\substack{k=0 \\ k \text{ even}}}^{m+1} H_k^m \xi^k\,. \tag{5.1}$$

This is known as a characterization of the image of the Radon transform [15, 169]. See App. B for details on this particular mathematical operator, well known in tomography applications, such as medical imaging.

Contrary to what is presented in App. B, here the degree of the polynomial is $m+1$, which does not allow to directly apply the theorem B.3. To circumvent this issue, we can consider for instance the difference quotient of H with respect to ξ, instead of H itself:

$$\int_{-1}^{1} x^m \frac{H\left(x,\xi\right) - H\left(x,0\right)}{\xi}\,\mathrm{d}x = \sum_{\substack{k=0 \\ k \text{ odd}}}^{m} H_{k+1}^m \xi^k\,. \tag{5.2}$$

Assuming that this difference quotient is well-behaved (which means more or less that we assume $\xi \mapsto H\left(x,\xi\right)$ to be differentiable on 0), we can now use the theorem B.3 and state the existence of a function $h_{\mathrm{T}}\left(\beta,\alpha\right)$[1,2] such that:

$$H\left(x,\xi\right) = H\left(x,0\right) + \xi \iint \mathrm{d}\beta\,\mathrm{d}\alpha\,\delta\left(x - \beta - \xi\alpha\right) h_{\mathrm{T}}\left(\beta,\alpha\right)\,, \tag{5.3}$$

---

[1]The somewhat strange non-alphabetical choice of variables is due to Ref. [170], and was kept also in the main reviews [1, 2], so we use it here to avoid further confusion.

[2]The choice of notation with a subscript T will be made clear in Sec. 5.3.6. It should not be confused with the notation used for transversity distributions, as we do not consider them at all in this thesis.

where h_{T} is called a *Double Distribution* (DD) and in this case is an odd function of α, given that H is ξ-even.

We can now verify by integrating Eq. (5.3) that the polynomiality property is indeed manifest:

$$\int_{-1}^{1} x^m H\left(x, \xi\right) \mathrm{d}x = \int_{-1}^{1} x^m H\left(x, 0\right) \mathrm{d}x + \xi \iint \mathrm{d}\beta \, \mathrm{d}\alpha \, \left(\beta + \xi \alpha\right)^m h_{\text{T}}\left(\beta, \alpha\right) , \qquad (5.4)$$

and that the Generalized Form Factors are given in terms of the DD h_{T} as:

$$H_0^m = \int_{-1}^{1} x^m H\left(x, 0\right) \mathrm{d}x ,$$

$$H_k^m = \binom{m}{k-1} h_{\text{T}}^{m-(k-1),\, k-1} , \qquad\qquad 1 \leq k \leq m+1 , \qquad (5.5)$$

where we defined the moments of h_{T} as

$$h_{\text{T}}^{j,k} = \iint \mathrm{d}\beta \, \mathrm{d}\alpha \, \beta^j \alpha^k \, h_{\text{T}}\left(\beta, \alpha\right) . \qquad (5.6)$$

In our context of GPDs, a DD representation is therefore the natural expression of polynomiality. In other words, a GPD can be represented as a Radon transform of a DD, and this is not just for modelling purposes, but a fundamental property.

5.2. Definition and properties of Double Distributions

In general, we can define two DDs f and g from the matrix element of Eq. (4.1), when using a two-dimensional Fourier transform this time:

$$\left\langle P + \frac{\Delta}{2} \middle| \bar{\psi}^q \left(-\frac{z^-}{2}\right) \gamma^+ \psi^q \left(\frac{z^-}{2}\right) \middle| P - \frac{\Delta}{2} \right\rangle \qquad (5.7)$$

$$= \iint_{\Omega} \mathrm{d}\beta \, \mathrm{d}\alpha \, e^{-i\beta P^+ z^- + i\alpha \frac{1}{2}\Delta^+ z^-} \left(2P^+ f\left(\beta, \alpha\right) - \Delta^+ g\left(\beta, \alpha\right)\right) .$$

The reason why there are two vector structures P^μ and Δ^μ (versus only one in the case of the GPD) is due to the two-dimensional Fourier transform; we are considering that $P^+ z^-$ and $\Delta^+ z^-$ are two independent variables, *i.e.* we do not fix the variable ξ.

The DD f has been independently introduced by Müller *et al.* [5] (under the denomination of "spectral function") and Radyushkin [97], while the need for an additional DD g was first pointed out by Polyakov and Weiss [171].

5.2.1. Relation to GPDs

By taking the Fourier transform (as in the definition of the GPD (4.1)) of Eq. (5.7),

$$\int \frac{\mathrm{d}z^-}{2\pi} e^{i x P^+ z^-} \left\langle P + \frac{\Delta}{2} \middle| \bar{\psi}^q \left(-\frac{z^-}{2}\right) \gamma^+ \psi^q \left(\frac{z^-}{2}\right) \middle| P - \frac{\Delta}{2} \right\rangle \qquad (5.8)$$

$$= 2P^+ \iint_{\Omega} \mathrm{d}\beta \, \mathrm{d}\alpha \int \frac{\mathrm{d}z^-}{2\pi} e^{i P^+ z^- (x - \beta - \alpha\xi)} \left(f\left(\beta, \alpha\right) + \xi \, g\left(\beta, \alpha\right)\right)$$

$$= 2P^+ \iint_{\Omega} \mathrm{d}\beta \, \mathrm{d}\alpha \, \delta\left(P^+ \left(x - \beta - \xi\alpha\right)\right) \left(f\left(\beta, \alpha\right) + \xi \, g\left(\beta, \alpha\right)\right),$$

we end up with the following relation between the GPD H and the DDs f and g, generalizing Eq. (5.3),

$$H\left(x,\xi\right) = \iint_\Omega \mathrm{d}\beta\,\mathrm{d}\alpha\,\delta\left(x - \beta - \xi\alpha\right)\left(f\left(\beta,\alpha\right) + \xi\,g\left(\beta,\alpha\right)\right). \tag{5.9}$$

The DDs are a natural solution of the polynomiality constraint, as shown in Sec. 5.1 and can be rewritten here in a more general way:

$$\int_{-1}^1 x^m H\left(x,\xi\right)\mathrm{d}x = \iint_\Omega \mathrm{d}\beta\,\mathrm{d}\alpha\,\left(\beta + \xi\alpha\right)^m\left(f\left(\beta,\alpha\right) + \xi\,g\left(\beta,\alpha\right)\right), \tag{5.10}$$

with the GFFs given by:

$$
\begin{aligned}
H_0^m &= f^{m,0}\,, \\
H_k^m &= \binom{m}{k} f^{m-k,\,k} + \binom{m}{k-1} g^{m-(k-1),\,k-1}\,, \qquad 1 \le k \le m\,, \\
H_{m+1}^m &= g^{0,\,m}\,,
\end{aligned} \tag{5.11}
$$

with the moments of f and g defined as in Eq. (5.6). It should be noted that only f contributes to zeroth order coefficients (*i.e.* the non-skewed limit), while only g contributes to the $(m+1)$-degree terms which correspond to what we called the D-term contributions. See Sec. 5.3.3.

Historically, DDs have been used to model GPDs based on extracted PDFs in the framework of the Radyushkin Double Distribution Ansatz [172]. We can cite for instance the popular Goloskokov-Kroll model [152, 155, 156] as an example of the family of models following this approach. Due to the success of these phenomenological models, DDs have been considered by most as a convenient way to implement polynomiality in GPD models. It may have become a common misconception to believe that DDs appear only in this restricted subset of GPD parametrizations. On the contrary, the reasoning in Sec. 5.1 and App. B shows that DDs are the *essence* of the polynomiality property. Obeying the polynomiality property is *exactly equivalent* to being constructed from a DD, and this is a key argument of the approach of Part. III.

5.2.2. Support

The compact support of DDs is the square

$$\Omega = \{(\beta,\alpha)\,/\,|\beta| + |\alpha| \le 1\} \tag{5.12}$$

and we refer to Refs. [97, 173] for the proof using the α-representation of Feynman diagrams. It can be however easily confirmed from the support of the GPD, as we will further clarify.

For the purpose of this paragraph, we will ignore the DD g and consider only f. H is in this case the Radon transform of f; it is obtained by integrating f over lines parametrized by x and ξ through the equation:

$$x - \beta - \alpha\,\xi = 0\,, \tag{5.13}$$

and whose slope is $-\frac{1}{\xi}$. We will denote these lines by $\mathcal{L}\left(x,\xi\right)$. This means we perform the line integral:

$$H\left(x,\xi\right) = \int_{\mathcal{L}(x,\xi)} f\left(\beta\left(s\right),\alpha\left(s\right)\right)\mathrm{d}s\,. \tag{5.14}$$
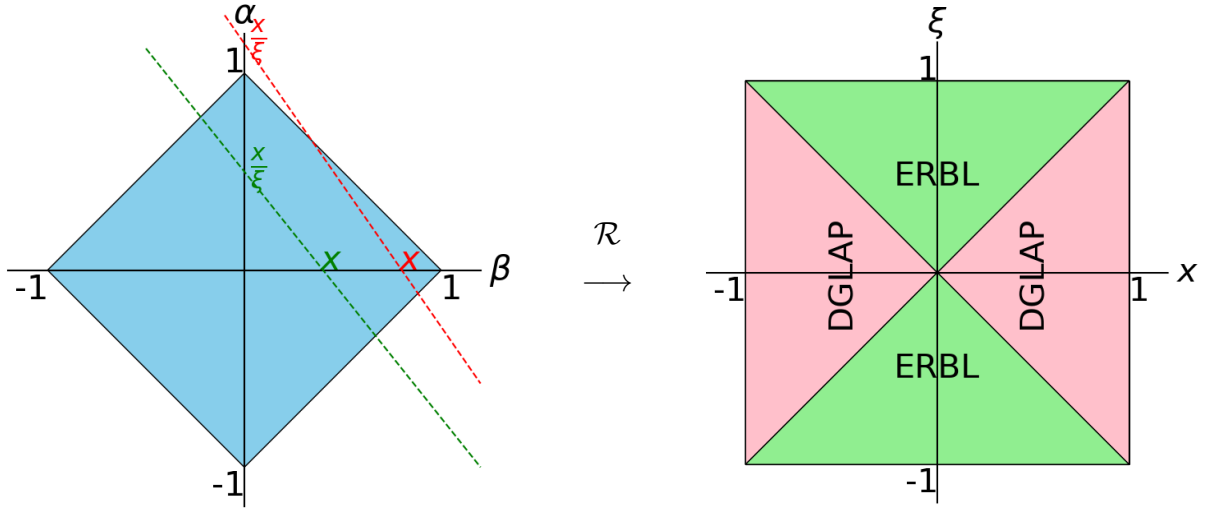
Figure 5.1. The domains $\Omega^<$ and $\Omega^>$ of the DD (resp. DGLAP and ERBL of the GPD) on the left (resp. right). The Radon transform $\mathcal{R}f(x,\xi) = \int d\beta d\alpha\, f(\beta,\alpha)\,\delta(x - \beta - \alpha\xi)$, which is an integration of f on a line parameterized by the couple (x,ξ), is the operation that sends one domain to the other. The red lines that cross the α axis on $x/\xi > 1$ correspond to DGLAP kinematics. ERBL lines are represented in green. In this example, both x and ξ are positive.

Figure 5.1 illustrates the DD domain and the above line integration. As can be seen, the considered lines cross the α-axis at $\alpha = x/\xi$ and the β-axis at $\beta = x$. When $|\xi| < 1$, a point (β, α) in the square Ω will only contribute to lines where $|x| < 1$, since the slope is constrained to be greater than 1 in absolute value. We recover the GPD support. On the other hand, a point outside Ω may also contribute to lines with $|\xi| < 1$ and $|x| > 1$, for which the GPD should be vanishing. Hence why the support of the DD is limited to Ω. This can also be proven rigorously using Thm. B.4.

An important but straightforward consequence of the ξ-parity of the GPD (and therefore of time reversal) is the following definite parity of the DDs:

$$f(\beta, -\alpha) = f(\beta, \alpha), \qquad\qquad g(\beta, -\alpha) = -g(\beta, \alpha), \qquad\qquad (5.15)$$

i.e. f is α-even, whereas g is α-odd. This reduces the domain of interest to only half the square.

5.2.3. Interpretation

A physical interpretation is significantly more difficult for DDs compared to GPDs, given the fact that they are not defined for fixed P and Δ (or equivalently for fixed P_1 and P_2) as it can be the case for GPDs (where we fix the constraint $\xi = -\frac{\Delta^+}{2P^+}$). We can nevertheless follow the diagram of Fig. 5.2 (left panel) as a guideline to get an understanding of the variables β and α.

In the forward limit, $\Delta = 0$, the momentum flows in the s-channel only, with the parton carrying a momentum fraction β of the hadron momentum P^+. We can therefore identify β with the usual PDF variable x. This is confirmed by the fact that the integration over α of the
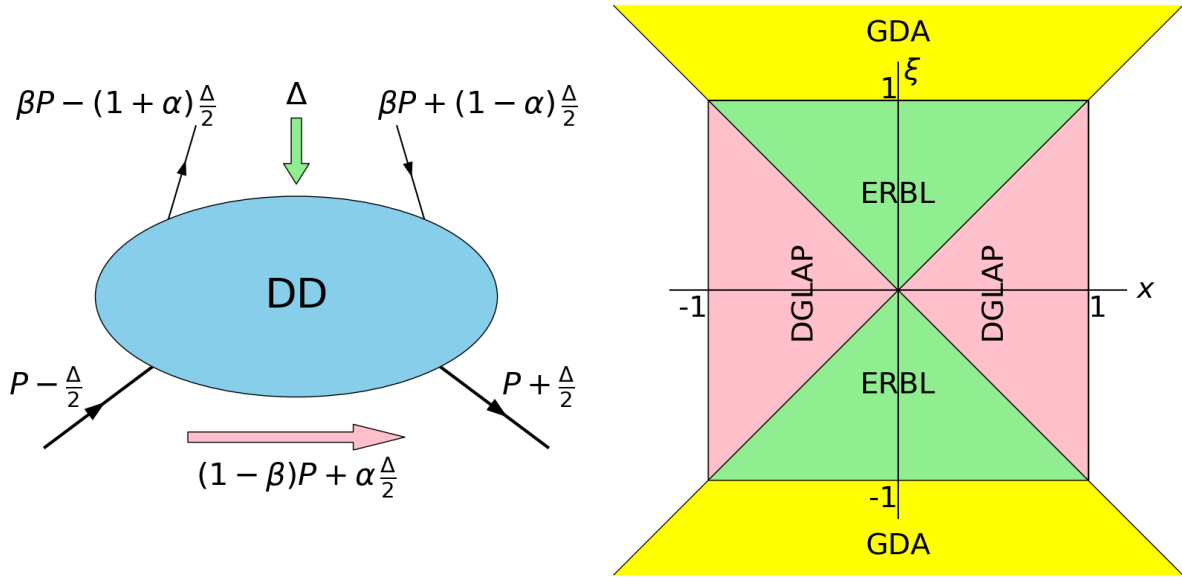
Figure 5.2. Left: DD diagram with associated momenta of hadrons and partons. Momentum flow in s-channel (in pink) and t-channel (in green). **Right**: GDA domain (in yellow) in GPD variables: $|\xi| \geq |x|$ and $|\xi| \geq 1$.

DD yields the PDF at $x = \beta$:

$$H(x, 0) = \int_{-1}^{1} \mathrm{d}\alpha \, f(x, \alpha) \ . \tag{5.16}$$

On the other hand, when $P = 0$, the momentum flows in the t-channel with the partons carrying momentum fractions $\frac{(1+\alpha)}{2}$ and $\frac{(1-\alpha)}{2}$ (if they are both taken as incoming) of Δ^+. The diagram looks like the one of a meson Distribution Amplitude, represented in Fig. 5.3 (right panel). The variable α can therefore be thought of as a DA variable.

This merger of two distinct non-perturbative distributions explains the origin of the name *Double Distribution*.

5.2.4. Extension to Generalized Distribution Amplitudes

All we know about the GPD support is that the DGLAP region $|x| \geq |\xi|$ for $|x| \geq 1$ is vanishing. On the other hand, the r.h.s. of Eq. (5.9) does not necessarily vanish on the extended ERBL region $|\xi| \geq |x|$ for $|\xi| \geq 1$ (represented in Fig. 5.2, right panel), despite not being part of the GPD domain.

In fact, it corresponds to the kinematics of Generalized Distribution Amplitudes (GDAs) [5, 174, 175]. These objects describe the transition from a quark-antiquark pair into a hadron-antihadron pair, instead of just one hadron as it is the case for Distributions Amplitudes. In a sense, they generalize DAs for larger numbers of hadrons[3].

Diagrammatically, they are the crossed-channel equivalent of GPDs. Turned upside down (*i.e.* rotated by $\frac{\pi}{2}$), the diagram of Fig. 4.1 would represent a GDA with incoming partons and

---

[3]Here, we are only considering two hadrons as we are interested in their link to GPDs.
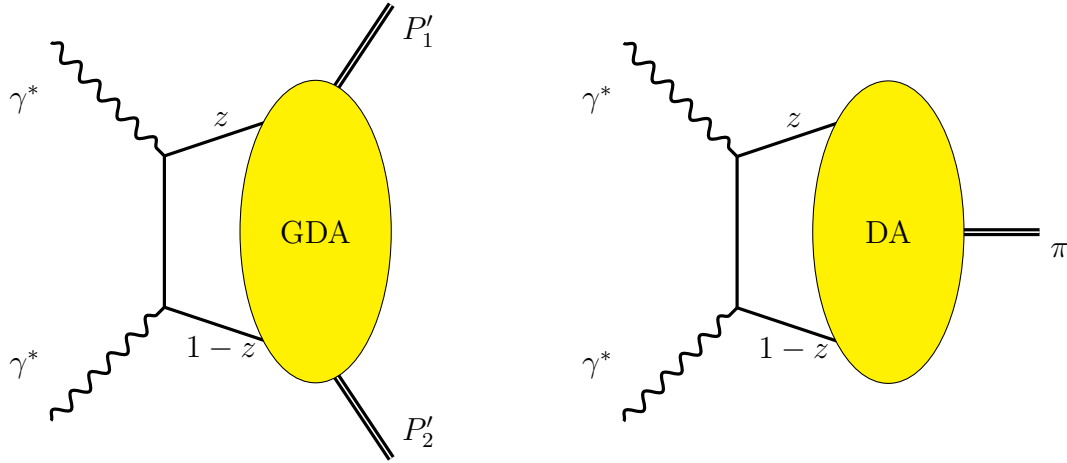
Figure 5.3. Handbag diagrams for $\gamma^*\gamma^* \to h\bar{h}$ (pair hadron-antihadron, left) and $\gamma^*\gamma^* \to \pi$ (right), where GDAs and DAs are respectively accessed.

outgoing hadrons. Following Ref. [1], we can use the following conventions with respect to the GPD momenta:

$$
\begin{aligned}
P'_1 &= P_2\,, & k'_1 &= k_2\,, \\
P'_2 &= -P_1\,, & k'_2 &= -k_1\,,
\end{aligned}
\tag{5.17}
$$

where the momenta for the GDA (denoted by a prime) are indexed by 1 for the hadron and quark, and 2 for the antihadron and antiquark. The same letter convention as for GPDs is used; k for partons and P for hadrons. Figure 5.3 represents the diagrams of GDAs and DAs in the simplest processes where they intervene.

The GDAs depend on three invariant scalars defined by:

$$
\begin{aligned}
z &= \frac{k'^{+}_1}{P'^{+}_1 + P'^{+}_2}\,, \\
\zeta &= \frac{P'^{+}_1}{P'^{+}_1 + P'^{+}_2}\,, \\
s &= \left(P'_1 + P'_2\right)^2\,.
\end{aligned}
\tag{5.18}
$$

From Eq. (5.17), we deduce that the Mandelstam variable $s \geq 0$ corresponds to the momentum transfer $t \leq 0$ in the case of GPDs, but in the timelike region. GDAs (timelike objects) are therefore analytic continuations of GPDs (spacelike objects). We also deduce the relations:

$$
1 - 2z = \frac{x}{\xi}\,, \qquad\qquad 1 - 2\zeta = \frac{1}{\xi}\,.
\tag{5.19}
$$

From the support $0 \leq z \leq 1$ and $0 \leq \zeta \leq 1$ of GDAs, we can confirm that the extended ERBL region of Fig. 5.2 (right panel) corresponds indeed to the GDA domain.

We can now write the GDA Φ, the analytic continuation of the GPD H, in terms of the

DDs (f, g):

$$-\frac{1}{2}\Phi(z, \zeta, s) = \iint_{\Omega} \mathrm{d}\beta \, \mathrm{d}\alpha \, \delta\left(1 - 2z - \beta(1 - 2\zeta) - \alpha\right)\left((1 - 2\zeta)f(\beta, \alpha, s) + g(\beta, \alpha, s)\right),$$

(5.20)

where the factor $-\frac{1}{2}$ is due to different conventions in the matrix element definitions of GPDs and GDAs. We used the same notation for the DDs and their analytic continuation to positive values of $t = s$.

5.2.5. Quark and anti-quark distributions

The DD f (and similarly for g) can be decomposed as follows:

$$f = f^> + f^<, \qquad \text{with} \qquad \begin{aligned} f^>(\beta, \alpha) &= f(\beta, \alpha)\,\theta(\beta), \\ f^<(\beta, \alpha) &= f(\beta, \alpha)\,\theta(-\beta), \end{aligned}$$

(5.21)

where $f^>$ and $f^<$ are called respectively "quark" (with support on $\Omega^> = \Omega \cap \{\beta > 0\}$), and "anti-quark" (with support on $\Omega^< = \Omega \cap \{\beta < 0\}$) distributions [1]. They yield the following "quark" and "anti-quark" GPDs (corresponding to Radyushkin's original GPDs [176]):

$$H^>(x, \xi) = \iint_{\Omega^>} \mathrm{d}\beta \mathrm{d}\alpha \, \delta(x - \beta - \alpha\xi)\left(f^>(\beta, \alpha) + \xi\, g^>(\beta, \alpha)\right),$$

(5.22)

with support $x \in [-\xi, +1]$, and

$$H^<(x, \xi) = \iint_{\Omega^<} \mathrm{d}\beta \mathrm{d}\alpha \, \delta(x - \beta - \alpha\xi)\left(f^<(\beta, \alpha) + \xi\, g^<(\beta, \alpha)\right),$$

(5.23)

with support on $x \in [-1, +\xi]$, the total GPD being of course $H = H^> + H^<$.

In particular, in the forward limit, we obtain the quark and anti-quark PDFs respectively:

$$\theta(x)\, q(x) \quad = H^{q>}(x, 0) = \int_{-1}^{1} \mathrm{d}\alpha \, f^{q>}(x, \alpha) \ ,$$

(5.24)

$$-\theta(-x)\, \bar{q}(-x) = H^{q<}(x, 0) = \int_{-1}^{1} \mathrm{d}\alpha \, f^{q<}(x, \alpha) \ ,$$

(5.25)

hence the chosen name of "quark" and "anti-quark" DDs or GPDs.

It should be noted that:

- In the DGLAP region, $H^>$ and $H^<$ are not correlated. They contribute independently to the positive x and the negative x DGLAP subdomains (which we may refer to in the following as DGLAP> and DGLAP<), respectively. In the ERBL region however, both interfere and they cannot be separated. The domain of $H^>$ for instance is sketched in Fig. 7.1.

- In the case of gluons, which are their own anti-particles, DDs are β-even (which reflects the x-parity of GPDs). $H^>$ and $H^<$ are not independent in that case, and one is recovered from the other by parity.

This nomenclature can be confusing since we are using the same name for both the full quark GPD H^q (with both quark and anti-quark contributions) and the quark contribution $H^{q>}$ (separated from its anti-quark counterpart). But in the following, we will consider only quark contributions to the GPD (*i.e.* the DD domain $\beta > 0$), unless explicitly stated otherwise. It should be therefore understood that H stands for $H^>$.

5.3. Different representations

5.3.1. Double Distributions ambiguity

As pointed out by Teryaev [16], the parametrization in terms of the DDs f and g is not unambiguous. If we consider for instance the Mellin moments (5.11) of the GPD H, we can see that they are invariant by the following transformation on the DDs moments:

$$f^{j,k} \longmapsto f^{j,k} - k\,\chi^{j,k-1}\,, \qquad\qquad g^{j,k} \longmapsto g^{j,k} + j\,\chi^{j-1,k}\,, \qquad (5.26)$$

which means that the decomposition (f, g) is not unique. Only the moments $f^{0,m}$ and $g^{m,0}$ determine the corresponding GFFs uniquely.

In the case of DDs vanishing on the edges of the square Ω[4], we can actually write the following transformation on (f, g) that leaves the GPD unchanged:

$$f(\beta, \alpha) \longmapsto f(\beta, \alpha) + \frac{\partial \chi}{\partial \alpha}(\beta, \alpha)\,, \qquad g(\beta, \alpha) \longmapsto g(\beta, \alpha) - \frac{\partial \chi}{\partial \beta}(\beta, \alpha)\,, \qquad (5.27)$$

assuming that χ fulfills the good parity property: $\chi(\beta, -\alpha) = -\chi(\beta, \alpha)$. This function is related to the previously written moments $\chi^{j,k}$ with the same definition as in Eq. (5.6). By analogy to electromagnetism, this is often called a "gauge transformation" in the literature. This analogy is not perfect and does not add much to the discussion, we therefore choose not to use it here. Instead of "gauges", we will just consider the ordinary terminology of (choice of) "representation".

The following subsections will delve deeper into these different choices, specifically the ones where we reduce the couple of DDs (f, g) to only one function h that we will abusively call *the* DD. Each representation will be referred to by the name of the physicist(s) who introduced it.

5.3.2. R representation

Historically, the DD g was overlooked. We will therefore denote by R (for "Radyushkin") the representation where only f is present:

$$f_{\mathrm{R}}(\beta, \alpha) = h_{\mathrm{R}}(\beta, \alpha)\,, \qquad\qquad g_{\mathrm{R}}(\beta, \alpha) = 0\,. \qquad (5.28)$$

This implies that the GPD fulfills a polynomiality property of degree m (in fact, it is the case considered in App. B), instead of $m + 1$ as it should be for the GPD H (both for the pion and the nucleon).

---

[4]See [177] for the generalization to DDs that are non-vanishing on the boundaries.

As an aside, let us explicit here the famous Radyushkin Double Distribution Ansatz (RDDA), mentioned in Sec. 5.2.1, fundamental ingredient of the DD-based phenomenological models. It was introduced in Ref. [172] as a modeling suggestion for the DD f. It goes as follows for a given flavor q:

$$f^q \left(\beta, \alpha, t \right) = \pi_N \left(\beta, \alpha \right) q \left(\beta, t \right) , \tag{5.29}$$

where $q \left(\beta, t \right)$ is of course the t-dependent PDF, and π_N is the profile function:

$$\pi_N \left(\beta, \alpha \right) = \frac{\Gamma \left(N + \frac{3}{2} \right)}{\sqrt{\pi} \, \Gamma \left(N + 1 \right)} \frac{\left((1 - \beta)^2 - \alpha^2 \right)^N}{(1 - \beta)^{2N+1}} . \tag{5.30}$$

The normalization of the profile function

$$\int_{-1+\beta}^{1-\beta} \mathrm{d}\alpha \, \pi_N \left(\beta, \alpha \right) = 1 \tag{5.31}$$

ensures the correct forward limit (5.16). The modeling approach goes then through a PDF parametrization and a choice of the parameter N (although it was taken to be 1 in most cases [23, 152, 155, 156]).

The RDDA does not say anything about the DD g. More generally, let us stress again that the R representation lacks the $(m+1)$-degree coefficient in the polynomiality property, which has no reason to vanish in the case of unpolarized GPDs.

5.3.3. D-term

To palliate this problem in a minimal way, *i.e.* by reducing the information in g to the strict minimum corresponding to the moments $g^{m,0}$ that cannot be reabsorbed in f, the authors of Ref. [171] introduced the so-called D-term:

$$g_{\mathrm{PW}} \left(\beta, \alpha \right) = \delta \left(\beta \right) D_{\mathrm{PW}} \left(\alpha \right) . \tag{5.32}$$

This generates the GFFs H_m^{m+1} only, the other ones generated entirely by h_{R}. The contribution to the GPD is the following:

$$H_{\mathrm{PW}} \left(x, \xi \right) = \iint_\Omega \mathrm{d}\beta \, \mathrm{d}\alpha \, \delta \left(x - \beta - \xi\alpha \right) \xi \, \delta \left(\beta \right) D_{\mathrm{PW}} \left(\alpha \right)$$

$$= \mathrm{sgn} \left(\xi \right) D_{\mathrm{PW}} \left(\frac{x}{\xi} \right) . \tag{5.33}$$

More generally, following Ref. [16], we can write for the D-term the following definition that is invariant by the transformations (5.27):

$$D \left(\alpha \right) = \int_{-1+|\alpha|}^{+1-|\alpha|} \mathrm{d}\beta \, g(\beta, \alpha) . \tag{5.34}$$

The support $[-1, 1]$ of D follows from the one of the DD. We also have that D is α-odd. From Eq. (5.33), we also deduce that the D-term contributes only to the ERBL region of the GPD, *i.e.* $|x| \le |\xi|$.

In every representation, we will denote by D_{PW} the "additional" (or "extra") D-term contributions not yielded by the reduced DD h itself. In the case of the R representation, it corresponds to the full D-term, since $f = h_{\mathrm{R}}$ does not contribute at all to Eq. (5.34).

5.3.4. BMKS **representation**

The authors of Ref. [178] suggested another way to generate all needed GFFs, while still keeping only one DD. This goes through the realization that $H(x,\xi)/x$ fulfills a polynomiality property of degree m, as can easily be seen from Eq. (5.1). Using the following representation:

$$H_{\text{BMKS}}(x,\xi) = x \iint_\Omega \mathrm{d}\beta\,\mathrm{d}\alpha\,\delta(x-\beta-\xi\alpha)\,h_{\text{BMKS}}(\beta,\alpha)\,, \tag{5.35}$$

we end up therefore with the correct order $m+1$ of polynomials for H:

$$\int_{-1}^{1} x^m H_{\text{BMKS}}(x,\xi)\,\mathrm{d}x = \iint_\Omega \mathrm{d}\beta\,\mathrm{d}\alpha\,(\beta+\xi\alpha)^{m+1}\,h_{\text{BMKS}}(\beta,\alpha)\,. \tag{5.36}$$

In terms of the DDs (f,g), we have the following relations:

$$f_{\text{BMKS}}(\beta,\alpha) = \beta\,h_{\text{BMKS}}(\beta,\alpha)\,, \qquad g_{\text{BMKS}}(\beta,\alpha) = \alpha\,h_{\text{BMKS}}(\beta,\alpha)\,, \tag{5.37}$$

with h_{BMKS} being α-even. In this case, the DD h_{BMKS} does generate an "intrinsic" D-term:

$$D_{\text{BMKS}}(\alpha) = \alpha\int_{-1+|\alpha|}^{+1-|\alpha|}\mathrm{d}\beta\,h_{\text{BMKS}}(\beta,\alpha)\,. \tag{5.38}$$

All this assumes of course the existence of h_{BMKS}. To proof it is more difficult, if not impossible. Indeed, to apply the theorem of App. B, we need the polynomiality property to be fulfilled for every Mellin moment. The zeroth moment of H/x corresponds to the x^{-1} moment of H, and we have no *a priori* knowledge on it. To fulfill the conditions of the theorem, we need it to be constant:

$$\int_{-1}^{1}\mathrm{d}x\,\frac{H(x,\xi)}{x} = \text{constant}\,. \tag{5.39}$$

But we do not even know if it is defined, *i.e.* that H/x is integrable[5], let alone constant. This issue renders the BMKS representation intractable in phenomenologically relevant cases. But we should point out that a regularization procedure was suggested in Refs. [179, 180] and then applied in Ref. [158].

5.3.5. P **representation**

In Refs. [17, 181], Pobylitsa introduced another representation[6]:

$$H_{\text{P}}(x,\xi) = (1-x)\iint_{\Omega^>}\mathrm{d}\beta\,\mathrm{d}\alpha\,\delta(x-\beta-\xi\alpha)\,h_{\text{P}}(\beta,\alpha)\,, \tag{5.40}$$

in his effort to provide frameworks where both positivity and polynomiality would be fulfilled. The parametrization of the DDs (f,g) is the following[6]:

$$f_{\text{P}}(\beta,\alpha) = (1-\beta)\,h_{\text{P}}(\beta,\alpha)\,, \qquad g_{\text{P}}(\beta,\alpha) = -\alpha\,h_{\text{P}}(\beta,\alpha)\,, \tag{5.41}$$

---

[5]In fact, from the knowledge of extracted PDFs, we know that it is most definitely not. The PDFs are already singular (even though integrable for the valence combinations). Further dividing by x only makes it worse.

[6]Here, we took for granted that only quark contributions are considered. Otherwise, a factor $(1+x)$ would be used instead of $(1-x)$ for $\Omega^<$, and Eq. (5.41) would be changed accordingly with additional $\text{sgn}(\beta)$ occurrences.

and this DD h_{P} generates the following D-term:

$$D_{\mathrm{P}}\left(\alpha\right) = -\alpha \int_{-1+|\alpha|}^{+1-|\alpha|} \mathrm{d}\beta\, h_{\mathrm{P}}(\beta,\alpha)\,. \tag{5.42}$$

Here, we considered that $H/\left(1-x\right)$ (instead of H or H/x) is in the image of the Radon transform. This representation is much more friendly when it comes to the behavior of the DD. Indeed, we know from perturbative QCD [182] that at large x, the pion GPD vanishes quadratically:

$$H_{\pi}\left(x,\xi\right) \underset{x\to 1}{\simeq} \frac{\left(1-x\right)^2}{1-\xi^2}\,, \tag{5.43}$$

while the nucleon GPD H vanishes with the third power:

$$H\left(x,\xi\right) \underset{x\to 1}{\simeq} \frac{\left(1-x\right)^3}{\left(1-\xi^2\right)^2}\,, \tag{5.44}$$

with the GPD E having an even stronger fall-off.

This means that $H/\left(1-x\right)$ is integrable, but we still need its integral to be independent of ξ to prove the existence of the DD as a well-behaved function:

$$\int_{-1}^{1} \mathrm{d}x\, \frac{H\left(x,\xi\right)}{1-x} = \mathrm{constant}\,, \tag{5.45}$$

a condition that does not follow from the polynomiality property. Nevertheless, it seems more suitable than the previous BMKS representation.

5.3.6. T **representation**

In Ref. [177], Tiburzi introduced what he called the "Drell-Yan gauge". We called this DD h_{T} and it was the subject of Sec. 5.1.

In this representation, the usual DDs (f,g) can be written as:

$$f_{\mathrm{T}}\left(\beta,\alpha\right) = \delta\left(\alpha\right) H\left(\beta,0\right)\,, \qquad\qquad g_{\mathrm{T}}\left(\beta,\alpha\right) = h_{\mathrm{T}}\left(\beta,\alpha\right)\,. \tag{5.46}$$

Let us stress again that, contrary to all the previous DDs h, this one is α-odd. Notice also the symmetry with respect to the R+PW representation where we would have:

$$f_{\mathrm{R}}\left(\beta,\alpha\right) = h_{\mathrm{R}}\left(\beta,\alpha\right)\,, \qquad\qquad g_{\mathrm{PW}}\left(\beta,\alpha\right) = \delta\left(\beta\right) D_{\mathrm{PW}}\left(\alpha\right)\,. \tag{5.47}$$

In the T representation, the information is maximized in the DD g, with a residual information on the line $\alpha = 0$ for the DD f, corresponding to the (t-dependent) PDF. The D-term plays the same role of residual information in the R+PW representation for the DD g on the line $\beta = 0$, with the information maximized in the DD f.

This T representation is interesting in the sense that it completely decouples the DD from the non-skewed limit $H\left(x,0\right)$ of the GPD, *i.e.* the (t-dependent) PDF, as written in Eq. (5.3). This potentially allows us to separate what we do know — the PDF, already extracted from inclusive experiments — or want to know — the t-dependent PDF, for hadron tomography —

from the part that is inherent to exclusive processes and is needed only for phenomenology, *i.e.* the non-vanishing skewness. This feature would help in fulfilling the various constraints in model building.

Moreover, the reasoning of Sec. 5.1 is more convincing that its counterparts for the BMKS or P representations. Indeed, the T representation does not require an additional polynomiality condition such as Eq. (5.45).

5.3.7. Note on the nucleon

As presented in Sec. 4.2, there are four chiral-even quark GPDs in the case of the nucleon, which calls for some remarks:

- The polarized ones, $\tilde{H}$ and $\tilde{E}$, fulfill a degree-m polynomiality property (see Eqs. (4.40)-(4.41)), which means that they don't present any D-term contribution. The R representation is sufficient in that case.

- The unpolarized GPDs, H and E, share the same D-term, with an opposite sign (see Eqs. (4.38)-(4.39)). This means that the combination $H + E$ is free from D-term contributions and can be written in the R representation again. This leaves one GPD (H or E, or any other independent combination) to be modeled in either the T, P or BMKS representations, and/or with an additional PW term. For the reasons mentioned above, we will not consider the BMKS representation in practical applications. The choice between the remaining options would be a model assumption.

5.3.8. Note on gluons

The gluon unpolarized GPDs having a degree-$(m + 2)$ polynomiality property, the previous representations would not fit. However, Pobylitsa suggested in Refs. [17, 181] a similar representation to Eq. (5.40) but with a factor $(1 - x)^2$ instead for gluons.

We will not go into further details and subtleties, since gluon DDs are beyond the scope of this present thesis. We will mainly concern ourselves with quark models, which we can think of as low-scale models that can be evolved to generate gluons perturbatively at larger scales.

5.4. Illustrations

5.4.1. Toy model

For the sake of clarity, let us consider a simple example of DD (as in Ref. [18]) in the BMKS representation:

$$h_{\mathrm{BMKS}}^{\mathrm{Toy}} (\beta, \alpha) = 15 \left((1 - \beta)^2 - \alpha^2 \right) \mathbf{1}_{\Omega >} (\beta, \alpha) , \qquad (5.48)$$

where $\mathbf{1}_{\Omega>}(\cdot)$ denotes the indicator function. This gives us the following GPD (using Eq. (5.35)):

$$H_{|\text{DGLAP}}^{\text{Toy}}(x,\xi) = \frac{20\,(1-x)^3\,x}{(1-\xi^2)^2}\,, \tag{5.49}$$

$$H_{|\text{ERBL}}^{\text{Toy}}(x,\xi) = \frac{5x(\xi+x)^2(-\xi(\xi+2)+2\xi x+x)}{\xi^3(\xi+1)^2}\,, \tag{5.50}$$

with support $x \in [-\xi, +1]$.

To obtain polynomial Mellin moments, one needs to integrate over both regions. The separate contributions are actually rational fractions in this case, as can be seen in the following:

$$\int_{+\xi}^{+1} dx\, x^m H^{\text{Toy}}(x,\xi) = \mathcal{P}_m^{\text{Toy,DGLAP}}(\xi) + \frac{R_{-1}^{\text{Toy}}(m)}{1+\xi} + \frac{R_{-2}^{\text{Toy}}(m)}{(1+\xi)^2}\,, \tag{5.51}$$

$$\int_{-\xi}^{+\xi} dx\, x^m H^{\text{Toy}}(x,\xi) = \mathcal{P}_m^{\text{Toy,ERBL}}(\xi) - \frac{R_{-1}^{\text{Toy}}(m)}{1+\xi} - \frac{R_{-2}^{\text{Toy}}(m)}{(1+\xi)^2}\,, \tag{5.52}$$

where $\mathcal{P}^{\text{Toy,DGLAP}}$ and $\mathcal{P}^{\text{Toy,ERBL}}$ are polynomials of degree $m+1$ whose sum gives the total Mellin moment:

$$\binom{n+5}{4}\left[\mathcal{P}_m^{\text{Toy,DGLAP}}(\xi) + \mathcal{P}_m^{\text{Toy,ERBL}}(\xi)\right] = \frac{5}{2}\sum_{\substack{k=0 \\ k\ \text{even}}}^{m+1}(k+2)\,\xi^k\,, \tag{5.53}$$

and R_{-1}^{Toy} and R_{-2}^{Toy} are the residues of the double pole $\xi = -1$ of the rational fractions:

$$R_{-1}^{\text{Toy}}(m) = 20(-1)^{m+1}\frac{7+2\,(m+(-1)^m)}{(5+2m+(-1)^m)\,(9+2m+(-1)^m)}\,, \tag{5.54}$$

$$R_{-2}^{\text{Toy}}(m) = 20(-1)^m\frac{2m^2+(12+2(-1)^m)\,m+16+5(-1)^m}{(5+2m+(-1)^m)\,(9+2m+(-1)^m)}\,. \tag{5.55}$$

We see here polynomiality in action, relating both regions through a cancellation of the same residual rational fractions.

Let us now turn to another representation, *e.g.* P. As our example was built in the BMKS representation, it obviously fulfills the extra condition (5.39), but does it fulfill also the one for the P representation, *i.e.* Eq. (5.45)? The answer is no:

$$\int_{-1}^{1} dx\, \frac{H^{\text{Toy}}(x,\xi)}{1-x} = \frac{5\left(\xi\,(2-\xi^2) - 2\,(1-\xi^2)\tanh^{-1}(\xi)\right)}{\xi^3}\,, \tag{5.56}$$

the r.h.s. being ξ-dependent!

To understand this, we can derive the P-DD, using the P$\leftrightarrow$BMKS conversion relations given in Ref. [183] (and in App. B of Ref. [18]):

$$h_{\text{P}}^{\text{Toy}}(\beta,\alpha) = 5\left(3\,\alpha^2\left(1 - \frac{1}{(1-\beta)^4}\right) + (4-3\beta)\,\beta + \frac{1}{(1-\beta)^2} - 1\right)\mathbf{1}_{\Omega>}(\beta,\alpha)\,. \tag{5.57}$$

This P-DD gives of course the same GPD as Eqs. (5.49)-(5.50), but if we look closely into it, we realize that is not actually integrable on Ω, despite the corresponding DDs $\left(f_{\mathrm{P}}^{\mathrm{Toy}}, g_{\mathrm{P}}^{\mathrm{Toy}}\right)$ (given by Eq. (5.41)) being integrable. We cannot therefore swap the order of integration between $\iint_\Omega \mathrm{d}\beta \mathrm{d}\alpha$ and $\int_{-1}^1 \mathrm{d}x$, hence why the extra condition (5.45) is not verified, despite seemingly having a DD in the P representation. The said condition is a necessary and sufficient property for *well-behaved* DDs in the P representation, which is not the case here.

We can isolate the minimal singular part of the DD as:

$$h_{\mathrm{P,\,Sing}}^{\mathrm{Toy}}(\beta, \alpha) = 5\left(\frac{1}{(1-\beta)^2} - \frac{3\,\alpha^2}{(1-\beta)^4}\right)\mathbf{1}_{\Omega>}(\beta, \alpha)\,, \tag{5.58}$$

with the regularized DD

$$\begin{aligned} h_{\mathrm{P,\,Reg}}^{\mathrm{Toy}}(\beta, \alpha) &= h_{\mathrm{P}}^{\mathrm{Toy}}(\beta, \alpha) - h_{\mathrm{P,\,Sing}}^{\mathrm{Toy}}(\beta, \alpha) \\ &= 5\left(3\alpha^2 - 3\beta^2 + 4\beta - 1\right)\mathbf{1}_{\Omega>}(\beta, \alpha) \end{aligned} \tag{5.59}$$

yielding a GPD that is identical in DGLAP but differs in the ERBL region by a D-term:

$$H_{|\mathrm{DGLAP}}^{\mathrm{Toy,\,Reg}}(x, \xi) = H_{|\mathrm{DGLAP}}^{\mathrm{Toy}}(x, \xi)\,, \tag{5.60}$$

$$H_{|\mathrm{ERBL}}^{\mathrm{Toy,\,Reg}}(x, \xi) = H_{|\mathrm{ERBL}}^{\mathrm{Toy}}(x, \xi) - 5\frac{x}{\xi}\left(1 - \left(\frac{x}{\xi}\right)^2\right)\,. \tag{5.61}$$

What have we learned? That a choice of representation where the DD is well-behaved comes with a choice of D-term in the ERBL region. This remark will be important for the covariant extension of Part. III.

5.4.2. Photon GPDs and DDs

As a second illustration, let us consider the known photon GPDs of Ref. [184]:

$$\begin{aligned} H_1^\gamma(x, \xi) &= \frac{x^2 + (1-x)^2 - \xi^2}{1 - \xi^2}\mathbf{1}_{\mathrm{DGLAP}>}(x, \xi) + \frac{x}{\xi}\frac{1-\xi}{1+\xi}\mathbf{1}_{\mathrm{ERBL}}(x, \xi) \\ &\quad - \frac{x^2 + (1+x)^2 - \xi^2}{1 - \xi^2}\mathbf{1}_{\mathrm{DGLAP}<}(x, \xi)\,, \end{aligned} \tag{5.62}$$

$$\begin{aligned} H_3^\gamma(x, \xi) &= \frac{x^2 - (1-x)^2 - \xi^2}{1 - \xi^2}\mathbf{1}_{\mathrm{DGLAP}>}(x, \xi) - \frac{1-\xi}{1+\xi}\mathbf{1}_{\mathrm{ERBL}}(x, \xi) \\ &\quad + \frac{x^2 - (1+x)^2 - \xi^2}{1 - \xi^2}\mathbf{1}_{\mathrm{DGLAP}<}(x, \xi)\,. \end{aligned} \tag{5.63}$$

The corresponding DDs have been derived in Ref. [185] in the R+PW representation:

$$h_{1\,\mathrm{R}}^\gamma(\beta, \alpha) = \mathrm{sgn}(\beta)(2(1 - |\beta| - |\alpha|) + \delta(\alpha) - 1)\,, \qquad h_{3\,\mathrm{R}}^\gamma(\beta, \alpha) = \delta(\alpha) - 1\,, \tag{5.64}$$

$$D_{1\,\mathrm{PW}}^\gamma(\alpha) = (|\alpha| - 1)(2|\alpha| + 1)\,\mathrm{sgn}(\alpha)\,, \qquad D_{3\,\mathrm{PW}}^\gamma(\alpha) = 0\,. \tag{5.65}$$

Notice that H_3 fulfills a degree-m polynomiality property, and therefore has no D-term.

The presence of a term $\delta\left(\alpha\right)$ suggests the use of the T representation (see Eq. (5.46)). Using the conversion relations given in Ref. [177], we can derive the T-DD (and the associated PDF) as:

$$H_1^\gamma\left(x,0\right) = \operatorname{sgn}\left(x\right) - 2x\left(1 - |x|\right), \tag{5.66}$$

$$h_{1\,\mathrm{T}}^\gamma\left(\beta,\alpha\right) = \operatorname{sgn}\left(\alpha\right)\left(1 - 2\left|\beta\right|\right) - 2\alpha + \delta\left(\beta\right)\operatorname{sgn}\left(\alpha\right)\left(|\alpha| - 1\right), \tag{5.67}$$

and

$$H_3^\gamma\left(x,0\right) = 2\left|x\right| - 1, \tag{5.68}$$

$$h_{3\,\mathrm{T}}^\gamma\left(\beta,\alpha\right) = -\operatorname{sgn}\left(\alpha\right)\operatorname{sgn}\left(\beta\right). \tag{5.69}$$

The representation for H_3^γ is now free of any singularity (*i.e.* the $\delta\left(\alpha\right)$ term). For H_1^γ however, there is still an explicit D-term like contribution, *i.e.* the $\delta\left(\beta\right)$ part. We can again get rid of this singular contribution and consider:

$$h_{1\,\mathrm{T}}^{\gamma,\mathrm{Reg}}\left(\beta,\alpha\right) = \operatorname{sgn}\left(\alpha\right)\left(1 - 2\left|\beta\right|\right) - 2\alpha, \tag{5.70}$$

with the corresponding GPD

$$H_{1,\mathrm{Reg}}^\gamma\left(x,\xi\right) = \frac{x^2 + \left(1 - x\right)^2 - \xi^2}{1 - \xi^2}\,\mathbf{1}_{\mathrm{DGLAP}>}\left(x,\xi\right) + \operatorname{sgn}\left(x\right)\frac{1 - 2\left|x\right| + \xi}{1 + \xi}\,\mathbf{1}_{\mathrm{ERBL}}\left(x,\xi\right) \tag{5.71}$$
$$- \frac{x^2 + \left(1 + x\right)^2 - \xi^2}{1 - \xi^2}\,\mathbf{1}_{\mathrm{DGLAP}<}\left(x,\xi\right).$$

which keeps the same DGLAP region, but is different in ERBL, as expected. This difference corresponds to the extra D-term of Eq. (5.67).

In these considered GPDs of the photon, there are both quark and antiquark contributions. If we wish to separate them as explained in Sec. 5.2.5, *i.e.* take:

$$H^>(x,0) = H(x,0)\,\theta(x), \tag{5.72}$$

$$h_{\mathrm{T}}^>(\beta,\alpha) = h_{\mathrm{T}}(\beta,\alpha)\,\theta(\beta), \tag{5.73}$$

for the quark contribution, and

$$H^<(x,0) = H(x,0)\,\theta(-x), \tag{5.74}$$

$$h_{\mathrm{T}}^<(\beta,\alpha) = h_{\mathrm{T}}(\beta,\alpha)\,\theta(-\beta), \tag{5.75}$$

for the antiquark, we would end up with:

$$H_{1,\mathrm{Reg}}^{\gamma\,>}\left(x,\xi\right) = \frac{x^2 + \left(1 - x\right)^2 - \xi^2}{1 - \xi^2}\,\mathbf{1}_{\mathrm{DGLAP}>}\left(x,\xi\right) - \frac{x\left(\xi + x\right)}{\xi\left(1 + \xi\right)}\,\mathbf{1}_{\mathrm{ERBL}}\left(x,\xi\right) \tag{5.76}$$
$$+ 1\,\mathbf{1}_{\mathrm{ERBL}>}\left(x,\xi\right) + 0\,\mathbf{1}_{\mathrm{DGLAP}<}\left(x,\xi\right),$$

$$H_3^{\gamma\,>}\left(x,\xi\right) = \frac{x^2 - \left(1 - x\right)^2 - \xi^2}{1 - \xi^2}\,\mathbf{1}_{\mathrm{DGLAP}>}\left(x,\xi\right) + \frac{x + \xi}{1 + \xi}\,\mathbf{1}_{\mathrm{ERBL}}\left(x,\xi\right) \tag{5.77}$$
$$- 1\,\mathbf{1}_{\mathrm{ERBL}>}\left(x,\xi\right) + 0\,\mathbf{1}_{\mathrm{DGLAP}<}\left(x,\xi\right),$$

and similarly for the antiquark contribution. We denoted by ERBL> the region $0 < x < \xi$. Notice that there is a discontinuity in the ERBL region at $x = 0$, but a "quark distribution" in ERBL has no physical meaning given that there is an emission of a pair quark-antiquark. It is only a mathematical definition, and the discontinuity disappears when considering the full GPD.

The toy model of the previous subsection and the present photon GPDs will be both used as benchmark for the covariant extension of Part. III.

Chapter 6.

Positivity and Light-front wave-functions

In this chapter, we turn to another representation of GPDs, the so-called overlap of light-front wave-functions [166, 186, 187]. First, we will briefly review the formalism with the necessary formulae, and then apply it to a few simple examples as an illustration.

6.1. Formalism

6.1.1. Light-front quantization

Light-front quantization allows the expansion of a hadron state $|P, \Lambda\rangle$ of momentum P and polarization Λ on a Fock basis [188, 189]:

$$|H; P, \Lambda\rangle = \sum_{N,\beta} \int [\mathrm{d}x]_N [\mathrm{d}^2\boldsymbol{k}_\perp]_N \Psi_{N,\beta}^\Lambda \left(x_1, \hat{\boldsymbol{k}}_{\perp 1}, ..., x_N, \hat{\boldsymbol{k}}_{\perp N} \right) |N, \beta; k_1, \ldots, k_N\rangle , \qquad (6.1)$$

where the $|N, \beta; k_1, \ldots, k_N\rangle$ denote the N-particles partonic states with each (massless) particle carrying a momentum (in light-cone coordinates, see App. A.1)

$$k_i = \left[x_i\, P^+, \frac{\boldsymbol{k}_{\perp i}^2}{2\, x_i\, P^+}, \boldsymbol{k}_{\perp i} \right] , \qquad (6.2)$$

and the hat denotes a relative coordinate such that:

$$\boldsymbol{k}_{\perp i} = \hat{\boldsymbol{k}}_{\perp i} + x_i \boldsymbol{P}_\perp . \qquad (6.3)$$

β stands for the parton composition of the state, and corresponding quantum numbers:

$$\beta = \{f_1, \lambda_1, c_1; \ldots; f_N, \lambda_N, c_N\} , \qquad (6.4)$$

where $f = g, u, d, \ldots$ denotes the nature of the parton (gluon or the quark flavor), λ its helicity and c its color.

These states are weighted by the so-called *Light-front Wave-functions* (LFWFs) $\Psi_{N,\beta}^\Lambda$, containing the non-perturbative physics. They depend only on the relative coordinates and are normalized as follows:

$$\sum_{N,\beta} \int [\mathrm{d}x]_N \left[\mathrm{d}^2\boldsymbol{k}_\perp \right]_N \left| \Psi_{N,\beta}^\Lambda \left(x_1, \hat{\boldsymbol{k}}_{\perp 1}, ... \right) \right|^2 = 1 . \qquad (6.5)$$

The measure element in Eqs. (6.1) and (6.5) fulfills momentum conservation by construction:

$$[\mathrm{d}x]_N = \prod_{i=1}^{N} \mathrm{d}x_i \,\delta\left(1 - \sum_{i=1}^{N} x_i\right), \tag{6.6}$$

$$[\mathrm{d}^2\boldsymbol{k}_\perp]_N = \frac{1}{(16\pi^3)^{N-1}} \left(\prod_{i=1}^{N} \mathrm{d}^2\boldsymbol{k}_{\perp i}\right) \delta^2\left(\sum_{i=1}^{N} \boldsymbol{k}_{\perp i} - \boldsymbol{P}_\perp\right), \tag{6.7}$$

where i labels the partons.

6.1.2. Frames and notations

We will consider only "hadron frames", *i.e.* reference frames where a hadron has zero transverse momentum. In particular, we define a symmetric frame (also called "average-frame" in Ref. [166]) in which P (the average of hadrons momenta, see Sec. 4.1) has a vanishing transverse component, *i.e.* $\boldsymbol{P}_\perp = \boldsymbol{0}_\perp$. In this frame, the hadron momenta can be parametrized as follows:

$$P = \frac{1}{2}(P_1 + P_2) = \left[P^+, P^- = \frac{M_H^2 + \boldsymbol{\Delta}_\perp^2/4}{2(1 - \xi^2) P^+}, \boldsymbol{0}_\perp\right], \tag{6.8}$$

$$\Delta = P_2 - P_1 = \left[-2\xi P^+, \frac{\xi(M_H^2 + \boldsymbol{\Delta}_\perp^2/4)}{(1 - \xi^2) P^+}, \boldsymbol{\Delta}_\perp\right]. \tag{6.9}$$

We denote with a bar the average of incoming and outgoing (denoted by a prime) parton momenta, with the average plus-momentum fraction being defined with respect to the average hadron momentum:

$$\bar{k}_i = \frac{k_i + k_i'}{2}, \qquad \bar{x}_i = \frac{\bar{k}_i^+}{P^+}, \qquad i = 1, \ldots, N. \tag{6.10}$$

The active (or "struck") parton of Fig. 4.1, denoted by the label a, has therefore the following plus-momentum fractions (defined once again with respect to P^+) and transverse momenta in the symmetric frame:

$$\text{incoming:} \qquad x_a = \bar{x}_a + \xi, \qquad \boldsymbol{k}_{\perp a} = \bar{\boldsymbol{k}}_{\perp a} - \frac{\boldsymbol{\Delta}_\perp}{2}, \tag{6.11}$$

$$\text{outgoing:} \qquad x_a' = \bar{x}_a - \xi, \qquad \boldsymbol{k}_{\perp a}' = \bar{\boldsymbol{k}}_{\perp a} + \frac{\boldsymbol{\Delta}_\perp}{2}, \tag{6.12}$$

while both incoming and outgoing parton momenta are equal to the average one $k_i = \bar{k}_i = k_i'$, for $i \neq a$, *i.e.* for spectator partons.

Moreover, we define a *hadron-in* and a *hadron-out* frames, corresponding to the incoming and outgoing hadrons, *i.e.* where $\boldsymbol{P}_{\perp 1} = \boldsymbol{0}_\perp$ and $\boldsymbol{P}_{\perp 2} = \boldsymbol{0}_\perp$ respectively. We denote parton momenta with superscripts "in" and "out" in these frames accordingly. In other words, the superscript "in" concerns momenta of incoming partons in the hadron-in frame, and likewise for the superscript "out" (with a prime appended, for pedantic consistency). These can be

related to the average momenta in the symmetric frame through the following transverse boost:

$$x_i^{\text{in}} = \frac{\bar{x}_i}{1+\xi}, \qquad \boldsymbol{k}_{\perp i}^{\text{in}} = \bar{\boldsymbol{k}}_{\perp i} + \frac{\bar{x}_i}{1+\xi}\frac{\boldsymbol{\Delta}_\perp}{2}, \qquad \text{for } i \neq a \qquad (6.13)$$

$$x_a^{\text{in}} = \frac{\bar{x}_a + \xi}{1+\xi}, \qquad \boldsymbol{k}_{\perp a}^{\text{in}} = \bar{\boldsymbol{k}}_{\perp a} - \frac{1 - \bar{x}_a}{1+\xi}\frac{\boldsymbol{\Delta}_\perp}{2}, \qquad (6.14)$$

$$x_i^{\text{out}\prime} = \frac{\bar{x}_i}{1-\xi}, \qquad \boldsymbol{k}_{\perp i}^{\text{out}\prime} = \bar{\boldsymbol{k}}_{\perp i} - \frac{\bar{x}_i}{1-\xi}\frac{\boldsymbol{\Delta}_\perp}{2}, \qquad \text{for } i \neq a \qquad (6.15)$$

$$x_a^{\text{out}\prime} = \frac{\bar{x}_a - \xi}{1-\xi}, \qquad \boldsymbol{k}_{\perp a}^{\text{out}\prime} = \bar{\boldsymbol{k}}_{\perp a} + \frac{1 - \bar{x}_a}{1-\xi}\frac{\boldsymbol{\Delta}_\perp}{2}, \qquad (6.16)$$

where the "in" plus-momentum fractions are defined with respect to P_1^+, and the "out" fractions with respect to P_2^+.

In the ERBL region, the partonic interpretation is that of an emission of a quark-antiquark pair, which means that the incoming hadron has $N+1$ partons, while the outgoing has $N-1$. For this reason, we introduce the notation $k_{a'} = -k_a'$ for the momentum of the active antiquark, which would have the following momentum in the hadron-in frame:

$$x_{a'}^{\text{in}} = -\frac{\bar{x}_a - \xi}{1+\xi}, \qquad \boldsymbol{k}_{\perp a'}^{\text{in}} = -\bar{\boldsymbol{k}}_{\perp a} - \frac{1 + \bar{x}_a}{1+\xi}\frac{\boldsymbol{\Delta}_\perp}{2}. \qquad (6.17)$$

6.1.3. Overlap representation of Generalized Parton Distributions

Using the Fock-space expansion (6.1), one can express GPDs in terms of LFWFs [166]. However, the partonic picture and therefore the way the GPDs are related to LFWFs depend on the considered kinematics. In the DGLAP region, the GPD is given by an overlap of LFWFs having the *same* number of constituents. In the ERBL region on the other hand, there is an overlap of LFWFs involving *different* numbers of constituents $N+1$ and $N-1$, due to the emission of a pair quark-antiquark (see Fig. 4.1).

Keeping our simple quark-pion case, we can write in the region $x \geq \xi$:

$$H^q(x, \xi, t) = \sum_{N,\beta} \left(\sqrt{1-\xi^2}\right)^{2-N} \sum_a \delta_{f_a, q} \int [\mathrm{d}\bar{x}]_N \left[\mathrm{d}^2 \bar{\boldsymbol{k}}_\perp\right]_N \delta(x - \bar{x}_a) \qquad (6.18)$$

$$\times \Psi_{N,\beta}^* \left(x_1^{\text{out}\prime}, \boldsymbol{k}_{\perp 1}^{\text{out}\prime}, \ldots, x_a^{\text{out}\prime}, \boldsymbol{k}_{\perp a}^{\text{out}\prime}, \ldots\right) \Psi_{N,\beta} \left(x_1^{\text{in}}, \boldsymbol{k}_{\perp 1}^{\text{in}}, \ldots, x_a^{\text{in}}, \boldsymbol{k}_{\perp a}^{\text{in}}, \ldots\right),$$

where all quarks of the same flavour as q are summed over as active/struck partons. Note that the t-dependence is recovered via Eq. (4.33). For the nucleon, the helicity-dependent matrix element $F_{\Lambda_2, \Lambda_1}^q$ would have an identical formula, but for an added nucleon helicity dependence on the wave-functions $\Psi_{N,\beta}^{*\Lambda_2}$ and $\Psi_{N,\beta}^{\Lambda_1}$.

In the "anti-quark" region $x \leq -\xi$, the result is similar, but for a global minus sign and a constraint $\bar{x}_a = -x$ for the momentum fraction of the active antiquark. In any case, in this thesis, we consider only quark contributions to the GPD.

The major difference arises in the ERBL region $-\xi \leq x \leq \xi$, as stated before, with the

following overlap:

$$H^q\left(x,\xi,t\right)=\sqrt{\frac{1-\xi}{1+\xi}}\sum_N\left(\sqrt{1-\xi^2}\right)^{2-N}\sum_{\beta,\beta'}\sum_{a,a'}\frac{1}{\sqrt{n_a n_{a'}}}\,\delta_{f_a,q}\,\delta_{f_a,\bar{f}_{a'}}\,\delta_{\lambda_a,-\lambda_{a'}}\,\delta_{c_a,\bar{c}_{a'}} \qquad (6.19)$$

$$\times\frac{1}{(16\pi^3)^{N-1}}\int \mathrm{d}\bar{x}_a\,\mathrm{d}^2\bar{\boldsymbol{k}}_{\perp a}\,\delta\left(x-\bar{x}_a\right)\delta\left(1-\xi-\sum_{\substack{i=1\\i\neq a,a'}}^{N+1}\bar{x}_i\right)$$

$$\times\,\delta^2\left(\frac{\boldsymbol{\Delta}_\perp}{2}-\sum_{\substack{i=1\\i\neq a,a'}}^{N+1}\bar{\boldsymbol{k}}_{\perp i}\right)\left[\prod_{\substack{i=1\\i\neq a,a'}}^{N+1}\mathrm{d}\bar{x}_i\,\mathrm{d}^2\bar{\boldsymbol{k}}_{\perp i}\,\delta_{\beta_i,\beta'_i}\right]$$

$$\times\,\Psi^*_{N-1,\beta'}\left(\left\{x_i^{\mathrm{out}\prime},\boldsymbol{k}_{\perp i}^{\mathrm{out}\prime},\,_{i\neq a,a'}^{i=1\ldots N+1}\right\}\right)\Psi_{N+1,\beta}\left(\left\{x_i^{\mathrm{in}},\boldsymbol{k}_{\perp i}^{\mathrm{in}},\,i=1\ldots N+1\right\}\right),$$

where n_a (resp. $n_{a'}$) denotes the number of partons in the incoming hadron with the same quantum numbers as the active quark (resp. antiquark). We sum over all pairs of quark and antiquark of appropriate flavor and opposite helicity and color, emitted from the initial hadron, and then over all spectator partons with matching quantum numbers between the incoming and outgoing hadron. We therefore labelled the indices from 1 to $N+1$ for both hadrons, even though the outgoing hadron lacks two partons (*i.e.* the active pair a and a'). Again, the case of the nucleon would be identical with added helicity dependence of the wave-functions.

In the case of gluons, the two formulae are identical but with a prefactor of $\sqrt{|x^2-\xi^2|}$.

For the details of the derivation, we refer to Ref. [166] where additional results for polarized GPDs are also given.

6.1.4. Probability density in impact parameter space

We have seen in Chap. 2 that GPDs, when taken at vanishing skewness $\xi=0$ and Fourier transformed to IPDs (2.14), provide us with a probabilistic interpretation. This can now be made explicit with the overlap representation (6.18). At $\xi=0$, there is still an interference with a relative shift in transverse momenta $\bar{\boldsymbol{k}}_{\perp i}+\bar{x}_i\frac{\boldsymbol{\Delta}_\perp}{2}$ and $\bar{\boldsymbol{k}}_{\perp i}-\bar{x}_i\frac{\boldsymbol{\Delta}_\perp}{2}$. But when Fourier transformed, the arguments of the wave-functions for the overlap in impact parameter space are identical and we end up with a density as integrand $\left|\Psi_{N,\beta}\left(\ldots,\bar{x}_i,\bar{\boldsymbol{b}}_{\perp i},\ldots\right)\right|^2$, hence why $H(x,\boldsymbol{b}_\perp^2)$ can be interpreted as a number density of partons. We kept here the notation Ψ also for the inverse Fourier transform of the wave-function:

$$\Psi_{N,\beta}\left(\ldots,x_i,\boldsymbol{b}_{\perp i},\ldots\right)=\int\left[\mathrm{d}^2\boldsymbol{k}_\perp\right]_N\exp\left(i\sum_{i=1}^N\boldsymbol{b}_{\perp i}\cdot\boldsymbol{k}_{\perp i}\right)\Psi_{N,\beta}\left(\ldots,x_i,\boldsymbol{k}_{\perp i},\ldots\right), \qquad (6.20)$$

where $\boldsymbol{b}_{\perp i}$ are the positions of partons with respect to the transverse center of plus-momentum (2.10) of the hadron, taken here at the origin, *i.e.* $\boldsymbol{R}_\perp=\boldsymbol{0}_\perp$. The details of the wave-function representation in impact parameter space are given in Ref. [74].

Notice that in the forward limit $t=0$, $\xi=0$, the overlap (6.18) gives also an integral of densities $\left|\Psi\left(\ldots,\bar{x}_i,\bar{\boldsymbol{k}}_{\perp i},\ldots\right)\right|^2$, as expected for PDFs, *i.e.* parton densities. This can also be obtained by integrating the impact parameter overlap representation over $\boldsymbol{b}_\perp$. On the other

hand, integrating over x would yield the overlap representation of impact parameter densities, or, by Fourier transform, the overlap representation of Form Factors.

6.1.5. Positivity property

One can notice that the overlap representation (6.18) in the DGLAP region has the structure of a scalar product

$$H^q(x, \xi, t) = (\phi_{-\xi, \mathbf{\Delta}_\perp} | \phi_{\xi, -\mathbf{\Delta}_\perp}) \tag{6.21}$$

between the two sequences of functions [1]:

$$\phi_{\xi, -\mathbf{\Delta}_\perp, N} : \left(\beta, \bar{x}_1, \bar{\mathbf{k}}_{\perp 1}, ..., \bar{x}_N, \bar{\mathbf{k}}_{\perp N} \right) \mapsto \sqrt{1+\xi}^{\,2-N} \Psi_{N, \beta} \left(x_1^{\text{in}}, \mathbf{k}_{\perp 1}^{\text{in}}, \ldots, x_N^{\text{in}}, \mathbf{k}_{\perp N}^{\text{in}} \right), \tag{6.22}$$

$$\phi_{-\xi, \mathbf{\Delta}_\perp, N} : \left(\beta, \bar{x}_1, \bar{\mathbf{k}}_{\perp 1}, ..., \bar{x}_N, \bar{\mathbf{k}}_{\perp N} \right) \mapsto \sqrt{1-\xi}^{\,2-N} \Psi_{N, \beta} \left(x_1^{\text{out}\prime}, \mathbf{k}_{\perp 1}^{\text{out}\prime}, \ldots, x_N^{\text{out}\prime}, \mathbf{k}_{\perp N}^{\text{out}\prime} \right).$$

We can therefore apply the Cauchy-Schwarz inequality

$$\left| (\phi_{-\xi, \mathbf{\Delta}_\perp} | \phi_{\xi, -\mathbf{\Delta}_\perp}) \right|^2 \leq (\phi_{-\xi, \mathbf{\Delta}_\perp} | \phi_{-\xi, \mathbf{\Delta}_\perp}) (\phi_{\xi, -\mathbf{\Delta}_\perp} | \phi_{\xi, -\mathbf{\Delta}_\perp}), \tag{6.23}$$

and using the change of variable

$$[\mathrm{d}\bar{x}]_N \left[\mathrm{d}^2 \bar{\mathbf{k}}_\perp \right]_N = (1+\xi)^{N-1} [\mathrm{d}x^{\text{in}}]_N \left[\mathrm{d}^2 \mathbf{k}_\perp^{\text{in}} \right]_N, \tag{6.24}$$

$$\delta(x - \bar{x}_a) = \frac{1}{1+\xi} \delta \left(\frac{x+\xi}{1+\xi} - x_a^{\text{in}} \right), \tag{6.25}$$

we obtain the PDF with the incoming parton's momentum fraction as argument:

$$(\phi_{\xi, -\mathbf{\Delta}_\perp} | \phi_{\xi, -\mathbf{\Delta}_\perp}) = H \left(\frac{x+\xi}{1+\xi}, 0, 0 \right) = q \left(\frac{x+\xi}{1+\xi} \right), \tag{6.26}$$

and similarly for the outgoing parton. We end up with the positivity property (4.22) of the pion:

$$|H^q(x, \xi, t)|^2 \leq q \left(\frac{x+\xi}{1+\xi} \right) q \left(\frac{x-\xi}{1-\xi} \right), \tag{6.27}$$

that is now proven.

The same approach, when generalized to consider a helicity structure, can lead to a proof of the relation given for the nucleon (4.50). See *e.g.* Ref. [1].

6.1.6. Two-body case

If we limit ourselves to the valence contribution to the pion, *i.e.* the first Fock sector $N = 2$, the relation (6.18) can be further simplified. Let us consider the π^+ case in which the first Fock sector would be $u\bar{d}$. We get the following GPD (for $x \geq \xi$):

$$H_{\pi^+}^u(x, \xi, t) = \int \frac{\mathrm{d}^2 \mathbf{k}_\perp}{16 \pi^3} \Psi_{u\bar{d}}^* \left(x^{\text{out}\prime}, \mathbf{k}_\perp^{\text{out}\prime} \right) \Psi_{u\bar{d}} \left(x^{\text{in}}, \mathbf{k}_\perp^{\text{in}} \right), \tag{6.28}$$

where the LFWF depends only on one set of momenta by virtue of Eqs. (6.6)-(6.7), and the boost relations used are those of either the active quark in Eqs. (6.14) and (6.16) or the spectator in Eqs. (6.13) and (6.15) (by symmetry of the LFWF). Note that for $x \leq -\xi$, the considered GPD is vanishing, as there is no valence antiquark u in the π^+. Moreover, as explained in Sec. 4.1.3, there is only one independent quark GPD, *e.g.* this one.

If we consider all helicity combinations for the two partons, we end up with the following two contributions in the overlap:

$$H^u_{\pi^+}(x, \xi, t) = \int \frac{\mathrm{d}^2 \boldsymbol{k}_\perp}{16\,\pi^3} \bigg[\Psi^*_{\uparrow\downarrow}\left(x^{\mathrm{out}\prime}, \boldsymbol{k}_\perp^{\mathrm{out}\prime}\right) \Psi_{\uparrow\downarrow}\left(x^{\mathrm{in}}, \boldsymbol{k}_\perp^{\mathrm{in}}\right) \qquad (6.29)$$
$$+ \boldsymbol{k}_\perp^{\mathrm{out}\prime} \cdot \boldsymbol{k}_\perp^{\mathrm{in}} \; \Psi^*_{\uparrow\uparrow}\left(x^{\mathrm{out}\prime}, \boldsymbol{k}_\perp^{\mathrm{out}\prime}\right) \Psi_{\uparrow\uparrow}\left(x^{\mathrm{in}}, \boldsymbol{k}_\perp^{\mathrm{in}}\right) \bigg] \,,$$

where the arrows denote the helicities of the quark and antiquark. $\Psi_{\uparrow\downarrow}$ is the scalar and $\Psi_{\uparrow\uparrow}$ the vector LFWF (*i.e.* with a sum of parton helicities equal to 1), the latter representing a state with non-vanishing orbital angular momentum (necessary to compensate the helicity). For more details on the helicity structure of wave-functions, see Ref. [190]. It should be noted that here the wave-functions are effective combinations of the ones introduced in the previous subsections, with color neutral parton states in particular. The two approaches are equivalent in the DGLAP region (as explained in Ref. [166]).

These two-body truncated formulae will be used in Sec. 6.2.

6.1.7. Distribution Amplitude

As an aside, let us mention quickly Distribution Amplitudes. Figure 5.3 (right panel) represents the diagram of a pion DA, in the simplest process where they can be accessed: $\gamma^*\gamma^* \to \pi$.

The leading-twist pion DA is obtained from the two-body LFWF of Eq. (6.28) with the integration:

$$f_\pi \, \Phi_\pi(z) = \int \frac{\mathrm{d}^2 \boldsymbol{k}_\perp}{16\,\pi^3} \Psi_{\uparrow\downarrow}(z, \boldsymbol{k}_\perp) \,, \qquad (6.30)$$

where

$$f_\pi = \int \mathrm{d}z \int \frac{\mathrm{d}^2 \boldsymbol{k}_\perp}{16\,\pi^3} \Psi_{\uparrow\downarrow}(z, \boldsymbol{k}_\perp) \qquad (6.31)$$

is the pion decay constant. The pion DA can be related to the GPD on the ERBL line $\xi = \pm 1$, via the soft pion theorem of Ref. [191] that states:

$$H^{I=0}_\pi(x, \xi = 1, t = 0) = 0 \,, \qquad (6.32)$$

$$H^{I=0}_\pi(x, \xi = 1, t = 0) = \Phi_\pi\left(\frac{1+x}{2}\right) \,, \qquad (6.33)$$

with the isoscalar and isovector pion GPDs defined in Sec. 4.1.3.

6.1.8. Consistent truncation: is it possible?

The different overlap structure in DGLAP and ERBL leads to a considerable issue: how to truncate consistently in both regions?

Let us fix for instance an order N at which we truncate in DGLAP, we are then left with a dilemma when it comes to the ERBL part. Do we truncate at the overlap $(N-2)/N$, or rather at $N/(N+2)$? Is an average truncation $(N-1)/(N+1)$ more sound? Which truncation would give a consistent GPD? By that we mean a GPD that corresponds to the same approximation in Fock space in both regions, and therefore a consistent function that is for instance:

- continuous at the cross-over line $|x| = |\xi|$ – this is crucial for the factorization of exclusive processes and therefore the experimental access to GPDs, as a discontinuity on this line would generate logarithmic divergences in observables as can be seen for instance in Eq. (3.19) (see also *e.g.* the discussion in section 3.13 of Ref. [1]);

- fulfills the polynomiality property – there does not seem to be any reason why one of the truncations would be favored by polynomiality over another, it rather ties together contributions from all Fock states in order to provide the cancellations between ERBL and DGLAP in Mellin moments of the GPD. For an illustration of the kind of cancellations needed, see Sec. 5.4.

To the best of our knowledge, there does not seem to be any good answer.

This question is nonetheless crucial to GPD modeling, and this thesis is mainly devoted to it. We will further explain its importance and show how to circumvent the answer, by providing an alternative method, in Chap. 7.

6.2. Examples

In this section, we illustrate the previous formalism by calculating a GPD from an overlap of LFWFs, for a few examples where the result can be obtained analytically. We consider the simple case of a pion in the first Fock sector as in Sec. 6.1.6. The subscript π^+ and superscript u will be however (mostly) dropped but implied.

6.2.1. Gaussian toy model

As a first illustration, we consider a LFWF with a Gaussian Ansatz (such Ansätze have been used for instance in AdS/QCD computations, see *e.g.* Refs. [192,193] and references therein). We choose to work with the following very simple one, with a unique mass parameter M:

$$\Psi\left(x, \boldsymbol{k}_\perp^2\right) = \frac{4\sqrt{15}\,\pi}{M}\,\sqrt{x\left(1-x\right)}\,\exp\left(-\frac{\boldsymbol{k}_\perp^2}{4M^2(1-x)x}\right).\tag{6.34}$$

where the x-dependent factor is used to obtain a correct PDF behavior, as will be shown later. The wave-function is already normalized such that:

$$\int \mathrm{d}x\,\frac{\mathrm{d}^2\boldsymbol{k}_\perp}{16\,\pi^3}\left|\Psi\left(x, \boldsymbol{k}_\perp^2\right)\right|^2 = 1\,.\tag{6.35}$$

Here, applying Eq. (6.28) does not lead to any difficulty, and the integration of this gaussian function can be carried out analytically [194] by considering for instance polar variables for the

integration in the transverse plane and choosing the first axis along $\boldsymbol{\Delta}_\perp$:

$$\boldsymbol{k}_\perp = \begin{pmatrix} k_\perp \cos\theta \\ k_\perp \sin\theta \end{pmatrix}, \qquad\qquad \boldsymbol{\Delta}_\perp = \begin{pmatrix} \Delta_\perp \\ 0 \end{pmatrix}, \qquad (6.36)$$

which would lead to:

$$H(x,\xi,t) = \int \frac{k_\perp \mathrm{d}k_\perp \mathrm{d}\theta}{16\,\pi^3}\, \Psi^* \left(\frac{x-\xi}{1-\xi}, k_\perp^2 + \left(\frac{1-x}{1-\xi}\right)^2 \frac{\Delta_\perp^2}{4} + \frac{1-x}{1-\xi} k_\perp \Delta_\perp \cos\theta \right) \qquad (6.37)$$

$$\times\, \Psi \left(\frac{x+\xi}{1+\xi}, k_\perp^2 + \left(\frac{1-x}{1+\xi}\right)^2 \frac{\Delta_\perp^2}{4} - \frac{1-x}{1+\xi} k_\perp \Delta_\perp \cos\theta \right),$$

and finally to the following GPD in DGLAP:

$$H(x,\xi,t) = \frac{30\,(1-x)^2\,(x^2-\xi^2)^{3/2}\,\exp\left(\frac{(1-\xi^2)(1-x)}{8((1+\xi^2)x-2\xi^2)}\frac{t}{M^2}\right)}{(1-\xi^2)\left((1+\xi^2)\,x - 2\xi^2\right)}, \qquad (6.38)$$

once we use the relation[1] $-t = \frac{\Delta_\perp^2}{1-\xi^2}$. This gives the reasonable PDF (see Sec. 6.2.3):

$$u_{\pi^+}(x) = H_{\pi^+}^u(x,0,0) = 30\,x^2\,(1-x)^2. \qquad (6.39)$$

To fix the mass parameter which governs the t-dependence, we can resort to the Form Factor sum rule[2,3]:

$$F_{\pi^+}(t) = \int_{-1}^{1} \mathrm{d}x\, H_{\pi^+}^u(x,\xi,t). \qquad (6.40)$$

The Form Factor is independent of ξ (polynomiality property), but as we do not have access to the ERBL region, $\xi = 0$ is the only value for which we can compute the integral in practice. The integral can therefore be taken between 0 and 1 as this GPD is vanishing on DGLAP<. We end up with an expression that we do not bother to write, as only the first order expansion is needed to define the pion's charge radius:

$$F_{\pi^+}(t) = 1 - \frac{3}{16\,M^2}\,(-t) + \mathcal{O}\left(t^2\right) \qquad (6.41)$$

$$= 1 - \frac{r_\pi^2}{6}\,(-t) + \mathcal{O}\left(t^2\right), \qquad (6.42)$$

which leads to a parameter value of $M \sim 0.315$ GeV, needed to recover the experimental value $r_\pi^2 = 0.439 \pm 0.008$ fm^2 of the NA7 collaboration [195].

As an illustration of the 3D hadron tomography of Chap. 2, we can also derive the IPD (see Eq. (2.14)) for this toy model:

$$H\left(x,\boldsymbol{b}_\perp^2\right) = \frac{60}{\pi}M^2\,(1-x)\,x^3\,e^{-2\,\boldsymbol{b}_\perp^2\,M^2\,\frac{x}{1-x}}, \qquad (6.43)$$

and we plotted the results for various values of x on Fig. 6.1.

---

[1]We neglected the pion mass in Eq. (4.33), *i.e.* we used the chiral limit.

[2]In truth, the pion Form Factor is a flavor combination $F_{\pi^+} = e_u F_{\pi^+}^u + e_d F_{\pi^+}^d$, with the electric charges being $e_u = \frac{2}{3}$ and $e_d = -\frac{1}{3}$. But using isospin symmetry and charge conjugation (as detailed in Sec. 4.1.3), we can show that $F_{\pi^+} = F_{\pi^+}^u$, hence the written sum rule.

[3]The pion Form Factor F_{π^+} is usually denoted simply F_π in the literature. We also have $F_{\pi^-} = -F_{\pi^+}$ and $F_{\pi^0} = 0$ by charge conjugation (see Eq. (4.15)).

$$x = 0.05 \qquad\qquad x = 0.5 \qquad\qquad x = 0.95$$
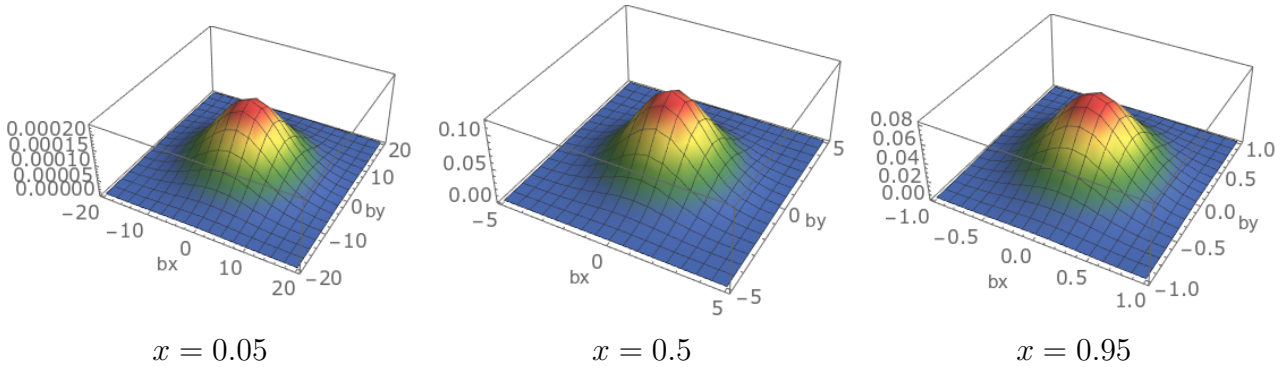
Figure 6.1. Impact parameter distribution $H\left(x, \boldsymbol{b}_\perp^2\right)$ at fixed values of $x = [0.05, 0.5, 0.95]$ for the Gaussian toy model of Sec. 6.2.1. See Eq. (6.43).

6.2.2. Roberts' toy model

Let us now consider the following LFWF model:

$$\Psi\left(x, \boldsymbol{k}_\perp^2\right) = \frac{2\sqrt{30}\,\pi\sqrt{(1-x)\,x}}{M\left(1 + \frac{\boldsymbol{k}_\perp^2}{4M^2(1-x)x}\right)}, \tag{6.44}$$

taken from Eq. (2.70) of Ref. [196], but adapted again with the necessary x-dependent factor to obtain the correct pion PDF (6.39).

In this case of rational fraction, the derivation of the GPD is trickier, and we will go into its details. Let us start by writing the integral:

$$H\left(x, \xi, t\right) = 480\,\pi^2\,M\left[x^{\text{in}}\left(1 - x^{\text{in}}\right)x^{\text{out}\prime}\left(1 - x^{\text{out}\prime}\right)\right]^{\frac{3}{2}} \tag{6.45}$$

$$\times \int \frac{\mathrm{d}^2\boldsymbol{k}_\perp}{16\,\pi^3} \frac{1}{\left(4\,M^2\,x^{\text{in}}\left(1 - x^{\text{in}}\right) + \boldsymbol{k}_\perp^{\text{in}\,2}\right)\left(4\,M^2\,x^{\text{out}\prime}\left(1 - x^{\text{out}\prime}\right) + \boldsymbol{k}_\perp^{\text{out}\prime\,2}\right)}.$$

We will call the integrand here $\mathcal{I}$.

To obtain an analytical result at the end, one must go through the following tricks:

- Apply Feynman parametrization:

$$\frac{1}{A^n\,B^n} = \frac{\Gamma\left(2\,n\right)}{\Gamma\left(n\right)^2}\int_0^1 \mathrm{d}u\,\frac{u^{n-1}\left(1-u\right)^{n-1}}{\left(u\,A + \left(1-u\right)B\right)^{2n}}, \tag{6.46}$$

which yields in this case:

$$\mathcal{I}\left(x, \xi, \boldsymbol{k}_\perp, \boldsymbol{\Delta}_\perp\right) = \int_0^1 \frac{\mathrm{d}u}{\left(4\,M^2\,[\ldots] + u\left(\boldsymbol{k}_\perp - \frac{1-x}{1+\xi}\frac{\boldsymbol{\Delta}_\perp}{2}\right)^2 + (1-u)\left(\boldsymbol{k}_\perp + \frac{1-x}{1-\xi}\frac{\boldsymbol{\Delta}_\perp}{2}\right)^2\right)^2}$$

$$= \int_0^1 \frac{\mathrm{d}u}{\left(\begin{array}{c}4\,M^2\,[\ldots] + k_\perp^2 + (1-x)\left(\frac{1-u}{1-\xi} - \frac{u}{1+\xi}\right)\boldsymbol{k}_\perp \cdot \boldsymbol{\Delta}_\perp \\ + (1-x)^2\left(\frac{1-u}{(1-\xi)^2} + \frac{u}{(1+\xi)^2}\right)\frac{\Delta_\perp^2}{4}\end{array}\right)^2} \tag{6.47}$$

where the square brackets are $[\ldots] = u\,x^{\text{in}}\left(1 - x^{\text{in}}\right) + (1-u)\,x^{\text{out}\prime}\left(1 - x^{\text{out}\prime}\right)$.

- "Complete the square":

$$\mathcal{I}\left(x,\xi,\boldsymbol{k}_\perp,\boldsymbol{\Delta}_\perp\right) = \int_0^1 \frac{\mathrm{d}u}{\left(4\,M^2\left[\ldots\right] + \left(\boldsymbol{k}_\perp + (1-x)\left(\frac{1-u}{1-\xi} - \frac{u}{1+\xi}\right)\frac{\boldsymbol{\Delta}_\perp}{2}\right)^2 + u\left(1-u\right)\left(\frac{1-x}{1-\xi^2}\right)^2\boldsymbol{\Delta}_\perp^2\right)^2} \tag{6.48}$$

and in doing so, apply a change of variable $\boldsymbol{k}_\perp + (1-x)\left(\frac{1-u}{1-\xi} - \frac{u}{1+\xi}\right)\frac{\boldsymbol{\Delta}_\perp}{2} \longmapsto \boldsymbol{k}_\perp$ to get rid of the angular dependence $\boldsymbol{k}_\perp \cdot \boldsymbol{\Delta}_\perp$ in the integrand.

- Using

$$\int_0^\infty k\,\mathrm{d}k\,\frac{b\,k^2 + c}{(a + k^2)^n} = \frac{a\,b + c\,(n-2)}{2\,(n-1)\,(n-2)\,a^{n-1}}\,, \tag{6.49}$$

with $b = 0$, one can now integrate over momentum:

$$\int \frac{\mathrm{d}^2\boldsymbol{k}_\perp}{16\,\pi^3}\,\mathcal{I}\left(x,\xi,\boldsymbol{k}_\perp,\boldsymbol{\Delta}_\perp\right) = \int_0^\infty \frac{k_\perp\,\mathrm{d}k_\perp}{8\,\pi^2}\,\mathcal{I}\left(x,\xi,\boldsymbol{k}_\perp,\boldsymbol{\Delta}_\perp\right)$$
$$= \int_0^1 \frac{\mathrm{d}u}{16\,\pi^2\left(4\,M^2\left[\ldots\right] + u\left(1-u\right)\left(\frac{1-x}{1-\xi^2}\right)^2\boldsymbol{\Delta}_\perp^2\right)}\,. \tag{6.50}$$

The integration over the Feynman parameter would then yield the GPD:

$$H\left(x,\xi,t\right) = \frac{240\,(1-x)^2\,(x^2-\xi^2)^{3/2}}{(1-\xi^2)\,\eta\left(x,\xi,t\right)}\,\tanh^{-1}\left(\frac{\eta\left(x,\xi,t\right)}{8\left(x - \xi^2\left(2-x\right)\right) + (1-\xi^2)\,(1-x)\,\frac{-t}{M^2}}\right)\,, \tag{6.51}$$

where

$$\eta\left(x,\xi,t\right) = \sqrt{\begin{array}{c} 64\left(\xi^3 + \xi - 2\xi x\right)^2 + (1-\xi^2)^2\,(1-x)^2\left(\frac{-t}{M^2}\right)^2 \\ + 16\,(1-\xi^2)\,(1-x)\left(x - \xi^2\left(2-x\right)\right)\frac{-t}{M^2} \end{array}}\,.$$

The PDF is identical to the previous case, and we can fix the mass parameter $M \sim 0.182$ GeV in the same way.

6.2.3. Algebraic Nakanishi-based model

We will consider now a much more physically sound model, but still algebraic which allows for the same kind of handy analytical calculations. It was introduced in Refs. [12, 13] and was one of the main motivations that led to this covariant extension effort that we will explain in Part. III. It concerns of course the pion as it is still our simple guiding case.

Our basic ingredient is again the two-body LFWF, but here it was obtained from the appropriate projection and integration of the Bethe-Salpeter wave-function resulting from the algebraic model described in [197] and based on its Nakanishi representation [198, 199].

As shown in Ref. [13] (the details of the computation can be found therein), there are two contributions[4] to the LFWF, the helicity-0 (or scalar):

$$\Psi_{\uparrow\downarrow}(x, \boldsymbol{k}_\perp) = 8\sqrt{15}\,\pi\,\frac{M^3}{\left(\boldsymbol{k}_\perp^2 + M^2\right)^2}\,(1-x)\,x\,, \tag{6.52}$$

and helicity-1 (or vector):

$$i\,k_\perp^j\,\Psi_{\uparrow\uparrow}(x, \boldsymbol{k}_\perp) = 8\sqrt{15}\,\pi\,\frac{k_\perp^j\,M^2}{\left(\boldsymbol{k}_\perp^2 + M^2\right)^2}\,(1-x)\,x\,, \qquad j = 1, 2\,, \tag{6.53}$$

where M is a model mass parameter introduced at the level of the quark propagator (a constituent-quark-like mass). Eqs. (6.52)-(6.53) correspond to specializing Eqs. (154) and (155) in Ref. [13] for the asymptotic case $\nu = 1$ therein[5].

Applying the overlap (6.29), the derivation of the GPD goes through the same steps as in Sec. 6.2.2. Let us separate the contributions and deal first with the scalar one:

$$H_{\uparrow\downarrow}(x, \xi, t) = 240\,\pi^2\,M^6 x^{\mathrm{in}}\left(1 - x^{\mathrm{in}}\right) x^{\mathrm{out}\prime}\left(1 - x^{\mathrm{out}\prime}\right)\int \frac{\mathrm{d}^2\boldsymbol{k}_\perp}{16\,\pi^3}\,\frac{1}{\left(\boldsymbol{k}_\perp^{\mathrm{in}\,2} + M^2\right)^2\left(\boldsymbol{k}_\perp^{\mathrm{out}\prime\,2} + M^2\right)^2}\,. \tag{6.54}$$

Here, applying Feynman parametrization (6.46) on the integrand and "completing the square" yields:

$$\mathcal{I}_{\uparrow\downarrow}(x, \xi, \boldsymbol{k}_\perp, \boldsymbol{\Delta}_\perp) = \int_0^1 \frac{u\,(1-u)\,\mathrm{d}u}{\left(M^2 + \left(\boldsymbol{k}_\perp + (1-x)\left(\frac{1-u}{1-\xi} - \frac{u}{1+\xi}\right)\frac{\boldsymbol{\Delta}_\perp}{2}\right)^2 + u\,(1-u)\left(\frac{1-x}{1-\xi^2}\right)^2\Delta_\perp^2\right)^4}\,. \tag{6.55}$$

Then integrating over $\boldsymbol{k}_\perp$ using (6.49) with the same change of variable, we end up with:

$$H_{\uparrow\downarrow}(x, \xi, t) = \int_0^1 \frac{5\,M^6 x^{\mathrm{in}}\left(1 - x^{\mathrm{in}}\right) x^{\mathrm{out}\prime}\left(1 - x^{\mathrm{out}\prime}\right) u\,(1-u)\,\mathrm{d}u}{\left(M^2 + u\,(1-u)\left(\frac{1-x}{1-\xi^2}\right)^2\Delta_\perp^2\right)^3}\,. \tag{6.56}$$

For the vector contribution, the derivation is similar. The only difference is that there will be an angular dependence $\boldsymbol{k}_\perp \cdot \boldsymbol{\Delta}_\perp$ in the numerator, but we can discard it, since the $\boldsymbol{k}_\perp$-odd contributions have a vanishing integral. We can therefore write:

$$H_{\uparrow\uparrow}(x, \xi, t) = 240\,\pi^2\,M^4 x^{\mathrm{in}}\left(1 - x^{\mathrm{in}}\right) x^{\mathrm{out}\prime}\left(1 - x^{\mathrm{out}\prime}\right) \tag{6.57}$$

$$\times \int \frac{\mathrm{d}^2\boldsymbol{k}_\perp}{16\,\pi^3}\int_0^1 \frac{\left(k_\perp^2 - u\,(1-u)\left(\frac{1-x}{1-\xi^2}\right)^2\Delta_\perp^2\right) u\,(1-u)\,\mathrm{d}u}{\left(M^2 + k_\perp^2 + u\,(1-u)\left(\frac{1-x}{1-\xi^2}\right)^2\Delta_\perp^2\right)^4}\,,$$

---

[4]By helicity here, we mean the sum of parton helicities. It should not be confused with the helicity of the pion, which is of course 0.

[5]There is a normalization mismatch between the two contributions in Ref. [13], which has been corrected in Refs. [18, 19].

which, once we integrate over momentum using (6.49) (this time with $b = 1$), leads to:

$$H_{\uparrow\uparrow}(x,\xi,t) = \int_0^1 \frac{5\, M^4 x^{\text{in}} \left(1 - x^{\text{in}}\right) x^{\text{out}\prime} \left(1 - x^{\text{out}\prime}\right) \left(M^2 - u\left(1-u\right)\left(\frac{1-x}{1-\xi^2}\right)^2 \Delta_\perp^2\right) u\left(1-u\right) \mathrm{d}u}{2\left(M^2 + u\left(1-u\right)\left(\frac{1-x}{1-\xi^2}\right)^2 \Delta_\perp^2\right)^3} \,.$$

$$(6.58)$$

In total, once we integrate over Feynman's parameter, we end up with the following GPD:

$$H(x,\xi,t) = \frac{15}{2} \frac{(1-x)^2 \left(x^2 - \xi^2\right)}{\left(1-\xi^2\right)^2 \left(1+\zeta\right)^2} \left(3 + \frac{1-2\zeta}{\sqrt{\zeta\left(1+\zeta\right)}} \operatorname{arctanh}\left(\sqrt{\frac{\zeta}{1+\zeta}}\right)\right), \qquad (6.59)$$

in DGLAP>, where:

$$\zeta = \frac{-t}{4M^2} \frac{(1-x)^2}{1-\xi^2} \qquad (6.60)$$

encodes the correlated dependence on the kinematical variables x and t, as a natural translation of the kinematical structure of Eqs. (6.52)-(6.53). It should be noticed that such a correlation is fully consistent with the results of pQCD when $x \to 1^-$, as any t-dependence in Eq. (6.59) appears suppressed by a factor $(1-x)^2$ [182]. Indeed, in this limit, Eq. (6.59) yields:

$$H\left(x,\xi,t\right) = 30 \frac{(1-x)^2}{1-\xi^2} \left(1 - 2\frac{1-x}{1-\xi^2} + \mathcal{O}\left((1-x)^2\right)\right), \qquad (6.61)$$

where the leading term plainly agrees with the one obtained in Ref. [182][6] as mentioned also in Sec. 5.3.5, while the first subleading correction is also shown not to depend on t. The forward limit is given by Eq. (6.39) and corresponds to the same result found in Ref. [11] as an excellent approximation for the pion's valence dressed-quark PDF [200].

Moreover, applying the sum rule for the pion electromagnetic Form Factor (6.40) yields:

$$F\left(t\right) = \frac{45}{\zeta_0^2} \left(1 - \sqrt{\frac{1+\zeta_0}{\zeta_0}} \operatorname{arctanh}\left(\sqrt{\frac{\zeta_0}{1+\zeta_0}}\right) + \frac{1}{3} \operatorname{arctanh}^2\left(\sqrt{\frac{\zeta_0}{1+\zeta_0}}\right)\right) \qquad (6.62)$$

$$= 1 - \frac{4}{21}\left(-\frac{t}{M^2}\right) + \mathcal{O}\left(t^2\right),$$

where we naturally used the notation $\zeta_0 = -t/\left(4M^2\right)$. The model mass parameter can now be identified as in Sec. 6.2.1:

$$M = \sqrt{\frac{24}{21}\frac{1}{r_\pi}} = 318 \pm 4\,\text{MeV}\,. \qquad (6.63)$$

This Form Factor compares fairly well with contemporary data [201] as shown in Ref. [19], up to $-t \simeq 2.5\,\text{GeV}^2$. At large t, nonetheless, Eq. (6.62) behaves as $1/t^2$, whereas the expected behavior is $1/t$ [202, 203]. This wrong behaviour can be well understood, as explained in Ref. [11], because Eqs. (6.52)-(6.53) have been derived from a Bethe-Salpeter wave function omitting contributions from the pseudovector components that are required for a complete description of the pion [204, 205].

---

[6]The limit $x \to 1^-$ given by Eq. (6.61) is equivalent to $u(x)/(1-\xi^2)$, as it is displayed by Eq. (4) of Ref. [182].

$$x = 0.05 \qquad\qquad x = 0.5 \qquad\qquad x = 0.95$$
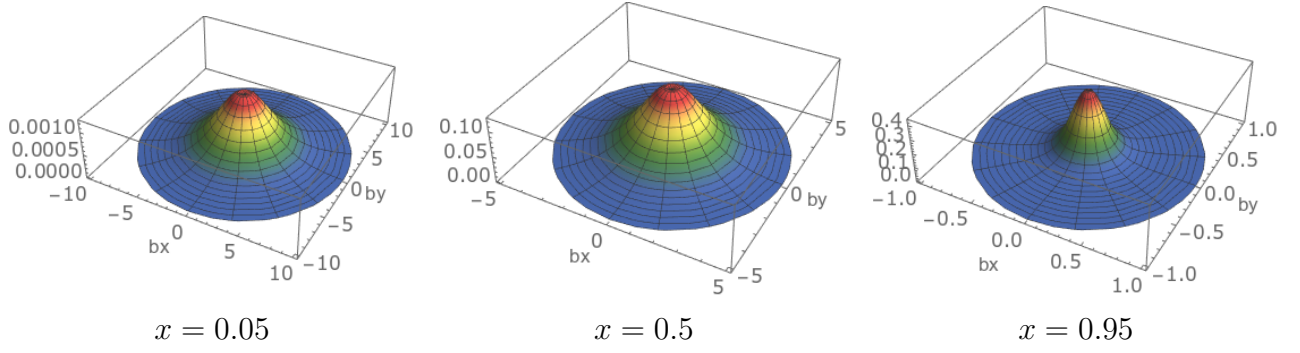
Figure 6.2. Impact parameter distribution $H\left(x, \boldsymbol{b}_\perp^2\right)$ at fixed values of $x = [0.05, 0.5, 0.95]$ for the algebraic model of Sec. 6.2.3.

We also plot on Fig. 6.2 the associated IPD $H\left(x, \boldsymbol{b}_\perp^2\right)$ as before. This Fourier integration is done numerically, but we can express the x-dependent rms impact parameter as:

$$\left\langle \boldsymbol{b}_\perp^2 \right\rangle (x) = -4 \left. \frac{\partial}{\partial\left(\boldsymbol{\Delta}_\perp^2\right)} H\left(x, 0, -\boldsymbol{\Delta}_\perp^2\right) \right|_{\boldsymbol{\Delta}_\perp^2 = 0}$$

$$= \frac{80}{M^2} x^2 (1-x)^4 . \tag{6.64}$$

Part III.

Covariant extension of Generalized Parton Distributions

Chapter 7.

Principle of the covariant extension

7.1. Motivation

As was stated in sections 2.2 and 2.3, we are mainly interested in accessing the GPD at the non-skewed limit $H(x, \xi = 0, t)$, where a probabilistic interpretation is possible [8], which would allow us to achieve the golden promise of hadron tomography.

However, we do not have a direct experimental access to GPDs. Indeed, they only enter the various exclusive processes (such as DVCS) via convolutions with hard-scattering kernels. We refer to Sec. 3.2.2 for the details on these Compton Form Factors. We see in Eq. (3.17) that the GPD is integrated over x, and in the case of a leading order analysis of DVCS, we can also have access to the crossover line $H(\xi, \xi, t)$ of the GPD (which still begs the question of how to link it to vanishing skewness but non-zero x), via the imaginary part of the CFF. Otherwise, a deconvolution in the variable x is necessary to access the GPD. Moreover, only finite values of ξ (and t) are accessible with exclusive processes. Inclusive processes allow one to access the forward limit ($t = 0$), which also implies $\xi = 0$, but we are interested in all values of t in the case of 3D imaging of the nucleon.

The effort to extract useful information for tomography can be summarized as follows:

- Deconvolute the x-dependence;

- Extrapolate from the finite values of the skewness ξ to vanishing ξ;

- Extrapolate to all values of t;

- Apply the inverse Fourier transform of Eq. (2.14).

The first three steps are not at all straightforward, and we cannot claim that phenomenological parametrizations [150, 155, 157, 206, 207] (with more or less arbitrary functional forms ranging from the most flexible but with poor predictive power to the least flexible but with poor data compatibility) are the final answer, despite great effort in that direction allowing to design experiments and make sense of them. We rather seek to rely as much as possible on QCD through nonperturbative frameworks with direct connection to it and models reproducing its features accurately (see *e.g.* Refs. [13, 14, 208–210] and references therein). We also seek to fulfill all (or as many as possible) known theoretical constraints on GPDs, the main ones being polynomiality and positivity (see sections 4.1.4 and 4.1.5). This is crucial to make sense of the extrapolation.

In that direction, two main roads can be followed:

Covariant approach: The first one is based on diagrammatic and covariant analyses which, in most cases, assume the so-called impulse approximation. It has the advantage of producing GPDs covering the entire kinematic domain and fulfilling polynomiality, but is plagued with several issues, such as the lack of positivity or issues with discrete symmetries when dealing with momentum dependent vertex models [11–14].

Light-front wave-functions approach: The second one is to use the expansion in Fock space in terms of LFWFs, as presented in Chap. 6. This way, positivity is naturally fulfilled as shown in Sec. 6.1.5. On the other hand, we encounter the truncation issue discussed in Sec. 6.1.8. This renders polynomiality unlikely to be fulfilled, nor the GPD to be consistent in both DGLAP and ERBL regions (continuous at the border $|x| = \xi$ in particular, which is crucial for factorization of exclusive processes), at any finite order of truncation N. It is rather expected to be achieved when all Fock states are summed over.

We suggest a solution to the last issue by considering the interplay between DGLAP and ERBL, linked through polynomiality. To the best of our knowledge, the first discussion of this link is the work of Müller and Schäfer [211]. Under analyticity assumptions, they argued that an extension of the GPD from the ERBL to the DGLAP region exists and is unique. But our goal here is the opposite.

Knowing the DGLAP region through a symmetric overlap truncation, we can use the polynomiality property to deduce the corresponding ERBL contribution. The latter will not likely represent any finite order truncation of the asymmetric overlap but probably corresponds to a projection on an arbitrary (infinite) number of Fock states. In other words, we probably pick partial contributions from each overlap $N-2/N$, $N/N+2$ and $N-1/N+1$ (and possibly others too), instead of the full contributions truncated at the first, second or third one. Doing so, we enforce polynomiality in a positivity-granted framework and ensure both constraints.

In practice, this goes through the use of Double Distributions, as the reader now understands that they are the natural expression of polynomiality. This method was first introduced by Hwang and Müller [20], who managed to derive analytically a DD in a simple model of scalar spectator diquark for the nucleon (mentioned in Sec. 9.2), from the knowledge of the symmetric overlap[1]. The DD then allows to extend the GPD to the whole kinematic domain.

More recently, we presented in Ref. [18] a general numerical method to achieve such goal.

7.2. Problem statement

We have so far discussed

- that the overlap representation makes sure the positivity of the GPD;

- that there is no simple way to exploit the overlap in the ERBL region and, for the same price, respect the polynomiality condition at any finite truncation order in Fock-space;

- and, finally, that the DD representation ensures this polynomiality.

---

[1]Müller also expanded on this recently in Ref. [212] for other LFWF models, given analyticity assumptions.

Therefore, a natural approach to model a GPD, by fulfilling both positivity and polynomiality conditions and exploiting the physical information encoded in the LFWFs would result from:

1. the computation of the overlap DGLAP GPD of Eq. (6.18), symmetric in Fock-space (overlap of LFWFs with the same number of constituents);

2. the derivation of a DD from this DGLAP GPD by an inverse problem;

3. the extension of the GPD to its full kinematic domain by means of the DD representation.

This is the program we will apply in the following.

In other words, given a GPD $H(x, \xi)$ with support $x \in [-1, +1]$ and with available non-trivial information only in the DGLAP region $0 \leq \xi \leq |x| \leq 1$, our goal is to find a DD h such that:

$$\hat{H}(x, \xi) = C^{>}(x, \xi) \int_{\Omega^{>}} \mathrm{d}\beta \mathrm{d}\alpha \, h(\beta, \alpha) \, \delta(x - \beta - \alpha\xi) \qquad (7.1)$$
$$+ C^{<}(x, \xi) \int_{\Omega^{<}} \mathrm{d}\beta \mathrm{d}\alpha \, h(\beta, \alpha) \, \delta(x - \beta - \alpha\xi) \, ,$$

where the definition of $\hat{H}$, $C^{>}$ and $C^{<}$ depends on the chosen representation:

R **representation:** $C^{>}$ and $C^{<}$ are both equal to 1 and either $\hat{H} = H$ is the GPD itself when it follows a degree-m polynomiality property or $\hat{H}(x, \xi) = H(x, \xi) - D_{\mathrm{PW}}\left(\frac{x}{\xi}\right)$, *i.e.* the GPD minus its D-term contribution in the R+PW representation.

BMKS **representation:** $C^{>}$ and $C^{<}$ are both equal to x, and $\hat{H} = H$.

P **representation:** $C^{>}(x, \xi) = 1 - x$ and $C^{>}(x, \xi) = 1 + x$, while $\hat{H} = H$.

T **representation:** $C^{>}$ and $C^{<}$ are both equal to ξ, and $\hat{H}(x, \xi) = H(x, \xi) - H(x, 0)$.

In the next section, we discuss the existence and uniqueness of a solution to such an inverse problem. And in the next chapter, we provide a numerical procedure to solve it.

But before, we make the following remarks:

- In principle we can add a PW term in all representations, not just the first one. But it is vanishing in the DGLAP region. Thus, in practice, $\hat{H}$ is always considered to be the GPD H itself, save in the T representation where we subtract the zero-skewness limit.

- As mentioned in Sec. 5.2.5, the quark and anti-quark GPDs are not correlated in the DGLAP region. In positive DGLAP ($0 \leq \xi \leq x$), only $H^{>}$ is present, while in negative DGLAP ($x \leq -\xi \leq 0$), only $H^{<}$ is. The two parts interfere in the ERBL region ($-\xi < x < \xi$) where $H = H^{>} + H^{<}$. Therefore, the task to accomplish is an independent inversion of

$$\hat{H}^{>}(x, \xi) = C^{>}(x, \xi) \int_{\Omega^{>}} \mathrm{d}\beta \mathrm{d}\alpha \, h^{>}(\beta, \alpha) \, \delta(x - \beta - \alpha\xi) \, , \qquad (7.2)$$

and

$$\hat{H}^{>}(x, \xi) = C^{<}(x, \xi) \int_{\Omega^{<}} \mathrm{d}\beta \mathrm{d}\alpha \, h^{<}(\beta, \alpha) \, \delta(x - \beta - \alpha\xi) \, . \qquad (7.3)$$
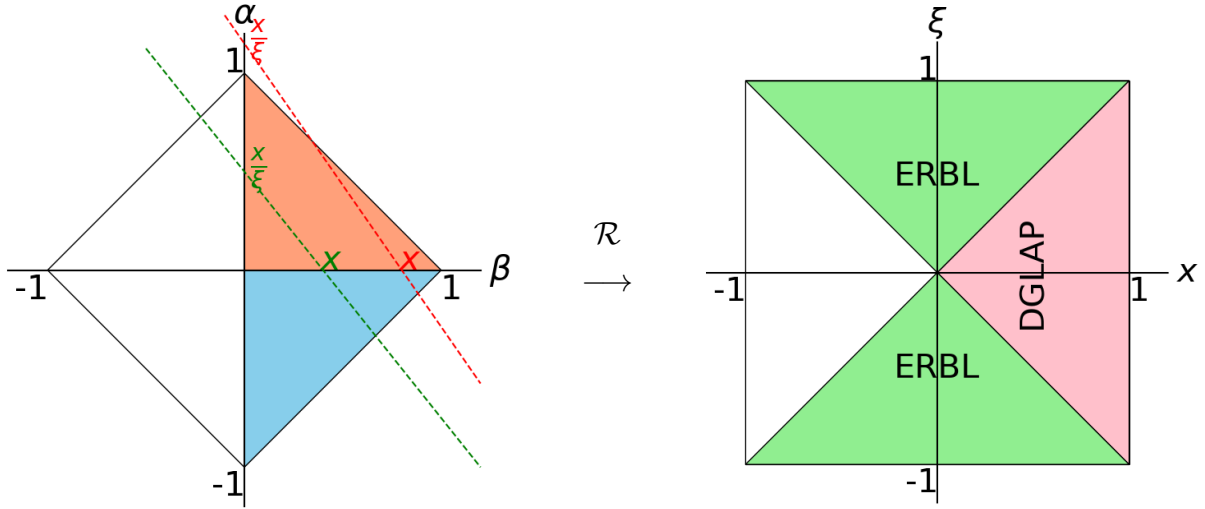
Figure 7.1. DD and GPD supports when only $\Omega^>$ is considered. Only the salmon red domain is used. The blue one is deduced by parity. And the white one, *i.e.* $\Omega^<$, is not correlated in DGLAP, and therefore can be dealt with separately.

- As mentioned in Sec. 5.2.2, h has a definite α-parity as the consequence of time reversal invariance: h_T is α-odd, while the others are α-even.

These last two properties together reduce the size of a numerical problem by 4 by comparison of a direct numerical inversion of Eq. (7.1). Indeed, we can separate a general GPD into two distinct problems $H^>$ and $H^<$, by virtue of linearity of Eq. (7.1) and the non-correlation in the DGLAP region. This limits us to half the DD domain (either $\Omega^>$ or $\Omega^<$) without loss of generality. And by parity, we reduce again the problem by half. Figure 7.1 summarizes this. This significantly decreases the computing cost of the numerical inversion[2] and further constrains the target solution.

As stated in Sec. 5.2.5, we will discuss only the case of quark DDs and GPDs. The treatment of anti-quark DDs and GPDs is essentially the same.

7.3. Existence and uniqueness or ambiguity of the extension

Asking whether a DGLAP GPD can be covariantly extended means the following consideration. Given a GPD H whose Mellin moments in the DGLAP sector can be written as

$$\int_\xi^1 \mathrm{d}x\, x^m H\left(x,\xi\right) = \mathcal{NP}_m\left(\xi\right) + \mathcal{P}_m^{\mathrm{DGLAP}}\left(\xi\right), \tag{7.4}$$

where we separated a non-polynomial contribution $\mathcal{NP}$ from a potential even polynomial $\mathcal{P}_m^{\mathrm{DGLAP}}$ of degree $m+1$, we may ask: can we compensate $\mathcal{NP}$ with an ERBL contribution?

---

[2]Given an algorithm with polynomial complexity $\mathcal{O}\left(N^p\right)$ where N is the size of the problem, solving two equal-size independent problems would have a $\mathcal{O}\left(2\,N^p\right)$ complexity, which is much better than a joint problem of complexity $\mathcal{O}\left((2N)^p\right)$.

In other words, can we find H^{ERBL} such that

$$\int_{-\xi}^{\xi} \mathrm{d}x\, x^m H^{\mathrm{ERBL}}(x,\xi) = -\mathcal{N}\mathcal{P}_m(\xi) + \mathcal{P}_m^{\mathrm{ERBL}}(\xi) \, , \tag{7.5}$$

where $\mathcal{P}_m^{\mathrm{ERBL}}$ is an arbitrary even polynomial of degree $m+1$, whose sum with $\mathcal{P}_m^{\mathrm{DGLAP}}$ would yield the final polynomial Mellin moment of the full GPD. Reformulating this to introduce Double Distributions, the question becomes about the existence of a DD (in a given representation) that would yield the known DGLAP GPD, and then allow to extend to ERBL. The existing criteria for the DD existence, *i.e.* the polynomiality property (complemented if necessary by the extra condition (5.39) or (5.45)), deal with the GPD known over its whole physical domain, not its restriction to the DGLAP region; in other words, it does not help us.

Nevertheless, we will admit that given models of LFWFs built from sufficiently covariant frameworks, the behavior (7.5) is granted. Anyway, given that we will turn to a least-squares formulation in Chap. 8, the existence of a solution is not an issue, the closest approximation being always favored.

On the other hand, it is crucial to know whether a solution is unique. We know that a D-term $\delta(\beta) D(\alpha)$ is visible only in the ERBL region and cannot be grasped from the knowledge of the DGLAP region only. This means the extension will only recover the ERBL contribution that is not due to a D-term. The choice of D-term would be left as model assumption. There is therefore a clear minimal ambiguity in the extension from DGLAP to ERBL. Is it the only one?

In other words, given two GPDs that are equal over the DGLAP region, are they necessarily equal over ERBL too? By linearity of the Radon transform (7.2), we can consider a GPD H that is vanishing on DGLAP and ask whether it is also zero in ERBL (modulo an extra D-term). By assuming the existence of the extension, we basically assumed the existence of a DD h_{T} (granted by polynomiality, see Sec. 5.1 and App. B). And we want to prove that it is vanishing.

Intuitively, as can be seen on Fig. 7.1, the DGLAP lines $\frac{x}{\xi} \geq 1$ never cross the $\beta = 0$ axis, as the D-term lives there, but all points of $\Omega^{>}\backslash\{\beta = 0\}$ are spanned by these lines. As the GPD is vanishing on DGLAP, the DD h_{T} must therefore be vanishing on $\Omega^{>}\backslash\{\beta = 0\}$. We can prove this.

Proof. Our starting point is that $\mathcal{R}h_{\mathrm{T}}(x,\xi) = 0$ for all $x \geq \xi > 0$[3]. Let us choose $x_0' > \xi_0 > 0$. Let x_0 be such that $x_0' > x_0 > \xi_0$, meaning that $\frac{\xi_0}{\sqrt{1+\xi_0^2}} < \frac{x_0}{\sqrt{1+\xi_0^2}}$. By continuity of $\xi \mapsto \frac{\xi}{\sqrt{1+\xi^2}}$, there exists $\epsilon > 0$ such that $0 < \frac{\xi}{\sqrt{1+\xi^2}} < \frac{x_0}{\sqrt{1+\xi_0^2}}$ for $|\xi - \xi_0| < \epsilon$. Then, for all x, ξ such that $\frac{x}{\sqrt{1+\xi^2}} > \frac{x_0}{\sqrt{1+\xi_0^2}}$ and $|\xi - \xi_0| < \epsilon$, we have $x > \xi > 0$ and therefore $\mathcal{R}h_{\mathrm{T}}(x,\xi) = 0$. We can apply the theorem B.4 and state that $h_{\mathrm{T}}(\beta,\alpha) = 0$ for all (β,α) on the half-plane $\beta + \alpha\xi_0 > x_0$. In particular, for $\beta + \alpha\xi_0 = x_0'$.

We showed that h_{T} is vanishing on all points spanned by DGLAP lines, *i.e.* vanishing on $\Omega^{>}\backslash\{\beta = 0\}$. $\qquad\square$

---

[3]The GPD (minus the zero-skewness part) in the T representation is $\xi\,\mathcal{R}h_{\mathrm{T}}(x,\xi)$, hence the hypothesis of $\xi \neq 0$.

In conclusion, a solution h of the inverse problem Eq. (7.2) is unique on $\Omega^> \backslash \{\beta = 0\}$.

We should remark that the T representation already provides its own D-term contribution (see Sec. 5.3.6), but we can use additional ones in a T+PW representation as model assumption. We proved rigorously the uniqueness of the inversion up to a D-term only for the T representation, but as we illustrated in Sec. 5.4, choosing a different representation with a well-behaved DD (as a numerical procedure would naturally pick) means choosing a different "intrinsic" D-term (in the sense discussed in Sec. 5.3, see *e.g.* Eqs. (5.38) and (5.42)), which is not an issue given what we already know of the ambiguity. The choice goes therefore through practical arguments, such as the numerical behavior. As was stated in Sec. 5.3, the P representation is quite convenient if the GPD vanishes sufficiently fast at $x \to 1$, which is a behavior we expect from the models of LFWFs considered. It will be therefore privileged in the following.

Chapter 8.

Numerical implementation of the covariant extension

8.1. Introduction

This chapter presents the considered numerical implementation of the covariant extension of a GPD from the DGLAP to the ERBL region with its challenges and results. In Chap. 7, we explained that we can solve our physics problem by inverting the Radon transform. This may seem straightforward since the Radon transform is linear, but this task is in fact quite difficult. Indeed, as mentioned in App. B, the inverse Radon transform may not be continuous and, in a loose sense, two "close" GPDs may be obtained as Radon transforms of very "different" DDs. This is an ill-posed problem in the sense of Hadamard. Since we are facing an incomplete data problem (we know the GPD only in the DGLAP region), the sensitivity to noise is expected to be even stronger than in the complete data problem, where we search a DD from the complete knowledge of a GPD and a GDA over their whole kinematic domains. In this respect, we note that reconstruction artifacts have already been reported [12, 16] for the latter situation.

One key remark is in order here. We do not know any closed-form formula for the inverse of the Radon transform restricted to the DGLAP region. In the recent Ref. [212], a possible step towards that direction was suggested using inverse Laplace transforms under some analyticity hypotheses of the LFWFs, but it is not clear how one could use this in practical applications in a general way. However we do not need a closed-form formula, and it would be of limited practical interest: the potential amplification of noise is related to the discontinuous nature of the inverse Radon transform. It is not the manifestation of a poor numerical scheme or of a badly-designed computing code. It is the inescapable consequence of a precise and general mathematical statement. Even if we had at our disposal a closed-form expression of the inverse Radon transform, we should expect this phenomenon of noise amplification except in the lucky but rare situations where all computations can be performed analytically. As soon as approximations enter the game, the discontinuous nature of the inverse Radon transform may generate some artifacts in the sought-after DD.

The way to go is well-known in the mathematical literature (see *e.g.* Ref. [213]). Assuming that the underlying DD is smooth enough, it is possible to numerically invert the Radon transform while keeping noise under control. This is called regularization.

This chapter falls into three sections. We first discretize our problem to reduce it to the computation of the pseudo-inverse of a rectangular matrix. Then we select adequate linear solver and regularization procedure. At last we validate our computing chain with simple but

relevant test case scenarios.

8.2. Discretization

The goal now is to obtain a discrete problem from the integral equation (7.2), and we will use the usual notation:

$$AX = B \,, \tag{8.1}$$

where A is a $m \times n$ matrix, X a vector of dimension n, and B a vector of dimension m.

8.2.1. Mesh

To obtain this finite-dimensional linear problem, the DD space should first be discretized. In an abstract way, we use a set of basis functions $\{v_j\}$ for the decomposition:

$$h \left(\beta, \alpha \right) = \sum_j h_j \, v_j \left(\beta, \alpha \right) \,, \tag{8.2}$$

where the index j labels the set of basis functions, and therefore the degrees of freedom. Adopting a formalism close to the one of Finite Element Methods (FEM) [214, 215], these basis functions are in one-to-one correspondence to given nodes in the DD domain. Indexing these nodes means indexing the basis functions. Applying this to a given mesh which is a set of vertices (or corners) and edges defining its elements, we can be more explicit. A basis function is non-zero only on elements adjacent to its corresponding node, and the restriction of a basis function to one such element is the Lagrange interpolation with respect to this node, *i.e.* the polynomial that is equal to 1 on the said node, and 0 on all others. See Fig. 8.1 for an example of such a basis function.

Following the conventions of FEM [216], we will consider the following classification:

P_n-**Lagrange** Used for triangular meshes, where the restriction of a basis function to a triangular element is an interpolating polynomial of total degree at most n. For example, for P_1, it would be a polynomial of the form $a + b\,\beta + c\,\alpha$.

Q_n-**Lagrange** Used for quadrilateral meshes, where the restriction of the basis function to a mesh element is an interpolating polynomial of partial degree at most n. For example, for Q_1, it would be a polynomial of the form $a + b\,\beta + c\,\alpha + d\,\beta\,\alpha$.

In the case of linear piece-wise functions (P_1 or Q_1), the considered nodes of the basis functions are the vertices of the mesh. For higher orders, the nodes also include other points (such as the middle of the edges for P_2 and Q_2). We will also consider constant piece-wise functions and we will call those elements P_0 (which corresponds to dP_0 in FEM notations). In this case, each basis function corresponds to one element (or any node in the interior of the element, *e.g.* the center of gravity, to keep the same correspondence between nodes and basis functions). Tab. 8.1 summarizes this.

Our unknowns $\{h_j\}$ of Eq. (8.2) correspond to the values of the DD h on the nodes j, and will be recast into the vector X of the discrete problem (8.1).

Order n	Basis function	Node
0	Piece-wise constant	Center of gravity of an element
1	Piece-wise linear	Vertex of the mesh
2	Piece-wise quadratic	Vertex or middle of an edge

Table 8.1. Summary of the different P_n elements. Each basis function has support on the elements surrounding the corresponding node. The restriction to an element is a Lagrange interpolation: it takes a value of 1 on the said node, and 0 on all the other nodes.

For the work presented here, we will consider only a triangular mesh, since the domain is a triangle anyway (see Fig. 7.1), with P_1 or P_0 elements.

We will always use the index j in the following to label the basis functions, *i.e.* the nodes, and the index k for labelling the triangular elements. Of course, in the case of P_0, the indices will be interchangeable, since a basis function is defined by an element.

8.2.2. Basis functions

In the case of a triangular mesh, it is natural to use barycentric coordinates to define the basis functions (instead of the Cartesian coordinates). For a given triangle k, we will denote by $\{\lambda_k^1(\beta, \alpha), \lambda_k^2(\beta, \alpha), \lambda_k^3(\beta, \alpha)\}$ the barycentric coordinates with respect to the three vertices. Note that the number of degrees of freedom is still 2, since $\lambda_k^1 + \lambda_k^2 + \lambda_k^3 = 1$. A given point (β, α) belongs to the triangle k if all three barycentric coordinates are positive. Moreover, for P_1 elements, they provide natural restrictions for the basis functions, since they are exactly the linear Lagrange interpolations at the vertices. If we denote by (β_i, α_i), $i = 1 \ldots 3$, the three vertices of a triangle, then the barycentric coefficient with respect to the first vertex can be written as:

Figure 8.1. Example of a P_1 basis function. The corresponding node (*i.e.* a vertex in this case) is represented in blue. The value of the basis function on this node is 1, and 0 on the others. The support is limited to the adjacent triangles (in salmon red color).

$$\lambda^1(\beta, \alpha) = \frac{\beta_3 \alpha_2 - \beta_2 \alpha_3 + (\alpha_3 - \alpha_2)\beta + (\beta_2 - \beta_3)\alpha}{\beta_3 \alpha_2 - \beta_2 \alpha_3 + (\alpha_3 - \alpha_2)\beta_1 + (\beta_2 - \beta_3)\alpha_1}, \tag{8.3}$$

and the others similarly by cycling indices.

The matrix of the linear problem is determined by the linear operator that transforms a DD into a GPD in Eq. (7.2). To build this matrix, we only need to know the Radon transform of a basis function:

$$\mathcal{R} v_j(x, \xi) = \int v_j(\beta, \alpha)\, \delta(x - \beta - \alpha\xi)\, \mathrm{d}\beta\, \mathrm{d}\alpha. \tag{8.4}$$

Let us first express this basis function in the P_0 and P_1 cases (superscripts 0 and 1 respectively):

$$v_j^0 (\beta, \alpha) = \theta \left(\lambda_j^1 (\beta, \alpha) \right) \theta \left(\lambda_j^2 (\beta, \alpha) \right) \theta \left(\lambda_j^3 (\beta, \alpha) \right) , \tag{8.5}$$

$$v_j^1 (\beta, \alpha) = \sum_{\substack{k \in \text{elements} \\ \text{adjacent to vertex } j}} \theta \left(\lambda_k^1 (\beta, \alpha) \right) \theta \left(\lambda_k^2 (\beta, \alpha) \right) \theta \left(\lambda_k^3 (\beta, \alpha) \right) \lambda_k^{\bar{j}} (\beta, \alpha) , \tag{8.6}$$

where $\bar{j}$ is the vertex j recast to the limited set $\{1, 2, 3\}$ of vertices of the element k. The P_1 basis function is also represented in Fig. 8.1. Applying the Radon transform on these basis functions yields:

$$\mathcal{R}v_j^0 (x, \xi) = \theta \left(\alpha_{\max}^j - \alpha_{\min}^j \right) \left(\alpha_{\max}^j - \alpha_{\min}^j \right) , \tag{8.7}$$

$$\mathcal{R}v_j^1 (x, \xi) = \sum_{\substack{k \in \text{elements} \\ \text{adjacent to vertex } j}} \theta \left(\alpha_{\max}^k - \alpha_{\min}^k \right) \int_{\alpha_{\min}^k}^{\alpha_{\max}^k} d\alpha \, \lambda_k^{\bar{j}} (x - \alpha\xi, \alpha) , \tag{8.8}$$

where the bounds of the integration $\left\{ \alpha_{\min}^k, \alpha_{\max}^k \right\}$ are determined with the three inequalities given by the Heaviside functions (positive barycentric coordinates). For higher order elements, the idea is the same, only the integrated function will change.

8.2.3. Sampling

The next step is then to discretize the GPD variables (x, ξ), *i.e.* to sample the set of straight lines intersecting the domain Ω. Given that we have only access to DGLAP kinematics, we will use the couples $(x, y) \in [-1, +1]^2$ with $y = \xi/x$. The choice of (x, y) will determine a line of the matrix. More precisely, the matrix A will have the coefficients:

$$A_{ij} = C^> (x_i, \xi_i) \, \mathcal{R}v_j (x_i, \xi_i) , \tag{8.9}$$

where $1 \leq i \leq m$ indexes the lines of the matrix, and $1 \leq j \leq n$ indexes the columns, *i.e.* the nodes in DD space. The $C^>$ factor was introduced in Eq. (7.2).

The size of the matrix is chosen such that we maximize the information, *i.e.* we need to integrate over lines that cross all the elements of the DD mesh. A value of $m \sim 4\,n$ is empirically satisfying. The matrix can be therefore built by picking random couples (x, y) until we attain the desired size. The results will of course depend on the matrix used and it is interesting to consider this as a source of "statistical error", whereas the regularization procedure (see the following section) would be the source of "systematic error". The statistical error can be managed quite easily and reduced considerably by picking as many samples as we want, whereas the systematic error remains a challenge to estimate.

Once the matrix is built, we use the set of chosen couples (x, y) to build the vector B r.h.s. of Eq. (8.1) with simply:

$$B_i = H^> (x_i, \xi_i) . \tag{8.10}$$

In summary, A is a matrix $m \times n$ where n is the number of mesh elements for P_0 (or number of vertices for P_1) and m the number of straight lines intersecting Ω. Each line will typically cross $\mathcal{O}(\sqrt{n})$ mesh elements, which means that only $\mathcal{O}(\sqrt{n})$ coefficients on a matrix line are non-zero and A is a sparse matrix. We need more constraints than parameters ($m > n$) and we usually use $m = 4n$, making the rank of $A \lesssim n$ (*i.e.* close to full-rank). B is a vector of dimension m, and X of dimension n.

8.3. Linear solver and regularization

An additional complexity arises in the selection of the matrix inversion routine.

In Sec. 7.3, we assumed the existence of a covariant extension of a DGLAP-restricted GPD $H_{|DGLAP}$ and showed its uniqueness up to the manifestations of ambiguities on the line $\beta = 0$. The question now is to know whether such an extension even exists? We will circumvent this issue by the following consideration.

A numerical solver may have to handle a linear system as in Eq. (8.1) but without one and only one solution. This is common in computerized tomography, not because the solution does not exist (there was one object inserted inside the scanning device), but because the experimental signal comes with noise which may apparently modify the original situation to an *inconsistent data problem*. In the framework of the Radon transform, causes may be multiple: the integration lines may not cross the same domain (no solutions), or they may be parallel and close to one another and bring redundant information (infinitely many solutions). One efficient way to ensure that the solution always exists and is unique is to turn to a least-squares formulation:

$$\text{Search } X \in \mathbf{R}^n \text{ such that } \|AX - B\|^2 \text{ is minimum,} \tag{8.11}$$

where $\|\cdot\|$ generically denotes a norm in a finite-dimensional vector space.

In the present work, we use a recent iterative conjugate-gradient type algorithm for sparse least-squares problems: LSMR [217]. For inconsistent problems (where the least-squares formulation is favored), it is equivalent to a Minimum Residual algorithm for the problem:

$$^tAA\,X = {}^tAB\,, \tag{8.12}$$

but it can also solve directly the problem (8.1) when it is consistent, *i.e.* when the numerical approximation of the target solution is equal to the exact function. In the P_0 case, it means functions that are already piece-wise constant, whereas a P_1 approximation can reproduce exactly a (piece-wise) linear polynomial.

This type of algorithms applies naturally its own regularization process, with the number of iterations being the regularization parameter. To illustrate this, we can use the so-called L-curve [21], which is a curve following a regularization parameter (which is in our case the number of iterations) and shows the compromise between the norm of the solution $\|X\|$ (the larger the norm, the larger the impact of noise) and the residual norm $\|r\|$, where $r = AX - B$ (which we desire to be small enough to converge to the real solution). This procedure gives the optimal regularization factor to choose for each problem, as the point of maximum curvature of the "L", as shown in Fig. 8.2.

In practice, as illustrated on Fig. 8.2, it is very difficult to determine this optimal regularization parameter for the considered problems. A better way to stop the iterations is to consider the stopping criteria used by these algorithms such as LSMR:

- For a consistent problem: $\|r\| \leq \mathtt{atol}\,\|A\|\,\|X\| + \mathtt{btol}\,\|B\|$;

- For a least-squares problem: $\|A\,r\| \leq \mathtt{atol}\,\|A\|\,\|r\|$,

where $\mathtt{atol}$ and $\mathtt{btol}$ are the input tolerances.
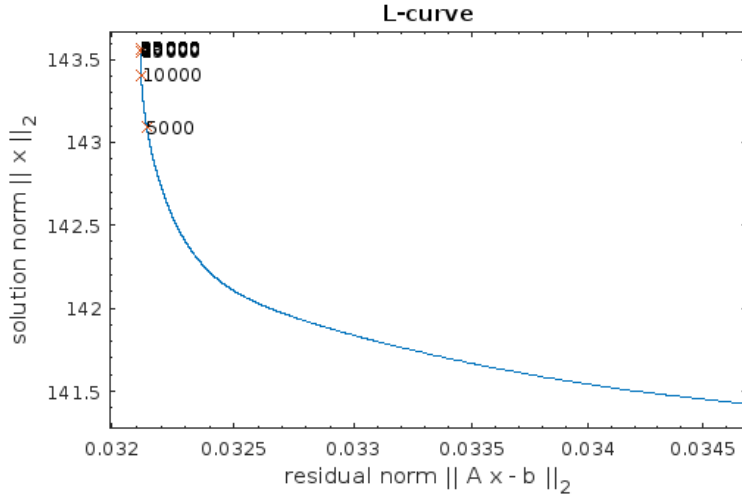
Figure 8.2. L-curve obtained with the number of iterations as regularization parameter for the case of Sec. 9.1.

An empirical value of 10^{-5} for the least-square tolerances gives a good compromise between noise and convergence, and this has the benefit of being valid for all considered cases. A 10^{-5} value for `atol` (resp. `btol`) means that the matrix A (resp. the right hand side B) is known exactly up to the fifth decimal, while the rest is numerical noise. Of course, in practice, we can compute analytically A (if the chosen basis functions and mesh allow us to compute the Radon transform without numerical integration, as it is the case for the method presented here) and B (if the GPD is known analytically), and they are therefore known exactly, up to machine precision. But in the inconsistent (*i.e.* least-squares) case, the considered vector B is different from the one due to a GPD calculated from the discrete numerical DD. This difference is the finite limit of the residual, in contrast with the consistent case where the residual has a zero limit. Even though small, when allied with the ill-posed character of the inversion, it can have a large impact on the solution. This is why we consider in practice that B (or equivalently A) is not known exactly and neglect higher decimals; we apply a regularization procedure by doing so.

8.4. Test and validation of the numerics

8.4.1. Smooth examples

The first immediate check we can perform to validate the numerical implementation described above, consists in the following. We first take a simple Ansatz for the DD, irrespective of the considered value of t (*e.g.* $t = 0$). We then compute the associated analytical GPD by applying the Radon transform, and use only its DGLAP part to apply our numerical inversion and obtain a numerical estimate of the DD. Finally, we compare this result with the original Ansatz. We will apply this testing procedure to the following three quark GPDs, each one of them deriving from a DD in the P representation:

(i) A constant DD $h_p^{\text{cst}}(\beta, \alpha)$ on the half-domain $\Omega^>$:

$$h_{\text{P}}^{\text{cst}}(\beta, \alpha) = \frac{3}{2} \mathbf{1}_{\Omega^>}(\beta, \alpha) \quad \Rightarrow \quad \begin{cases} H_{|\text{DGLAP}>}^{\text{cst}}(x, \xi) = \dfrac{3(1-x)^2}{1-\xi^2}, \\ H_{|\text{ERBL}}^{\text{cst}}(x, \xi) = \dfrac{(1-x)(x+\xi)}{\xi(1+\xi)}. \end{cases} \tag{8.13}$$

(ii) the example defined by Eq. (5.59) and already introduced in Sec. 5.4.1,

(iii) and a simplified case of the RDDA (5.29):

$$h_{\mathrm{P}}^{\mathrm{RDDA}}(\beta,\alpha) = \pi_N(\beta,\alpha)\,\frac{q(\beta)}{1-\beta}\,\mathbf{1}_{\Omega>}(\beta,\alpha)\,, \tag{8.14}$$

where the quotient $(1-\beta)$ compensates for the P representation (see the relations (5.41)). In particular, we specialize for the case $N=1$ and take[1] $q(\beta) = 30\,\beta^2(1-\beta)^2$. We thus obtain a closed algebraic formula for the GPD:

$$H_{|\mathrm{DGLAP}>}^{\mathrm{RDDA}}(x,\xi) = \frac{30\,(1-x)^2}{\xi^3\,(1-\xi^2)^2}\Big(-3\xi\,(2-x) + \xi^3\,(10-(5-x)\,x) - 3\xi^5 \tag{8.15}$$

$$+\,3\left(1-\xi^2\right)^2(2-x)\tanh^{-1}(\xi)\Big),$$

$$H_{|\mathrm{ERBL}>}^{\mathrm{RDDA}}(x,\xi) \;=\; \frac{15\,(1-x)}{2\xi^3\,(1+\xi)^2}\Big((x+\xi)\big(-(2+\xi)\,(6+(6-\xi)\,\xi) - (1+2\xi)\,x^2$$

$$+\,(3+\xi)\,(4+5\xi)\,x\big) - 6\,(2-x)\,(1-x)\,(1+\xi)^2\log\left(\frac{1-x}{\xi+1}\right)\Big), \tag{8.16}$$

which, in turn, can be numerically inverted with the procedure described above.

In all cases, we adopted the P representation as it appears to be convenient for GPD models derived through a covariant extension of an overlap of LFWFs, as discussed in Sec. 5.3.5 and Sec. 7.3. In the leftmost plots of Fig. 8.3, we display the comparison of the exact algebraic and numerically approximated $h_{\mathrm{P}}^{\mathrm{cst}}(\beta,\alpha)$ for the case (i), while the rightmost ones stand for the comparison of the GPDs directly obtained from both DDs. The upper and lower plots have been obtained, respectively, with piecewise constant (*i.e.* P_0 elements) and piecewise linear (*i.e.* P_1) basis functions when discretizing the DD space for the reduction to a finite-dimensional problem, as explained in Sec. 8.2. Analogous plots, and similarly arranged, are displayed in Fig. 8.4 for case (ii) and Fig. 8.5 for case (iii).

The mesh was generated using the `Triangle` software [218] with a requirement of maximal area for the triangular elements equal to 0.001, which produced a mesh of 427 vertices and 780 elements. The linear solver used is described in Sec. 8.3. As justified before, we used a tolerance of 10^{-5} as a regularization procedure.

All in all, as an overall conclusion we can assert that the numerical inversion approximates very well the three known GPDs as they appear not to differ significantly in all the cases. Several important points should be however stressed out:

- The numerical inversion relies only on the knowledge of the GPD within the DGLAP region and its extension to the ERBL is our main goal, therefore the examination of algebraic and numeric GPDs over the ERBL region is the main outcome of Figs. 8.3-8.5.

- The numerical reconstruction of the DDs may seem quite noisy or far off in some cases, but these discrepancies do not hinder the reconstruction of the GPD, for which the

---

[1]See Sec. 6.2.3.
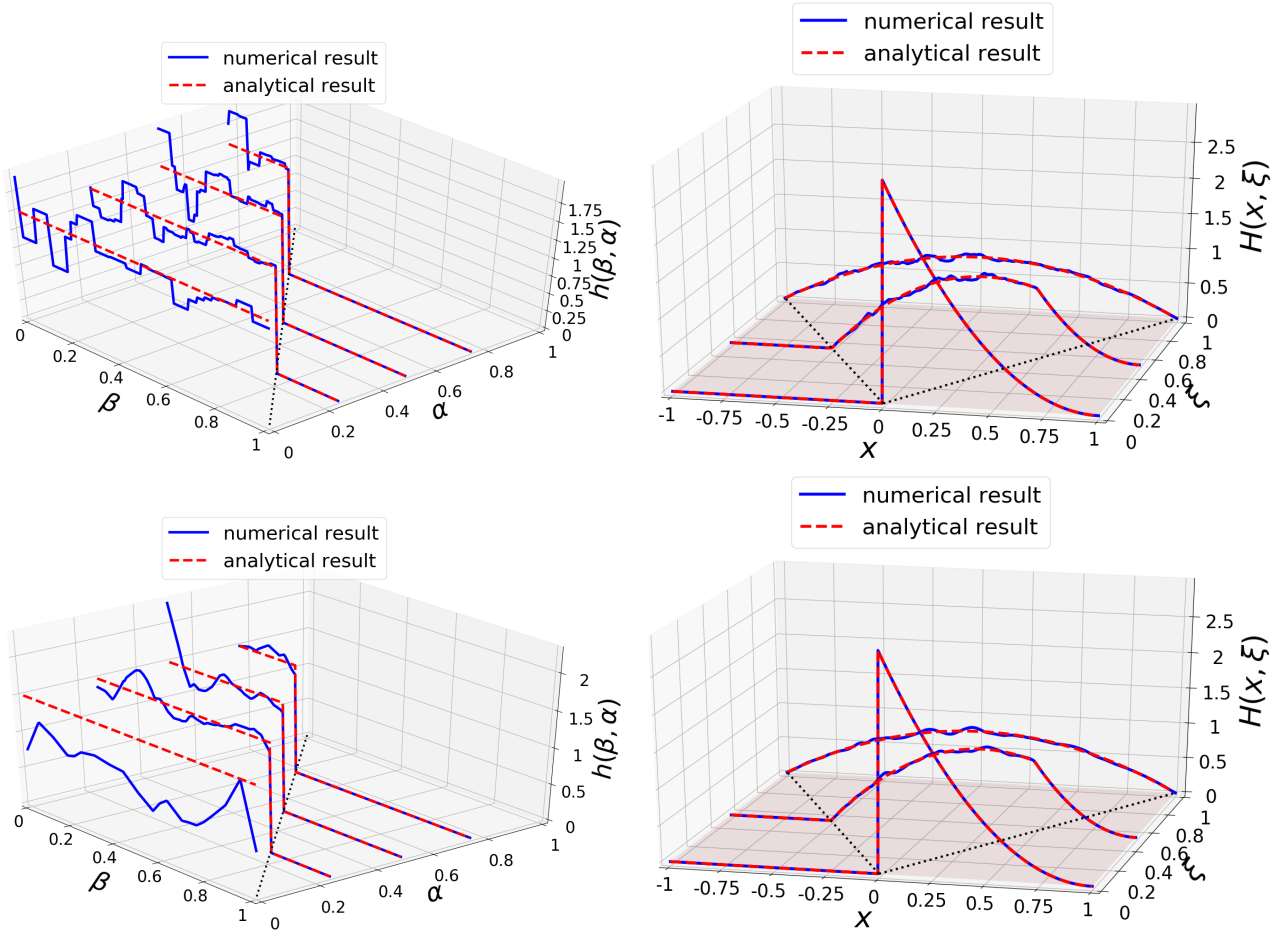
Figure 8.3. Comparison between algebraic, given by Eq. (8.13), and numerical results for the DD $h_{\mathrm{P}}^{\mathrm{cst}}(\beta, \alpha)$ at fixed values of $\alpha = [0, 0.25, 0.5, 0.75]$ (left panel) and the corresponding GPD $H^{\mathrm{cst}}(x, \xi)$ at fixed values of $\xi = [0, 0.5, 1]$ (right panel) for the case (i). The blue solid curves display the numerical results while the red dashed ones show the algebraic results. The black dotted curves indicate either the line $\beta + \alpha = 1$ (left panel) or $x \pm \xi = 0$ (right panel). The upper panel stands for a discretization obtained with P_0 elements, while the lower panel displays the results with P_1 elements.

convolution helps smooth these defects[2]. The physical object of interest is the GPD, not the DD, therefore these discrepancies are not an issue. For this reason, in Chap. 9, we will display only the GPD plots when illustrating the procedure with real applications to LFWFs occurring in descriptions of hadron structure.

- It should be noted however that the constant DD can be reconstructed numerically exactly (up to machine precision). Indeed, the regularization in that case is not needed, since there is no distinction between the analytical DD and its discretized version. We could

---

[2]This should not come as a surprise. The Radon transform is a smoothing operator, since it integrates a DD over lines. Conversely, the inverse Radon operator has to undo this smoothing to reconstruct the DD, hence provoking noise amplification.
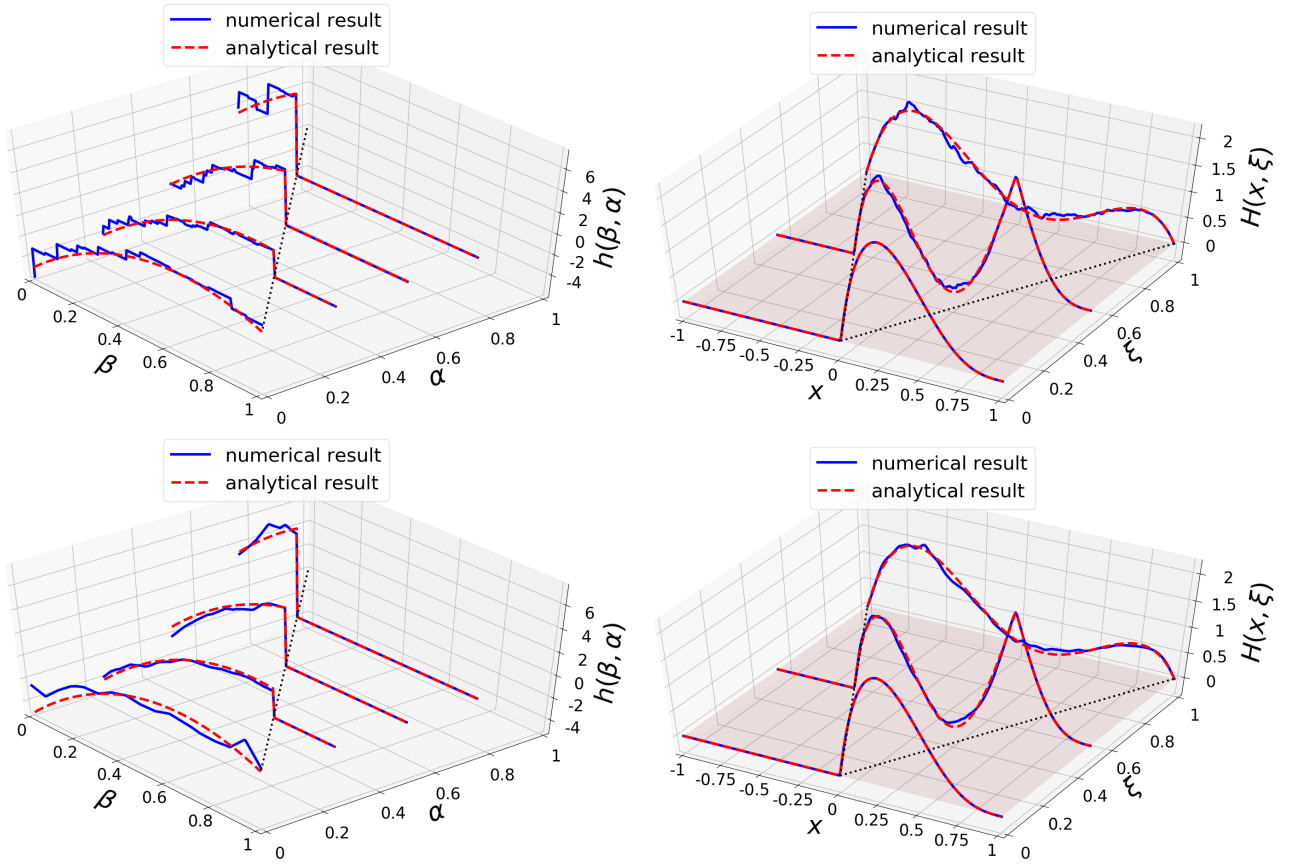
Figure 8.4. Comparison between algebraic, given by Eqs. (5.59)-(5.61), and numerical results for the DD $h_{\mathrm{P,\,Reg}}^{\mathrm{Toy}}(\beta,\alpha)$ (left panel) and the corresponding GPD $H^{\mathrm{Toy,\,Reg}}(x,\xi)$ (right panel) for the case (ii). Same conventions as in Fig. 8.3.

therefore directly invert the discrete problem and recover the exact DD (which would be equivalent to using a tolerance of 0 instead of 10^{-5}), but for the sake of homogeneity, we decided to employ the same method for all shown examples.

- It may seem from the plots that the P_1 discretization does not improve on the P_0 result, but this is not true. We chose here to use the same mesh for both P_0 and P_1 elements. This particular mesh has 427 vertices and 780 triangular elements. Hence, the number of degrees of freedom for P_1 (*i.e.* the number of vertices) is half the one for P_0 (*i.e.* number of elements). In other words, we attain with P_1 a similar result to the P_0 one but with half the degrees of freedom, *i.e.* at a much lower cost. It is therefore a significant improvement. Consequently, in Chap. 9, we will keep only the P_1 method.

8.4.2. Parametrization with Regge behabior

All the previous examples dealt with GPDs smoothly behaving at $x = 0$. However, phenomenological models for valence quark GPDs often exhibit an integrable singularity, typically a $1/\sqrt{x}$ behavior. If such a GPD is related to a DD h_{P} in the P representation, then it can
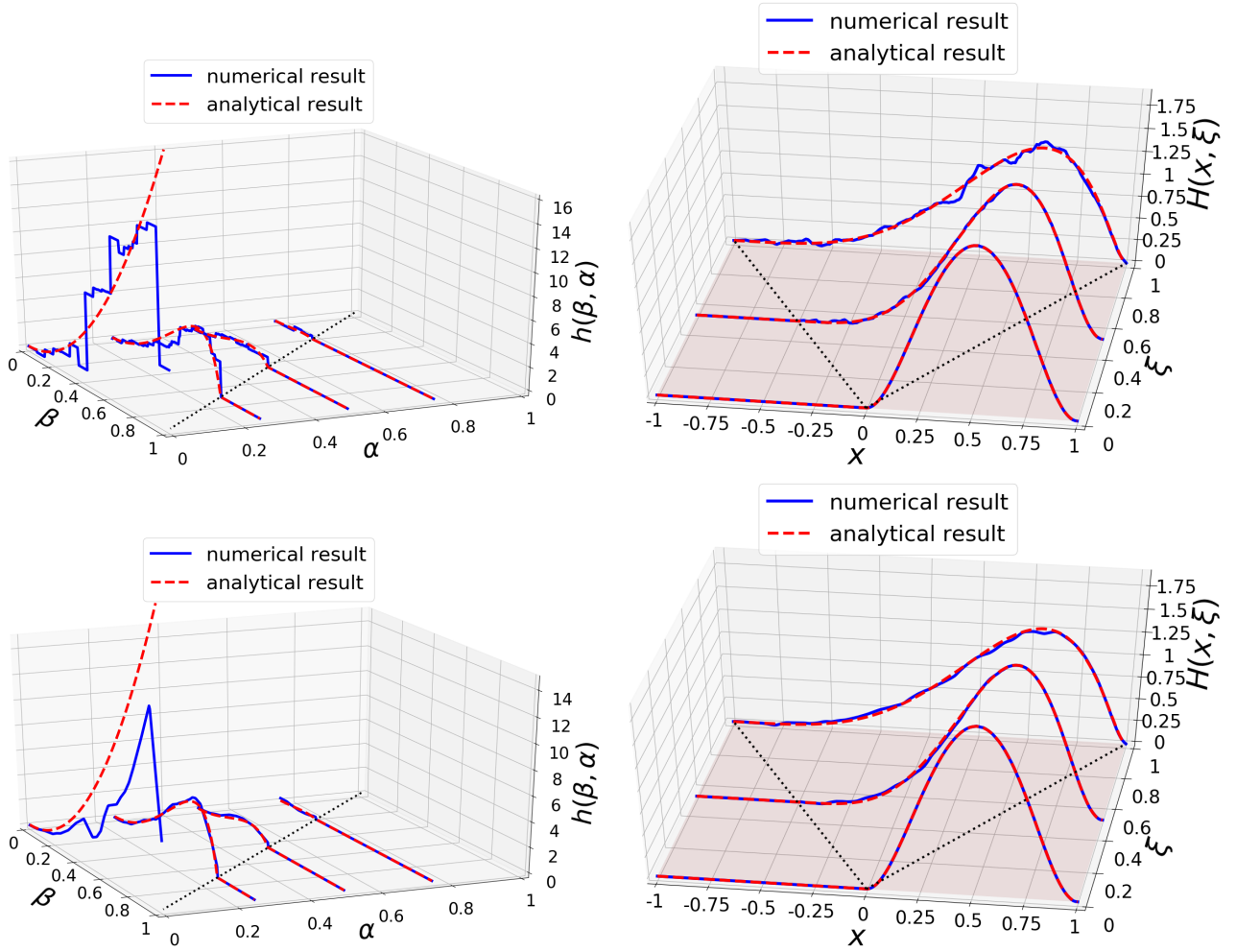
Figure 8.5. Comparison between algebraic, given by Eqs. (8.14)-(8.16), and numerical results for the DD $h_{\mathrm{P}}^{\mathrm{RDDA}}(\beta, \alpha)$ (left panel) and the corresponding GPD $H^{\mathrm{RDDA}}(x, \xi)$ (right panel) for the case (iii). Same conventions as in Fig. 8.3.

be shown that $H(x, 0) \sim \int_{-1}^{+1} d\alpha\, h_{\mathrm{P}}(x, \alpha)$ at small x. Therefore h_{P} itself may also exhibit an integrable singularity $1/\sqrt{\beta}$. The numerical method presented up to now approximates the target DD by piecewise constant or piecewise linear functions on Ω. In particular all approximations are bounded, even if in principle they can be more and more peaked when the mesh gets thinner. As discussed in Sec. 8.2 and Sec. 8.3, careful choices of the size of the mesh and of the number of iterations are essential for the resolution of the inverse problem with adequate control of the numerical noise. With a naive discretization, it is difficult when dealing with singularities to make sense of a solution; it would probably require a number of iterations that is not attainable due to the necessary truncation of the regularization. We thus adopt a more educated discretization; knowing that we are dealing with Regge-type singularities, we can adapt our method accordingly, by discretizing:

$$h_{\mathrm{P}}'(\beta, \alpha) = \sqrt{\beta}\, h_{\mathrm{P}}(\beta, \alpha) \tag{8.17}$$

which will be less singular that h_P, possibly even free of singularities. This change of target function only modifies the kernel of Eq. (7.2) (it is not a Radon transform anymore), otherwise everything readily follows the same procedure.
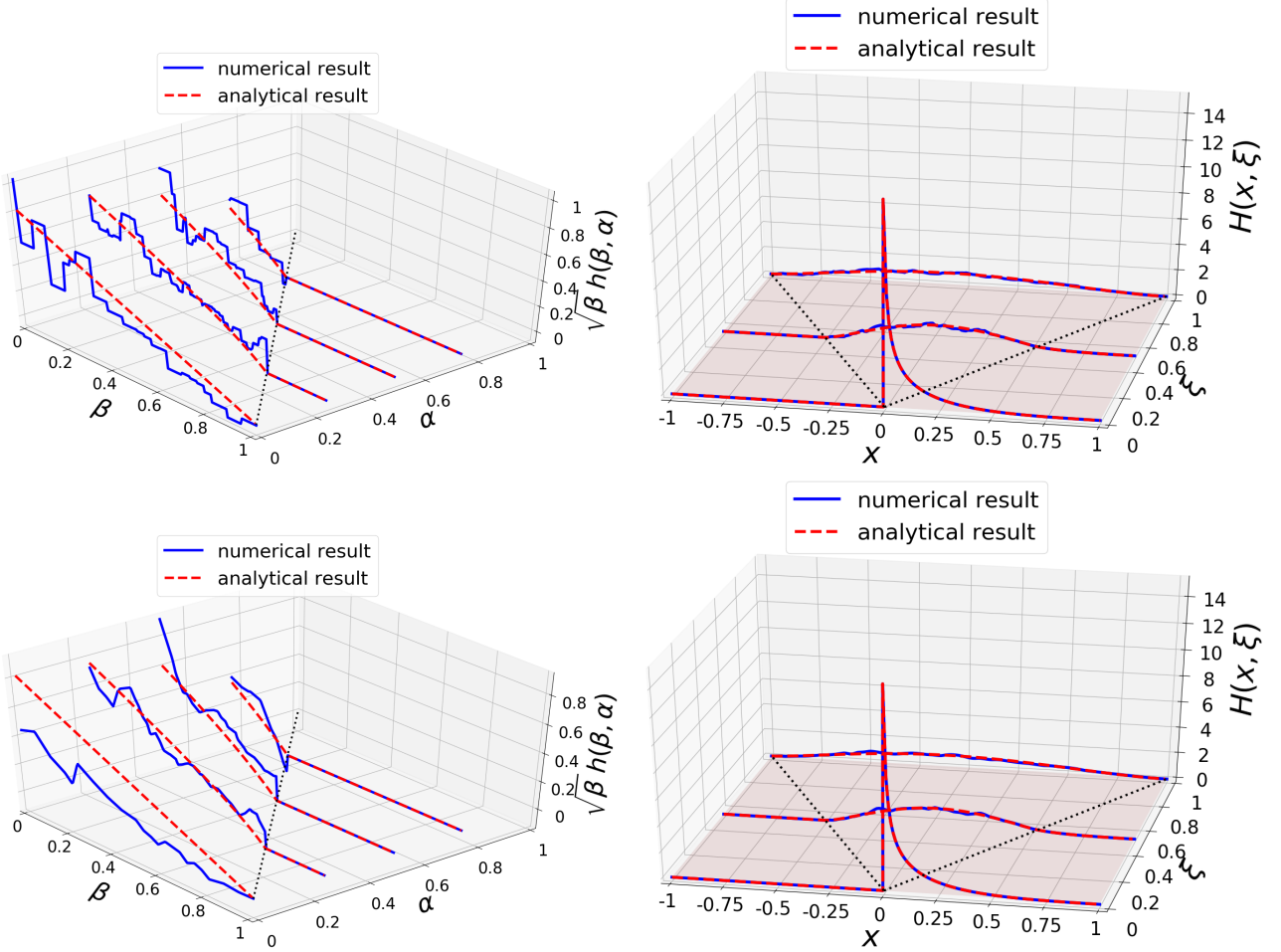
Figure 8.6. Comparison between algebraic, given by Eqs. (8.19)-(8.21), and numerical results for the DD $h_\mathrm{P}^\mathrm{Regge}(\beta, \alpha)$ (left panel) and the corresponding GPD $H^\mathrm{Regge}(x, \xi)$ (right panel). Same conventions as in Fig. 8.3.

Let us exemplify this technique on a simple parametrization of nucleon DD for which, once again, the expression is already known. We use the RDDA as presented in Sec. 5.3.2 and Eq. (8.14) for $N = 1$, but this time with a singular PDF[3]:

$$q^\mathrm{Regge}(x) = \frac{35\,(1-x)^3}{32\,\sqrt{x}}\,, \tag{8.18}$$

which would give the following DD (with a $1/\sqrt{\beta}$ singularity) on $\Omega^>$:

$$h_\mathrm{P}^\mathrm{Regge}(\beta, \alpha) = \frac{105\left((1-\beta)^2 - \alpha^2\right)}{128\,(1-\beta)\,\sqrt{\beta}}\,. \tag{8.19}$$

---

[3]This simple model is similar in spirit to the parametrizations of the nucleon GPDs H, E, $\tilde{H}$ and $\tilde{E}$ used in popular phenomenological models, see *e.g.* the review Ref. [26] and refs therein.

The corresponding GPD is[4]

$$H^{\text{Regge}}_{|\text{DGLAP}>}(x,\xi) = H^{\text{Regge}}_{|\text{ERBL}}(x,\xi) + H^{\text{Regge}}_{|\text{ERBL}}(x,-\xi) \,, \tag{8.20}$$

$$H^{\text{Regge}}_{|\text{ERBL}}(x,\xi) \quad = \frac{35}{64}\frac{1-x}{\xi^3}\left[\sqrt{\frac{x+\xi}{1+\xi}}\left(3+\xi(1+2\xi)-x(5+\xi)\right)\right. \tag{8.21}$$

$$\left. - 3(1-x)^2\tanh^{-1}\left(\sqrt{\frac{x+\xi}{1+\xi}}\right)\right] .$$

The comparison between the algebraic GPD and the result obtained through the numerical reconstruction of the DD with DGLAP information is shown on Fig. 8.6.

8.4.3. Photon GPDs

Let us now turn to the photon GPDs described in Sec. 5.4.2. We apply again the same procedure described in this chapter, but this time in the T representation instead of P, with only P_1 elements for the discretization. The results for both GPDs $H^{\gamma,>}_{1,\text{Reg}}$ (5.76) and $H^{\gamma,>}_3$ (5.77) are displayed in figures 8.7 and 8.8 respectively[5]. For the iterative algorithm, we first used the same tolerance 10^{-5} as previously, which would allow us to regularize the ill-posed problem. But here, the examples considered are piece-wise constant and piece-wise linear DDs (see Eqs. (5.69)-(5.70)), which can be reproduced exactly by the P_1 discretization, so, as explained in sections 8.3 and 8.4.1, there is no need for regularization in this simple case. We can therefore lower the tolerance of the iterative method (*e.g.* to 10^{-10}) or use a direct pseudo-inverse routine, to achieve a much better precision. This means we do not need to trade-off between convergence and noise; we can attain an arbitrarily good result, as can be seen in the lower panels of figures 8.7 and 8.8.

The discrepancies that appear on these lower plots concern the lines of discontinuity for the DD, *e.g.* $\alpha = 0$. Indeed, both DDs $h^{\gamma,\text{Reg}}_{1\,\text{T}}$ (5.70) and $h^{\gamma}_{3\,\text{T}}$ (5.69) are defined in terms of the sign function and the value of $\text{sgn}(0)$ is a matter of convention. Here, for the analytical result, we use $\text{sgn}(0) = 0$. On the other hand, numerically, we invert the Radon transform by considering only the domain $\alpha \geq 0$ and complete by parity (see Sec. 7.2 for more details), *i.e.* in the case of the T representation $h_\text{T}(\beta,\alpha) = -h_\text{T}(\beta,-\alpha)$ for $\alpha < 0$. This means that the value of the DD at $\alpha = 0$ is obtained by a continuous extension of the values at $\alpha > 0$, the algorithm not being aware at all of the sheer existence of the domain $\alpha < 0$. Hence the discrepancies that we see on the plots. However, the value of the DD (when it is a function and not a *distribution*) on a single line does not matter for the integration and therefore for the GPD. Therefore, this is a non-issue. We could have also artificially glossed over it if we had used $\text{sgn}(0) = 1$ for the analytical curve.

---

[4]We abused notation in Eq. (8.20), by considering $H_{|\text{ERBL}}(x,\xi)$ outside its domain. Note that this relation between $H_{|\text{DGLAP}>}$ and $H_{|\text{ERBL}}$ is always valid when considering Double Distributions, but it implies some analytic continuation [211]. Here, there is no issue since we have a closed form fomula that can be evaluated outside the physical domain.

[5]The conventions for these figures are the same as previously, save for the meaning of upper and lower panels. See the corresponding captions.
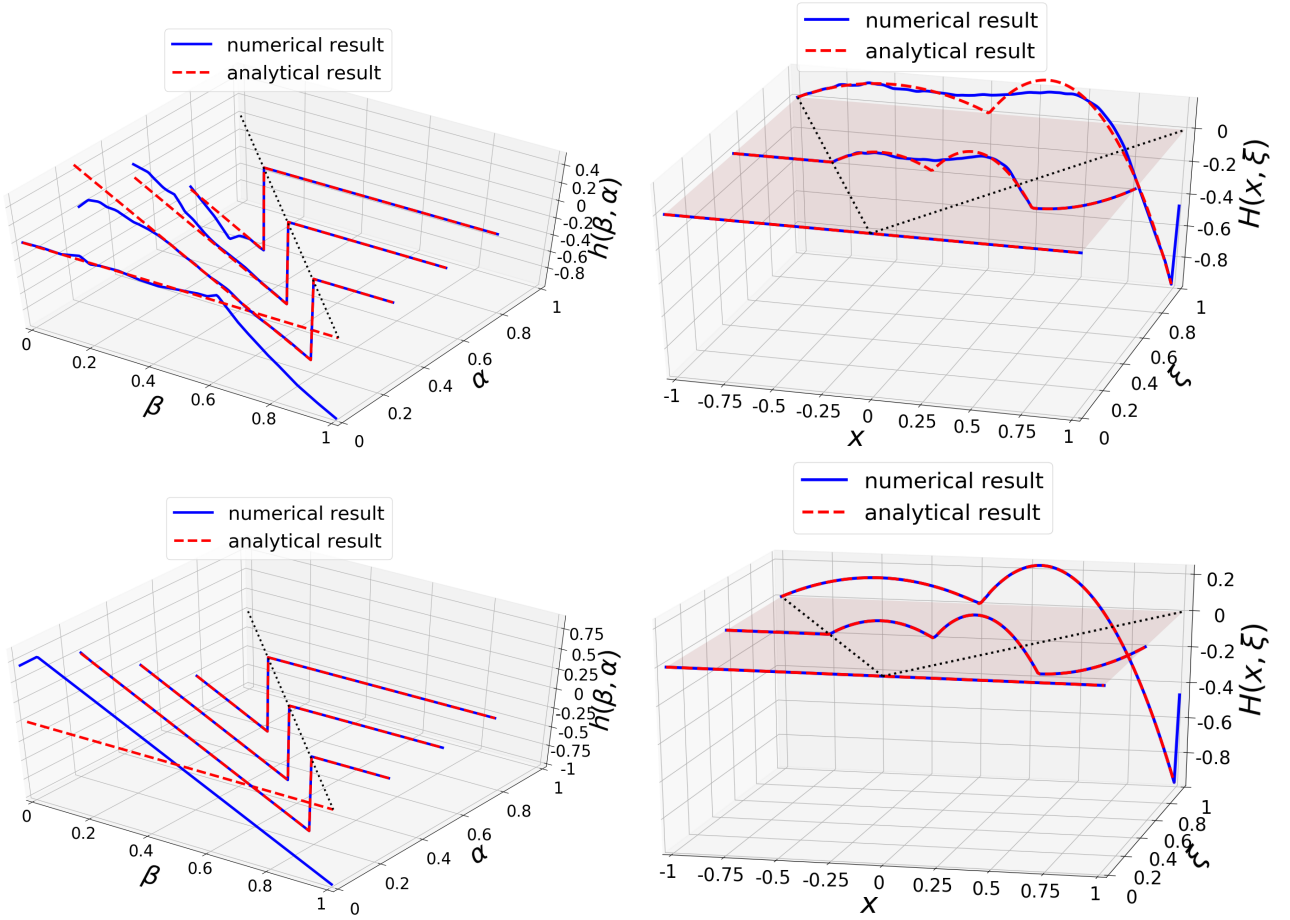
Figure 8.7. Results of the covariant extension from DGLAP to ERBL, for the GPD $H_{1,\mathrm{Reg}}^{\gamma>}$. Comparison between the numerical result (solid blue) and the known analytical target result (dashed red) of Eq. (5.76). **Left panels**: Plots of the DD $h_{1\mathrm{T}}^{\gamma,\mathrm{Reg}>}$ at fixed values of $\alpha \in \{0, 0.25, 0.5, 0.75\}$. **Right panels**: Plots of the difference $H_{1,\mathrm{Reg}}^{\gamma>}(x,\xi) - H_{1,\mathrm{Reg}}^{\gamma>}(x,0)$ at fixed values of $\xi \in \{0, 0.5, 1\}$. **Upper panels**: Tolerance for the least-squares algorithm of 10^{-5}. **Lower panels**: Tolerance of 10^{-10}.

We can also notice a discrepancy at $x = \xi = 1$. This is due to the fact that both GPDs H_1^γ and H_3^γ are not well-defined on that point. Indeed, we have for instance in the case of H_1:

$$H_1^\gamma (x = 1, \xi) = \frac{1 - \xi^2}{1 - \xi^2} = 1 \xrightarrow[\xi \to 1]{} 1 , \qquad (8.22)$$

while

$$H_1^\gamma (x = \xi, \xi) = \frac{(1 - \xi)^2}{1 - \xi^2} = \frac{1 - \xi}{1 + \xi} \xrightarrow[\xi \to 1]{} 0 . \qquad (8.23)$$

We get a different value whether we take the limit $(x, \xi) \longrightarrow (1, 1)$ on the direction $x = \xi$ or on the direction $x = 1$. Therefore, the GPDs are not continuous at this particular point, despite being continuous at the cross-over $x = \xi$. Hence, the apparent discrepancy should not come as a surprise.
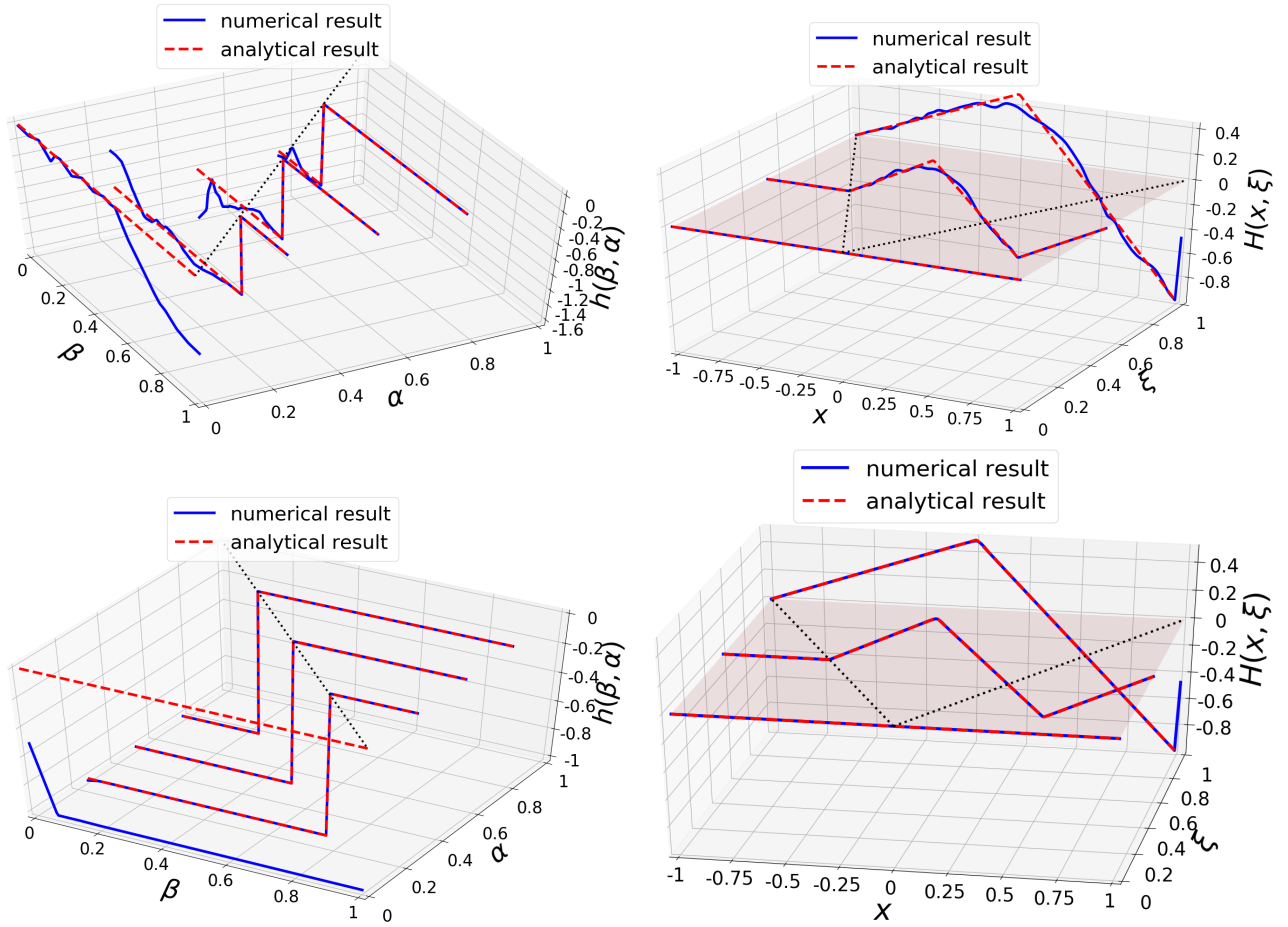
Figure 8.8. Results of the covariant extension from DGLAP to ERBL, for the GPD $H_3^{\gamma>}$. Comparison between the numerical result (solid blue) and the known analytical target result (dashed red) of Eq. (5.77). **Left panels**: Plots of the DD $h_{3\,\mathrm{T}}^{\gamma>}$ at fixed values of $\alpha \in \{0, 0.25, 0.5, 0.75\}$. **Right panels**: Plots of the difference $H_3^{\gamma>}(x,\xi) - H_3^{\gamma>}(x,0)$ at fixed values of $\xi \in \{0, 0.5, 1\}$. **Upper panels**: Tolerance for the least-squares algorithm of 10^{-5}. **Lower panels**: Tolerance of 10^{-10}.

Let us emphasize again that the GPD we obtain from a covariant extension of the DGLAP region is unique, up to a D-term like contribution. Since H_3^{γ} fulfills a degree-m polynomiality condition, there is no associated D-term, and therefore no ambiguity when extending the DGLAP region. We recover exactly the original GPD. For H_1^{γ} however, there is no hope to recover it numerically, at least in the present T representation, due to the explicit D-term like part in $h_{1\,\mathrm{T}}^{\gamma}$. We can only recover $H_{1,\mathrm{Reg}}^{\gamma}$, which is consistent with what is known and stated before in this thesis about the D-term ambiguity; H_1^{γ} is indeed part of the infinite set of solutions defined by $H_{1,\mathrm{Reg}}^{\gamma}$. This shows that our method is indeed general and can be applied to any model of GPD.

We see also that the T representation is particularly well-suited for such endeavor, and does not have the limitation of the P representation when it comes to the behavior of the GPD at $x \to 1$. Here, the GPDs do not vanish on this limit, which renders the use of the

P representation impossible. The presence of $\delta(\alpha)$ terms also makes the R representation intractable, but is not an issue for the T representation, as shown in Sec. 5.4.2.

In practice, for the next chapter, we will go back to the P representation as the examples considered have the good pQCD behavior at $x \to 1$.

Chapter 9.

Examples of application of the covariant extension

The approach described in Chap. 7 can be either applied to numerous existing LFWF-based GPD models to covariantly extend them from the DGLAP region to the ERBL one, or used to build a covariant GPD model, reliable on both DGLAP and ERBL regions, from the knowledge of the LFWF. Although in some particular cases, an analytical derivation of the DD is possible and a full GPD in both DGLAP and ERBL regions can be obtained, one can only proceed systematically by applying a numerical technique such as the one introduced in section Chap. 8. In this chapter, aiming to illustrate the procedure without the intention of being exhaustive, we provide four examples of GPD models, two of which can be extended to the ERBL region both analytically and numerically, allowing us to benchmark our algorithm. Three of these examples concern the pion and were introduced in Sec. 6.2.

9.1. Algebraic Nakanishi-based model

9.1.1. Extension to ERBL

We first consider the pion model of Sec. 6.2.3 based on a Nakanishi parametrization with the GPD given in Eq. (6.59). In this case, we managed to derive the DD analytically, through a sensible choice of trial functions, in the P representation:

$$h_{\mathrm{P}}(\beta, \alpha, t) = \frac{15}{2} \frac{1 - 3\alpha^2 - 2\beta + 3\beta^2 + \frac{-t}{4M^2}\left(1 - \alpha^4 + 2\alpha^2\beta^2 - \beta^4 + 4\beta^2 - 4\beta\right)}{\left(1 + \frac{-t}{4M^2}\left((1-\beta)^2 - \alpha^2\right)\right)^3} \mathbf{1}_{\Omega>}(\beta, \alpha) \ . \tag{9.1}$$

This result can then be plugged into Eq. (5.40), to provide us with a covariant extension of the model given in Sec. 6.2.3 to the ERBL kinematic domain. The ERBL GPD reads:

$$H(x, \xi, t) = -\frac{15\left(\xi^2 - x^2\right)}{4\left(1 + \zeta\right)^{5/2}\left(1 - \xi^2\right)^{3/2}\left(1 - x\right)^2\sqrt{\zeta\left(1 - \xi^2\right)}\left(\xi^2 + \frac{\zeta(1-\xi^2)(\xi^2 - x^2)}{(1-x)^2}\right)^2} \tag{9.2}$$

$$\times \Bigg(\sqrt{\zeta(\zeta + 1)}\Big(-\zeta\xi\left(1 - \xi^2\right)(1 - x)$$

Figure 9.1. Comparison between algebraic and numerical results for the pion GPD H in the Nakanishi-based model of Sec. 6.2.3. As it was the case in Fig. 8.3, the blue solid curves display the numerical results while the red dashed ones show the results algebraically derived and given by Eqs. (6.59) and (9.2). The left panel stands for the case $t = 0$ for fixed values of $\xi = [0, 0.5, 1]$ and the right one shows the t-behavior for fixed values $[0, -0.25, -0.5]$ at $\xi = 0.5$. We retain only P_1 elements. For more details, see Sec. 8.4.

$$\times \left(\xi^4 + 6\xi (1 - x) x^2 - 6\xi^3 (1 - x) + \xi^2 (4 - 3 (3 - x) x) + x (4 - x (8 - 5x)) \right)$$
$$+ \left(\zeta \left(1 - \xi^2 \right) \right)^2 \left(\xi^3 (3\xi - 2) + 3x^4 - 4\xi x^3 - 6(\xi - 1)\xi x^2 + 2\xi \left(\xi^2 - 1 \right) x \right)$$
$$+ (x - 1)^3 \left(\xi^5 + 3\xi^4 (x - 1) + \xi^3 (2 - 5x) + 2\xi x \right) \Big)$$
$$+ (1 - 2\zeta) \Big(\zeta \left(1 - \xi^2 \right) \left(\xi^2 - x^2 \right) + \xi^2 (x - 1)^2 \Big)^2$$
$$\times \left(\tanh^{-1} \left(\sqrt{\frac{\zeta}{1 + \zeta}} \right) - \tanh^{-1} \left(\sqrt{\frac{\zeta}{1 + \zeta}} \frac{\xi^2 - x}{\xi (1 - x)} \right) \right) \Bigg),$$

where we used again the notation ζ of Eq. (6.60). In the limit $t \to 0$, we can write:

$$H(x, \xi, 0) = \frac{15}{2} \frac{(1 - x) (\xi^2 - x^2)}{\xi^3 (1 + \xi)^2} \left(x + 2x\xi + \xi^2 \right). \tag{9.3}$$

These analytical expressions allow us to benchmark our numerical procedure, in the same principle as Sec. 8.4, but this time with a real application to a LFWF model. Thus, we compare the results given by Eq. (6.59) and Eq. (9.2), respectively derived for the DGLAP and ERBL kinematics, with those obtained by the numerical inversion of the linear problem described in Chap. 8, and display the outcome in Fig. 9.1. As can be seen, both numerical and algebraic results compare strikingly well, not only at a qualitative but also a quantitative level. The left

panel corresponds to the limit $t = 0$, while the right one displays the evolution at other values of t and a constant value of $\xi = 0.5$.

9.1.2. Soft pion theorem and D-term contributions

As we have stressed in Sec. 7.3, this extension is unique up to a D-term, or more generally up to terms defined on the line $\beta = 0$. These terms are necessarily *distributions*, as mere functions do not contribute to the integration on a single line (a line is negligible on the plane for Lebesgue integration). One example of such distributions is the said extra D-term $g_{\mathrm{PW}}(\beta, \alpha) = \delta(\beta) D_{\mathrm{PW}}(\alpha)$, but we could also have derivatives of the Dirac distribution[1], *e.g.* a term of the form $g_{\delta'}(\beta, \alpha) = \delta'(\beta) D_1(\alpha)$. Such a term in the DD g contributes to the GPD as:

$$H_{\delta'}(x, \xi) = \frac{1}{|\xi|} D_1'\left(\frac{x}{\xi}\right). \tag{9.4}$$

Notice the derivative of D_1. It is equivalent to a contribution of the Dirac distribution in the DD f, *i.e.* $f_\delta(\beta, \alpha) = \delta(\beta) D_1'(\alpha)$, and D_1' was called D^+ in Refs. [18, 19].

What matters is that we can now fulfill the soft pion theorem of Eqs. (6.32)-(6.33), which allows us to constrain the extra D-terms at $t = 0$. Indeed, D_{PW}, being α-odd, contributes only to Eq. (6.32), while D_1', being α-even, contributes only to Eq. (6.33). Knowing the DA in the present model from the definition (6.30) (see also the wave-function (6.52)):

$$\Phi(z) = 6 z (1 - z), \tag{9.5}$$

which corresponds to the so-called asymptotic DA, we can deduce the necessary D_{PW} and D_1' terms:

$$D_{\mathrm{PW}}(\alpha, t = 0) = -\frac{15}{4} \alpha \left(1 - \alpha^2\right), \tag{9.6}$$

$$D_1'(\alpha, t = 0) = -\frac{9}{8} \left(1 - \alpha^2\right) \left(1 - 5\alpha^2\right). \tag{9.7}$$

We thus removed the ambiguity, but only at $t = 0$ and in the simple case of the pion. This procedure is detailed in Ref. [19].

How to constrain the D-term at any value of t (and for the nucleon) remains an open subject, but several directions can be followed, such as the Mellin moments Lattice calculations, or a phenomenological parametrization of the D-term with free parameter(s) in fits to experimental data, to quote a few of them.

9.2. Algebraic spectator diquark model

If LFWFs have been widely used in attempts to model the pion, the case of the nucleon has also been treated previously, in particular in the pioneering paper of Hwang and Müller [20]. They

---

[1]Note that in this case, the dispersion relations of Sec. 3.2.2 would need more than one subtraction constant.
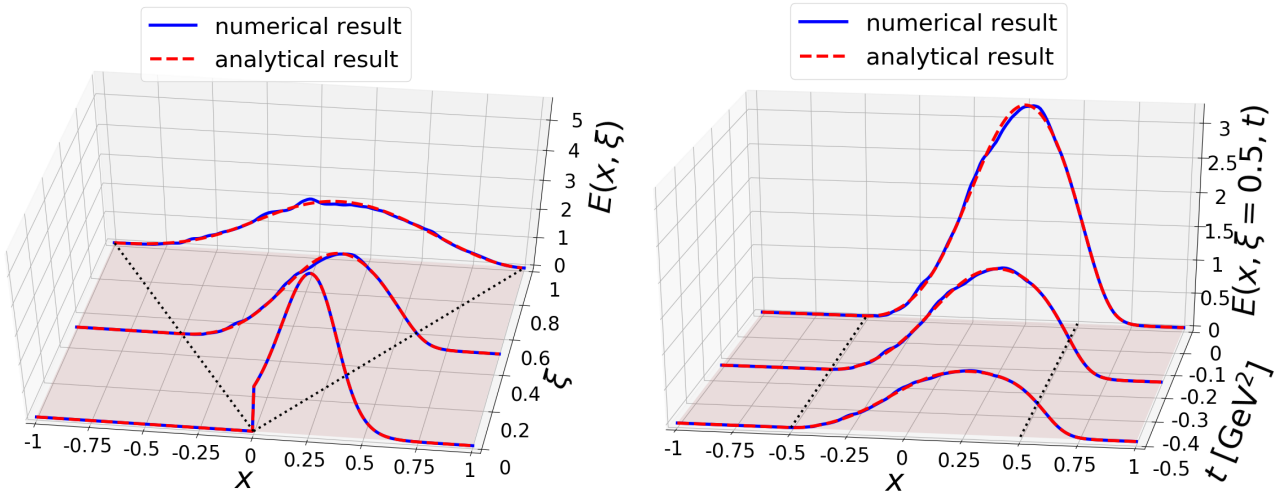
Figure 9.2. Comparison for the GPD E, in the spectator diquark model, between our numerical algorithm and the algebraic result of Ref. [20]. Same conventions as in Fig. 9.1.

have developed an algebraic parametrization for two-body LFWFs of the nucleon (described by a constituent quark and a spectator scalar diquark):

$$\Psi^{\uparrow}_{+1/2}(x, \boldsymbol{k}_\perp) = \Psi^{\downarrow}_{-1/2}(x, \boldsymbol{k}_\perp) = \left(M + \frac{m}{x}\right)\varphi(x, \boldsymbol{k}_\perp), \tag{9.8}$$

$$\Psi^{\uparrow}_{-1/2}(x, \boldsymbol{k}_\perp) = -\frac{k^1 + ik^2}{x}\varphi(x, \boldsymbol{k}_\perp), \quad \Psi^{\downarrow}_{+1/2}(x, \boldsymbol{k}_\perp) = \frac{k^1 - ik^2}{x}\varphi(x, \boldsymbol{k}_\perp), \tag{9.9}$$

$$\varphi(x, \boldsymbol{k}_\perp) = \frac{\sqrt{2N}\, 2\pi\, \Gamma(p+1)}{\sqrt{\Gamma(2p+1)(1-x)}} M^{2p}x^{-p}\left(M^2 - \frac{\boldsymbol{k}_\perp^2 + m^2}{x} - \frac{\boldsymbol{k}_\perp^2 + \lambda^2}{1-x}\right)^{-p-1}, \tag{9.10}$$

where M, m and λ are respectively the nucleon, quark and spectator masses, p is an additional free parameter and N is a normalization constant. The authors have shown that with such a model, after calculating the overlap of wave functions (see Sec. 6.1.3 or Eqs. (13-14) of Ref. [20]), one can write the GPD E in the P representation:

$$E(x, \xi, t) = (1-x)\int_0^1 \mathrm{d}\beta \int_{-1+\beta}^{1-\beta} \mathrm{d}\alpha\, e(\beta, \alpha, t)\,\delta(x - \beta - \xi\alpha), \tag{9.11}$$

and they have been able to extract analytically:

$$e(\beta, \alpha, t) = \frac{N\left(\beta + \frac{m}{M}\right)\left((1-\beta)^2 - \alpha^2\right)^p}{\left(2\left(\frac{(1-\beta)m^2}{M^2} + \frac{\beta\lambda^2}{M^2} - (1-\beta)\beta - \frac{t((1-\beta)^2 - \alpha^2)}{4M^2}\right)\right)^{2p+1}}, \tag{9.12}$$

where N is the same constant[2] as in Eq. (9.10) and can be determined from the usual PDF normalization (obtained with the GPD H, and not E). Therefore, the authors managed to extend their specific model in the ERBL region. Consequently, we use this model as an additional benchmark for our numerical technique.

---

[2]The definition of N here differs from that of Ref. [20] by a factor 2^{2p+1}.

The comparison between our numerical reconstruction and the algebraic result is shown on Fig. 9.2[3]. We use the same values of parameters as in Ref. [20], *i.e.* $M = 1$ GeV, $m = 0.45$ GeV, $\lambda = 0.75$ GeV and $p = 1$. In this case, the normalization constant for the DD is $N \sim 0.176$. We stress that in Fig. 9.2, the qualifying terms "analytical" and "numerical" refer to the DDs. In other words, "analytical result" means that the GPD is calculated through a numerical integration of the "analytical" DD (9.12) in the ERBL region (or through the numerical integration of Eq. (15) in Ref. [20] in the DGLAP region), whereas "numerical result" means that the GPD is calculated from the "numerically" reconstructed DD (from DGLAP information only), via analytical integrations of the basis functions (see *e.g.* Eqs. (8.2), (8.8) and (9.11)).

9.3. Pion wave-functions
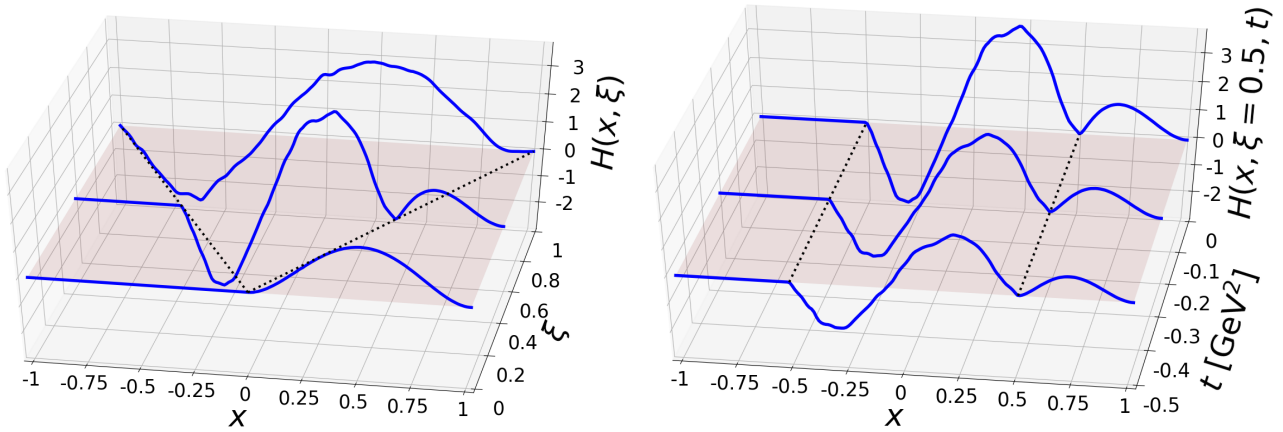
Figure 9.3. Results obtained for the GPD H (6.38) in the case of a Gaussian LFWF (6.34). Same conventions as in Fig. 9.1, but without analytical benchmark.

Now, let us consider the other examples of pion LFWFs of Sec. 6.2, the first one being the Gaussian parametrization (6.38). We do not know any algebraic expression for the associated DD (if it exists). We anyhow examine this case for illustrative purposes and display in Fig. 9.3 the results for the GPD in both DGLAP and ERBL derived from the DDs obtained with our numerical inversion. Indeed, some qualitative similarities in the shape can be noticed when compared to the results previously obtained with the Nakanishi-based LFWF and depicted in Fig. 9.1.

We did the same for the rational fraction LFWF of Sec. 6.2.2, and displayed the results in Fig. 9.4. Note that even though these plots are quite similar, these pion models give each rise to a very different picture in impact parameter space (see Sec. 6.2), which highlights the notion that the t-extrapolation is a delicate matter.

---

[3]The reader may have noticed that we consider unphysical values of t even though we are dealing with a nucleon and the constraint Eq. (4.34) cannot be neglected. This model being completely algebraic, evaluating in unphysical regions is not an issue.
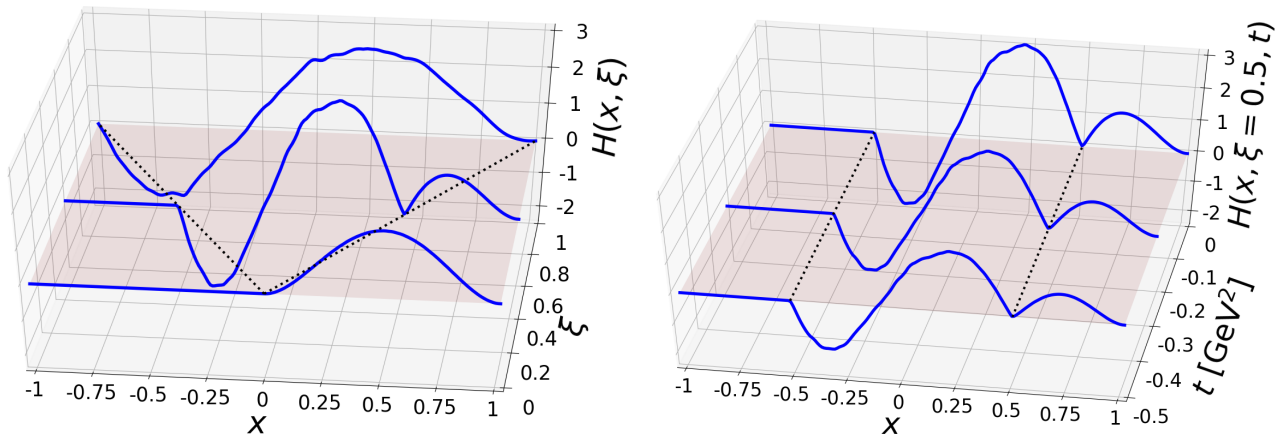
Figure 9.4. Results obtained for the GPD H (6.51) in the case of the LFWF (6.44). Same conventions as in Fig. 9.1, but without analytical benchmark.

Conclusion

The promise of hadron tomography has driven a very large experimental effort, be it to extract GPDs, or their cousins, TMDs. For the former, the leading-twist framework was validated within the experimental accuracy already achieved, but the upcoming data with a wide kinematic coverage and a high accuracy will need robust models to make sense of them. In order to learn new insights on QCD dynamics inside hadrons, these models need to be based on *ab initio* computations.

The usual method of triangle diagram calculations does not allow to fulfill all theoretical constraints on GPDs, namely the positivity property is not guaranteed. On the other hand, the overlap representation in terms of LFWFs naturally fulfills positivity but lacks the important polynomiality feature of GPDs, as it is very unlikely to appear at any finite order of truncation, due to the interplay between different Fock states in the DGLAP and ERBL regions, and only in the case where all Fock states are summed over can we be sure of fulfilling it. Nevertheless, by limiting ourselves to a truncation in the DGLAP region only, we can use the natural expression of polynomiality, in other words the DD representation, to extend the GPD to the ERBL region and in doing so fulfill both constraints. With such a method, we can directly relate the $\xi = 0$ line of GPDs, needed for hadron tomography, to the regions of non-vanishing skewness that are accessible in experiments and therefore give potential solutions to the necessary extrapolation.

The procedure described in this thesis applies this principle, which consists in solving an ill-posed inverse problem. Indeed, GPD and DD are related through the well-known Radon transform, fundamental tool of computerized tomography, whose inverse is a discontinuous operator. This means that the inverse Radon transform cannot be computed in a straightforward manner, as a regularization procedure is needed. Nevertheless, as long as the original LFWF model is built in a covariant framework, the corresponding DGLAP GPD can be extended numerically to the ERBL region as intended. This was tested on several simple pion GPD models, as well as the nucleon scalar diquark model for which an analytical extension was already known and was at the origin of this promising method. This allowed to benchmark the procedure itself that can be then applied to any phenomenologically sound model.

However, the so-called D-term remains elusive, as it is a pure ERBL contribution. In fact, contributions of the DD on the $\beta = 0$ line cannot be grasped from DGLAP information only. Other means of constraining the D-term are therefore necessary. Nevertheless, most GPDs do not feature any D-term. For instance, among all twist-2 quark GPDs of the nucleon, only one independent GPD (for a given flavor) out of eight (if we count chiral-odd GPDs) is in need of a D-term. For all the other GPDs, the procedure is sufficient in itself.

The next step is to apply this method to a LFWF-based nucleon model (in the vein of constituent quark models for instance) that was not previously known in the ERBL region. This would allow a first phenomenological study of that model by computing *e.g.* DVCS observables and comparing to experimental data, with the help of the PARTONS framework where the computing chain from GPDs to cross-sections is already implemented together with

the evolution in the factorization scale. As we expect in the near future the publication of the new JLab 12 GeV data for the valence region, this study would be most welcome. Doing so, we could test the relevance at low scale of a valence truncation of LFWFs and pave the way for a systematic phenomenology of LFWFs through exclusive processes and GPDs. This could potentially lead *in fine* to a unified phenomenology of both GPDs and TMDs.

Appendices

Appendix A.

Conventions and Notations

A.1. Conventions

We follow basically the conventions of QFT and Particle Physics textbooks (*e.g.* Ref. [66]).

Units

We work in the natural units of Particle Physics:

$$\hbar = c = 1 \,, \tag{A.1}$$

in the Lorentz-Heaviside convention for electromagnetism:

$$\epsilon_0 = \mu_0 = 1 \,, \tag{A.2}$$

and every dimensionful quantity is given in powers of GeV.

Minkowski vectors and coordinates

We denote by characters with roman font the four-vectors in Minkowski space, *e.g.* $p = (p^0, p^1, p^2, p^3)$, with bold font 3D vectors, *e.g.* $\boldsymbol{p} = (p^1, p^2, p^3)$, and we add a $\perp$ symbol for 2D vectors (in the transverse plane, usually orthogonal to the z-direction), *e.g.* $\boldsymbol{p}_\perp = (p^1, p^2)$. We use Greek indices $\mu, \nu, \ldots \in [\![0, 3]\!]$ for the coordinates of a four-vector, *e.g.* p^μ, and Roman indices $i, j, \ldots \in [\![1, 2 \text{ or } 3]\!]$ for 2D or 3D vectors, *e.g.* $p^i_\perp$.

The metric, denoted $\eta^{\mu\nu}$, has a signature $(+ - - -)$, such that

$$u \cdot v = u_\mu v^\mu = \eta_{\mu\nu} u^\nu v^\mu = u^0 v^0 - \boldsymbol{u} \cdot \boldsymbol{v} = u^0 v^0 - u^1 v^1 - u^2 v^2 - u^3 v^3 \,, \tag{A.3}$$

and

$$p^2 = p_\mu p^\mu = E_p^2 - \boldsymbol{p}^2 = m^2 \,, \tag{A.4}$$

for an on-shell particle of four-momentum p, energy $E_p = p^0$ and mass m. Following Einstein's convention, contracted indices are summed over.

The light-cone coordinates for a four-vector u are defined as:

$$u^+ = \frac{1}{\sqrt{2}} \left(u^0 + u^3 \right) \,, \qquad u^- = \frac{1}{\sqrt{2}} \left(u^0 - u^3 \right) \,, \qquad \boldsymbol{u}_\perp = \left(u^1, u^2 \right) \,, \tag{A.5}$$

Appendix A. Conventions and Notations

and the scalar product writes:

$$u \cdot v = u^+ v^- + u^- v^+ - \boldsymbol{u}_\perp \cdot \boldsymbol{v}_\perp \,. \tag{A.6}$$

For a momentum p, the light-cone coordinate p^+ is either called in this thesis "plus-momentum" or "longitudinal momentum", as in the limit $p^3 \to \infty$ (Infinite Momentum Frame), p^+ becomes proportional to p^3 (and E_p). Note that for an on-shell particle (A.4), $E_p \geq \sqrt{\boldsymbol{p}^2} \geq |p^3|$ and therefore p^+ and p^- are always positive.

Dirac matrices and spinors

The Dirac matrices are defined as:

$$\{\gamma^\mu, \gamma^\nu\} = 2\eta^{\mu\nu} \,, \qquad\qquad \gamma^5 = i\gamma^0\gamma^1\gamma^2\gamma^3 \,, \qquad\qquad \sigma^{\mu\nu} = \frac{i}{2}\left[\gamma^\mu, \gamma^\nu\right] \,, \tag{A.7}$$

where $\{\cdot\,,\,\cdot\}$ and $[\cdot\,,\,\cdot]$ represent the anti-commutator and commutator respectively. For a four-vector p, the usual notation $\not{p}$ stands for $p_\mu\gamma^\mu$. These matrices can be expressed in the Weyl representation as:

$$\gamma^0 = \begin{pmatrix} \boldsymbol{0} & \boldsymbol{1} \\ \boldsymbol{1} & \boldsymbol{0} \end{pmatrix} \,, \qquad\qquad \gamma^i = \begin{pmatrix} \boldsymbol{0} & \sigma^i \\ -\sigma^i & \boldsymbol{0} \end{pmatrix} \,, \tag{A.8}$$

where $\sigma^i, i \in [\![1,3]\!]$, are the Pauli matrices.

In this representation, the plane-wave spinors for spin-1/2 particles are given by:

$$u^\uparrow(p) = \frac{\sqrt{p^0 - |\boldsymbol{p}|} - \sqrt{p^0 + |\boldsymbol{p}|}}{2\,|\boldsymbol{p}|} \begin{pmatrix} p^3 \\ p^1 + ip^2 \\ -p^3 \\ -(p^1 + ip^2) \end{pmatrix} + \frac{\sqrt{p^0 - |\boldsymbol{p}|} + \sqrt{p^0 + |\boldsymbol{p}|}}{2} \begin{pmatrix} 1 \\ 0 \\ 1 \\ 0 \end{pmatrix} \,, \tag{A.9}$$

$$u^\downarrow(p) = \frac{\sqrt{p^0 - |\boldsymbol{p}|} - \sqrt{p^0 + |\boldsymbol{p}|}}{2\,|\boldsymbol{p}|} \begin{pmatrix} p^1 - ip^2 \\ -p^3 \\ -(p^1 - ip^2) \\ p^3 \end{pmatrix} + \frac{\sqrt{p^0 - |\boldsymbol{p}|} + \sqrt{p^0 + |\boldsymbol{p}|}}{2} \begin{pmatrix} 0 \\ 1 \\ 0 \\ 1 \end{pmatrix} \,, \tag{A.10}$$

$$v^\uparrow(p) = \frac{\sqrt{p^0 - |\boldsymbol{p}|} - \sqrt{p^0 + |\boldsymbol{p}|}}{2\,|\boldsymbol{p}|} \begin{pmatrix} p^3 \\ p^1 + ip^2 \\ p^3 \\ p^1 + ip^2 \end{pmatrix} + \frac{\sqrt{p^0 - |\boldsymbol{p}|} + \sqrt{p^0 + |\boldsymbol{p}|}}{2} \begin{pmatrix} 1 \\ 0 \\ -1 \\ 0 \end{pmatrix} \,, \tag{A.11}$$

$$v^\downarrow(p) = \frac{\sqrt{p^0 - |\boldsymbol{p}|} - \sqrt{p^0 + |\boldsymbol{p}|}}{2\,|\boldsymbol{p}|} \begin{pmatrix} p^1 - ip^2 \\ -p^3 \\ p^1 - ip^2 \\ -p^3 \end{pmatrix} + \frac{\sqrt{p^0 - |\boldsymbol{p}|} + \sqrt{p^0 + |\boldsymbol{p}|}}{2} \begin{pmatrix} 0 \\ 1 \\ 0 \\ -1 \end{pmatrix} \,, \tag{A.12}$$

with the normalization

$$\bar{u}^\lambda(p)\,u^{\lambda'}(p) = -\bar{v}^\lambda(p)\,v^{\lambda'}(p) = 2\,m\,\delta^{\lambda\lambda'} \,. \tag{A.13}$$

We denoted by λ the longitudinal polarization (*i.e.* along the z-direction), and by m the mass of the particle.

Fourier transform

We use the asymmetric convention for Fourier transforms. For integrals over momentum, the measure will always have a $(2\pi)^n$ denominator (where n is the dimension considered), while in position space there is no such denominator[1]. The Fourier transform and its inverse writes in Minkowski space:

$$\mathcal{F}f(p) = \int \mathrm{d}^4r \, f(r) \, e^{i\,p\cdot r}, \tag{A.14}$$

$$f(r) = \int \frac{\mathrm{d}^4p}{(2\pi)^4} \, \mathcal{F}f(p) \, e^{-i\,r\cdot p}. \tag{A.15}$$

Note however that for spatial Fourier transforms in 2D or 3D, due to the metric (A.3), there would be a minus sign for the exponential of Eq. (A.14) and no sign for Eq. (A.15).

A.2. Nomenclature

Acronyms

BH	Bethe-Heitler.
CFF	Compton Form Factor.
DA	Distribution Amplitude.
DD	Double Distribution.
DDVCS	Double Deeply Virtual Compton Scattering.
DIS	Deep Inelastic Scattering.
DVCS	Deeply Virtual Compton Scattering.
DVMP	Deeply Virtual Meson Production.
EIC	Electron Ion Collider.
FF	Form Factor.
GDA	Generalized Distribution Amplitude.
GFF	Generalized Form Factor.
GPD	Generalized Parton Distribution.
GTMD	Generalized Transverse Momentum Dependent PDF.
IMF	Infinite Momentum Frame.

---

[1]Except in the definition of parton distributions, *e.g.* Eq. (4.1), due to their normalization.

Appendix A. Conventions and Notations

IPD	Impact Parameter Distribution.
l.h.s., r.h.s.	Left hand side, right hand side.
LFWF	Light-Front Wave-function.
LO	Leading Order.
NLO	Next-to-Leading Order.
OPE	Operator Product Expansion.
PDF	Parton Distribution Function.
QCD	Quantum Chromodynamics.
QED	Quantum Electrodynamics.
RDDA	Radyushkin Double Distribution Ansatz.
TCS	Time-like Compton Scattering.
TMD	Transverse Momentum Dependent PDF.

Symbols

$\mathbf{1}_A\left(\,\cdot\,\right)$	Indicator function for set A.
$A, B, C, \ldots$	Gravitational Form Factors.
$\alpha_{em} = \frac{e^2}{4\pi}$	Fine structure constant.
$\alpha_S = \frac{g^2}{4\pi}$	Strong coupling constant.
$\boldsymbol{b}_\perp$	Impact parameter (transverse position from $\boldsymbol{R}_\perp$).
$\delta\left(\,\cdot\,\right)$	Dirac distribution.
e	Positron or proton charge.
$e_\ell, e_q, \ldots$	Charge of particles in unit of e.
$\epsilon^{ij}, \epsilon^{ijk}, \epsilon^{\mu\nu\rho\sigma}$	Levi-Civita symbols.
$\eta^{\mu\nu}$	Metric tensor.
$F, F_1, F_2, G_E, G_M, G_A, G_P, \ldots$	Elastic Form Factors.
$f, g, h, e \ldots$	Double Distributions.
$\mathcal{F}, \mathcal{R}$	Fourier transform, Radon transform.
$g, u, d, \ldots$	Partons (quark flavors and gluons) or associated PDFs.

$\mathcal{H}, \mathcal{E}, \tilde{\mathcal{H}}, \dots$	Compton Form Factors.
$H, E, \tilde{H}, \tilde{E}, \dots$	GPDs or IPDs.
$\boldsymbol{k}_\perp$	Transverse momentum of partons.
$k, k_1, k_2, \dots$	Parton momenta.
$l, l', \dots$	Lepton momenta.
$M_H, M_N, M_p, \dots$	Mass of hadron, nucleon, proton...
μ_F	Factorization scale.
$P, P_1, P_2, \dots$	Hadron momenta.
Ψ	Light-front Wave-function.
$\psi^q, A^\mu, G^{\mu\nu}$	Quark field, gluon field and gluon field strength tensor.
Q^2	Momentum transfer on leptons (usually photon virtuality).
$q, q_1, q_2, \dots$	Photon momenta.
$\boldsymbol{R}_\perp$	Center of plus-momentum of hadron.
$\boldsymbol{r}_\perp$	Transverse position from the spectators' center.
$\boldsymbol{S}, \boldsymbol{S}_\perp, \Lambda$	Spin. Transverse and longitudinal components.
$t = \Delta^2$	Momentum transfer on the target.
$\theta(\,\cdot\,)$	Heaviside step function.
$W_1, W_2, F_1, F_2, \dots$	Structure functions.
x	Longitudinal momentum fraction of partons.
x_B, ξ	Bjorken variable, skewness.

Appendix B.

Radon transform

B.1. Definition and properties

Given that we concern ourselves with GPDs and DDs only, the latter having a compact support Ω (see Sec. 5.2.2), we will limit ourselves in this appendix to distributions and smooth functions with compact support, usually denoted by $\mathcal{E}'$ and $\mathcal{D}$ respectively in the literature (see *e.g.* the appendices of Refs. [100, 169]).

The two-dimensional *Radon transform* [15] is a linear operator defined as follows for a given function f[1]:

$$\tilde{\mathcal{R}}h\left(\rho,\phi\right) = \iint_{\mathbf{R}^2} \mathrm{d}\beta \mathrm{d}\alpha\, h\left(\beta,\alpha\right) \delta\left(\rho - \beta\cos\phi - \alpha\sin\phi\right) . \tag{B.1}$$

For $\rho \geq 0$, this transform benefits from the geometric interpretation of Fig. B.1 (left panel). We integrate over lines parametrized by ρ and ϕ. For $\rho < 0$, we can recover the same interpretation by noticing the redundancy:

$$
\begin{aligned}
\tilde{\mathcal{R}}h\left(-\rho,\phi\right) &= \iint_{\mathbf{R}^2} \mathrm{d}\beta \mathrm{d}\alpha\, h\left(\beta,\alpha\right) \delta\left(-\rho - \beta\cos\phi - \alpha\sin\phi\right) \\
&= \iint_{\mathbf{R}^2} \mathrm{d}\beta \mathrm{d}\alpha\, h\left(\beta,\alpha\right) \delta\left(\rho - \beta\cos\left(\phi\pm\pi\right) - \alpha\sin\left(\phi\pm\pi\right)\right) \\
&= \tilde{\mathcal{R}}h\left(\rho,\phi\pm\pi\right) .
\end{aligned}
\tag{B.2}
$$

We can summarize this by reducing the target set of the transform to $\mathcal{D}\left(\mathcal{P}^2\right)$ instead of $\mathcal{D}\left(\mathbf{R}\times[0,2\pi]\right)$, where $\mathcal{P}^2$ is the set of lines of $\mathbf{R}^2$. Does it correspond to the image? Not really, as it is further constrained by the following property:

$$
\begin{aligned}
\int_{\mathbf{R}} \rho^m\, \tilde{\mathcal{R}}h\left(\rho,\phi\right) \mathrm{d}\rho &= \iint_{\mathbf{R}^2} \mathrm{d}\beta \mathrm{d}\alpha \int_{\mathbf{R}} \rho^m\, \mathrm{d}\rho\, h\left(\beta,\alpha\right) \delta\left(\rho - \beta\cos\phi - \alpha\sin\phi\right) \\
&= \iint_{\mathbf{R}^2} \mathrm{d}\beta \mathrm{d}\alpha\, h\left(\beta,\alpha\right) \left(\beta\cos\phi + \alpha\sin\phi\right)^m ,
\end{aligned}
\tag{B.3}
$$

i.e. that the Mellin moments of a Radon transform are homogeneous polynomials of degree $\leq m$ on $(\cos\phi, \sin\phi)$. We will denote by $\mathcal{D}_{\mathrm{H}}\left(\mathcal{P}^2\right)$ the functions of $\mathcal{D}\left(\mathcal{P}^2\right)$ fulfilling this condition[2].

---

[1]On the other hand, the Radon transform of *distributions* is defined through the adjoint Radon transform of test functions, but we will not go into these details.

[2]This corresponds to the *polynomiality* property of GPDs.

We can now say that $\mathcal{D}_{\mathrm{H}}(\mathcal{P}^2)$ is indeed the image of the Radon transform, as the following theorem[3,4] states [219]:

Theorem B.1 (Helgason, 1980)**.** *The Radon transform is a bijection of $\mathcal{D}(\mathbf{R}^n)$ onto $\mathcal{D}_{\mathrm{H}}(\mathcal{P}^n)$.*

For compactly-supported distributions $\mathcal{E}'$, there is also a similar theorem from Hertle [220] concerning the existence of the inverse image.

Finally, as we need it for the covariant extension of Chap. 7, let us mention (in a simplified form) the following support theorem by Boman and Quinto [221]:

Theorem B.2 (Boman and Quinto, 1987)**.** *For $h \in \mathcal{E}'(\mathbf{R}^2)$ and $\phi_0 \in [0, 2\pi]$, $\rho_0 > 0$, if there exists $\epsilon > 0$ such that $\tilde{\mathcal{R}}h(\rho, \phi) = 0$ for all (ρ, ϕ) such that $\rho > \rho_0$ and $|\phi - \phi_0| < \epsilon$, then $h(\beta, \alpha) = 0$ for all (β, α) on the half-plane $\beta \cos\phi_0 + \alpha \sin\phi_0 > \rho_0$.*

An important mathematical literature has been dedicated to the Radon transform, notably because of its central role in the field of computerized tomography. Inverting the Radon transform indeed allows to unravel the internal structure of an object exposed to some kind of radiation propagating along straight lines (in two dimensions).

The aforementioned theorem of Boman and Quinto gives some examples of situations where a function is uniquely determined by its Radon transform. This allows to define the inverse Radon transform. However, it has early been shown on simple but general examples that the inverse Radon transform may not be continuous. In that case, nothing prevents the artificial amplification of noise (numerical or experimental when dealing with actual measurements) when inverting the Radon transform. It is an example of ill-posed problem in the sense of Hadamard.

For more details on the Radon transform, we refer to the literature (*e.g.* Refs. [169, 213]).

B.2. Relation to GPDs

A possible correspondence between the canonical variables (ρ, ϕ) of the Radon transform and the GPD variables (x, ξ) is given by:

$$\begin{cases} x &= \dfrac{\rho}{\cos\phi} \\ \xi &= \tan\phi \end{cases} \quad \Longleftrightarrow \quad \begin{cases} \rho &= \dfrac{x}{\sqrt{1+\xi^2}} \\ \phi &= \arctan\xi \end{cases} . \tag{B.4}$$

The domain considered for ϕ is $\left]-\frac{\pi}{2}, \frac{\pi}{2}\right[$ since $\cos\phi = \frac{1}{\sqrt{1+\xi^2}}$ is always positive, but that is not an issue due to the redundancy (B.2); we can still consider all the lines of the plane since ρ can take negative values.

We should note that the GPD is indeed compactly-supported when it comes to the variables (ρ, ϕ), even counting the GDA domain. Indeed, for $\rho > 1$, we would have $x^2 > 1 + \xi^2$, *i.e.* both

---

[3]We write the theorem in the general way it was stated even though we are only interested in the two-dimensional case.

[4]Helgason also showed a similar version for $\mathcal{S}$ (the space of rapidly-decreasing smooth functions) instead of $\mathcal{D}$.
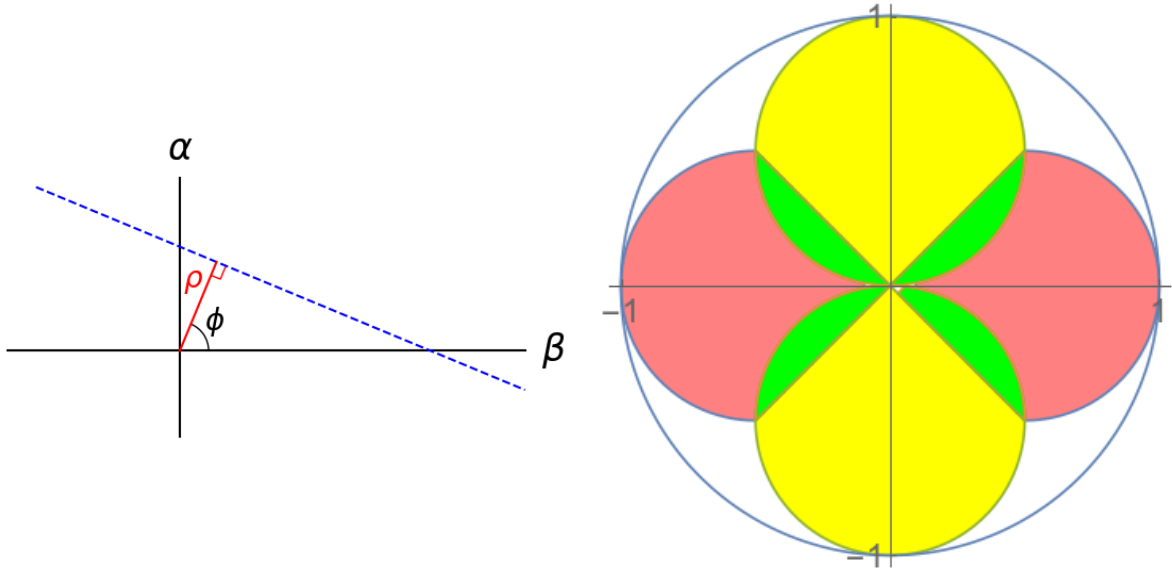
Figure B.1. Left: Geometric interpretation of the Radon transform. Integration over a line (in dashed blue) parametrized by (ρ, ϕ). **Right**: Support of GPD in polar variables (ρ, ϕ). In pink, DGLAP region. In green, ERBL region for GPD. In yellow, GDA domain.

$|x| > |\xi|$ (which corresponds to DGLAP) and $|x| > 1$, a region for which we know the GPD is vanishing. We can summarize the different domains as follows:

$$
\begin{aligned}
\text{DGLAP:} \quad & |\xi| \leq |x| \leq 1 & \iff & \quad |\sin \phi| \leq |\rho| \leq |\cos \phi| \,, \\
\text{ERBL (GPD):} \quad & |x| \leq |\xi| \leq 1 & \iff & \quad |\rho| \leq |\sin \phi| \leq |\cos \phi| \,, \\
\text{ERBL (GDA):} \quad & \begin{cases} |x| \leq |\xi| \\ |\xi| \geq 1 \end{cases} & \iff & \quad \begin{cases} |\rho| \leq |\sin \phi| \\ |\cos \phi| \leq |\sin \phi| \end{cases} .
\end{aligned}
\tag{B.5}
$$

This is also sketched in Fig. B.1 (right panel).

We remind the relation between GPD and DD[5]:

$$
\begin{aligned}
H(x, \xi) &= \iint \mathrm{d}\beta \, \mathrm{d}\alpha \, \delta(x - \beta - \xi\alpha) \, h(\beta, \alpha) \\
&= \frac{1}{\sqrt{1 + \xi^2}} \iint \mathrm{d}\beta \, \mathrm{d}\alpha \, \delta\left(\frac{x}{\sqrt{1 + \xi^2}} - \frac{\beta}{\sqrt{1 + \xi^2}} - \alpha \frac{\xi}{\sqrt{1 + \xi^2}} \right) h(\beta, \alpha) \\
&= \frac{1}{\sqrt{1 + \xi^2}} \, \tilde{\mathcal{R}} h\left(\frac{x}{\sqrt{1 + \xi^2}}, \arctan \xi \right) \\
&\equiv \mathcal{R} h(x, \xi) \,,
\end{aligned}
\tag{B.6}
$$

where we defined the operator $\mathcal{R}$ with a ξ-dependent factor compared to the usual Radon transform of the literature, for convenience.

Going back to Thm. B.1, we can now state its formal equivalent for GPDs:

---

[5]In the simple case of the R representation.

Appendix B. Radon transform

Corollary B.3. *A GPD H fulfills the polynomiality property:*

$$\int_{-1}^{1} x^m \, H\left(x,\xi\right) \mathrm{d}x = \sum_{k=0}^{m} H_m^k \, \xi^k \,, \tag{B.7}$$

if and only if it is a Radon transform of a DD h:

$$H\left(x,\xi\right) = \mathcal{R}h\left(x,\xi\right), \tag{B.8}$$

and this DD is unique.

Proof. In canonical variables, we have

$$\int_{-1}^{1} \rho^m \, H\left(\frac{\rho}{\cos\phi}, \tan\phi\right) \mathrm{d}\rho = \int_{-1}^{1} x^m \, H\left(x, \tan\phi\right) \cos^{m+1}\phi \, \mathrm{d}x$$

$$= \cos^{m+1}\phi \sum_{k=0}^{m} H_m^k \, \tan^k\phi \tag{B.9}$$

$$= \cos\phi \sum_{k=0}^{m} H_m^k \, \sin^k\phi \, \cos^{m-k}\phi \,.$$

From Thm. B.1, we conclude that

$$\sqrt{1+\xi^2} \, H\left(x,\xi\right) = \frac{H\left(\frac{\rho}{\cos\phi}, \tan\phi\right)}{\cos\phi} = \tilde{\mathcal{R}}h\left(\rho,\phi\right), \tag{B.10}$$

hence the result, the converse being trivial (see Chap. 5). $\qquad\square$

Let us now consider the translation of Thm. B.2 into GPD language, which would be:

Corollary B.4. *For $h \in \mathcal{E}'\left(\mathbf{R}^2\right)$ and $x_0 > 0, \xi_0 \in \mathbf{R}$, if there exists $\epsilon > 0$ such that $\mathcal{R}h\left(x,\xi\right) = 0$ for all (x,ξ) such that $\frac{x}{\sqrt{1+\xi^2}} > \frac{x_0}{\sqrt{1+\xi_0^2}}$ and $|\xi - \xi_0| < \epsilon$, then $h\left(\beta,\alpha\right) = 0$ for all (β,α) on the half-plane $\beta + \alpha\xi_0 > x_0$.*

Proof. This follows immediately from the theorem, given the dictionary (B.4) and that tan is a continuous function: we can find $\epsilon' > 0$ such that $|\phi - \phi_0| = |\arctan\xi - \arctan\xi_0| < \epsilon'$ implies $|\xi - \xi_0| < \epsilon$ and we would therefore have $\mathcal{R}h\left(x,\xi\right) = 0$ in that restricted set. The theorem can then be applied. $\qquad\square$

For a thorough study of the Radon transform in the context of GPDs we refer to the habilitation thesis [160].

Figures and Tables

List of Figures

Figures and Tables

126

List of Tables

Index

Index

Bibliography

[1] M. Diehl, "Generalized parton distributions," *Phys.Rept.* **388** (2003) 41–277, `arXiv:hep-ph/0307382 [hep-ph]`. On pages iv, xii, 30, 32, 33, 41, 44, 46, 47, 51, 56, 57, 71, and 73.

[2] A. Belitsky and A. Radyushkin, "Unraveling hadron structure with generalized parton distributions," *Phys.Rept.* **418** (2005) 1–387, `arXiv:hep-ph/0504030 [hep-ph]`. On pages iv, 32, 33, 43, 44, and 51.

[3] E. Jones, T. Oliphant, P. Peterson, *et al.*, "SciPy: Open source scientific tools for Python," 2001–. `http://www.scipy.org/`. [Online; accessed 2018-09-19]. On page iv.

[4] J. D. Hunter, "Matplotlib: A 2d graphics environment," *Computing in Science Engineering* **9** no. 3, (May, 2007) 90–95. On page iv.

[5] D. Mueller, D. Robaschik, B. Geyer, F. Dittes, and J. Hořejši, "Wave functions, evolution equations and evolution kernels from light ray operators of QCD," *Fortsch.Phys.* **42** (1994) 101–141, `arXiv:hep-ph/9812448 [hep-ph]`. On pages xi, 26, 41, 52, and 55.

[6] A. Radyushkin, "Scaling limit of deeply virtual Compton scattering," *Phys.Lett.* **B380** (1996) 417–425, `arXiv:hep-ph/9604317 [hep-ph]`. On pages xi, 26, and 41.

[7] X.-D. Ji, "Deeply virtual Compton scattering," *Phys.Rev.* **D55** (1997) 7114–7125, `arXiv:hep-ph/9609381 [hep-ph]`. On pages xi and 41.

[8] M. Burkardt, "Impact parameter dependent parton distributions and off forward parton distributions for zeta —> 0," *Phys. Rev.* **D62** (2000) 071503, `arXiv:hep-ph/0005108 [hep-ph]`. [Erratum: Phys. Rev.D66,119903(2002)]. On pages xi, 18, 20, 21, 22, and 83.

[9] A. V. Belitsky, D. Mueller, and A. Kirchner, "Theory of deeply virtual Compton scattering on the nucleon," *Nucl.Phys.* **B629** (2002) 323–392, `arXiv:hep-ph/0112108 [hep-ph]`. On pages xi, 28, and 29.

[10] B. Pire, J. Soffer, and O. Teryaev, "Positivity constraints for off - forward parton distributions," *Eur.Phys.J.* **C8** (1999) 103–106, `arXiv:hep-ph/9804284 [hep-ph]`. On pages xii and 46.

[11] C. Mezrag, L. Chang, H. Moutarde, C. Roberts, J. Rodríguez-Quintero, *et al.*, "Sketching the pion's valence-quark generalised parton distribution," *Phys.Lett.* **B741** (2014) 190–196, `arXiv:1411.6634 [nucl-th]`. On pages xii, 78, and 84.

131

Bibliography

[12] C. Mezrag, *Generalised Parton Distributions : from phenomenological approaches to Dyson-Schwinger equations.* PhD thesis, IRFU, SPhN, Saclay, 2015. `https://tel.archives-ouvertes.fr/tel-01180175`. On pages xii, 43, 76, 84, and 89.

[13] C. Mezrag, H. Moutarde, and J. Rodriguez-Quintero, "From Bethe–Salpeter Wave functions to Generalised Parton Distributions," *Few Body Syst.* **57** no. 9, (2016) 729–772, `arXiv:1602.07722 [nucl-th]`. On pages xii, xiv, 76, 77, 83, 84, and 125.

[14] B. C. Tiburzi and G. Verma, "Violation of Positivity Bounds in Models of Generalized Parton Distributions," *Phys. Rev.* **D96** no. 3, (2017) 034020, `arXiv:1706.05849 [hep-ph]`. On pages xii, 83, and 84.

[15] J. Radon, "On the determination of functions from their integral values along certain manifolds," *Medical Imaging, IEEE Transactions on* **5** no. 4, (Dec, 1986) 170–176. On pages xiii, 51, and 121.

[16] O. Teryaev, "Crossing and radon tomography for generalized parton distributions," *Phys.Lett.* **B510** (2001) 125–132, `arXiv:hep-ph/0102303 [hep-ph]`. On pages xiii, 58, 59, and 89.

[17] P. Pobylitsa, "Solution of polynomiality and positivity constraints on generalized parton distributions," *Phys.Rev.* **D67** (2003) 034009, `arXiv:hep-ph/0210150 [hep-ph]`. On pages xiii, 60, and 62.

[18] N. Chouika, C. Mezrag, H. Moutarde, and J. Rodríguez-Quintero, "Covariant Extension of the GPD overlap representation at low Fock states," *Eur. Phys. J.* **C77** no. 12, (2017) 906, `arXiv:1711.05108 [hep-ph]`. On pages xiii, 62, 63, 77, 84, and 107.

[19] N. Chouika, C. Mezrag, H. Moutarde, and J. Rodríguez-Quintero, "A Nakanishi-based model illustrating the covariant extension of the pion GPD overlap representation and its ambiguities," *Phys. Lett.* **B780** (2018) 287–293, `arXiv:1711.11548 [hep-ph]`. On pages xiv, 77, 78, 107, and 125.

[20] D. Hwang and D. Mueller, "Implication of the overlap representation for modelling generalized parton distributions," *Phys.Lett.* **B660** (2008) 350–359, `arXiv:0710.1567 [hep-ph]`. On pages xiv, 84, 107, 108, 109, and 128.

[21] P. C. Hansen, "Regularization Tools version 4.0 for Matlab 7.3," *Numerical Algorithms* **46** no. 2, (2007) 189–194. On pages xiv and 93.

[22] B. Berthou *et al.*, "PARTONS: PARtonic Tomography Of Nucleon Software," *Eur. Phys. J.* **C78** no. 6, (2018) 478, `arXiv:1512.06174 [hep-ph]`. On pages xiv, 35, 37, and 126.

[23] P. Kroll, H. Moutarde, and F. Sabatie, "From hard exclusive meson electroproduction to deeply virtual Compton scattering," *Eur.Phys.J.* **C73** (2013) 2278, `arXiv:1210.6975 [hep-ph]`. On pages xv, 29, 32, 35, and 59.

[24] A. V. Belitsky, D. Müller, and Y. Ji, "Compton scattering: from deeply virtual to quasi-real," *Nucl.Phys.* **B878** (2014) 214–268, `arXiv:1212.6674 [hep-ph]`. On pages xv, 29, and 36.

[25] C. Lorcé, B. Pasquini, and M. Vanderhaeghen, "Unified framework for generalized and transverse-momentum dependent parton distributions within a 3Q light-cone picture of the nucleon," *JHEP* **1105** (2011) 041, `arXiv:1102.4704 [hep-ph]`. On pages xv, xvi, 19, 47, and 125.

[26] M. Guidal, H. Moutarde, and M. Vanderhaeghen, "Generalized Parton Distributions in the valence region from Deeply Virtual Compton Scattering," *Rept.Prog.Phys.* **76** (2013) 066202, `arXiv:1303.6600 [hep-ph]`. On pages xv, 30, and 99.

[27] **CLAS** Collaboration, S. Pisano *et al.*, "Single and double spin asymmetries for deeply virtual Compton scattering measured with CLAS and a longitudinally polarized proton target," *Phys. Rev.* **D91** no. 5, (2015) 052014, `arXiv:1501.07052 [hep-ex]`. On pages xvi, 33, and 125.

[28] F. Halzen and A. D. Martin, *QUARKS AND LEPTONS: An Introductory Course in Modern Particle Physics*. John Wiley and Sons, Inc., 1984. On page 7.

[29] D. Griffiths, *Introduction to elementary particles*. Physics textbook. Wiley, 1987. On page 7.

[30] P. Aurenche, "La QCD et son histoire : partons d'un bon pied!," Sept., 2006. `https://cel.archives-ouvertes.fr/cel-00093000`. Lecture, École Joliot Curie 2005. On page 7.

[31] E. Rutherford, "LIV. Collision of α particles with light atoms. IV. An anomalous effect in nitrogen," *The London, Edinburgh, and Dublin Philosophical Magazine and Journal of Science* **37** no. 222, (1919) 581–587. On page 7.

[32] D. M. Dennison, "A note on the specific heat of the hydrogen molecule," *Proceedings of the Royal Society of London A: Mathematical, Physical and Engineering Sciences* **115** no. 771, (1927) 483–486. On page 7.

[33] R. Frisch and O. Stern, "Über die magnetische Ablenkung von Wasserstoffmolekülen und das magnetische Moment des Protons. I," *Zeitschrift für Physik* **85** no. 1, (Jan, 1933) 4–16. On page 7.

[34] I. Estermann and O. Stern, "Über die magnetische Ablenkung von Wasserstoffmolekülen und das magnetische Moment des Protons. II," *Zeitschrift für Physik* **85** no. 1, (Jan, 1933) 17–24. On page 7.

[35] I. I. Rabi, J. M. B. Kellogg, and J. R. Zacharias, "The magnetic moment of the proton," *Phys. Rev.* **46** (Aug, 1934) 157–163. On page 7.

[36] I. I. Rabi, J. M. B. Kellogg, and J. R. Zacharias, "The magnetic moment of the deuton," *Phys. Rev.* **46** (Aug, 1934) 163–165. On page 7.

Bibliography

[37] C. F. Perdrisat, V. Punjabi, and M. Vanderhaeghen, "Nucleon Electromagnetic Form Factors," *Prog. Part. Nucl. Phys.* **59** (2007) 694–764, `arXiv:hep-ph/0612014 [hep-ph]`. On pages 8 and 125.

[38] H. Moutarde, *Nucleon Reverse Engineering: Structuring the nucleon with quarks and gluons.* École Joliot Curie, 2013. `http://ejc2013.sciencesconf.org/conference/ejc2013/Moutarde_ejc2013.pdf`. On page 8.

[39] I. Sick, "Proton charge radius from electron scattering," *Atoms* **6** no. 1, (2018) 2, `arXiv:1801.01746 [nucl-ex]`. On page 9.

[40] R. Mcallister and R. Hofstadter, "Elastic Scattering of 188-MeV Electrons From the Proton and the α Particle," *Phys.Rev.* **102** (1956) 851–856. On page 9.

[41] R. Hofstadter, "Electron scattering and nuclear structure," *Rev.Mod.Phys.* **28** (1956) 214–254. On page 9.

[42] M. N. Rosenbluth, "High Energy Elastic Scattering of Electrons on Protons," *Phys. Rev.* **79** (1950) 615–619. On page 9.

[43] Y. Ne'eman, "Derivation of strong interactions from a gauge invariance," *Nuclear Physics* **26** no. 2, (1961) 222 – 229. On page 9.

[44] M. Gell-Mann, "Symmetries of baryons and mesons," *Phys. Rev.* **125** (Feb, 1962) 1067–1084. On page 9.

[45] M. Gell-Mann, "A Schematic Model of Baryons and Mesons," *Phys. Lett.* **8** (1964) 214–215. On page 9.

[46] G. Zweig, "An SU(3) model for strong interaction symmetry and its breaking. Version 2," in *DEVELOPMENTS IN THE QUARK THEORY OF HADRONS. VOL. 1. 1964 - 1978*, D. Lichtenberg and S. P. Rosen, eds., pp. 22–101. 1964. `http://inspirehep.net/record/4674/files/cern-th-412.pdf`. On page 9.

[47] J.-B. Zuber, *Invariances in Physics and Group Theory.* Master ENS International Center for Fundamental Physics, Jan., 2015. On page 10.

[48] O. W. Greenberg, "Spin and Unitary Spin Independence in a Paraquark Model of Baryons and Mesons," *Phys. Rev. Lett.* **13** (1964) 598–602. On page 10.

[49] N. Bogoliubov, B. Struminsky, and A. Tavkhelidze, "On the composite models in theories of elementary particles," *JINR Publication D-1968* (1965) . On page 10.

[50] M. Han and Y. Nambu, "Three Triplet Model with Double SU(3) Symmetry," *Phys.Rev.* **139** (1965) B1006–B1010. On page 10.

[51] D. Lichtenberg, *Unitary symmetry and elementary particles.* Academic Press, 1970. On page 10.

[52] H. Fritzsch, M. Gell-Mann, and H. Leutwyler, "Advantages of the Color Octet Gluon Picture," *Phys.Lett.* **B47** (1973) 365–368. On page 10.

[53] S. Weinberg, "Nonabelian Gauge Theories of the Strong Interactions," *Phys. Rev. Lett.* **31** (1973) 494–497. On page 10.

[54] S. Weinberg, "Current algebra and gauge theories. 2. NonAbelian gluons," *Phys. Rev.* **D8** (1973) 4482–4498. On page 10.

[55] E. D. Bloom, D. Coward, H. DeStaebler, J. Drees, G. Miller, *et al.*, "High-Energy Inelastic e p Scattering at 6-Degrees and 10-Degrees," *Phys.Rev.Lett.* **23** (1969) 930–934. On pages 11 and 13.

[56] M. Breidenbach, J. I. Friedman, H. W. Kendall, E. D. Bloom, D. Coward, *et al.*, "Observed Behavior of Highly Inelastic electron-Proton Scattering," *Phys.Rev.Lett.* **23** (1969) 935–939. On pages 11 and 13.

[57] R. Feynman, *Photon-Hadron Interactions.* Frontiers in physics. W.A. Benjamin, 1972. On page 12.

[58] J. Bjorken, "Asymptotic Sum Rules at Infinite Momentum," *Phys.Rev.* **179** (1969) 1547–1553. On page 12.

[59] J. Callan, Curtis G. and D. J. Gross, "High-energy electroproduction and the constitution of the electric current," *Phys.Rev.Lett.* **22** (1969) 156–159. On page 13.

[60] **Particle Data Group** Collaboration, C. Patrignani *et al.*, "Review of Particle Physics," *Chin. Phys.* **C40** no. 10, (2016) 100001. On pages 13, 14, 34, and 125.

[61] **NNPDF** Collaboration, R. D. Ball *et al.*, "Parton distributions for the LHC Run II," *JHEP* **04** (2015) 040, arXiv:1410.8849 [hep-ph]. On pages 14 and 125.

[62] G. Sterman, *An Introduction to Quantum Field Theory.* Cambridge University Press, 1993. On pages 14, 25, and 33.

[63] V. N. Gribov and L. N. Lipatov, "Deep inelastic e p scattering in perturbation theory," *Sov. J. Nucl. Phys.* **15** (1972) 438–450. [Yad. Fiz.15,781(1972)]. On page 15.

[64] G. Altarelli and G. Parisi, "Asymptotic Freedom in Parton Language," *Nucl. Phys.* **B126** (1977) 298–318. On page 15.

[65] Y. L. Dokshitzer, "Calculation of the Structure Functions for Deep Inelastic Scattering and e+ e- Annihilation by Perturbation Theory in Quantum Chromodynamics.," *Sov. Phys. JETP* **46** (1977) 641–653. [Zh. Eksp. Teor. Fiz.73,1216(1977)]. On page 15.

[66] M. E. Peskin and D. V. Schroeder, *An Introduction to quantum field theory.* Addison-Wesley, Reading, USA, 1995. http://www.slac.stanford.edu/~mpeskin/QFT.html. On pages 15, 43, and 115.

[67] E. P. Wigner, "On the quantum correction for thermodynamic equilibrium," *Phys.Rev.* **40** (1932) 749–760. On page 17.

[68] H. Weyl, "Quantum mechanics and group theory," *Z. Phys.* **46** (1927) 1. On page 17.

[69] J. Moyal, "Quantum mechanics as a statistical theory," *Proc.Cambridge Phil.Soc.* **45** (1949) 99–124. On page 18.

[70] X.-d. Ji, "Viewing the proton through 'color' filters," *Phys.Rev.Lett.* **91** (2003) 062001, `arXiv:hep-ph/0304037 [hep-ph]`. On page 18.

[71] A. V. Belitsky, X.-d. Ji, and F. Yuan, "Quark imaging in the proton via quantum phase space distributions," *Phys.Rev.* **D69** (2004) 074014, `arXiv:hep-ph/0307383 [hep-ph]`. On page 18.

[72] C. Lorcé and B. Pasquini, "Quark Wigner Distributions and Orbital Angular Momentum," *Phys.Rev.* **D84** (2011) 014015, `arXiv:1106.0139 [hep-ph]`. On page 18.

[73] J. B. Kogut and D. E. Soper, "Quantum Electrodynamics in the Infinite Momentum Frame," *Phys. Rev.* **D1** (1970) 2901–2913. On page 18.

[74] M. Diehl, "Generalized parton distributions in impact parameter space," *Eur.Phys.J.* **C25** (2002) 223–232, `arXiv:hep-ph/0205208 [hep-ph]`. On pages 18, 19, 23, and 70.

[75] M. Diehl, "QCD and Hadron structure," June, 2016. HUGS Summer School, Jefferson Lab. On pages 18, 20, 23, and 26.

[76] S. Meissner, A. Metz, M. Schlegel, and K. Goeke, "Generalized parton correlation functions for a spin-0 hadron," *JHEP* **0808** (2008) 038, `arXiv:0805.3165 [hep-ph]`. On page 19.

[77] S. Meissner, A. Metz, and M. Schlegel, "Generalized parton correlation functions for a spin-1/2 hadron," *JHEP* **0908** (2009) 056, `arXiv:0906.5323 [hep-ph]`. On page 19.

[78] M. Burkardt, "Impact parameter space interpretation for generalized parton distributions," *Int. J. Mod. Phys.* **A18** (2003) 173–208, `arXiv:hep-ph/0207047 [hep-ph]`. On page 21.

[79] M. Diehl and P. Hägler, "Spin densities in the transverse plane and generalized transversity distributions," *Eur. Phys. J.* **C44** (2005) 87–101, `arXiv:hep-ph/0504175 [hep-ph]`. On page 21.

[80] S. Boffi and B. Pasquini, "Generalized parton distributions and the structure of the nucleon," *Riv.Nuovo Cim.* **30** (2007) 387, `arXiv:0711.2625 [hep-ph]`. On page 21.

[81] M. Burkardt, "GPDs with zeta not equal 0," `arXiv:0711.1881 [hep-ph]`. On page 23.

[82] X.-D. Ji, "Gauge-Invariant Decomposition of Nucleon Spin," *Phys. Rev. Lett.* **78** (1997) 610–613, `arXiv:hep-ph/9603249 [hep-ph]`. On page 23.

[83] X.-D. Ji, "Lorentz symmetry and the internal structure of the nucleon," *Phys. Rev.* **D58** (1998) 056003, `arXiv:hep-ph/9710290 [hep-ph]`. On page 23.

[84] M. V. Polyakov, "Generalized parton distributions and strong forces inside nucleons and nuclei," *Phys. Lett.* **B555** (2003) 57–62, `arXiv:hep-ph/0210165 [hep-ph]`. On page 24.

[85] M. V. Polyakov and P. Schweitzer, "Forces inside hadrons: pressure, surface tension, mechanical radius, and all that," `arXiv:1805.06596 [hep-ph]`. On page 24.

[86] E. Leader and C. Lorcé, "The angular momentum controversy: What's it all about and does it matter?," *Phys. Rept.* **541** no. 3, (2014) 163–248, `arXiv:1309.4235 [hep-ph]`. On page 24.

[87] X.-D. Ji, "Off forward parton distributions," *J.Phys.* **G24** (1998) 1181–1205, `arXiv:hep-ph/9807358 [hep-ph]`. On page 24.

[88] E. R. Berger, M. Diehl, and B. Pire, "Time - like Compton scattering: Exclusive photoproduction of lepton pairs," *Eur.Phys.J.* **C23** (2002) 675–689, `arXiv:hep-ph/0110062 [hep-ph]`. On page 25.

[89] M. Guidal and M. Vanderhaeghen, "Double deeply virtual Compton scattering off the nucleon," *Phys. Rev. Lett.* **90** (2003) 012001, `arXiv:hep-ph/0208275 [hep-ph]`. On page 25.

[90] A. V. Belitsky and D. Mueller, "Exclusive electroproduction of lepton pairs as a probe of nucleon structure," *Phys. Rev. Lett.* **90** (2003) 022001, `arXiv:hep-ph/0210313 [hep-ph]`. On page 25.

[91] L. Mankiewicz, G. Piller, and T. Weigl, "Hard exclusive meson production and nonforward parton distributions," *Eur. Phys. J.* **C5** (1998) 119–128, `arXiv:hep-ph/9711227 [hep-ph]`. On page 25.

[92] M. Vanderhaeghen, P. A. M. Guichon, and M. Guidal, "Hard electroproduction of photons and mesons on the nucleon," *Phys. Rev. Lett.* **80** (1998) 5064–5067. On pages 25 and 36.

[93] L. L. Frankfurt, P. V. Pobylitsa, M. V. Polyakov, and M. Strikman, "Hard exclusive pseudoscalar meson electroproduction and spin structure of a nucleon," *Phys. Rev.* **D60** (1999) 014010, `arXiv:hep-ph/9901429 [hep-ph]`. On page 25.

[94] S. B. Libby and G. F. Sterman, "Mass Divergences in Two Particle Inelastic Scattering," *Phys.Rev.* **D18** (1978) 4737. On page 25.

[95] J. Collins, *Foundations of Pertubative QCD*. Cambridge Monographs On particle physics, nuclear physics and cosmology, 2011. On page 25.

[96] R. L. Jaffe, "Spin, twist and hadron structure in deep inelastic processes," in *The spin structure of the nucleon. Proceedings, International School of Nucleon Structure, 1st Course, Erice, Italy, August 3-10, 1995*, pp. 42–129. 1996. `arXiv:hep-ph/9602236 [hep-ph]`. On page 26.

[97] A. Radyushkin, "Nonforward parton distributions," *Phys.Rev.* **D56** (1997) 5524–5557, `arXiv:hep-ph/9704207 [hep-ph]`. On pages 26, 52, and 53.

[98] X.-D. Ji and J. Osborne, "One loop corrections and all order factorization in deeply virtual Compton scattering," *Phys.Rev.* **D58** (1998) 094018, `arXiv:hep-ph/9801260 [hep-ph]`. On page 26.

[99] J. C. Collins and A. Freund, "Proof of factorization for deeply virtual Compton scattering in QCD," *Phys.Rev.* **D59** (1999) 074009, `arXiv:hep-ph/9801262 [hep-ph]`. On page 26.

[100] H. Nussenzveig, *Causality and Dispersion Relations.* Mathematics in Science and Engineering. Elsevier Science, 1972. On pages 26 and 121.

[101] A. Bacchetta, U. D'Alesio, M. Diehl, and C. A. Miller, "Single-spin asymmetries: The Trento conventions," *Phys.Rev.* **D70** (2004) 117504, `arXiv:hep-ph/0410050 [hep-ph]`. On pages 29 and 126.

[102] A. V. Belitsky and D. Mueller, "Refined analysis of photon leptoproduction off spinless target," *Phys.Rev.* **D79** (2009) 014017, `arXiv:0809.2890 [hep-ph]`. On page 29.

[103] A. Belitsky and D. Mueller, "Exclusive electroproduction revisited: treating kinematical effects," *Phys.Rev.* **D82** (2010) 074010, `arXiv:1005.5209 [hep-ph]`. On page 29.

[104] M. Diehl and S. Sapeta, "On the analysis of lepton scattering on longitudinally or transversely polarized protons," *Eur. Phys. J.* **C41** (2005) 515–533, `arXiv:hep-ph/0503023 [hep-ph]`. On page 29.

[105] P. Guichon and M. Vanderhaeghen, "Analytic ee'γ cross section." in *Atelier DVCS, Laboratoire de Physique Corpusculaire, Clermont-Ferrand, June 30 - July 01, 2008*. On pages 29 and 36.

[106] H. Moutarde, "Extraction of the Compton Form Factor H from DVCS measurements at Jefferson Lab," *Phys.Rev.* **D79** (2009) 094021, `arXiv:0904.1648 [hep-ph]`. On pages 29 and 35.

[107] M. Vanderhaeghen, P. A. Guichon, and M. Guidal, "Deeply virtual electroproduction of photons and mesons on the nucleon: Leading order amplitudes and power corrections," *Phys.Rev.* **D60** (1999) 094017, `arXiv:hep-ph/9905372 [hep-ph]`. On pages 29 and 36.

[108] B. Pire, L. Szymanowski, and J. Wagner, "NLO corrections to timelike, spacelike and double deeply virtual Compton scattering," *Phys.Rev.* **D83** (2011) 034009, `arXiv:1101.0555 [hep-ph]`. On pages 30 and 36.

[109] H. Moutarde, B. Pire, F. Sabatie, L. Szymanowski, and J. Wagner, "On timelike and spacelike deeply virtual Compton scattering at next to leading order," *Phys.Rev.* **D87** (2013) 054029, `arXiv:1301.3819 [hep-ph]`. On pages 30 and 36.

[110] K. Kumericki, S. Liuti, and H. Moutarde, "GPD phenomenology and DVCS fitting," *Eur. Phys. J.* **A52** no. 6, (2016) 157, `arXiv:1602.02763 [hep-ph]`. On pages 30, 32, and 35.

[111] O. V. Teryaev, "Analytic properties of hard exclusive amplitudes," in *11th International Conference on Elastic and Diffractive Scattering: Towards High Energy Frontiers: The 20th Anniversary of the Blois Workshops, 17th Rencontre de Blois (EDS 05) Chateau de Blois, Blois, France, May 15-20, 2005.* 2005. `arXiv:hep-ph/0510031 [hep-ph]`. On page 31.

[112] I. V. Anikin and O. V. Teryaev, "Dispersion relations and subtractions in hard exclusive processes," *Phys. Rev.* **D76** (2007) 056007, `arXiv:0704.2185 [hep-ph]`. On page 31.

[113] A. V. Radyushkin, "Sum rules for nucleon generalized parton distributions and border function formulation," *Phys. Rev.* **D88** no. 5, (2013) 056010, `arXiv:1307.6781 [hep-ph]`. On page 31.

[114] J. Blumlein, B. Geyer, and D. Robaschik, "The Virtual Compton amplitude in the generalized Bjorken region: twist-2 contributions," *Nucl.Phys.* **B560** (1999) 283–344, `arXiv:hep-ph/9903520 [hep-ph]`. On page 32.

[115] A. Radyushkin, "Double distributions and evolution equations," *Phys.Rev.* **D59** (1999) 014030, `arXiv:hep-ph/9805342 [hep-ph]`. On page 32.

[116] A. V. Belitsky, A. Freund, and D. Mueller, "Evolution kernels of skewed parton distributions: Method and two loop results," *Nucl.Phys.* **B574** (2000) 347–406, `arXiv:hep-ph/9912379 [hep-ph]`. On page 32.

[117] A. Freund and M. McDermott, "A Detailed next-to-leading order QCD analysis of deeply virtual Compton scattering observables," *Eur.Phys.J.* **C23** (2002) 651–674, `arXiv:hep-ph/0111472 [hep-ph]`. On page 32.

[118] A. Efremov and A. Radyushkin, "Factorization and Asymptotical Behavior of Pion Form-Factor in QCD," *Phys.Lett.* **B94** (1980) 245–250. On page 33.

[119] G. P. Lepage and S. J. Brodsky, "Exclusive Processes in Quantum Chromodynamics: Evolution Equations for Hadronic Wave Functions and the Form-Factors of Mesons," *Phys.Lett.* **B87** (1979) 359–365. On page 33.

[120] A. Vinnikov, "Code for prompt numerical computation of the leading order GPD evolution," `arXiv:hep-ph/0604248 [hep-ph]`. On pages 33 and 36.

[121] **HERMES** Collaboration, A. Airapetian *et al.*, "Measurement of the beam spin azimuthal asymmetry associated with deeply virtual Compton scattering," *Phys. Rev. Lett.* **87** (2001) 182001, `arXiv:hep-ex/0106068 [hep-ex]`. On page 33.

[122] **HERMES** Collaboration, A. Airapetian *et al.*, "The Beam-charge azimuthal asymmetry and deeply virtual compton scattering," *Phys. Rev.* **D75** (2007) 011103, `arXiv:hep-ex/0605108 [hep-ex]`. On page 33.

[123] **HERMES** Collaboration, A. Airapetian *et al.*, "Measurement of Azimuthal Asymmetries With Respect To Both Beam Charge and Transverse Target Polarization in Exclusive Electroproduction of Real Photons," *JHEP* **06** (2008) 066, `arXiv:0802.2499 [hep-ex]`. On page 33.

[124] **HERMES** Collaboration, A. Airapetian *et al.*, "Separation of contributions from deeply virtual Compton scattering and its interference with the Bethe-Heitler process in measurements on a hydrogen target," *JHEP* **11** (2009) 083, `arXiv:0909.3587 [hep-ex]`. On page 33.

[125] **HERMES** Collaboration, A. Airapetian *et al.*, "Exclusive Leptoproduction of Real Photons on a Longitudinally Polarised Hydrogen Target," *JHEP* **06** (2010) 019, `arXiv:1004.0177 [hep-ex]`. On page 33.

[126] **HERMES** Collaboration, A. Airapetian *et al.*, "Measurement of double-spin asymmetries associated with deeply virtual Compton scattering on a transversely polarized hydrogen target," *Phys. Lett.* **B704** (2011) 15–23, `arXiv:1106.2990 [hep-ex]`. On page 33.

[127] **HERMES** Collaboration, A. Airapetian *et al.*, "Beam-helicity and beam-charge asymmetries associated with deeply virtual Compton scattering on the unpolarised proton," *JHEP* **07** (2012) 032, `arXiv:1203.6287 [hep-ex]`. On page 33.

[128] **H1** Collaboration, C. Adloff *et al.*, "Measurement of deeply virtual Compton scattering at HERA," *Phys. Lett.* **B517** (2001) 47–58, `arXiv:hep-ex/0107005 [hep-ex]`. On page 33.

[129] **H1** Collaboration, A. Aktas *et al.*, "Measurement of deeply virtual compton scattering at HERA," *Eur. Phys. J.* **C44** (2005) 1–11, `arXiv:hep-ex/0505061 [hep-ex]`. On page 33.

[130] **H1** Collaboration, F. D. Aaron *et al.*, "Measurement of deeply virtual Compton scattering and its t-dependence at HERA," *Phys. Lett.* **B659** (2008) 796–806, `arXiv:0709.4114 [hep-ex]`. On page 33.

[131] **H1** Collaboration, F. D. Aaron *et al.*, "Deeply Virtual Compton Scattering and its Beam Charge Asymmetry in e+- Collisions at HERA," *Phys. Lett.* **B681** (2009) 391–399, `arXiv:0907.5289 [hep-ex]`. On page 33.

[132] **ZEUS** Collaboration, S. Chekanov *et al.*, "Measurement of deeply virtual Compton scattering at HERA," *Phys. Lett.* **B573** (2003) 46–62, `arXiv:hep-ex/0305028 [hep-ex]`. On page 33.

[133] **ZEUS** Collaboration, S. Chekanov *et al.*, "A Measurement of the Q**2, W and t dependences of deeply virtual Compton scattering at HERA," *JHEP* **05** (2009) 108, `arXiv:0812.2517 [hep-ex]`. On page 33.

[134] **CLAS** Collaboration, S. Stepanyan *et al.*, "Observation of exclusive deeply virtual Compton scattering in polarized electron beam asymmetry measurements," *Phys. Rev. Lett.* **87** (2001) 182002, `arXiv:hep-ex/0107043 [hep-ex]`. On page 33.

[135] **CLAS** Collaboration, S. Chen *et al.*, "Measurement of deeply virtual compton scattering with a polarized proton target," *Phys. Rev. Lett.* **97** (2006) 072002, `arXiv:hep-ex/0605012 [hep-ex]`. On page 33.

[136] **CLAS** Collaboration, F. X. Girod *et al.*, "Measurement of Deeply virtual Compton scattering beam-spin asymmetries," *Phys. Rev. Lett.* **100** (2008) 162002, `arXiv:0711.4805 [hep-ex]`. On page 33.

[137] **CLAS** Collaboration, G. Gavalian *et al.*, "Beam spin asymmetries in deeply virtual Compton scattering (DVCS) with CLAS at 4.8 GeV," *Phys. Rev.* **C80** (2009) 035206, `arXiv:0812.2950 [hep-ex]`. On page 33.

[138] **CLAS** Collaboration, H. S. Jo *et al.*, "Cross sections for the exclusive photon electroproduction on the proton and Generalized Parton Distributions," *Phys. Rev. Lett.* **115** no. 21, (2015) 212003, `arXiv:1504.02009 [hep-ex]`. On page 33.

[139] **Jefferson Lab Hall A, Hall A DVCS** Collaboration, C. M. Camacho *et al.*, "Scaling tests of the cross-section for deeply virtual compton scattering," *Phys. Rev. Lett.* **97** (2006) 262002, `arXiv:nucl-ex/0607029 [nucl-ex]`. On page 33.

[140] **Jefferson Lab Hall A** Collaboration, M. Defurne *et al.*, "E00-110 experiment at Jefferson Lab Hall A: Deeply virtual Compton scattering off the proton at 6 GeV," *Phys. Rev.* **C92** no. 5, (2015) 055202, `arXiv:1504.05453 [nucl-ex]`. On page 33.

[141] M. Defurne *et al.*, "A glimpse of gluons through deeply virtual compton scattering on the proton," *Nature Commun.* **8** no. 1, (2017) 1408, `arXiv:1703.09442 [hep-ex]`. On page 33.

[142] A. Accardi *et al.*, "Electron Ion Collider: The Next QCD Frontier," *Eur. Phys. J.* **A52** no. 9, (2016) 268, `arXiv:1212.1701 [nucl-ex]`. On pages 34 and 126.

[143] M. Guidal, "A Fitter code for Deep Virtual Compton Scattering and Generalized Parton Distributions," *Eur. Phys. J.* **A37** (2008) 319–332, `arXiv:0807.2355 [hep-ph]`. [Erratum: Eur. Phys. J.A40,119(2009)]. On page 35.

[144] M. Guidal and H. Moutarde, "Generalized Parton Distributions from Deeply Virtual Compton Scattering at HERMES," *Eur. Phys. J.* **A42** (2009) 71–78, `arXiv:0905.1220 [hep-ph]`. On page 35.

[145] M. Guidal, "Generalized Parton Distributions from Deep Virtual Compton Scattering at CLAS," *Phys. Lett.* **B689** (2010) 156–162, `arXiv:1003.0307 [hep-ph]`. On page 35.

[146] M. Guidal, "Constraints on the $\tilde{H}$ Generalized Parton Distribution from Deep Virtual Compton Scattering Measured at HERMES," *Phys. Lett.* **B693** (2010) 17–23, `arXiv:1005.4922 [hep-ph]`. On page 35.

[147] K. Kumerički, D. Müller, and M. Murray, "HERMES impact for the access of Compton form factors," *Phys. Part. Nucl.* **45** no. 4, (2014) 723–755, `arXiv:1301.1230 [hep-ph]`. On page 35.

[148] M. Boër and M. Guidal, "Generalized Parton Distributions and Deeply Virtual Compton Scattering," *J. Phys.* **G42** no. 3, (2015) 034023, `arXiv:1412.4651 [hep-ph]`. On page 35.

[149] K. Kumericki, D. Mueller, and K. Passek-Kumericki, "Towards a fitting procedure for deeply virtual Compton scattering at next-to-leading order and beyond," *Nucl. Phys.* **B794** (2008) 244–323, `arXiv:hep-ph/0703179 [HEP-PH]`. On page 35.

[150] K. Kumerički and D. Mueller, "Deeply virtual Compton scattering at small x_B and the access to the GPD H," *Nucl. Phys.* **B841** (2010) 1–58, `arXiv:0904.0458 [hep-ph]`. On pages 35 and 83.

[151] H. Moutarde, P. Sznajder, and J. Wagner, "Border and skewness functions from a leading order fit to DVCS data," `arXiv:1807.07620 [hep-ph]`. On page 35.

[152] S. Goloskokov and P. Kroll, "The Role of the quark and gluon GPDs in hard vector-meson electroproduction," *Eur.Phys.J.* **C53** (2008) 367–384, `arXiv:0708.3569 [hep-ph]`. On pages 35, 36, 53, and 59.

[153] T. Lautenschlager, D. Muller, and A. Schaefer, "Global analysis of generalized parton distributions – collider kinematics –," `arXiv:1312.5493 [hep-ph]`. On page 35.

[154] K. Kumericki, D. Mueller, and A. Schafer, "Neural network generated parametrizations of deeply virtual Compton form factors," *JHEP* **07** (2011) 073, `arXiv:1106.2808 [hep-ph]`. On page 35.

[155] S. Goloskokov and P. Kroll, "Vector meson electroproduction at small Bjorken-x and generalized parton distributions," *Eur.Phys.J.* **C42** (2005) 281–301, `arXiv:hep-ph/0501242 [hep-ph]`. On pages 36, 53, 59, and 83.

[156] S. Goloskokov and P. Kroll, "An Attempt to understand exclusive pi+ electroproduction," *Eur.Phys.J.* **C65** (2010) 137–151, `arXiv:0906.0460 [hep-ph]`. On pages 36, 53, and 59.

[157] M. Guidal, M. Polyakov, A. Radyushkin, and M. Vanderhaeghen, "Nucleon form-factors from generalized parton distributions," *Phys.Rev.* **D72** (2005) 054013, `arXiv:hep-ph/0410251 [hep-ph]`. On pages 36 and 83.

[158] C. Mezrag, H. Moutarde, and F. Sabatié, "Test of two new parameterizations of the Generalized Parton Distribution H," *Phys.Rev.* **D88** (2013) 014001, `arXiv:1304.7645 [hep-ph]`. On pages 36 and 60.

[159] J. D. Noritzsch, "Heavy quarks in deeply virtual Compton scattering," *Phys. Rev.* **D69** (2004) 094016, `arXiv:hep-ph/0312137 [hep-ph]`. On page 36.

[160] H. Moutarde, "Nucleon reverse engineering: Structuring hadrons with colored degrees of freedom," *to appear in EPJA* (2018) . On pages 41 and 124.

[161] M. Diehl and T. Gousset, "Time ordering in off diagonal parton distributions," *Phys.Lett.* **B428** (1998) 359–370, `arXiv:hep-ph/9801233 [hep-ph]`. On page 43.

[162] A. Bilal, *Lecture notes in Quantum Field Theory.* Master ENS International Center for Fundamental Physics, Sept., 2014. On page 43.

[163] S. Weinberg, *The Quantum Theory of Fields.* No. vol. 1. Cambridge University Press, 1995. On page 43.

[164] N. Kivel and M. V. Polyakov, "One loop chiral corrections to hard exclusive processes: 1. Pion case," `arXiv:hep-ph/0203264 [hep-ph]`. On page 44.

[165] C. Mezrag, H. Moutarde, J. Rodríguez-Quintero, and F. Sabatié, "Towards a Pion Generalized Parton Distribution Model from Dyson-Schwinger Equations," `arXiv:1406.7425 [hep-ph]`. On page 44.

[166] M. Diehl, T. Feldmann, R. Jakob, and P. Kroll, "The Overlap representation of skewed quark and gluon distributions," *Nucl.Phys.* **B596** (2001) 33–65, `arXiv:hep-ph/0009255 [hep-ph]`. On pages 47, 67, 68, 69, 70, and 72.

[167] P. Pobylitsa, "Inequalities for generalized parton distributions H and E," *Phys.Rev.* **D65** (2002) 077504, `arXiv:hep-ph/0112322 [hep-ph]`. On page 50.

[168] P. Pobylitsa, "Disentangling positivity constraints for generalized parton distributions," *Phys.Rev.* **D65** (2002) 114015, `arXiv:hep-ph/0201030 [hep-ph]`. On page 50.

[169] S. Deans, *The Radon transform and some of its applications.* A Wiley-Interscience publication. Wiley, 1983. On pages 51, 121, and 122.

[170] K. Goeke, M. V. Polyakov, and M. Vanderhaeghen, "Hard exclusive reactions and the structure of hadrons," *Prog.Part.Nucl.Phys.* **47** (2001) 401–515, `arXiv:hep-ph/0106012 [hep-ph]`. On page 51.

[171] M. V. Polyakov and C. Weiss, "Skewed and double distributions in pion and nucleon," *Phys.Rev.* **D60** (1999) 114017, `arXiv:hep-ph/9902451 [hep-ph]`. On pages 52 and 59.

[172] I. Musatov and A. Radyushkin, "Evolution and models for skewed parton distributions," *Phys.Rev.* **D61** (2000) 074027, `arXiv:hep-ph/9905376 [hep-ph]`. On pages 53 and 59.

[173] A. Radyushkin, "Alpha representation and spectral properties of multiparton functions," *Theor.Math.Phys.* **61** (1985) 1144. On page 53.

[174] M. Diehl, T. Gousset, B. Pire, and O. Teryaev, "Probing partonic structure in gamma* gamma —> pi pi near threshold," *Phys.Rev.Lett.* **81** (1998) 1782–1785, `arXiv:hep-ph/9805380 [hep-ph]`. On page 55.

[175] M. Diehl, T. Gousset, and B. Pire, "Exclusive production of pion pairs in gamma* gamma collisions at large Q**2," *Phys.Rev.* **D62** (2000) 073014, `arXiv:hep-ph/0003233 [hep-ph]`. On page 55.

[176] A. Radyushkin, "Symmetries and structure of skewed and double distributions," *Phys.Lett.* **B449** (1999) 81–88, `arXiv:hep-ph/9810466 [hep-ph]`. On page 57.

[177] B. Tiburzi, "Double distributions: Loose ends," *Phys.Rev.* **D70** (2004) 057504, `arXiv:hep-ph/0405211 [hep-ph]`. On pages 58, 61, and 65.

[178] A. V. Belitsky, D. Mueller, A. Kirchner, and A. Schafer, "Twist three analysis of photon electroproduction off pion," *Phys.Rev.* **D64** (2001) 116002, `arXiv:hep-ph/0011314 [hep-ph]`. On page 60.

[179] A. Radyushkin, "Generalized Parton Distributions and Their Singularities," *Phys.Rev.* **D83** (2011) 076006, `arXiv:1101.2165 [hep-ph]`. On page 60.

[180] A. Radyushkin, "Modeling Nucleon Generalized Parton Distributions," *Phys.Rev.* **D87** no. 9, (2013) 096017, `arXiv:1304.2682 [hep-ph]`. On page 60.

[181] P. V. Pobylitsa, "Integral representations for nonperturbative GPDs in terms of perturbative diagrams," *Phys. Rev.* **D67** (2003) 094012, `arXiv:hep-ph/0210238 [hep-ph]`. On pages 60 and 62.

[182] F. Yuan, "Generalized parton distributions at x —> 1," *Phys. Rev.* **D69** (2004) 051501, `arXiv:hep-ph/0311288 [hep-ph]`. On pages 61 and 78.

[183] D. Mueller, "Generalized Parton Distributions – visions, basics, and realities –," *Few Body Syst.* **55** (2014) 317–337, `arXiv:1405.2817 [hep-ph]`. On page 63.

[184] S. Friot, B. Pire, and L. Szymanowski, "Deeply virtual compton scattering on a photon and generalized parton distributions in the photon," *Phys. Lett.* **B645** (2007) 153–160, `arXiv:hep-ph/0611176 [hep-ph]`. On page 64.

[185] I. R. Gabdrakhmanov and O. V. Teryaev, "Analyticity and sum rules for photon GPDs," *Phys. Lett.* **B716** (2012) 417–424, `arXiv:1204.6471 [hep-ph]`. On page 64.

[186] M. Diehl, T. Feldmann, R. Jakob, and P. Kroll, "Linking parton distributions to form-factors and Compton scattering," *Eur. Phys. J.* **C8** (1999) 409–434, `arXiv:hep-ph/9811253 [hep-ph]`. On page 67.

[187] S. J. Brodsky, M. Diehl, and D. S. Hwang, "Light cone wave function representation of deeply virtual Compton scattering," *Nucl. Phys.* **B596** (2001) 99–124, `arXiv:hep-ph/0009254 [hep-ph]`. On page 67.

[188] S. J. Brodsky, T. Huang, and G. P. Lepage, "Hadronic wave functions and high momentum transfer interactions in quantum chromodynamics," *Conf. Proc.* **C810816** (1981) 143–199. On page 67.

[189] S. J. Brodsky, H.-C. Pauli, and S. S. Pinsky, "Quantum chromodynamics and other field theories on the light cone," *Phys. Rept.* **301** (1998) 299–486, `arXiv:hep-ph/9705477 [hep-ph]`. On page 67.

[190] X.-d. Ji, J.-P. Ma, and F. Yuan, "Classification and asymptotic scaling of hadrons' light cone wave function amplitudes," *Eur. Phys. J.* **C33** (2004) 75–90, `arXiv:hep-ph/0304107 [hep-ph]`. On page 72.

[191] M. V. Polyakov, "Hard exclusive electroproduction of two pions and their resonances," *Nucl.Phys.* **B555** (1999) 231, `arXiv:hep-ph/9809483 [hep-ph]`. On page 72.

[192] S. J. Brodsky, G. F. de Teramond, H. G. Dosch, and J. Erlich, "Light-Front Holographic QCD and Emerging Confinement," *Phys. Rept.* **584** (2015) 1–105, `arXiv:1407.8131 [hep-ph]`. On page 73.

[193] A. Bacchetta, S. Cotogno, and B. Pasquini, "The transverse structure of the pion in momentum space inspired by the AdS/QCD correspondence," *Phys. Lett.* **B771** (2017) 546–552, `arXiv:1703.07669 [hep-ph]`. On page 73.

[194] Wolfram Research, Inc., "Mathematica, Version 11.3.". Champaign, IL, 2018. On page 73.

[195] **NA7 Collaboration** Collaboration, S. Amendolia *et al.*, "A Measurement of the Space - Like Pion Electromagnetic Form-Factor," *Nucl.Phys.* **B277** (1986) 168. On page 74.

[196] C. D. Roberts, "Three Lectures on Hadron Physics," *J. Phys. Conf. Ser.* **706** no. 2, (2016) 022003, `arXiv:1509.02925 [nucl-th]`. On page 75.

[197] L. Chang, I. Cloet, J. Cobos-Martinez, C. Roberts, S. Schmidt, *et al.*, "Imaging dynamical chiral symmetry breaking: pion wave function on the light front," *Phys.Rev.Lett.* **110** (2013) 132001, `arXiv:1301.0324 [nucl-th]`. On page 76.

[198] N. Nakanishi, "Partial-Wave Bethe-Salpeter Equation," *Phys.Rev.* **130** (1963) 1230–1235. On page 76.

[199] N. Nakanishi, "A General survey of the theory of the Bethe-Salpeter equation," *Prog.Theor.Phys.Suppl.* **43** (1969) 1–81. On page 76.

[200] L. Chang, C. Mezrag, H. Moutarde, C. D. Roberts, J. Rodriguez-Quintero, *et al.*, "Basic features of the pion valence-quark distribution function," *Phys.Lett.* **B737** (2014) 23–29, `arXiv:1406.5450 [nucl-th]`. On page 78.

[201] **Jefferson Lab** Collaboration, G. Huber *et al.*, "Charged pion form-factor between Q**2 = 0.60-GeV**2 and 2.45-GeV**2. II. Determination of, and results for, the pion form-factor," *Phys.Rev.* **C78** (2008) 045203, `arXiv:0809.3052 [nucl-ex]`. On page 78.

Bibliography

[202] A. Efremov and A. Radyushkin, "Asymptotical Behavior of Pion Electromagnetic Form-Factor in QCD," *Theor.Math.Phys.* **42** (1980) 97–110. On page 78.

[203] G. P. Lepage and S. J. Brodsky, "Exclusive Processes in Perturbative Quantum Chromodynamics," *Phys.Rev.* **D22** (1980) 2157. On page 78.

[204] P. Maris, C. D. Roberts, and P. C. Tandy, "Pion mass and decay constant," *Phys.Lett.* **B420** (1998) 267–273, `arXiv:nucl-th/9707003 [nucl-th]`. On page 78.

[205] S.-X. Qin, C. D. Roberts, and S. M. Schmidt, "Ward–Green–Takahashi identities and the axial-vector vertex," *Phys. Lett.* **B733** (2014) 202–208, `arXiv:1402.1176 [nucl-th]`. On page 78.

[206] M. V. Polyakov and K. M. Semenov-Tian-Shansky, "Dual parametrization of GPDs versus double distribution Ansatz," *Eur.Phys.J.* **A40** (2009) 181–198, `arXiv:0811.2901 [hep-ph]`. On page 83.

[207] G. R. Goldstein, J. O. G. Hernandez, and S. Liuti, "Flexible Parametrization of Generalized Parton Distributions from Deeply Virtual Compton Scattering Observables," *Phys.Rev.* **D84** (2011) 034007, `arXiv:1012.3776 [hep-ph]`. On page 83.

[208] C. Fanelli, E. Pace, G. Romanelli, G. Salmè, and M. Salmistraro, "Pion Generalized Parton Distributions within a fully covariant constituent quark model," *Eur. Phys. J.* **C76** no. 5, (2016) 253, `arXiv:1603.04598 [hep-ph]`. On page 83.

[209] A. E. Dorokhov, W. Broniowski, and E. Ruiz Arriola, "Generalized Quark Transversity Distribution of the Pion in Chiral Quark Models," *Phys.Rev.* **D84** (2011) 074015, `arXiv:1107.5631 [hep-ph]`. On page 83.

[210] W. Broniowski, E. Ruiz Arriola, and K. Golec-Biernat, "Generalized parton distributions of the pion in chiral quark models and their QCD evolution," *Phys.Rev.* **D77** (2008) 034023, `arXiv:0712.1012 [hep-ph]`. On page 83.

[211] D. Mueller and A. Schäfer, "Complex conformal spin partial wave expansion of generalized parton distributions and distribution amplitudes," *Nucl.Phys.* **B739** (2006) 1–59, `arXiv:hep-ph/0509204 [hep-ph]`. On pages 84 and 100.

[212] D. Müller, "Double distributions and generalized parton distributions from the parton number conserved light front wave function overlap representation," `arXiv:1711.09932 [hep-ph]`. On pages 84 and 89.

[213] F. Natterer, *The Mathematics of Computerized Tomography.* Classics in Applied Mathematics. Society for Industrial and Applied Mathematics, 2001. On pages 89 and 122.

[214] H. P. Langtangen and K.-A. Mardal, *Introduction to Numerical Methods for Variational Problems.* Sept., 2016. `http://hplgit.github.io/fem-book/doc/web/`. On page 90.

[215] H. Le Dret, *Lecture notes in Numerical Approximation of PDEs*. Université Pierre et Marie Curie, Jan., 2012.
`https://www.ljll.math.upmc.fr/ledret/M1ApproxPDE.html`. On page 90.

[216] D. N. Arnold and A. Logg, "Periodic Table of the Finite Elements," *SIAM News* **47** (2014) . `https://femtable.org/`. On page 90.

[217] D. Fong and M. Saunders, "LSMR: An iterative algorithm for sparse least-squares problems," *ArXiv e-prints* (June, 2010) , `arXiv:1006.0758 [cs.MS]`.
`http://web.stanford.edu/group/SOL/software/lsmr/`. On page 93.

[218] J. R. Shewchuk, "Triangle: Engineering a 2D Quality Mesh Generator and Delaunay Triangulator," in *Applied Computational Geometry: Towards Geometric Engineering*, M. C. Lin and D. Manocha, eds., vol. 1148 of *Lecture Notes in Computer Science*, pp. 203–222. Springer-Verlag, May, 1996. From the First ACM Workshop on Applied Computational Geometry. On page 95.

[219] S. Helgason, *The Radon transform*. Progress in mathematics. Birkhäuser, 1980. On page 122.

[220] A. Hertle, "Continuity of the radon transform and its inverse on euclidean space.," *Mathematische Zeitschrift* **184** (1983) 165–192. `http://eudml.org/doc/173356`. On page 122.

[221] J. Boman and E. T. Quinto, "Support theorems for real-analytic radon transforms," *Duke Math. J.* **55** no. 4, (12, 1987) 943–948. On page 122.

Titre : Distributions de Partons Généralisées et extension covariante : vers une tomographie du nucléon

Mots-clés : Chromodynamique Quantique, Distributions de Partons Généralisées, Structure du nucléon, Diffusion Compton Profondément Virtuelle, Transformée de Radon, Doubles Distributions

Résumé : Les Distributions de Partons Généralisées (GPDs) encodent les corrélations entre impulsion longitudinale et position transverse des partons dans les hadrons et permettent d'imager la structure du nucléon en 2+1 dimensions. Elles ont été étudiées théoriquement et expérimentalement pendant deux décennies et une nouvelle ère expérimentale débute actuellement (à Jefferson Lab et COMPASS, mais aussi à l'avenir à un collisionneur électron-ion) pour les extraire avec grande précision.

La difficulté est que seul un accès expérimental indirect est possible, à travers divers canaux de diffusion exclusive et les observables associés. Cela implique de prendre nécessairement en compte les nombreuses contraintes théoriques si l'on veut concevoir des modèles fiables pour la phénoménologie. En particulier, deux contraintes cruciales sont les propriétés de "polynomialité" et de "positivité". L'approche de cette thèse consiste à tirer partie des deux propriétés en modélisant d'abord les fonctions d'onde sur le cône de lumière des premiers états de Fock du nucléon, permettant d'obtenir une GPD dans la région appelée DGLAP via overlap où le nombre de partons est conservé, puis l'étendre de manière covariante à la région ERBL, avec une inversion de transformée de Radon.

In fine, le but est d'appliquer cette procédure à un modèle de quark-constituant pour GPDs de valence, ce qui permettrait de produire de manière inédite pour ce genre de modèle des résultats à comparer à l'expérience (sur le processus de diffusion Compton profondément virtuelle en l'occurrence). Pour atteindre cette objectif, on utilise la librairie PARTONS sous différentes hypothèses perturbatives.

Title: Generalized Parton Distributions and their covariant extension: towards nucleon tomography

Keywords: Quantum Chromodynamics, Generalized Parton Distributions, Nucleon structure, Deeply Virtual Compton Scattering, Radon transform, Double Distributions

Abstract: Generalized Parton Distributions (GPDs) encode the correlations between longitudinal momentum and transverse position of partons inside hadrons and can give access to a picture of the nucleon structure in 2+1 dimensions. They have been studied theoretically and experimentally for almost two decades and a new experimental era is starting (at JLab and COMPASS currently, and in the future at an EIC) to extract them.

The difficulty is that only an indirect experimental access is so far possible, through different exclusive channels and various observables. Therefore, one has to take into account the many theoretical constraints to be able to produce accurate models and rely on their phenomenology. Two important constraints are called the polynomiality and positivity properties. The approach of this thesis is to make use of both of them by first modeling low Fock states light-front wave-functions, which gives a GPD in the DGLAP region by a parton number conserved overlap, and then covariantly extending this GPD to the ERBL region, through an inverse radon transform.

In fine, the goal is to apply this on a constituent quark-like model for valence GPDs, which would allow to produce a phenomenological output (on DVCS data for instance) from this kind of models, which was impossible before. We make use of the versatile PARTONS framework to achieve this under various perturbative QCD assumptions.